FRIEDRICH-SCHILLER-
UNIVERSITÄT
JENA

# Beiträge zur Chemie der Azaacene

Dissertation
(kumulativ)

zur Erlangung des akademischen Grades

doctor rerum naturalium (Dr. rer. nat.)

vorgelegt dem Rat der Chemisch-Geowissenschaftlichen Fakultät

der Friedrich-Schiller-Universität Jena

von Dipl.-Chem. Dominique Mario Gampe

geboren am 16.12.1989 in Plauen

Gutachter:

1. Prof. Dr. Rainer Beckert
   Friedrich-Schiller-Universität Jena
   Institut für Organische Chemie und Makromolekulare Chemie
   Humboldtstr. 10
   07743 Jena
2. Prof. Dr. Pablo Wessig
   Universität Potsdam
   Institut für Chemie
   Karl-Liebknecht-Str. 24-25
   D-14476 Potsdam
3. Prof. Dr. Kalina Peneva
   Institute of Organic Chemistry and Macromolecular Chemistry
   Jena Center of Soft Matter
   Friedrich Schiller University of Jena
   Lessingstr. 8th
   07743 Jena

Tag der öffentlichen Verteidigung: 24.01.2018

*„Alles Schwierige auf Erden beginnt einfach, alles Große beginnt klein.“*
(Lao-Tse)

# Inhaltsverzeichnis

# Dokumentation der Publikationsäquivalente

**P1)** "Stable and Easily Accessible Functional Dyes: Dihydrotetraazaanthracenes as Versatile Precursors for Higher Acenes"

D. M. Gampe,[1] M. Kaufmann,[2] D. Jakobi,[3] T. Sachse,[4] M. Presselt,[5] R. Beckert,[6] H. Görls,[7] *Chem. Eur. J.* **2015**, *21*, 7571-7581.

DOI: 10.1002/chem.201500230

http://onlinelibrary.wiley.com/doi/10.1002/chem.201500230/abstract

| Autor | 1 | 2 | 3 | 4 | 5 | 6 | 7 |
|---|---|---|---|---|---|---|---|
| Konzept | | | | | | X | |
| Synthese | X | X | X | | | | |
| Spektroskopie | X | X | X | | | | |
| DFT / TD-DFT Berechnungen | | | | X | | | |
| RKSA | | | | | | | X |
| Anfertigen des Manuskripts | X | X | | X | | | |
| Korrektur des Manuskripts | X | X | X | X | X | X | X |
| Betreuung | | | | | X | X | |
| Vorschlag der Publikationsäquivalente | 0,5 | | | | | | |

**P2)** "Surprising Characteristics of D-A-Type Functional Dyes by Introducing 4-Alkoxythiazoles as the Donor-Unit"

D. M. Gampe,[1] F. Nöller,[2] V. G Hänsch,[3] S. Schramm,[4] A. Darsen,[5] S. H. Habenicht,[6] S. Ehrhardt,[7] D. Weiß,[8] H. Görls,[9] R. Beckert,[10] *Tetrahedron* **2016**, *72*, 3232-3239.

DOI: 10.1016/j.tet.2016.04.046

http://www.sciencedirect.com/science/article/pii/S0040402016303167

| Autor | 1 | 2 | 3 | 4 | 5 | 6 | 7 | 8 | 9 | 10 |
|---|---|---|---|---|---|---|---|---|---|---|
| Konzept | X | | | | | | | X | | X |
| Synthese Edukte | X | X | X | | X | X | X | | | |
| Synthese Zielprodukte | X | X | X | | | | | | | |
| Spektroskopie / Elektrochemie | X | X | | | | | | | | |
| DFT / TD-DFT Berechnungen | | | | X | | | | | | |
| RKSA | | | | | | | | | X | |
| Anfertigen des Manuskripts | X | | | X | | | | | | |
| Korrektur des Manuskripts | X | | | X | | | | X | X | X |
| Betreuung | | | | | | | | X | | X |
| Vorschlag der Publikationsäquivalente | 1,0 | | | | | | | | | |

**P3)** "Pushing to the Low Limits: Tetraazaanthracenes with Very Low-Lying LUMO Levels and Near-Infrared Absorption"

D. M. Gampe,[1] S. Schramm,[2] F. Nöller,[3] D. Weiß,[4] H. Görls,[5] P. Naumov,[6] R. Beckert,[7] *Chem. Commun.* **2017**, *53*, 10220-10223.

DOI: 10.1039/C7CC05224C

http://pubs.rsc.org/en/content/articlelanding/2017/cc/c7cc05224c#!divAbstract

| Autor | 1 | 2 | 3 | 4 | 5 | 6 | 7 |
|---|---|---|---|---|---|---|---|
| Konzept | X | | | X | | | X |
| Synthese | X | | X | | | | |
| Spektroskopie / Elektrochemie | X | | | | | | |
| DFT / TD-DFT Berechnungen | | X | | | | | |
| RKSA | | | | | X | | |
| Anfertigen des Manuskripts | X | X | | | | | |
| Korrektur des Manuskripts | X | X | X | X | X | X | X |
| Betreuung | | | | | | X | X |
| Vorschlag der Publikationsäquivalente | 1,0 | | | | | | |

**P4)** "Mixing Chromophores: Novel D-A-type Dyes with low lying LUMOs and narrow Bandgaps by Connecting 4-Alkoxythiazoles and Azaacenes"

D. M. Gampe,[1] V. G Hänsch,[2] S. Schramm,[3] R. Menzel,[4] D. Weiß,[5] R. Beckert,[6] *Eur. J. Org. Chem.* **2017**, *2017*, 1369-1379.

DOI: 10.1002/ejoc.201601521

http://onlinelibrary.wiley.com/doi/10.1002/ejoc.201601521/abstract

| Autor | 1 | 2 | 3 | 4 | 5 | 6 |
|---|---|---|---|---|---|---|
| Konzept | X | | | X | X | X |
| Synthese | X | X | | | | |
| Spektroskopie / Elektrochemie | X | | | | | |
| DFT / TD-DFT Berechnungen | | | X | | | |
| Anfertigen des Manuskripts | X | | | | | |
| Korrektur des Manuskripts | X | X | X | X | X | X |
| Betreuung | | | | | | X |
| Vorschlag der Publikationsäquivalente | 1,0 | | | | | |

**P5)** "*N*-Phenylfluorubine: one functional dye - chromophor, fluorophor, electron-acceptor and more"

D. M. Gampe,[1] S. Schramm,[2] M. Kaufmann,[3] H. Görls,[4] R. Beckert,[5] *New J. Chem.* **2016**, *40*, 10100-10107.

DOI: 10.1039/C6NJ02544G

http://pubs.rsc.org/en/Content/ArticleLanding/2016/NJ/C6NJ02544G#!divAbstract

| Autor | 1 | 2 | 3 | 4 | 5 |
|---|---|---|---|---|---|
| Konzept | X | | X | | X |
| Synthese | X | | | | |
| Spektroskopie / Elektrochemie | X | | | | |
| DFT / TD-DFT Berechnungen | | X | | | |
| Anfertigen des Manuskripts | X | | | | |
| Korrektur des Manuskripts | X | X | X | X | X |
| Betreuung | | | | | X |
| Vorschlag der Publikationsäquivalente | 1,0 | | | | |

**P6)** "From Highly Fluorescent Donors to Strongly Absorbing Acceptors: The Tunable Properties of Fluorubines"

D. M. Gampe,[1] S. Schramm,[2] S. Ziemann,[3] M. Westerhausen,[4] H. Görls,[5] P. Naumov,[6] R. Beckert,[7] *J. Org. Chem.* **2017**, *82*, 6153-6162.

DOI: 10.1021/acs.joc.7b00676

http://pubs.acs.org/doi/abs/10.1021/acs.joc.7b00676

| Autor | 1 | 2 | 3 | 4 | 5 | 6 | 7 |
|---|---|---|---|---|---|---|---|
| Konzept | X | | | | | | X |
| Synthese Edukte | X | | X | | | | |
| Synthese Zielprodukte | X | | | | | | |
| Spektroskopie / Elektrochemie | X | | | | | | |
| DFT / TD-DFT Berechnungen | | X | | | | | |
| RKSA | | | | | X | | |
| Anfertigen des Manuskripts | X | | | | | | |
| Korrektur des Manuskripts | X | X | X | X | X | X | X |
| Betreuung | | | | X | | X | X |
| Vorschlag der Publikationsäquivalente | 1,0 | | | | | | |

**Erklärung zu den Eigenanteilen des Promovenden/der Promovendin sowie der weiteren Doktoranden/Doktorandinnen als Koautoren an den Publikationen und Zweitpublikationsrechten bei einer kumulativen Dissertation**

**Für alle in dieser kumulativen Dissertation verwendeten Manuskripte liegen die notwendigen Genehmigungen der Verlage („Reprint permissions“) für die Zweitpublikation vor.**

**Die Co-Autoren der in dieser kumulativen Dissertation verwendeten Manuskripte sind sowohl über die Nutzung, als auch über die oben angegebenen Eigenanteile informiert und stimmen dem zu.**

**Ich bin mit der Abfassung der Dissertation als publikationsbasiert, d.h. kumulativ, einverstanden und bestätige die vorstehenden Angaben. Eine entsprechend begründete Befürwortung mit Angabe des wissenschaftlichen Anteils des Doktoranden/der Doktorandin an den verwendeten Publikationen werde ich parallel an den Rat der Fakultät der Chemisch-Geowissenschaftlichen Fakultät richten.**

Dominique M. Gampe Datum Jena _____

Prof. Dr. Rainer Beckert Datum Jena _____

# Abbildungsverzeichnis

# Schemenverzeichnis

# Abkürzungsverzeichnis

| | |
|---|---|
| $\Delta E_{CV}$ | Elektrochemisch ermittelte Bandlücke |
| $\Delta E_{opt}$ | Absorptionsspektroskopisch ermittelte Bandlücke |
| Ar | aromatischer Rest |
| BHJ | bulk heterojunction; mittels vermischtem Donor- und Akzeptormaterial sensibilisierte Solarzelle |
| BINAP | 2,2'-Bis(diphenylphosphino)-1,1'-binaphthyl |
| Bt | 2,1,3-Benzothiadiazol |
| CT | charge transfer; Ladungsverschiebung |
| CV | Cyclovoltammetrie |
| D-A | Donor-Akzeptor |
| DDQ | 2,3-Dichlor-5,6-dicyano-benzochinon |
| DFT / TD-DFT | Dichtefunktionaltheorie / Zeitabhängige ~ |
| DMA | Dimethylacetamid |
| DSSC | dye sensitized solar cell; mittels Farbstoffen sensibilisierte Solarzelle |
| *et al.* | et alii; und andere |
| EtOH | Ethanol |
| $Fc/Fc^+$ | Ferrocen/Ferrocenium |
| $\varepsilon$ | molarer Extinktionskoeffizient |
| HOMO | highest occupied molecular orbital; höchstes besetztes Molekülorbital |
| Hünig-Base | Di-*iso*-propylethylamin |
| ITO | Indium-Zinn-Oxid |
| $KO^tBu$ | Kalium-*tert*-butanolat |
| $\lambda$ | Wellenlänge |
| LUMO | lowest unoccupied molecular orbital; niedrigstes unbesetztes Molekülorbital |
| NaAc | Natriumacetat |
| NBS | *N*-Bromsuccinimid |
| NIR | nah-infraroter Bereich des Lichts |
| NMP | *N*-Methylpyrrolidin |
| OPV | organic photovoltaic; mittels organischen Materialien sensibilisierte Solarzelle |
| OFET | organic field-effect transistor; mittels organischen Halbleiters gesteuerter Transistor |
| OLED | organic light-emitting diode; mittels organischen Emitters strahlende Leuchtdiode |
| PCBM | Phenyl-$C_{61}$-buttersäuremethylester |

| | |
|---|---|
| $Pd(dba)_2$ | Bis(dibenzylidenaceton)palladium(0) |
| $\Phi_{FL}$ | Fluoreszenzquantenausbeute |
| P3HT | Poly-3-hexylthiophen |
| Ph | Phenylrest |
| RuPhos | 2-Dicyclohexylphosphino-2',6'-diisopropoxybiphenyl |
| SCE | Saturated calomel elektrode; Kalomelelektrode |
| SPhos | 2-Dicyclohexylphosphino-2',6'-dimethoxybiphenyl |
| $TBAPF_6$ | Tetrabutylammoniumhexafluorophosphat |
| TCNQ | Tetracyanochinodimethan |
| THF | Tetrahydrofuran |
| UV/Vis | Ultraviolettes / sichtbares Licht |
| $\upsilon$ | Stoke's shift |

# 1 Einleitung

Im Laufe der letzten Jahrhunderte gewannen farbige organische Substanzen aus ästhetischen Gründen immer mehr an Bedeutung für die Gesellschaft. Um große Mengen produzieren zu können, wurde die künstliche Herstellung – die Synthese – von Farben immer wichtiger. Mit der Entwicklung der „Teerfarben“ (Mauvein, Fuchsin und diversen Azo-Farbstoffen) Mitte des 19. Jahrhunderts begann das gezielte Moleküldesign, um verschiedenen Eigenschaftsansprüchen, zum Beispiel der Farbgebung und Prozessierbarkeit, gerecht zu werden.[1] Durch den stetigen Technologiefortschritt während des 20. Jahrhunderts bedurfte es auch einer konstant wachsenden Menge an speziellen Farbstoffen. So entstanden farbige Lacke, Anstriche, Druckerfarben oder auch Farbindikatoren.[2] Heute existieren noch viele weitere spezielle Anwendungsbereiche, welche vorrangig mit der medizinischen Diagnostik, bildgebenden Verfahren oder der Entwicklung von elektronischen Bauteilen zusammenhängen.[3]

Vor allem die Verwendung von funktionellen Farbstoffen[1] in der heutigen Hochtechnologie erfordert gut abgestimmte Eigenschaften der organischen Materialien. Neben einer breiten und starken Lichtabsorption ist beispielsweise auch die Ladungsträgerbeweglichkeit eines Farbstofffilms wichtig für eine Anwendung in organischen Solarzellen (OPV – organic photovoltaics).[4] Eine gute Leitfähigkeit und schmale Bandlücken sind ebenso bei einem Einsatz als halbleitendes Material in organischen Transistoren (OFET – organic field-effect transistor) vorteilhaft.[5] Werden lichtemittierende Farbstoffe (z.B. Fluorophore) in organischen Leuchtdioden (OLED) verwendet, sollte neben einer hohen Quantenausbeute auch eine geringe Reorganisierungsenergie vorhanden sein.[6] Durch kleine Änderungen der Struktur ist es zwar beispielsweise möglich, potente OPV Materialien zu Halbleitern für Transistoren umzufunktionieren, jedoch ist ein erfolgreicher Einsatz nicht unbedingt gewährleistet. Alle optischen, elektrischen oder optoelektrischen Bauteile besitzen dennoch eine Gemeinsamkeit: sie sollten stabil über große Zeiträume sein.[7] Dabei spielt sowohl die chemische als auch die Photostabilität eine große Rolle.

Eine große Klasse von funktionellen Farbstoffen sind die Acene,[8] wie beispeilsweise: Anthracen (**1**) oder Tetracen (**2**, siehe Abbildung 1). Seit der Einführung dieser in diversen optoelektronischen Bauteilen und der Entdeckung ihrer hervorragenden lochleitenden (p-Typ halbleitenden) Eigenschaften wurden viele verschiedene Acene synthetisiert und untersucht.[9] Pentacen (**3**) wurde schließlich die Referenzsubstanz für p-Typ Halbleiter.[10]

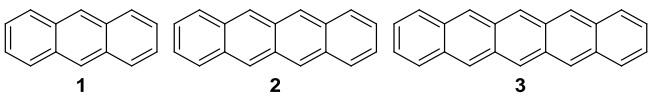


Abbildung 1: Drei der wichtigsten Acene: Anthracen (**1**), Tetracen (**2**) und Pentacen (**3**).

[1] Funktionelle Farbstoffe sind organische Materialien, die nicht wegen ihrer ästhetischen Farb-, sondern aufgrund spezieller Eigenschaften Anwendung finden. Das älteste bekannte Beispiel hierfür ist Chlorophyll.[3c]

Jedoch sind Instabilität, schlechte Lösungsprozessierbarkeit und eingeschränkte Modifizierbarkeit der Struktur Gründe für die Limitierung der Einsatzgebiete. Die Suche nach stabilen und modifizierbaren Alternativen mündete unter anderem in der Integration von Heteroatomen in das System (meistens Stickstoff oder Schwefel).[11]

Mit der Substitution von CH-Einheiten durch Stickstoffatome entstehen die sogenannten Azaacene, welche zwar schon Ende des 19. Jahrhunderts erste Erwähnung fanden, jedoch zeitweise in Vergessenheit gerieten.[12] Bereits 1890 gelang es Fischer und Hepp das erste Azapentacen darzustellen.[13] Fluorindin (Dihydro-tetraazapentacen, **5**, siehe Abbildung 2) war aufgrund seiner außerordentlich starken und lösungsmittelabhängigen Fluoreszenzeigenschaften Anlass kontroverser Diskussionen.[14] Hinsberg verfasste 1901 den ersten Übersichtsartikel „Über mehrgliedrige stickstoffhaltige Ringsysteme“ (unter anderem auch über Dihydronaphtazin **4**), in dem er intensiv auf das jeweilige Redoxpaar: Dihydro-Azaacen ⇄ Azaacen einging.[15] Dieses Redoxverhalten zieht drastische Eigenschaftsänderungen nach sich und stand schon damals im Zentrum der Studien. Bevor es Hinsberg und Schwantes 1903 gelang Fluorubin (Dihydro-hexaazapentacen **6**) zu synthetisieren, waren außerdem die Protonierungsgleichgewichte der Dihydro-Azaacene nahezu unbeachtet geblieben.[16] Besonders beeindruckt waren sie dabei von der pH-sensitiven Fluoreszenzemission, welche sich über vier Protonierungsschritte variieren ließ.

Harsche Synthesebedingungen, schwierige Isolierung und schlechte Löslichkeit waren wahrscheinlich die Gründe für das lange Brachliegen dieser Stoffklasse. Erst während der letzten 20 Jahre erfuhren die Azaacene, durch die oben beschriebene Suche nach stabilen Pentacen-Derivaten, eine Renaissance.[17] Nuckolls und Mitarbeiter wiesen 2003 als erste erfolgreich lochleitende Eigenschaften eines Azaacens (Dihydronaphthazin **4**) nach.[18] Nachdem es ein Jahr später gelang Elektronenleitfähigkeit (n-Typ Halbleiter) von Tetraazaanthracenen[19] zu detektieren, begannen intensive, bis zum heutigen Tage andauernde Untersuchungen an dieser Stoffklasse. Zunächst beschäftigten sich viele Studien mit der Synthese neuartiger Azaacen Derivate. Erfolgreiche, nunmehr etablierte Herstellungsverfahren, wie in Schema 1 dargestellt, begannen mit der Zyklisierung von vicinalen Diaminen **A** und bis-Elektrophilen **B** (X = OH, Halogen, CN) durch zweifache nukleophile aromatische Substitution.[20]

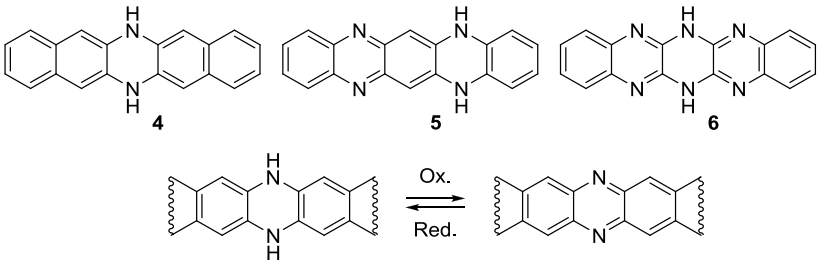


Abbildung 2: Erste hergestellte Dihydro-Azapentacene (Dihydronaphtazin **4**, Fluorindin **5**, Fluorubin **6**) und allgemeine Darstellung der Redoxpaare.

Schema 1: Grundlegende Herstellungsverfahren von Aza-substituierten Acenen.

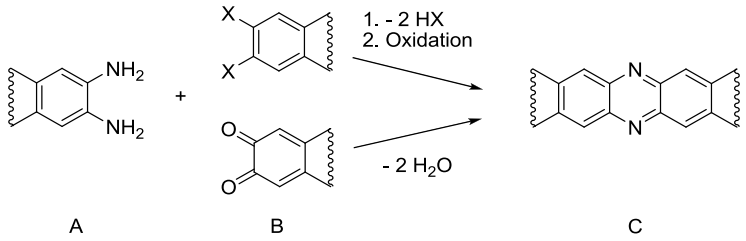


Neben einigen eher exotischen Synthesewegen, wie *ortho*-Annelierung,[21] Domino-Reaktion[22] oder der Umsetzung von *in situ* generierten Chinodimethiden,[23] spielt zunehmend die Buchwald - Hartwig - Kreuzkupplung eine große Rolle.[24]

Die schon 1901 von Hinsberg erwähnten, drastischen Eigenschaftsunterschiede der Redoxpaare[15] können heutzutage genau ermittelt werden (Abbildung 2 unten). Die reduzierten Spezies weisen beispielweise starke Fluoreszenzemission, pH-Sensibilität, erhöhte Stabilität und die Tendenz zur Aggregation durch Wasserstoffbrücken auf. Im Vergleich dazu zeigen die oxidierten Pendants eine schmalere Bandlücke, die mit einer bathochromen Verschiebung der Absorption verbunden ist, verringerte Lagen des niedrigsten unbesetzten Molekülorbitals (LUMO – lowest unoccupied molecular orbital) und verbesserte Löslichkeit in organischen Lösungsmitteln.[25]

Neben dem Einsatz als Halbleiter in OFETs könnten Aza-substituierte Acene aufgrund der allgemein hohen Stabilität und dem breiten Eigenschaftsspektrum für eine Vielzahl von Anwendungsmöglichkeiten interessant werden.[26] Beispielsweise sind manche Derivate brauchbare Emitter für OLEDs, während andere als Sensoren für Anionen oder Metallionen fungieren.[27] Durch die freien Elektronenpaare der Stickstoffatome ist weiterhin der Einsatz als Liganden für Übergangsmetall-Komplexe denkbar.[28] Die photospektroskopischen Eigenschaften sprechen für eine Applikation als Sensibilisator in Farbstoff-Solarzellen. 2017 gelang beispielsweise auch erstmals die Integration von Azaacenen als Akzeptorsubstanz in bulk heterojunction Solarzellen (BHJ – mittels vermischtem Donor- und Akzeptormaterial sensibilisierte Solarzelle).[29]

Um die Zugänglichkeit zu Azaacenen mit zugeschnittenen Eigenschaften sicherzustellen, muss dennoch weiterhin an den Grundlagen geforscht werden. Zum einen sind die Synthesen von geeigneten Bausteinen unausgereift. Vicinale Diamine sind aufgrund ihrer oxidativen Instabilität noch immer unterrepräsentiert und potente bis-Elektrophile entweder redoxaktiv (z. B. Chinone) oder sie reagieren unselektiv mit jeder Art von Nukleophil. Zum anderen gilt es, die vorhandenen Zyklisierungsmöglichkeiten zu optimieren, sei es durch Kreuzkupplungsreaktionen oder „synthetische Umwege“ über stabile Intermediate.

Die grundlegenden Charakteristika von Azaacenen sollten außerdem erweitert werden. Die starke pH-Abhängigkeit der Eigenschaften wurde zwar von einigen Wissenschaftlern bemerkt, jedoch nur von wenigen quantifiziert. Derlei Variabilität stellt ein nützliches Werkzeug für die Erweiterung des Anwendungsspektrums dar.

Diese Dissertation beschäftigt sich mit der Synthese und Charakterisierung von Azaacen Derivaten. Während der Forschungen zu diesem Thema waren unter anderem neuartige und attraktive Vorstufen bedeutsam. Die Kombination von verschiedenen funktionellen Farbstoffen mit Azaacenen konnte dadurch zum ersten Mal erfolgreich realisiert werden. Abbildung 3 zeigt eine Übersicht der während dieser Arbeit untersuchten Azaacene. Über die verschiedenen Reste R können die Eigenschaften gezielt modifiziert werden, wobei vor allem die Reste $R^6$ (grün) eine große Rolle zum Aufbau von höheren Azaacenen spielen. Mittels *N*-Substitution ($R^4$, $R^5$) wird die Dihydro-Form fixiert, wodurch es möglich ist eine pH-Sensitivität zu erhalten, sowie Löslichkeit und Kristallisation zu begünstigen. Sind diese Reste ($R^4$, $R^5$) Protonen, ergibt sich ein leichter Zugang zur oxidierten Spezies und somit zu einer meist reversiblen Redoxaktivität. Wird eine Substitution am Kohlenstoff-Grundgerüst vorgenommen ($R^1$, $R^2$, $R^3$) können Eigenschaften wie Redox-, Absorptions- und Emissionsverhalten variiert werden.

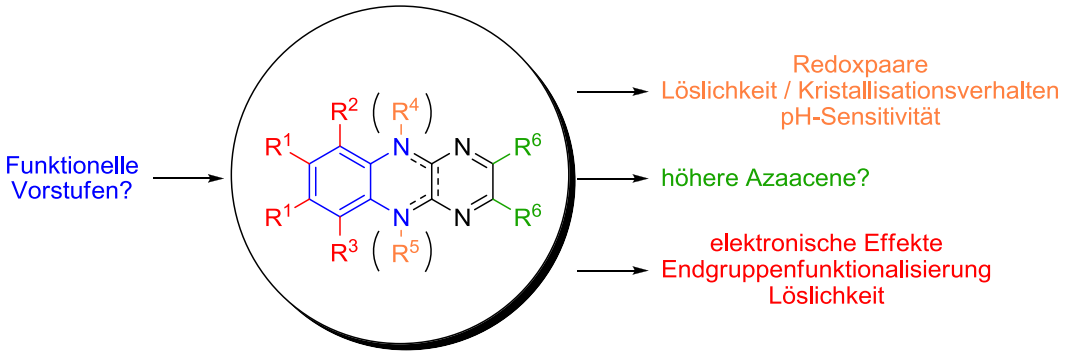


Abbildung 3: Generelle Struktur und Vielseitigkeit der in dieser Arbeit diskutierten Azaacene.

# 2 Funktionelle Vorstufen

## 2.1 Dihydro-tetraazaanthracene

Teile dieses Kapitels sind publiziert in: D. M. Gampe, M. Kaufmann, D. Jakobi, T. Sachse, M. Presselt, R. Beckert, H. Görls, *Chem. Eur. J.* **2015**, *21*, 7571-7581.

Die Einführung von Stickstoff in Acen-Grundgerüste führt zu neuartigen Eigenschaften, wie schmaleren Bandlücken und vor allem zu drastisch erhöhten chemischen Stabilitäten.[30] Neben den, in Schema 1 gezeigten, allgemeinen Synthesemöglichkeiten existieren außergewöhnliche Zugänge, welche in Schema 2 dargestellt sind. Die Arbeitsgruppe um Wudl nutzte 1998 die oxidative *ortho*-Annelierung, um ihr zwitterionisches Tetraphenylhexaazaanthracen (Schema 2A; Y = CH; $Ar^1 = Ar^2$ = Ph) zu synthetisieren und Langer *et al.* erweiterten die Fülle an möglichen Produkten um verschieden substituierte Hexaazaacridine (Y = N).[31] Oxidative *ortho*-Annelierungen sind vor allem ein probater Syntheseweg zu *N*-funktionalisierten Azaacenen mit hoher Stickstoffanzahl, welche intensiv in unserer Arbeitsgruppe untersucht wurden. Auf diese Art können Imidazochinoxaline, chinoide Oktaazahexacene oder Fluorubine dargestellt werden.[32] Fleischhauer *et al.* entdeckten zudem einen Weg zu kationischen Fluorubinen (Schema 2B), welche bei der photoinduzierten Domino Reaktion aus 1,2-Diazetinen entstehen.[22]

Schema 2: Außergewöhnliche Synthesewege zu Azaacenen. A) Oxidative *ortho*-Annelierung; B) Photoinduzierte Domino-Reaktion.

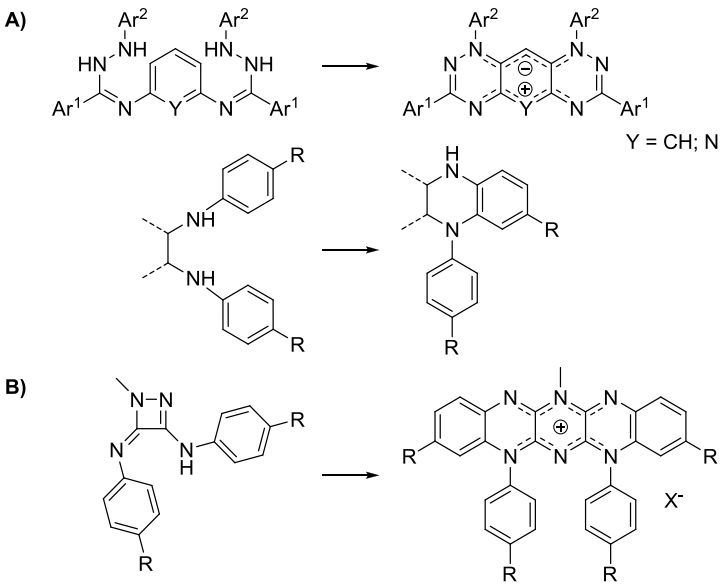

Azaacene sind als Ladungstransportmaterialien noch immer unterrepräsentiert. Das liegt vor allem an problematischen Synthesen und Isolierungen, aufgrund folgender Umstände:

- beschränkter Zugang zu geeigneten Diaminen und entsprechenden bis-elektrophilen Partnern,[33]
- niedrige Ausbeuten der Zyklisierungen, zum Teil trotz Pd-Katalyse,[34]
- schlechte Löslichkeit der Zielstrukturen wegen starker Aggregationsphänomene.[35]

Um diese Probleme lösen zu können, wollten wir den Zugang zu stabilen Edukten erweitern. Neben der Darstellung diverser *N*-substituierter Diamine nutzten wir Dichlor-dicyano-pyrazin als hochreaktives bis-Elektrophil, um eine rasche Zyklisierung, verbunden mit erhöhten Ausbeuten, zu erzwingen. Weiterhin konnten dadurch elektronenziehende Nitril-Gruppen, welche die LUMO-Energien absenken sollten, eingeführt werden. Ried nutzte Dichlor-dicyano-pyrazin 1988 für die erstmalige Synthese von Dihydro-Tetraazaanthracenen.[36] Die Verwendung von Tetraazaanthracenen als n-Typ Halbleiter in OFETs erfolgte jedoch erst 2004.[19] Wir waren daran interessiert, durch *N*-Substitution ($R^1$, siehe Abbildung 4) zum einen die entsprechenden Dihydroformen zu konservieren und zum anderen löslichkeitsvermittelnde, morphologische und bestimmte elektronische Eigenschaften zu beeinflussen.

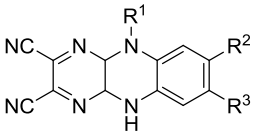


**7a-i**

$R^1 = C_6H_5$; $R^2 = R^3 = H$: **7a**
$R^1 = C_6H_5$; $R^2 = NH\text{-}C_6H_5$; $R^3 = NO_2$: **7b**
$R^1 = p\text{-}C_6H_4\text{-}{}^n(C_4H_9)$; $R^2 = NH\text{-}p\text{-}C_6H_4\text{-}{}^n(C_4H_9)$; $R^3 = NO_2$: **7c**
$R^1 = {}^nC_6H_{13}$; $R^2 = NH\text{-}{}^nC_6H_{13}$; $R^3 = NO_2$: **7d**
$R^1 = (CH_2)_5\text{-}COOEt$; $R^2 = NH\text{-}(CH_2)_5\text{-}COOEt$; $R^3 = NO_2$: **7e**
$R^1 = p\text{-}C_6H_4\text{-}N(CH_3)_2$; $R^2 = NH\text{-}p\text{-}C_6H_4\text{-}N(CH_3)_2$; $R^3 = NO_2$: **7f**
$R^1 = m\text{-}C_6H_4\text{-}CF_3$; $R^2 = NH\text{-}m\text{-}C_6H_4\text{-}CF_3$; $R^3 = NO_2$: **7g**

$R^2$; $R^3$ = 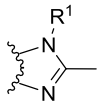


$R^1 = C_6H_5$: **7h**
$R^1 = {}^nC_6H_{13}$: **7i**

Abbildung 4: Allgemeine Struktur der synthetisierten Dihydro-Tetraazaanthracene und Definierung der Reste.

Die neuen Vertreter der Dihydro-Tetraazaanthracene **7** ließen sich leicht aus einem funktionalisierten Diamin (**8**) herstellen. Wie in Schema 3 dargestellt, wurde der einfachste Vertreter (**7a**) durch Zyklisierung von *N*-Phenyl-*o*-phenylendiamin (**8a**) und 2,3-Dichlor-5,6-dicyanopyrazin (**9**) in Ausbeuten von 95% erhalten. Ausgehend von 1,5-Dichlor-2,4-dinitrobenzen wurden über dessen Aminolyseprodukte **10** die vicinalen Diamine **8b-g** durch eine einfache Reduktionsreaktion ($N_2H_4$ / Raney-Ni) hergestellt und mit **9** in moderaten Ausbeuten zu **7b-g** umgesetzt. Die Reduktion beider Nitrogruppen in **10** zu den bis-Diaminen **8h-i** gestaltete sich als relativ einfach, jedoch erwiesen sich diese Tetraamino-Derivate als sehr oxidationsempfindlich. Deshalb lag es nahe, die generierten bis-Diamine **8h-i** *in situ* mit zwei Äquivalenten von **9** unter strengem Sauerstoffausschluss umzusetzen. Das führte zu den gelb-fluoreszierenden Imidazoanthracenen **7h** und **7i**. Ursache für die Entstehung dieser fusionierten Fünfringe könnte das Oxidationsvermögen des Pyrazins **9** sein. Möglicherweise wurden geringe Mengen des Lösungsmittels Ethanol durch **9** zu Essigsäure oxidiert, welche in einer Folgereaktion mit den semizyklisierten Produkten zum 2-Methylimidazolderivat **7h-i** abreagierten.

Schema 3: Synthese der Dihydro-Tetraazanthracene.

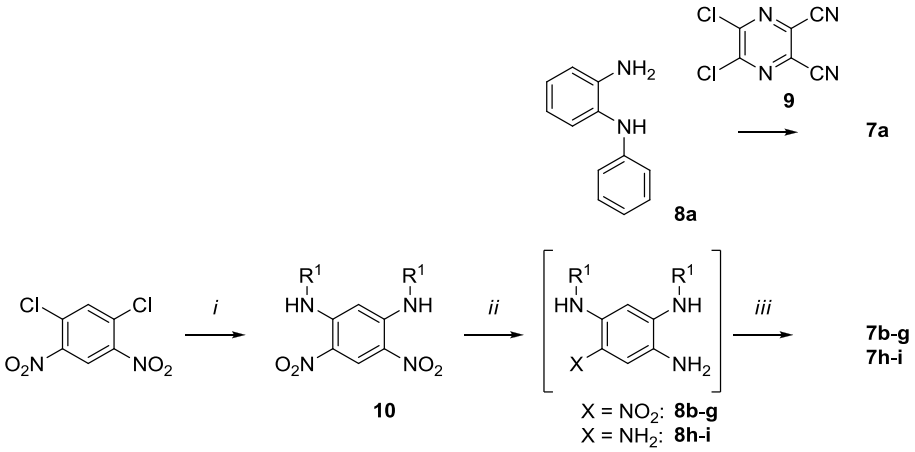


*i*) 2 äqu. $H_2N\text{-}R^1$, EtOH, 40-97%.
*ii*) Raney-Ni, $N_2H_4{*}H_2O$, EtOH, $N_2$, quantitativ.
*iii*) **7b-g**: **8b-g**, **9**, Dioxan, 12 h, 18-50%.
**7h-i**: **8h-i**, 2 äqu. **9**, Dioxan, 12 h, 30%.

Alle Derivate besitzen die nötigen Strukturelemente für den Aufbau höherer Azaacene. Beispielsweise kann die vicinale Dinitril Substruktur im Sinne eines Pseudohalogenids als doppelte nucleofuge Gruppe betrachtet werden. So etablierten Richards und Mitarbeiter einen effizienten Syntheseweg zu stickstoffreichen Azaacenen durch die Substitution von elektronenarmen *ortho*-Dinitrilen mit Diaminen.[37] Weiterhin können neuartige *ortho*-Diamine bei der Reduktion der Nitro-Derivate **7b-g** freigesetzt werden. Die photo- und elektrochemische Charakterisierung dieser Tetraazaanthracene brachte Eigenschaften hervor, welche sie zu einer interessanten Klasse funktioneller Farbstoffe machen.

In Abbildung 5 sind die UV/Vis-Absorptionsspektren der Phenyl-Derivate vergleichend dargestellt. Alle drei Derviate zeigen eine starke Absorptionsbande im ultravioletten Spektralbereich ($\lambda_{max}$ = 267 - 305 nm) und eine weitere mit Maximum nahe des sichtbaren Bereichs ($\lambda_{max}$ = 374 - 408 nm). Wie erwartet, ist die Absorption von **7h** im Vergleich zu **7a**, aufgrund des erweiterten $\pi$-Systems, leicht bathochrom verschoben ($\Delta\lambda_{max}$ = 15 nm). Im Falle von **7b** erschwert die komplexe Zusammensetzung von elektronenschiebenden und -ziehenden Substrukturen die Erklärung der einzelnen Banden. Einerseits erscheint die Bande um 374 nm bei niedrigeren Wellenlängen im Vergleich zu den anderen Phenyl-Derivaten, was wahrscheinlich am elektronenziehenden Effekt der Nitro-Gruppe liegt. Jedoch führt eben diese zu zwei weiteren überlagerten Absorptionsbanden bei 504 und ~535 nm. Nitro-Funktionen sind weiterhin dafür bekannt, Fluoreszenzemissionen zu unterdrücken.[38] Während **7a**, **7h** und **7i** gelb-orangene Emissionen zeigen (siehe Publikation 1 im Anhang), fluoresziert keines der hergestellten Nitro-anthracene (**7b-g**).

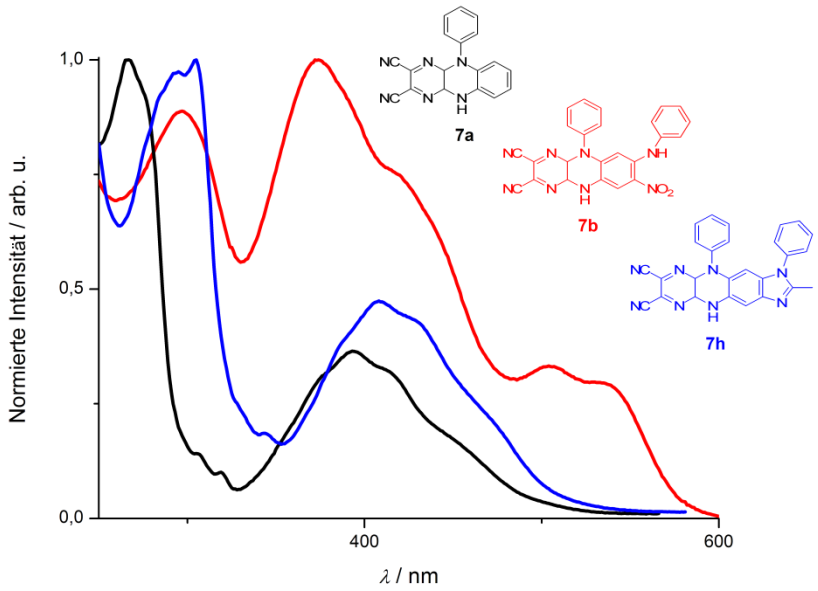


Abbildung 5: UV/Vis-Absorptionsspektren der Phenyl-substituierten Derivate **7a**, **b** und **h** (in $CH_3CN$).

Aufgrund der langwelligen Absorption der Nitro-Derivate, welche für einen Einsatz in OPVs interessant wäre, lag es nahe auch die Lagen der Grenzorbitale mittels Cyclovoltammetrie (CV) zu bestimmen. In Abbildung 6 sind beispielhaft die CV Spektren von **7c** und **7d** dargestellt, welche extern gegen Ferrocen/Ferrocenium ($Fc/Fc^+$) kalibriert wurden. Alle Vertreter besitzen eine reversible Oxidation ($E_{1/2}$ = 0,3 V) sowie je eine irreversible ($E$ = -1,5 V) und eine reversible Reduktion ($E_{1/2}$ = -1,9 V). Die irreversible Reduktion bei -1,5 V führt zur Bildung einer neuen Spezies, welche selbst bei rund -0.8 V redoxaktiv ist.

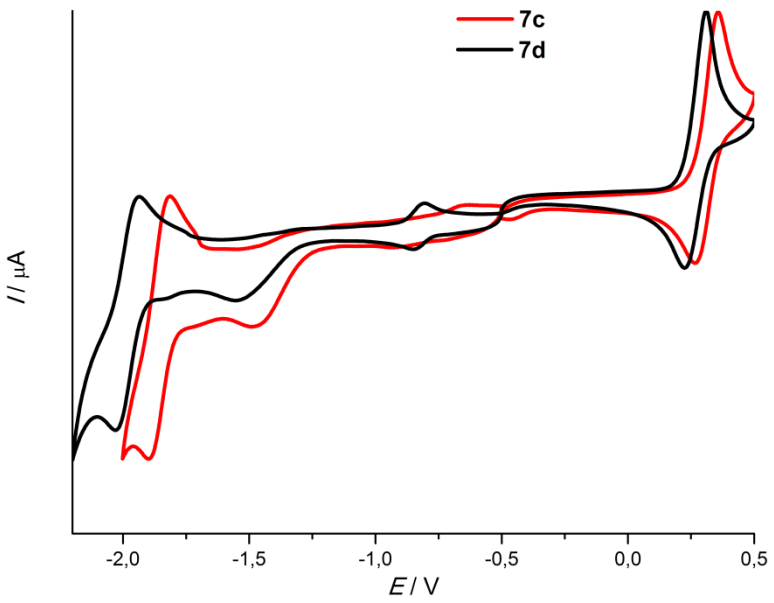


Abbildung 6: Cyclovoltammogramme von **7c** und **d**, extern gegen $Fc/Fc^+$ kalibriert.

Über die sogenannten „onset"-Werte (Wendepunkte des Kurvenverlaufs) der Oxidation und Reduktion werden die Ionisierungsenergie (korreliert mit HOMO – highest occupied molecular orbital) und Elektronenaffinität (korreliert mit LUMO) berechnet.[39] Wie in Tabelle 1 zusammengefasst, weisen die studierten Derivate elektrochemische Bandlücken (Energiedifferenz zwischen HOMO und LUMO) von 1,6 bis 1,8 eV auf. HOMO-Energien von -5,3 eV und LUMO-Energien von -3.7 eV deuten auf einen möglichen ambipolaren Charakter, wie es bei Miaos Diazapentacen der Fall ist ($E_{HOMO}$ = -5,34 und $E_{LUMO}$ = -3,68 eV).[40] Dieses kann als Lochleiter und als Elektronenleiter fungieren. Aufgrund der energetischen Grenzorbitallagen können solche Derivate weder als klassischer Lochleiter, was eine hohe HOMO-Energie voraussetzt, noch als klassischer Elektronenleiter mit niedriger LUMO-Energie aufgefasst werden, sondern werden als ambipolar bezeichnet.

Tabelle 1: Zusammenfassung der elektrochemischen Daten.

| Substanz | **7c** | **7d** | **7e** | **7g** |
|---|---|---|---|---|
| $E_{onset}$ (ox) / V [a] | 0,26 | 0,22 | 0,245 | 0,05 |
| $E_{onset}$ (red) / V [a] | -1,29 | -1,32 | -1,42 | -1,76 |
| $E_{HOMO}$ / eV [b] | -5,36 | -5,32 | -5,35 | -5,15 |
| $E_{LUMO}$ / eV [b] | -3,81 | -3,78 | -3,68 | -3,34 |
| $\Delta E_{CV}$ / eV [c] | 1,55 | 1,54 | 1,67 | 1,81 |

[a] Bestimmt durch CV in 0,1 M Lösung von $TBAPF_6$ in THF (Elektroden: Graphit, Pt, Ag/AgCl) und extern kalibriert gegen $Fc/Fc^+$.
[b] Berechnet über: $E_{HOMO}$ = -[$E_{onset}$ (ox vs. $Fc/Fc^+$)+5.1 eV]; $E_{Lumo}$ = -[$E_{onset}$ (red vs. $Fc/Fc^+$)+5.1 eV].
[c] $\Delta E$ = -($E_{HOMO}$-$E_{LUMO}$).

Es ist uns gelungen, vielversprechende Vertreter der Dihydro-Tetraazaanthracene zu synthetisieren. Dabei entdeckten wir die langwellig absorbierenden Nitro-Derivate (**7b**-**g**), welche einerseits als bis-Elektrophil oder andererseits als Diamin-Baustein für die Synthese von höheren Azaacenen genutzt werden können. Diese „Zwischenstufen" zeigen jedoch selbst interessante Eigenschaften, wie beispielsweise kurze π-π-Abstände im kristallinen Zustand (**7a**), starke Absorptionsbanden (**7b**) und Fluoreszenzemissionen (**7h**). Die Nitro-Anthracene **7c**-**e** besitzen schmale elektrochemische Bandlücken, wobei die Grenzorbitalenergien auf einen ambipolaren Charakter deuten.

## 2.2 Donor-Akzeptor-Farbstoffe durch Verknüpfung von 4-Hexyloxy-thiazolen mit 2,1,3-Benzothiadiazolen

Teile dieses Kapitels sind publiziert in: D. M. Gampe, F. Nöller, V. G. Hänsch, S. Schramm, A. Darsen, S. H. Habenicht, S. Ehrhardt, D. Weiß, H. Görls, R. Beckert, *Tetrahedron* **2016**, *72*, 3232-3239.

Die Synthesemöglichkeiten zu funktionalisierten Azaacenen sind, wie vorstehend angedeutet, noch immer begrenzt. Neben den bis-Elektrophilen ist die Synthese von probaten Diamin-Bausteinen ein Problem.[33] Die unter 2.1 beschriebenen Synthesen stellen einen Weg zu *N*-funktionalisierten Diaminen dar. Im Folgenden soll eine mögliche Route zu *C*-substituierten Aryldiaminen gezeigt werden. Um Substituenten am Kohlenstoff-Gerüst einzuführen, bedarf es meist einer Blockierung der Diamin-Substruktur. Wie in Schema 4 dargestellt, existieren verschiedene Wege, Diamine nach entsprechender Funktionalisierung freizusetzen. In den einfachsten Fällen kann entweder von einer *ortho*-Dinitro-Verbindung (Weg A) oder von *N*-geschützten Aminen (Weg B) ausgegangen werden. Die offensichtlichen Probleme der Verwendung von Dinitro-Aromaten, wie elektronische und sterische Effekte bei der Zweitsubstitution, können umgangen werden indem die Nitrierung zuletzt stattfindet. Jedoch müssen die $NO_2$-Gruppen dann *ortho*-ständig einführbar sein. Die Diamine werden im Anschluss reduktiv freigesetzt und - je nach Reduktionsmethode - *in situ* zyklisiert. *N*-geschützte Diamine (Weg B) haben den Vorteil einer leichten Generierung und Entschützung. Nachteile sind allerdings säure- bzw. basenlabile sowie meist teure Schutzgruppen und eine schlechte Atomökonomie.

Schema 4: Mögliche Synthesewege zu *ortho*-Phenylendiaminen.

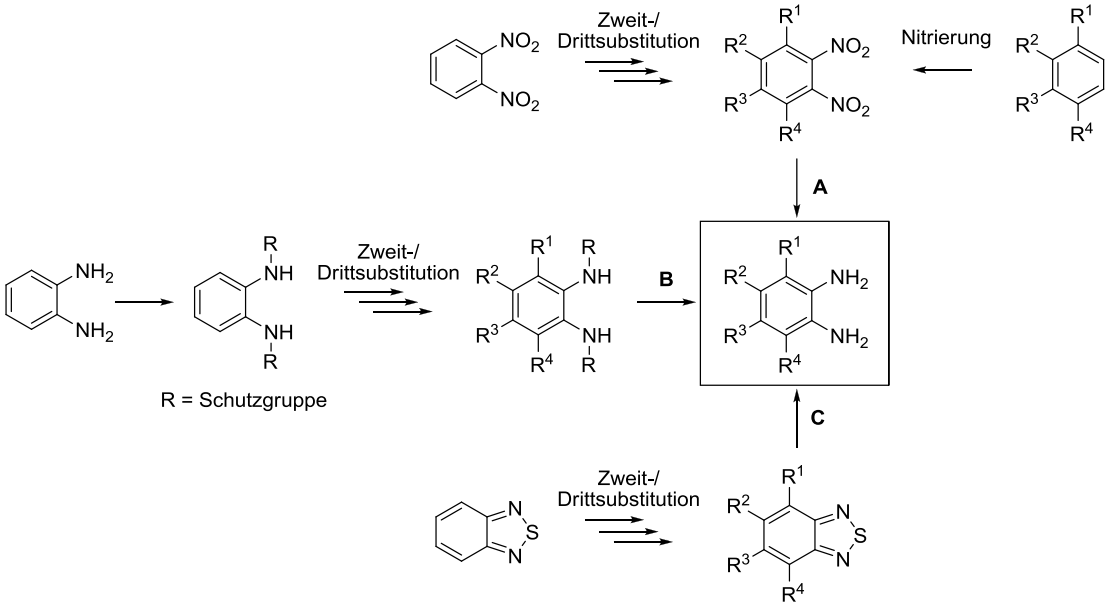

In der letzten Zeit gewann daher eine weitere Funktionalität immer mehr Aufmerksamkeit als Diamin-Vorstufe (Weg C).[41] 2,1,3-Benzothiadiazole (Bt) sind eine gut untersuchte Stoffklasse[42] und werden leicht durch reduktive Entschwefelung in das jeweilige *ortho*-Phenylendiamin überführt.[43] Die Bt-Einheit ist stabil gegenüber allen Reaktionsbedingungen (außer reduktiven) und zeigt sich bei Zweitsubstitutionen deutlich reaktiver als die entsprechenden Dinitro-Verbindungen. Dadurch ist es beispielsweise möglich, Halogene für folgende Kreuzkupplungen oder nukleophile Substitutionen einzuführen, um letztlich hochfunktionalisierte Diamine darzustellen.[44]

Unser Ziel war es die von unserer Gruppe intensiv studierten 4-Alkoxythiazole mit Azaacenen zu verknüpfen.[45] Doch schon die generierten Bt-Vorstufen (siehe Abbildung 7) überzeugten mit überraschenden Eigenschaften. Aufgrund ihrer Elektronenaffinität sind Bt-Einheiten sehr beliebte Elektronenakzeptoren für Donor-Akzeptor (D-A) Moleküle[46] oder Copolymere[47] und die eingeführten 4-Hexyloxythiazole fungieren als gute Elektronendonoren, was von uns erstmalig gezeigt werden konnte. Thiazole wurden sonst als schwache Akzeptoreinheiten[48] oder, im Falle der 4-Hydroxythiazole, als π-konjugierte Brücken in D-A Materialien eingesetzt.[49]

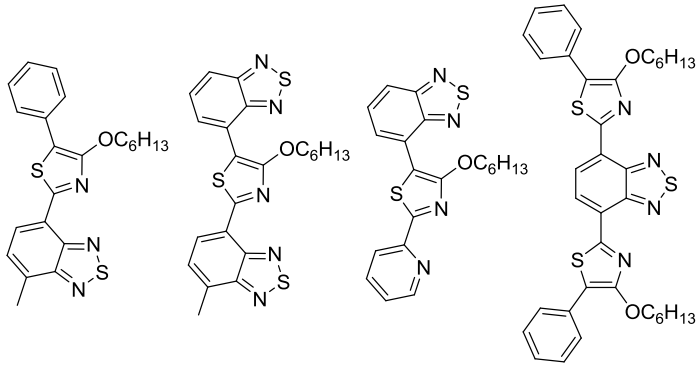


Abbildung 7: Darstellung der Bt-basierten D-A Farbstoffe.

Die Synthese der Zielstrukturen gelang über konsekutive, mehrstufige Reaktionen ausgehend von Bt (**20**) bzw. 4-Methyl-Bt (**19**, siehe Schema 5). Für die geplanten Thiazolsynthesen nach Hantzsch werden ein Carbothioamid (z.B. **16**) und ein *α*-Brom-Arylessigester (z.B. **17**) benötigt.[50] Thioamid **16** wurde synthetisiert über eine Bromierung von **19**. Die anschließende Rosenmund-von-Braun-Reaktion mit Kupfer(I)-cyanid erzeugte ein Carbonitril,[51] welches durch Addition von Schwefelwasserstoff in Thioamid **16** überführbar war. Um Derivat **17** herzustellen, wurde die benzylische Methyl-Gruppe von **19** genutzt. Nach der Bromierung konnte durch nukleophile Substitution ein Nitril erzeugt werden.[52] Die anschließende Hydrolyse im sauren Milieu generierte eine Bt-substituierte Essigsäure, welche nach der Veresterung lediglich in *α*-Position bromiert werden musste. Di-thioamid **18** wurde, wie Thioamid **16**, über eine dreistufige Reaktionssequenz bestehend aus zweifacher Bromierung, Cyanierung und $H_2S$-Addition, ausgehend von **20**, synthetisiert. Die klassische Hantzsch Zyklisierung zwischen den entsprechenden *α*-Brom-Phenylessigestern und Thioamiden und eine finale Veretherung mit Hexyliodid lieferte die Bt-basierten D-A Farbstoffe (detaillierte Darstellung in Publikation 2).

Schema 5: Synthesewege zu den Bt-thiazolen **11** – **14**.

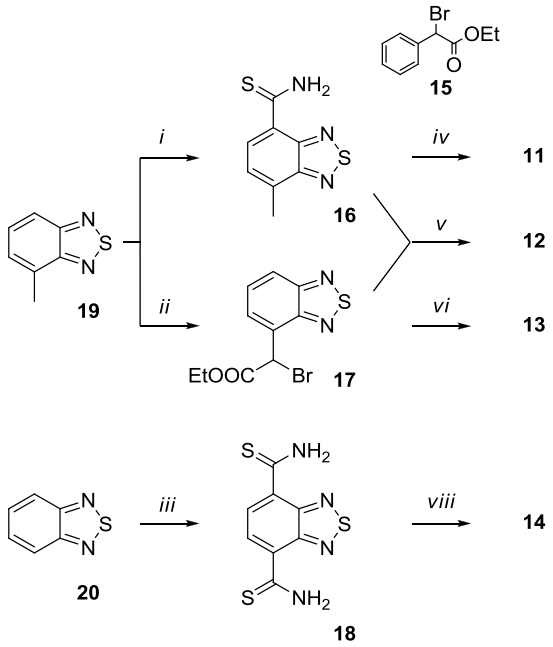


*i*) 1.) $Br_2$, HAc, 62%; 2.) CuCN, NMP, 74%; 3.) $HPS_2(OEt)_2$, EtOH, 84%.
*ii*) 1.) NBS, $C_2Cl_4$, 69%; 2.) KCN, EtOH, 65%; 3.) HCl, 69%; 4.) $SOCl_2$, EtOH, 80%; 5.) NBS, $CCl_4$, 42%.
*iii*) 1.) 2 äqu. $Br_2$, HBr, 87%; 2.) 2 äqu. CuCN, Pyridin, NaI, DMF, 56%; 3.) $HPS_2(OEt)_2$, EtOH, 62%.
*iv*) 1.) Ethyl-2-brom-2-phenylacetat (**15**), NaAc, EtOH, 53%; 2.) I-$C_6H_{13}$, $K_2CO_3$, Aceton, 68%.
*v*) 1.) NaAc, EtOH, 76%; 2.) I-$C_6H_{13}$, $K_2CO_3$, Aceton, 74%.
*vi*) 1.) Pyridin-2-carbothioamid, NaAc, EtOH, 78%; 2.) I-$C_6H_{13}$, $K_2CO_3$, Aceton, 48%.
*vii*) 1.) 2 äqu. **15**, NaAc, EtOH, 42%; 2.) 2 äqu. I-$C_6H_{13}$, $K_2CO_3$, Aceton, 16%.

Wie es für 4-Alkoxythiazole bekannt ist,[53] bilden auch die mit einem Bt-Rest ausgestatteten Vertreter farbige Lösungen mit starken Fluoreszenzerscheinungen, die mittels UV/Vis-Absorptions- und Fluoreszenz-Emissionsspektroskopie (siehe Abbildung 8) untersucht wurden.

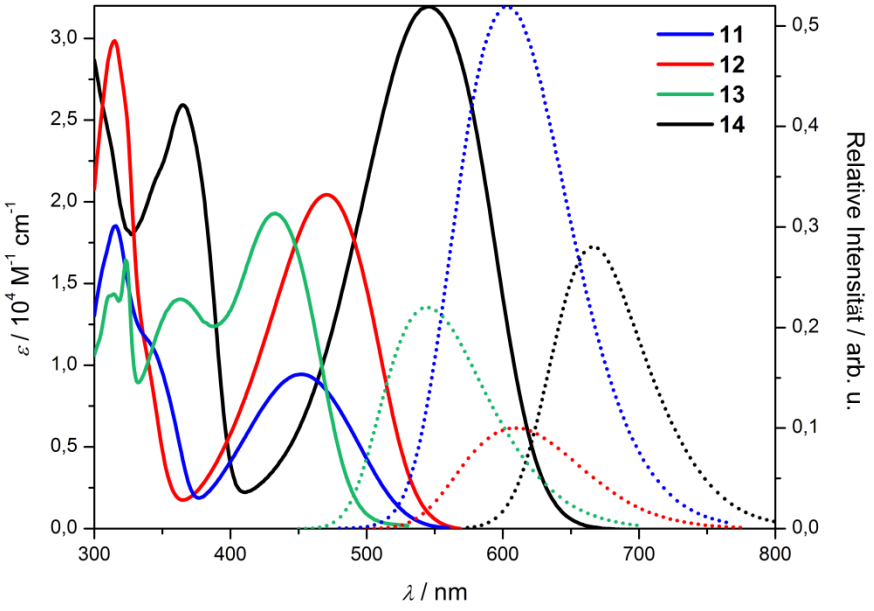


Abbildung 8: Vergleichende Darstellung der UV/Vis-Absorptions- (Linien) und Fluoreszenzemissionsspektren (Punkte) der Bt-Thiazol-Farbstoffe (in THF).

Alle Derivate zeigen eine stark ausgeprägte Bande im UV-Bereich und eine weitere, sehr breite Bande im sichtbaren Teil des Spektrums. Vor allem beim Vergleich der Derivate **11** und **14** wird die Donorstärke der 4-Hexyloxythiazol-Einheit deutlich. Während die maximale Absorption des sichtbaren Lichts von Thiazol **11** bei 450 nm ($\varepsilon$ = 9000 $M^{-1}cm^{-1}$) liegt, ist die von bis-Thiazol **14** um rund 100 nm (≙ 0,47 eV) bathochrom verschoben und mit einem molaren Extinktionskoeffizienten ($\varepsilon$) von 32000 $M^{-1}cm^{-1}$ um den Faktor 3 höher. Die untersuchten Zielstrukturen zeichnen sich weiterhin durch ihre starken Fluoreszenz-Emissionen im gelben bis roten Spektralbereich, mit Quantenausbeuten von bis zu 50% (**11**), aus.

Cyclovoltammetrische Messungen offenbarten die elektrochemische Aktivität der neuartigen Hybridfarbstoffe, welche auf die irreversible Oxidation der Thiazol- und eine reversible Reduktion der Bt-Einheit rückführbar ist. Auf der Grundlage dieser Redoxaktivität ließen sich die Grenzorbitalenergien errechnen (siehe Tabelle 2). Hervorzuheben ist die schmale Bandlücke des Derivats **14**, welche im Bereich von Bt-basierten D-A-D Materialien, ausgestattet mit klassischen Donoren wie Diarylaminen, liegt.[54]

Tabelle 2: Zusammenfassung der photo- und elektrochemischen Daten der Bt-Thiazole.

| Substanz | **11** | **12** | **13** | **14** |
|---|---|---|---|---|
| $\lambda_{Abs}$ / nm [$\varepsilon$ / $10^4 M^{-1}cm^{-1}$] [a] | 316 [1,9]; 452 [0,9] | 315 [3,0]; 470 [2,0] | 323 [1.64]; 363 [1.4]; 433 [1.9] | 365 [2,6]; 545 [3,2] |
| $\lambda_{Em}$ / nm [a] | 602 | 609 | 543 | 667 |
| $\upsilon$ / $cm^{-1}$ [b] | 5510 | 4856 | 4680 | 3556 |
| $\Phi_{FL}$ / % [c] | 52 | 9 | 22 | 28 |
| $E_{HOMO}$ / eV [d] | -5,82 | -5,92 | -5,83 | -5,78 |
| $E_{LUMO}$ / eV [d] | -3,38 | -3,48 | -3,28 | -3,72 |
| $\Delta E_{CV}$ / eV [e] | 2,44 | 2,44 | 2,55 | 2,06 |
| $\Delta E_{opt}$ / eV [f] | 2,35 | 2,28 | 2,52 | 1,97 |

[a] Gemessen in THF.
[b] Relativ zum Maximum der Absorption.
[c] Gemessen in Cyclohexan, relativ zu Rhodamin 6G ($\Phi_{FL}$ = 0.95) und Fluorescein ($\Phi_{FL}$ = 0.91).[55]
[d] Bestimmt durch CV in 0,1 M Lösung von $TBAPF_6$ in THF, extern kalibriert gegen $Fc/Fc^+$ und berechnet über: $E_{HOMO}$ = -[$E_{onset}$ (ox vs. $Fc^+$/Fc)+5.1 eV]; $E_{Lumo}$ = -[$E_{onset}$ (red vs. $Fc^+$/Fc)+5.1 eV].
[e] $\Delta E$ = -($E_{HOMO}$-$E_{LUMO}$).
[f] Kalkuliert über den onset (10%) der Absorption.

Benzothiadiazole sind vielversprechende Vorstufen auf dem Weg zu Azaacenen und ihre außerordentliche Stabilität gegenüber vielen Reaktionstypen konnte erfolgreich untermauert werden. Wir waren weiterhin in der Lage, erstmalig 4-Alkoxythiazole als Elektronendonor in D-A Farbstoffen einzuführen und erhielten Derivate mit aussichtsreichen Eigenschaften für eine Verwendung in optoelektronischen Bauelementen. Besonders D-A-D Derivat **14** überzeugt mit leichter Zugänglichkeit, hoher Absorbanz und einer schmalen Bandlücke.

# 3 Tetraazaanthracene als Elektronenakzeptor

## 3.1 Kombination von Thiazolen mit Tetraazaanthracenen

Teile dieses Kapitels sind publiziert in: D. M. Gampe, S. Schramm, F. Nöller, D. Weiß, H. Görls, P. Naumov, R. Beckert, *Chem. Commun.* **2017**, *53*, 10220-10223.

Es existieren zwei grundlegende Arten, um Licht durch organische Moleküle in Strom umzuwandeln. Zum einen die sogenannte Grätzel-Zelle (DSSC – dye sensitized solar cell), welche einen kovalent an Titandioxid ($TiO_2$) gebundenen Farbstoff nutzt. Zum anderen die heterojunction Solarzelle (meistens: BHJ), welche durch ein Donor- und ein Akzeptormaterial photosensibilisiert wird (siehe Abbildung 9).[56] Bei der DSSC (Abbildung 9A) wird der Farbstoff durch Licht angeregt, überträgt ein Elektron mittels $TiO_2$ auf die Anode (hier: ITO – Indiumzinnoxid) und relaxiert in einen energetisch niedrigeren Zustand. Der oxidierte, kationische Farbstoff wird mittels Triiodid ($I_3^-$) rückreduziert, welches seinerseits über kathodische Reduktion (hier: Platin) aus Iod generiert wird. Im Falle der BHJ (Abbildung 9B) wird durch Sonnenlicht beispielsweise das Donormaterial (hier: P3HT – Poly-3-hexylthiophen) angeregt, welches vereinfacht ein Elektron und ein Loch bildet. An der Grenzfläche zwischen Donor und Akzeptor (hier: PCBM – Phenyl-$C_{61}$-buttersäuremethylester) wird das Elektron auf den Akzeptor (energetisch niedrigeres LUMO) übertragen, während das Loch in der Donorschicht (energetisch höheres HOMO) verbleibt. Die folglich separierten Ladungen diffundieren durch die jeweiligen Schichten zu den Elektroden (hier: ITO, Silber) und es fließt Strom.

Vor allem auf dem Gebiet der BHJ Solarzellen konnten in den letzten Jahren kontinuierlich Fortschritte durch die Aufklärung der Teilprozesse erzielt werden.[57] Meist gelang die stetige Steigerung der Wirkungsgrade bei der Verwendung eines Copolymer-Donors und eines Fulleren-Akzeptors.

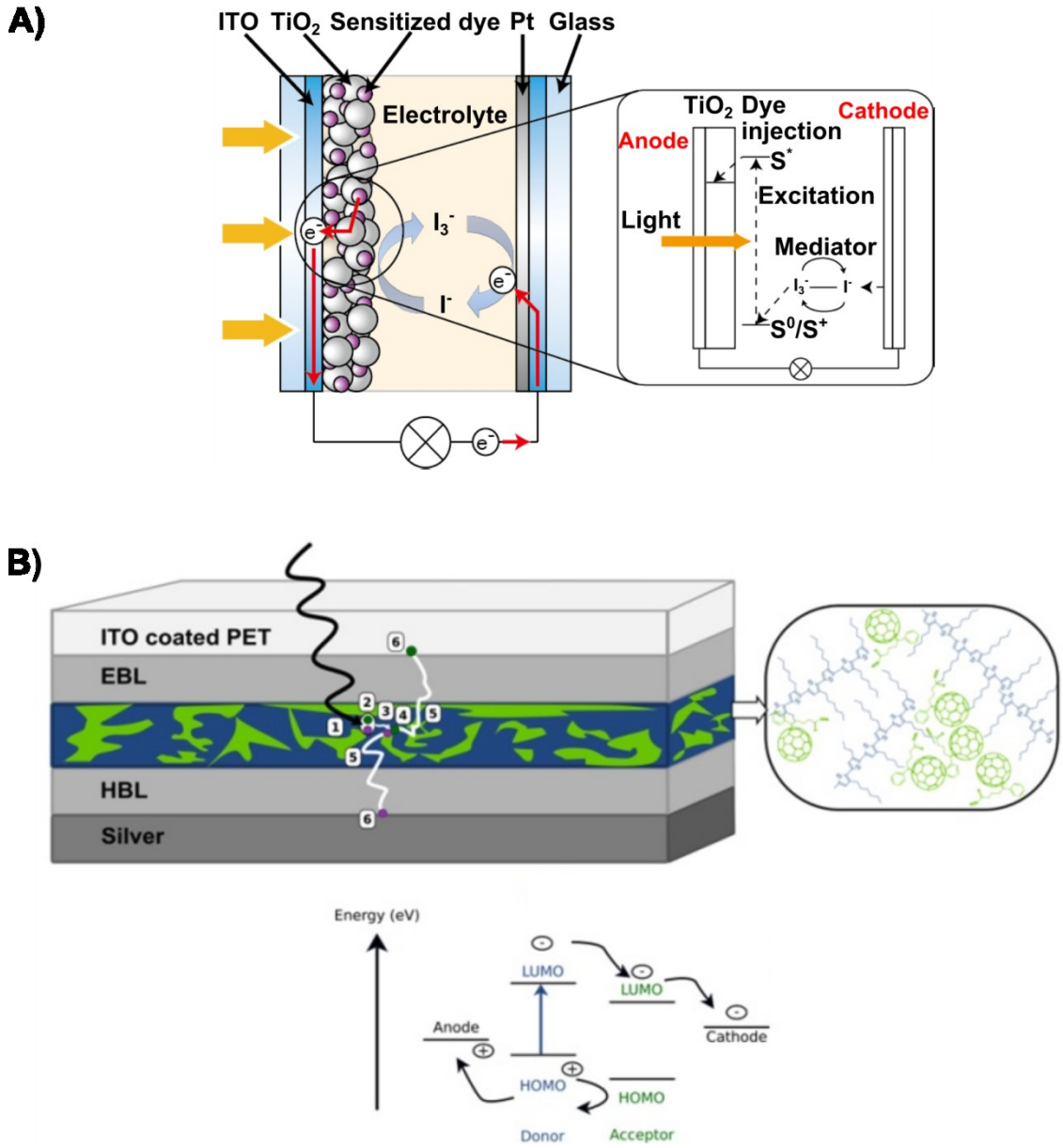


Abbildung 9: A) Darstellung einer Grätzel-Zelle. B) Darstellung einer BHJ-Solarzelle (EBL ist die Elektronensperrschicht und HBL die Lochsperrschicht).[58]

Jedoch scheinen die Nachteile der beteiligten Substanzklassen den Erfolg der BHJ Solarzellen zu begrenzen. Polymere Donoren tragen mit schlechter Reproduzierbarkeit und ihrer Polydispersität zu den Nachteilen der klassischen BHJ bei, während Einzelmolekül-Donoren immer gleiche Eigenschaften und sogar höhere Ladungsträgerbeweglichkeiten aufweisen.[59] Die neuesten Studien von Einzelmolekül-basierten BHJs suggerieren ihre Konkurrenzfähigkeit gegenüber den Polymeren.[60] Auf der anderen Seite wird derzeit intensiv nach alternativen Akzeptormaterialien gesucht, da die kommerziell verwendeten Fulleren-Derivate verschiedene Nachteile, wie schlechte Prozessierbarkeit,[61] schwache Lichtabsorption im sichtbaren/nah-infraroten Bereich,[62] kostenintensive Herstellung[63] und schwierige Modifizierbarkeit aufweisen.[64] Die geforderten Eigenschaften neuartiger Akzeptoren sind demnach sehr breit gefächert. Neben einer Minimierung der anhand der Fullerene aufgeführten Nachteile sollten sich diese durch reversible Elektronenaufnahme

(Reduktion), dreidimensionale Elektronenleitfähigkeit und geringe Reorganisationsenergie (nötige Energie, um nach dem Leitungsprozess in den Grundzustand zurückzugelangen) auszeichnen.

Um die Anforderungen an Elektronendonor- bzw. Akzeptormaterialien zu erfüllen, werden immer häufiger monodisperse, metallfreie Einzelmoleküle des D-A Typs verwendet.[65] Durch die D-A Struktur wird ein Charge-Transfer (CT) Charakter generiert und die Bandlücke verringert, wodurch eine Absorption im nah-infraroten (NIR) Spektralbereich hervorgerufen werden kann.[66] Da das HOMO durch den jeweiligen Donor-Part definiert wird, das LUMO hingegen auf der Akzeptoreinheit liegt, ist es weiterhin möglich, die energetischen Lagen durch die Art der Bausteine und geschicktes Moleküldesign festzulegen.

Wie unter 2.2 beschrieben, besitzen 4-Alkoxythiazole hervorragende photochemische Eigenschaften und können außerdem als Elektronendonoren in D-A Farbstoffen eingesetzt werden. Um die für eine Anwendung als Akzeptormaterial erforderlichen, tiefen LUMO-Lagen[67] zu generieren, sind Tetraazaanthracen Einheiten prädestiniert[68] und wurden mit den Thiazolen kombiniert (siehe Abbildung 10). Ausgangsmaterial bildeten die im vorigen Abschnitt beschriebenen Benzothiadiazole (**11**-**14**), welche durch eine reduktive Entschwefelung in die entsprechenden *o*-Phenylendiamine überführbar waren (siehe Schema 6). Nach erfolglosen Versuchen mittels Zinkstaub bzw. Zinndichlorid und Salzsäure[69] gelang die Reduktion zur Diamin Substruktur mit Hilfe von Natriumborhydrid und katalytischen Mengen Cobalt(II)chlorid. [70] Aufgrund der bekannten Instabilität solcher *ortho*-Phenylendiamine wurden diese nach einer Extraktion sofort mit Dichlor-dicyano-pyrazin (**9**) umgesetzt. Der abschließende Reaktionsschritt zu den D-A Derivaten **21** - **24** (die Oxidation der Dihydro-tetraazaanthracene **25** – **28**) glückte mittels 2,3-Dichlor-5,6-dicyano-benzochinon (DDQ).

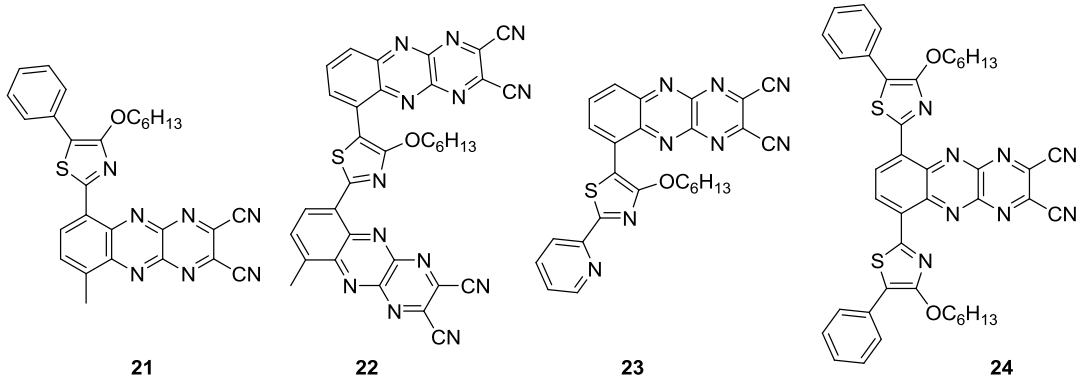


Abbildung 10: Zielstrukturen durch die Kombination von Thiazolen mit Azaacenen.

Schema 6: Syntheseweg der Tetraazaanthracen-basierten Donor-Akzeptor-Farbstoffe.

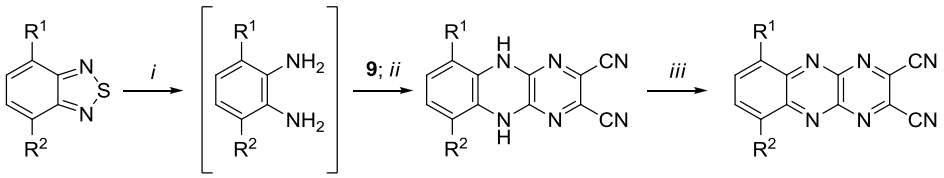


**11**: $R^1$ = phenyl-thiazol-2-yl; $R^2$ = Methyl: **25** **21**
**13**: $R^1$ = pyridin-2-yl-thiazol-5-yl; $R^2$ = H: **27** **23**
**14**: $R^1$ = phenyl-thiazol-2-yl; $R^2$ = phenyl-thiazol-2-yl: **28** **24**

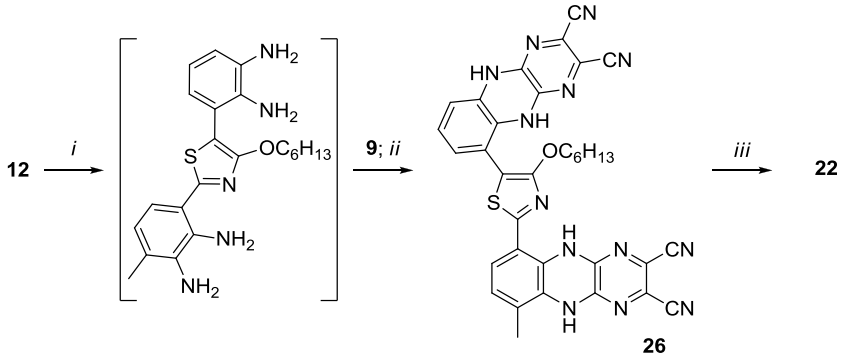


*i*) 9 äqu. $NaBH_4$, $CoCl_2$ (kat.), EtOH/THF 3:1, $N_2$; quant.
*ii*) 2,3-Dichlor-5,6-dicyanopyrazin (**9**), Dioxan, $N_2$; **25**: 54%; **26**: 32%; **27**: 58%; **28**: 33%.
*iii*) DDQ, THF, $N_2$; **21**: 56%; **22**: 91%; **23**: 57%; **24**: 90%.

Ausgesprochen breite CT-Banden über den gesamten sichtbaren bis in den NIR Bereich sind in den UV/Vis-Spektren zu erkennen (siehe Abbildung 11). Die Derivate **21** - **23** absorbieren Licht bis 900 nm, wodurch sich optische Bandlücken von rund 1,4 eV errechnen lassen. D-A-D Farbstoff **24** zeigt eine sehr breite CT-Bande von 550 bis 1100 nm mit einem Maximum bei 839 nm ($\varepsilon$ = 6350 $M^{-1}cm^{-1}$) und einer bemerkenswert schmalen optischen Bandlücke von $\Delta E_{opt}$ = 1,1 eV.

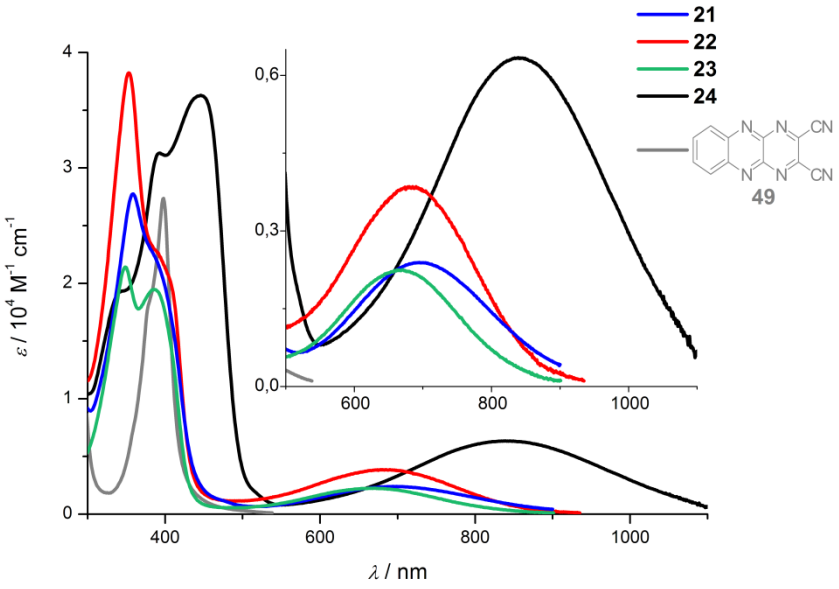


Abbildung 11: UV/Vis-Absorptionsspektren der Thiazolo-Anthracene (**21**-**24**) und vergleichend, das des unsubstituierten Tetraazaanthracens (**49**, synthetisiert nach Referenz [19]), gemessen in THF.

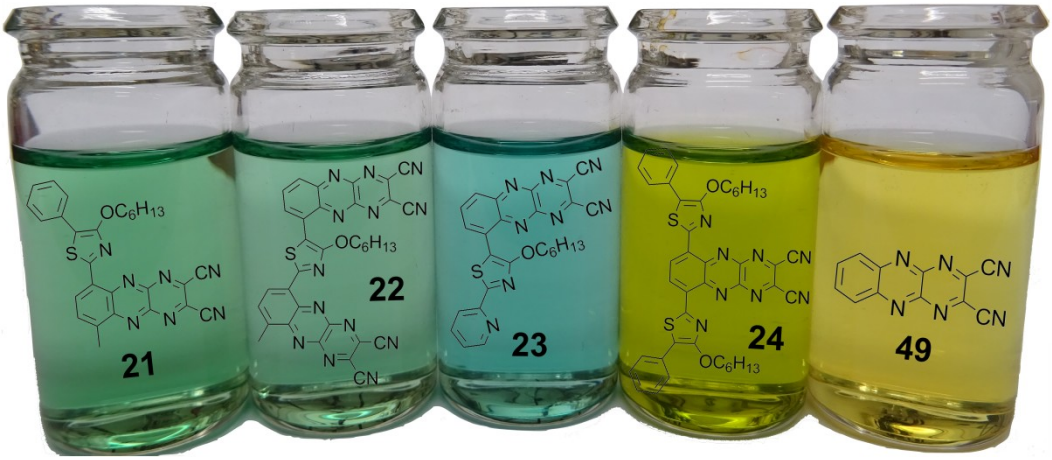


Abbildung 12: Fotografische Darstellung der Thiazolo-Anthracene **21**-**24** und des unsubstituierten Tetraazaanthracens **49**, gelöst in THF (~$10^{-5}$ M).

Abbildung 12 stellt den visualisierten Beweis für die guten Donoreigenschaften der Thiazol-Substrukturen dar. Während die Lösung des literaturbekannten, unsubstituierten Tetraazaanthracens **49** gelb erscheint, lösen sich die Thiazol-substituierten Derivate unter Ausbildung einer türkis bis gelb-schwarzen Farbe.

Aus den zwei reversiblen Reduktionsschritten innerhalb der Cyclovoltammogramme (siehe Publikation 3) kann die Bildung von stabilen Radikalanionen und Dianionen geschlussfolgert werden.[71] Weiterhin finden diese bei hohen Reduktionspotentialen (**22**, **23**: ~0 V / **24**: 0,16 V gegen SCE saturated calomel electrode) statt, was nicht nur elektrochemische Stabilität gegenüber Wasser und Sauerstoff garantiert, sondern auch auf sehr niedrige LUMO Lagen hindeutet.[72] Mit Energien von -4,6 eV (**22**, **23**) werden die Lagen der kommerziellen Fullerene ($PC_{61}BM$: -3,8 / $PC_{71}BM$: -4,3 eV) deutlich unterschritten und bis-Thiazol **24** stellt gar einen Spitzenreiter mit einem Wert von -4.8 eV dar.[73] Unserem Wissen nach weisen bisher lediglich perfluorierte Tetracyanochinodimethane solch tiefe LUMO-Lagen auf.[74]

Wir waren in der Lage, den Tetraazaanthracen-Baustein in D-A Systemen zu etablieren. Dadurch ergeben sich sehr niedrige LUMO-Lagen sowie Charge-Transfer-Banden bis in den NIR-Bereich, was einen Einsatz als Akzeptormaterial in BHJ Solarzellen nahelegt.

## 3.2 Gemischte Chromophore: Diarylamine, 4-Alkoxythiazole und verschiedene Akzeptorblöcke

Teile dieses Kapitels sind publiziert in: D. M. Gampe, V. G. Hänsch, S. Schramm, R. Menzel, D. Weiß and R. Beckert, *Eur. J. Org. Chem.* **2017**, *2017*, 1369-1379.

Der Donor-Charakter der 4-Alkoxythiazole sollte durch die Integration von Diarylaminen weiterhin verstärkt werden. Damit geht eine stärkere Separation der Grenzorbitale einher, was zu schmaleren Bandlücken führt. Diarylamine sind nicht nur exzellente Elektronendonoren, sie zeichnen sich außerdem durch ihre nicht-linearen optischen und lochleitenden Eigenschaften aus und sind weiterhin in der Lage, stabile Radikale zu bilden.[75] Teil dieses Projekts war konsequenterweise die Verwendung von drei verschiedenen cyclischen Diarylaminen als Elektronendonoren: Carbazol, Phenoxazin und Phenothiazin.

Als Akzeptoreinheit sollten weiterhin drei verschiedene Substanzklassen untersucht und miteinander verglichen werden. Pyrazin als schwacher Elektronenakzeptor, Benzothiadiazol als starke und etablierte Akzeptoreinheit und Tetraazaanthracen als neuartiger Baustein in D-A Molekülen.[76] Tetraazaanthracene sind, wie in 3.1 dargestellt, durch ihre sehr tief liegenden LUMOs bekannte Vertreter elektronenarmer Materialien und wurden schon erfolgreich als n-Typ Halbleiter in OFETs eingesetzt.[77] Außerdem sind sie bekannt für hohe Stabilität, interessante photochemische Eigenschaften und ihre Vielseitigkeit (siehe Kapitel 2.1). Gepaart mit den elektronenschiebenden Eigenschaften der Diarylamin-substituierten Thiazole sollten D-A Typ Moleküle mit tief liegenden LUMOs und sehr engen Bandlücken generiert werden. Aufgrund einstellbarer Orbitalenergien und einer kostengünstigeren Herstellung werden derartige Elektronenakzeptoren intensiv als Fullerenersatz getestet.[78] Aktuelle Ergebnisse zeigen, dass die Fulleren-freien BHJ Solarzellen in ihrer Effizienz bereits mit den Fulleren-basierten vergleichbar sind.[64]

Die Kombination der eben beschriebenen Donor- und Akzeptoreinheiten liefert neun verschiedene Derivate der in Abbildung 13 dargestellten D-A Struktur.

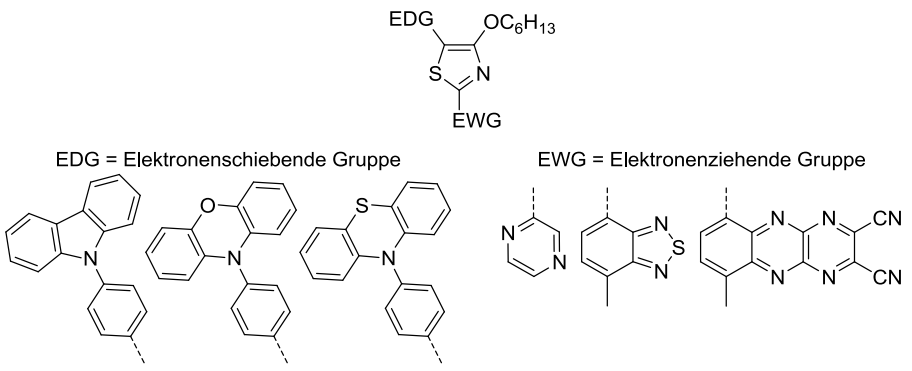


Abbildung 13: Allgemeines Strukturmotiv der D-A Derivate und Darstellung der verwendeten Bausteine.

Die zentrale Einheit bildet das 4-Alkoxythiazol, welches die an 5-Position substituierte, elektronenschiebenden Gruppe (Donor) mit der in 2-Position angebrachten, elektronenziehenden (Akzeptor) verbinden soll. Dieses Substituentenmuster hat einen starken CT Charakter zur Folge.[79]

Wie in Schema 7 abgebildet, begann die Synthese mit Hantzsch Zyklisierungen zwischen *para*-Brom-substituiertem Phenylessigester **30** und dem entsprechenden Thioamid (**16** oder **29**). Danach wurden Williamson-Ethersynthesen mit Hexyliodid durchgeführt, um die gut löslichen, kupplungsfähigen 4-Hexyloxythiazole **31A** und **B** in guten Ausbeuten zu erhalten. Über Buchwald-Hartwig-Kreuzkupplungen war es möglich, die Diarylamin-modifizierten Pyrazine (**PyrC**, **PyrO**, **PyrS**) und Piazthiole (**BtC**, **BtO**, **BtS**) zu generieren. Buchwald-Hartwig-Aminierungen sind Palladium-katalysierte Reaktionen zur C-N-Bindungsknüpfung aus Arylhalogeniden und primären, bzw. sekundären Aminen.[80] Über starke Basen und phosphororganische Liganden ist diese Art der Kreuzkupplung steuerbar.[81]

Schema 7: Synthese der Thiazol-verbrückten D-A Systeme.

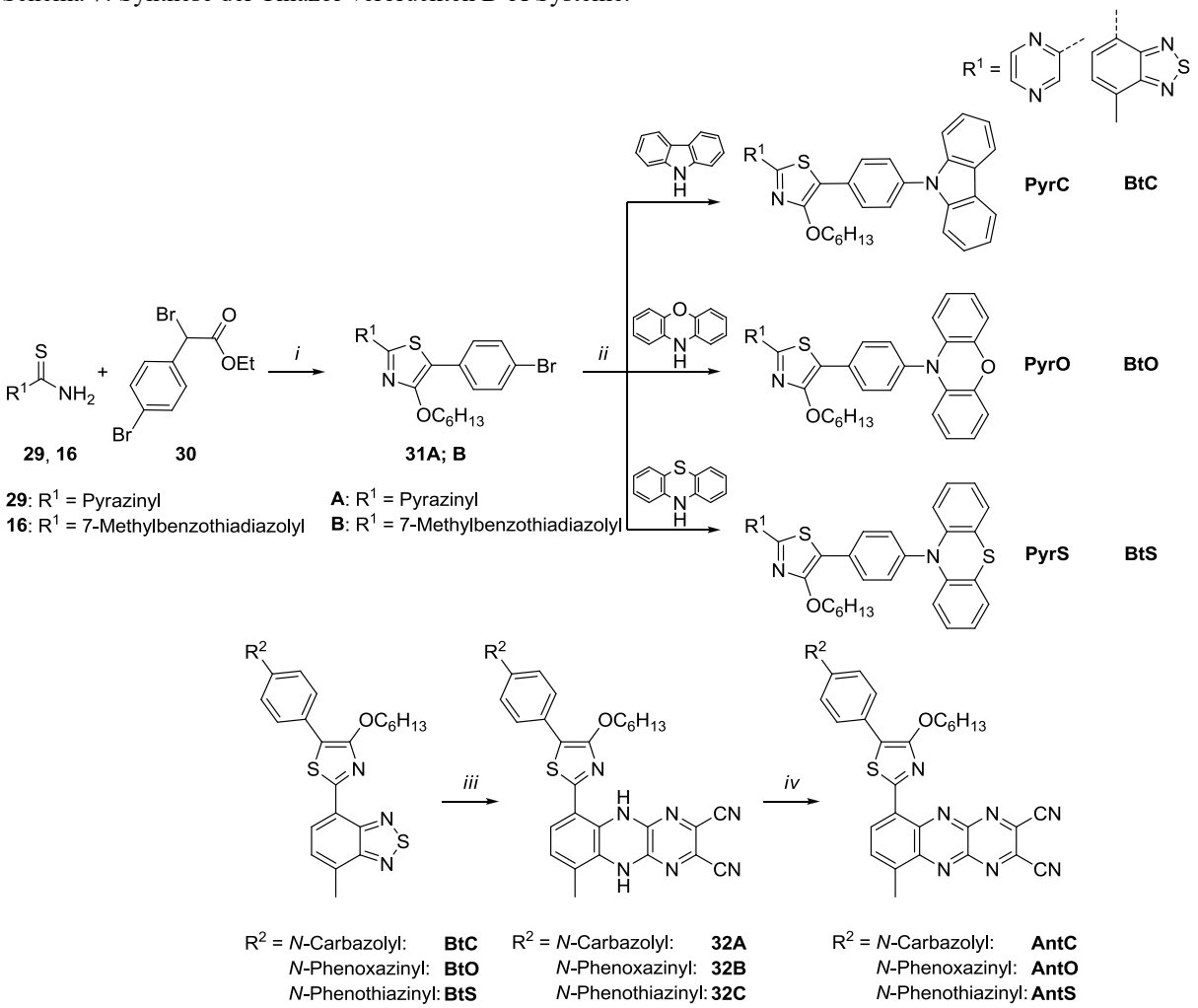


*i*) **31A**: 1.) **29**, NaAc, EtOH, 25%; 2.) I-$C_6H_{13}$, $K_2CO_3$, Aceton, 80%;
**31B**: 1.) **16**, NaAc, EtOH, 87%; 2.) I-$C_6H_{13}$, $K_2CO_3$, Aceton, 72%.
*ii*) $Pd(dba)_2$, SPhos, KO$^t$Bu, Toluen, $N_2$, **PyrC**: 53%; **PyrO**: 46%; **PyrS**: 35%; **BtC**: 83%; **BtO**: 95%; **BtS**: 80%.
*iii*) 1.) $NaBH_4$, $CoCl_2$ (cat.), EtOH/THF, $N_2$, quant.; 2.) **9**, dioxane, $N_2$, **32A**: 54%; **32B**: 30%; **32C**: 45%.
*iv*) DDQ, THF, $N_2$, **AntC**: 53%; **AntO**: 57%; **AntS**: 58%.

Die Darstellung der drei Bt-Derivate beweist dadurch erneut die Robustheit und Vielseitigkeit der Bt-Einheit, da sie stabil gegenüber starken Basen wie KO$^t$Bu ist und Pd-katalysierte Kreuzkupplungen toleriert. Die Freisetzung der *ortho*-Diamin Substruktur gelang, wie bereits in Schema 6 gezeigt, mittels Natriumborhydrid. Anschließende Zyklisierungen mit Pyrazin **9** erzeugten die Dihydro-Tetraazaanthracene (**32A-C**), welche durch Oxidation mit Hilfe von DDQ in die Tetraazaanthracene **AntC**, **AntO** und **AntS** überführbar waren.

Aufgrund der photo- und elektrochemischen Eigenschaften können Rückschlüsse zu Donor- und Akzeptorstärke gezogen werden. Deshalb war es notwendig, alle Derivate per UV/Vis-Absorptions- und Fluoreszenzspektroskopie sowie Cyclovoltammetrie zu charakterisieren (siehe Abbildung 14). Abhängig von der jeweiligen Akzeptorstärke verschiebt sich die Absorption bathochrom um ca. 50 nm (≙ 0,4 eV) von Pyrazin zu Bt und um weitere 250 nm (≙ 0,95 eV) im Falle der Anthracene (siehe Tabelle 3). Dadurch werden die optischen Bandlücken ($\Delta E_{opt}$) von 2,7 (**PyrX**) zu 2,3 (**BtX**) bzw. 1,3 eV (**AntX**) verringert. Während die Pyrazine (**PyrX**) und Piazthiole (**BtX**) mit moderaten bis guten Fluoreszenzquantenausbeuten ihrer grünen bzw. orangenen Emission aufwarten, zeigen die Anthracene (**AntX**) keine messbare Fluoreszenzemission bis 900 nm.

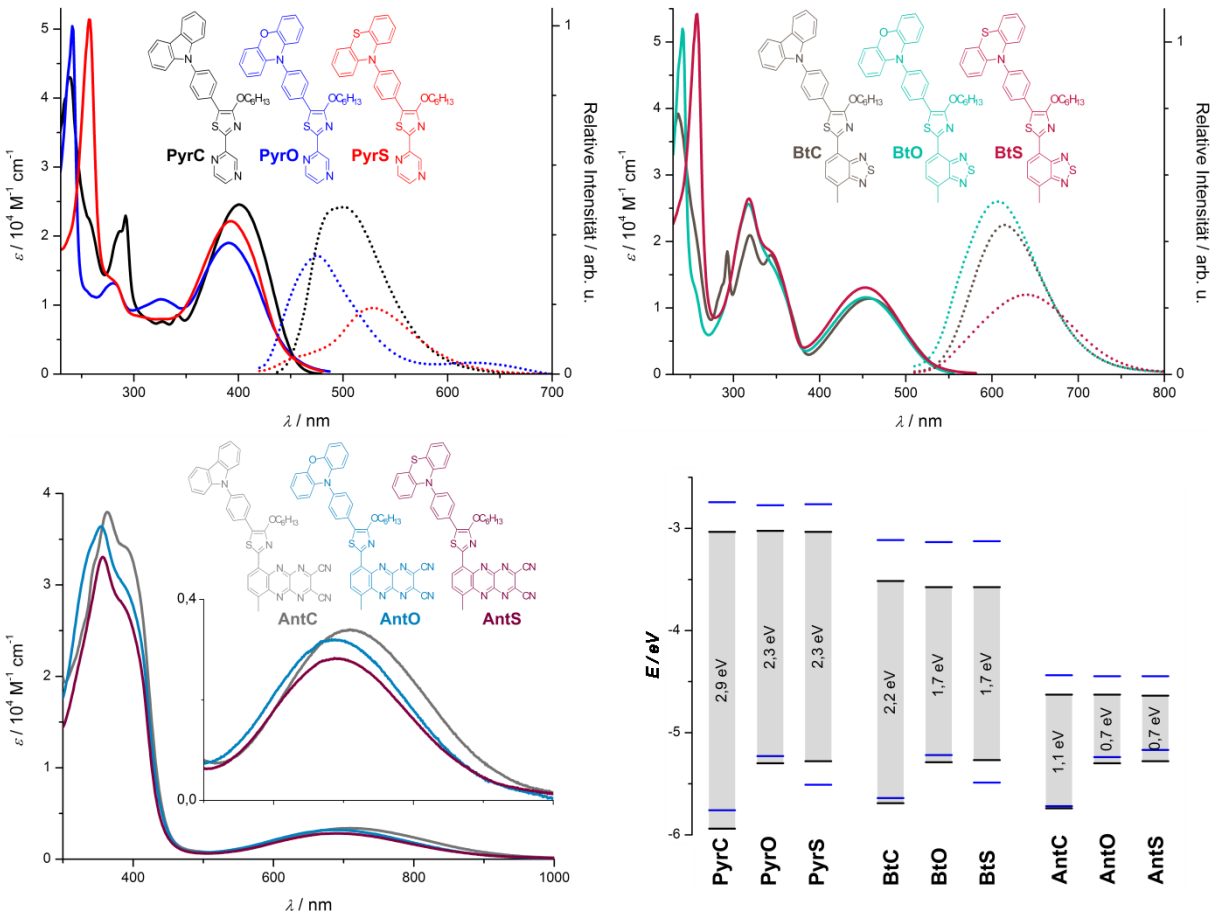


Abbildung 14: UV/Vis-Absorptions- (Linien) und Fluoreszenzspektren (der fluoreszierenden Vertreter; Punkte) der D-A Thiazole (in THF). Unten rechts: Grafische Darstellung der elektrochemisch (schwarz) und theoretisch (blau) bestimmten Grenzorbitalenergien.

Die Grenzorbitalenergien (Abbildung 14) ließen sich über die Redoxpotentiale aus cyclovoltammetrischen Messungen bestimmen (siehe Publikation 4). Zunächst kann festgestellt werden, dass die HOMO-Energie lediglich von der Art des Diarylamins abhängt und gänzlich unbeeinflusst vom jeweiligen Akzeptor ist. Umgekehrt hat die Diarylamin Einheit keinen Einfluss auf das LUMO, da dieses vom Akzeptor definiert wird. Carbazole besitzen nicht die für Diarylamine übliche reversible Oxidation,[85] wodurch die HOMO-Energien im Vergleich zu den anderen Diarylaminen um 0,4 eV herabgesetzt sind. Dies wird auch bei Betrachtung der molekularen Verteilung der HOMOs in Abbildung 15 ersichtlich. Während die HOMOs der Carbazole (**PyrC**, **BtC**, **AntC**) über das gesamte System verteilt sind, liegen die der Phenoxazine und Phenothiazine ausschließlich auf der Diarylamin-Einheit. Drastische Änderungen werden jedoch beim Vergleich der untersuchten Akzeptorblöcke deutlich. Die Energien der LUMOs sinken mit zunehmender Akzeptorstärke von Pyrazin (-3,1 eV) über Bt (-3,7 eV) zu Tetraazaanthracen (-4,7 eV). Bei **AntO** und **AntS** führt die strikte räumliche Trennung der Grenzorbitale (siehe Abbildung 15) zu einem wirksamen CT, wodurch sehr schmale elektrochemische Bandlücken von 0,65 eV generiert werden konnten. Auffällig wirkt der Vergleich der optischen mit den elektrochemischen Bandlücken (siehe Tabelle 3). Überraschenderweise sind die optischen Bandlücken aus der Absorptionsspektroskopie deutlich höher als die elektrochemisch ermittelten. Hinsichtlich der Widerstände und Diffusionsabhängigkeit bei der Cyclovoltammetrie verhält es sich im Normalfall genau umgekehrt ($\Delta E_{opt} < \Delta E_{CV}$).[86] Durch zwei entgegengesetzte Betrachtungsweisen kann dieser Fakt allerdings erklärt werden. Einerseits führt die Torsion der Moleküle in Lösung (sichtbar in Abbildung 15) zu einer ineffektiven Konjugation des π-Systems, die Diarylamin-Ebene steht nahezu senkrecht zur Thiazol-Ebene, was die optischen Lücken erhöht. Bei der CV werden andererseits die Substrukturen infolge der gut separierten Grenzorbitale einzeln betrachtet, weshalb die Torsion keine Rolle spielt.

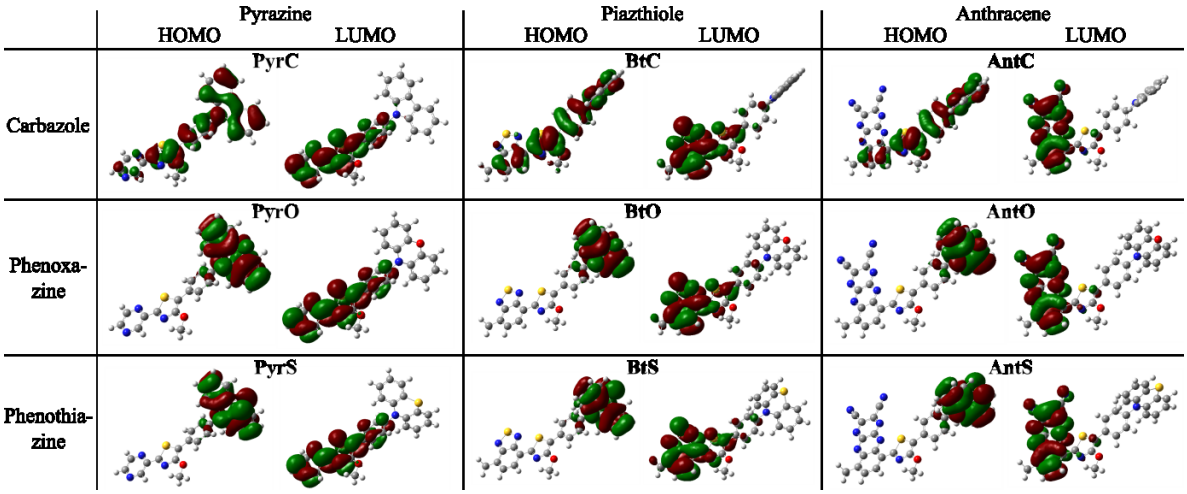


Abbildung 15: Verteilung der Grenzorbitale aller untersuchten Derivate.

Zur Optimierung der Grundzustandsgeometrien diente eine initiale systematische Konformerensuche mittels Merck molecular force field,[82] gefolgt von einer Optimierung mit anschließender Frequenzberechnung zur Validierung des lokalen Minimums mit Hilfe von CAM-B3LYP/6-31+G(d,p)48,[83] implementiert wie in Gaussian 09.[84] HOMO und LUMO Energien wurden über B3LYP/6-31+G(d,p)48 basierend auf den erhaltenen Grundzustandsgeometrien berechnet.

Tabelle 3: Zusammenfassung der photo- und elektrochemischen Daten der Phenothiazine.

| Substanz | **PyrS** | **BtS** | **AntS** |
|---|---|---|---|
| $\lambda_{Abs}$ / nm [$\varepsilon$ / $10^4$ $M^{-1}cm^{-1}$] [a] | 393 [4,35]; 257 [4,71] | 453 [4,12]; 318 [4,42]; 258 [4,73] | 694 [3,45]; 357 [4,52] |
| $\lambda_{Em}$ / nm [a] | 530 | 641 | / |
| $\upsilon$ / $cm^{-1}$ [b] | 6056 | 6475 | / |
| $\Phi_{FL}$ / % [c] | 19 | 24 | / |
| $E_{HOMO}$ / eV [d] | -5,38 | -5,35 | -5,38 |
| $E_{LUMO}$ / eV [d] | -3,12 | -3,66 | -4,73 |
| $\Delta E_{CV}$ / eV [e] | 2,26 | 1,69 | 0,65 |
| $\Delta E_{opt}$ / eV [f] | 2,73 | 2,32 | 1,33 |

[a] Gemessen in THF.
[b] Relativ zum Maximum der Absorption.
[c] Gemessen in Cyclohexan, relativ zu Chininsulfat ($\Phi_{FL}$ = 0.53) und Fluoreszein ($\Phi_{FL}$ = 0.91).
[d] Bestimmt durch CV in 0,1 M Lösung von $TBAPF_6$ in THF und extern kalibriert gegen $Fc/Fc^+$ und berechnet über: $E_{HOMO}$ = -[$E_{onset}$ (ox vs. $Fc^+$/Fc)+5.1 eV]; $E_{Lumo}$ = -[$E_{onset}$ (red vs. $Fc^+$/Fc)+5.1 eV].
[e] $\Delta E$ = -($E_{HOMO}$-$E_{LUMO}$).
[f] Kalkuliert über den onset (10%) der Absorption.

Über Buchwald-Hartwig Kreuzkupplungen waren wir in der Lage, Diarylamine mit Thiazolen zu verknüpfen. Weiterhin konnten drei verschiedene Akzeptorstrukturen integriert und vergleichend untersucht werden. Jede Substruktur brachte die erhofften Eigenschaften in die Zielmoleküle ein. Während sich die Pyrazine (**PyrX**) und Piazthiole (**BtX**) als gute Fluorophore erwiesen, zeigten die Anthracene (**AntX**), verbunden mit schmalen Bandlücken, Absorptionsbanden bis in den NIR-Bereich. Durch geschickte Wahl des Diarylamin-Donors ist es schlussendlich möglich, die Eigenschaften genau abzustimmen. Carbazole führen zu niedrigen HOMO-Lagen und höheren Quantenausbeuten, der im Vergleich hypsochrom verschobenen Fluoreszenz. Durch Substitution mit Phenoxazin wird die HOMO-Energie angehoben und die Derivate besitzen gute Fluoreszenzquantenausbeuten. Die Integration von Phenothiazin mündet in einer bathochromen Verschiebung der Fluoreszenz und einer strikten räumlichen Trennung von HOMO und LUMO.

# 4 Fluorubine

## 4.1 Einleitung

Die erste Erwähnung des Fluorubin Grundkörpers (**6**, siehe Abbildung 2) geschah 1903 durch Hinsberg und Schwantes. Neben der schlechten Löslichkeit wurde hauptsächlich auf die starke grüne Fluoreszenz in alkalischen Lösungen und deren bathochromer shift (gelb - rot) in Säuren als herausstechende Eigenschaft verwiesen.[16] Sowohl die schlechte Löslichkeit als auch die schwierige Isolierung aufgrund vieler, ebenfalls schwer-löslicher Nebenprodukte war anscheinend Hauptgrund dafür, dass diese Stoffklasse erst nach längerer Zeit wieder in den Fokus der Wissenschaft geriet. Nachdem es Akimoto 1955 erstmals gelang, Fluorubin (**6**) spektroskopisch zu charakterisieren,[87] wurden viele Patentschriften zur Herstellung und Applikation von dessen Derivaten (**33**, siehe Abbildung 16) veröffentlicht.[88] Nach der Beschreibung der ersten kationischen Derivate durch die Arbeitsgruppe um Prof. Beckert (siehe Schema 2B, unter 2.1), entwickelten sie einen unabhängigen Syntheseweg zu weiteren Substitutionsmustern, woraus das erste zwitterionische Fluorubin resultierte (**34B**).[89] Die Stabilität dieser Derivate, verbunden mit hohen Extinktionskoeffizienten (bis zu $12\times10^4$ $M^{-1}$ $cm^{-1}$) und Quantenausbeuten bis zu 99% macht sie interessant für Anwendungen in OLEDs oder OPVs. Zudem kann die Feinabstimmung der Eigenschaften leicht durch die Änderung des pH-Wertes geschehen.

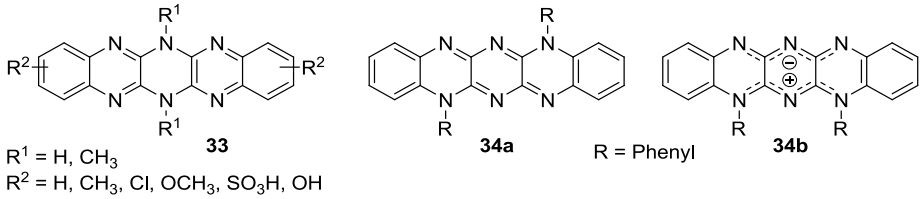


Abbildung 16: Strukturen der patentierten (**33**) und der von Fleischhauer (**34**) entwickelten Fluorubin-Derivate.

Ein moderner Ansatz zum Aufbau höherer Azaacene ist die nukleophile Substitution von vicinalen Dinitril-Vorstufen durch Diamine, wie von Richards *et al.* beschrieben (siehe Schema 8).[37] Die Arbeitsgruppe um Miao bediente sich dieser Syntheseroute um ihre „stark elektronenarmen" Hexaazapentacene aufzubauen und deren Redoxgleichgewicht mit ihren Dihydro-Formen (Fluorubinen) zu untersuchen.[90] Beide Arbeitsgruppen nutzten die oxidierten, gegenüber Nukleophilen hochreaktiven Azaacen-dinitrile als Edukte.

Schema 8: Darstellung der von Richards *et al.* entwickelten Substitution von Dinitrilen durch Diamine.

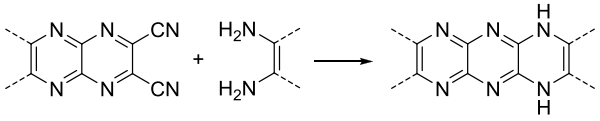

## 4.2 *N*-Phenylfluorubin

Teile dieses Kapitels sind publiziert in: D. M. Gampe, S. Schramm, M. Kaufmann, H. Görls, R. Beckert, *New J. Chem.* **2016**, *40*, 10100-10107.

Wir waren interessiert an den Dihydro-Azapentacenen, welche im Gegensatz zu ihren oxidierten Pendants stabiler und stärkere Fluorophore sind.[25c] Weiterhin war es kürzlich gelungen, Dihydro-Azapentacene als halbleitendes Material in OFETs einzusetzen,[91] sodass diese Eigenschaft nicht länger allein den oxidierten Azaacenen vorbehalten ist. Konsequenterweise nutzten wir 5-Phenyl-5,10-dihydro-[1,4,5,10]-tetraazaanthracen **7a** (siehe Schema 9), welches eine fixierte Dihydro-Form besitzt, für die folgende Dinitril-Substitution mit **36**. *N*-Phenylfluorubin **35** ist demnach erhältlich über zwei einfache Zyklisierungsschritte, ausgehend von günstigen Edukten, besitzt eine Reihe interessanter Eigenschaften, welche nachfolgend vorgestellt werden und stellte das erste unsymmetrische, *N*-substituierte Fluorubin dar.

Über den von uns optimierten Syntheseweg ($Na_2CO_3$, DMA) war es erstmals gelungen, ein Dihydro-Azaacen in einer nukleophilen Reaktion mit Ausbeuten von 14% umzusetzen. Im Gegensatz zu den literaturbeschriebenen Umsetzungen ist **7a** unreaktiv gegenüber Nukleophilen, da durch die Dihydro-Form Elektronendichte auf die zu substituierenden Kohlenstoff-Bindungen transferiert wird. Dies führt letztlich zur Notwendigkeit von sehr harschen Reaktionsbedingungen und langen Reaktionszeiten (siedendes DMA, >72 h). Die finale Oxidation von Tetrahydro-Hexaazapentacen **35a** zu **35** findet augenblicklich bei Kontakt mit Luftsauerstoff statt. Aufwendig ausgearbeitete Isolierungsprozeduren führten zur Möglichkeit, Fluorubin **35** auch aus größeren Reaktionsansätzen (getestet bis zu 10 g von **7a**) in reiner Form isolieren zu können.

Einige Arbeitsgruppen beschrieben die starke pH-Sensitivität der Dihydro-Azaacene, jedoch quantifizierten sie, wenn überhaupt, lediglich die Änderungen der optischen Eigenschaften.[92] Mittels UV/Vis-Absorptionstitration ermittelten wir zunächst die Umschlagspunkte, welche in Schema 10 dargestellt sind. Um die einzelnen Spezies zu untersuchen war es notwendig, die Lösungen von **35** durch Zugabe von Base bzw. entsprechender Säure in die jeweiligen pH-Bereiche zu überführen (z. B. methanolische Lösungen mit Natronlauge, Essigsäure oder Salzsäure für die Absorptions- und Emissionsspektroskopie).

Schema 9: Synthese von *N*-Phenylfluorubin (mit Nummerierung der N-Atome).

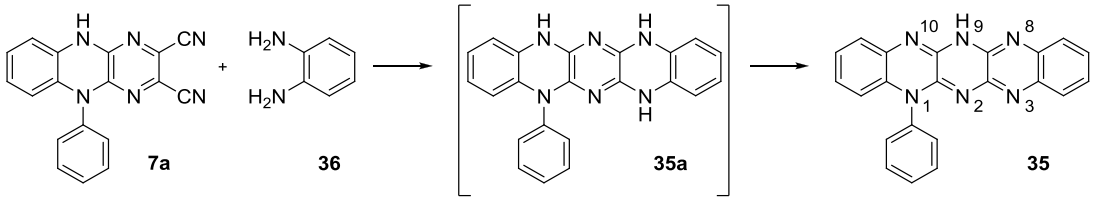

Schema 10: Mögliche Protonierungszustände von **35**, in Abhängigkeit des pH-Werts. Die laut DFT / TD-DFT stabilsten Tautomere wurden abgebildet, weiterführende Informationen stehen in Publikation 5 im Anhang..

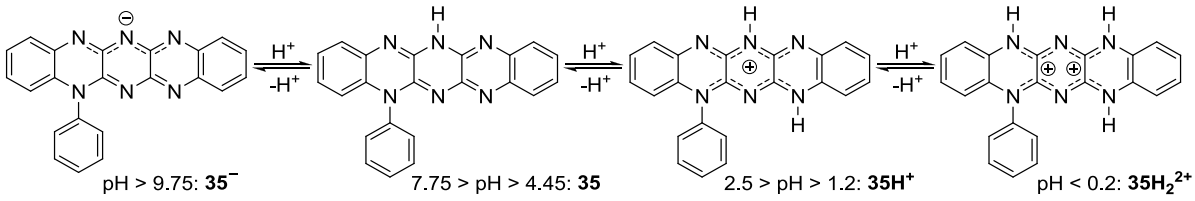


Über die Änderung des Milieus kann die Absorption des Moleküls, von einem Maximum bei 472 nm in der Neutralform bis 561 nm im Falle der zweifach protonierten Spezies mit nahezu gleichbleibend hohen Extinktionskoeffizienten (log $\varepsilon$ > 4,2), verschoben werden. Dabei rückt auch die Fluoreszenzemission vom grünen in den roten Spektralbereich. Während die neutrale (**35**) und deprotonierte Spezies (**35**$^-$) mit Quantenausbeuten von über 90% aufwarten, sinken diese mit dem Grad der Protonierung. Durch vermehrte Schwingungsdeaktivierung der einfach (**35H**$^+$), bzw. zweifach protonierten Spezies (**35H$_2$**$^{2+}$) können die auf 60% bzw. 20% sinkenden Quantenausbeuten erklärt werden.

Erstmalige Untersuchungen zur Beeinflussung der Grenzorbitalenergien durch Variation des pH-Wertes führten zu bemerkenswerten Ergebnissen. Durch die Deprotonierung des Fluorubins **35** zu **35**$^-$ werden die Grenzorbitalenergien von -6,6 auf -5,0 eV (HOMO) bzw. von -4,0 auf -2,7 eV (LUMO) angehoben (siehe Abbildung 17). Bei Protonierung kann ein gegenteiliger Effekt beobachtet werden. Die Elektronenaffinität nimmt drastisch zu, einhergehend mit der Absenkung der Grenzorbitalenergien. So führt das Protonieren zur LUMO-Energie von 4,3 eV (**35H**$^+$) und zweifache Protonierung (**35H$_2$**$^{2+}$) zum herausragend niedrigen LUMO-Level von -4,7 eV, was für eine Anwendung als Akzeptormaterial in BHJs spricht.

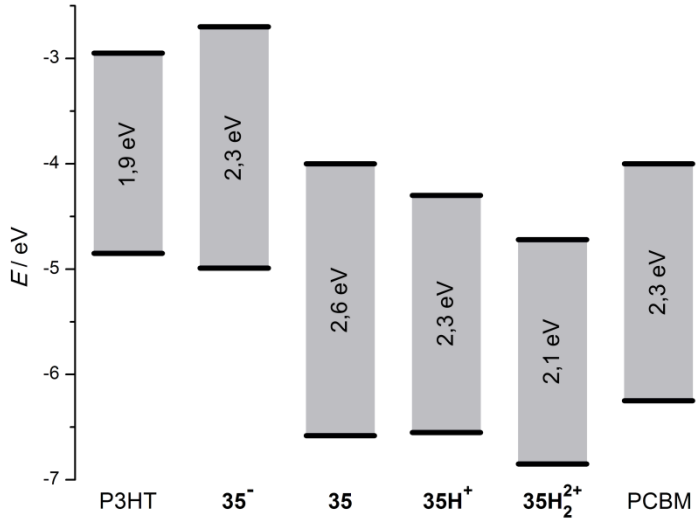


Abbildung 17: Vergleichende Darstellung der Grenzorbitallagen des Derivats **35** bei verschiedenen Protonierungszuständen mit den konventionellen Materialien einer BHJ Solarzelle P3HT und $PC_{61}BM$.

Durch simples Ändern des pH-Wertes ist es möglich, die Eigenschaften von *N*-Phenylfluorubin **35** über einen weiten Bereich einzustellen. Die Fluoreszenzemission kann von grün über gelb (**35**$^{-}$) und orange (**35H**$^{+}$) bis rot (**35H$_2$**$^{2+}$) variiert werden. Dabei werden auch die Lagen der Grenzorbitale drastisch verschoben. So kann es von einem Elektronendonor (**35**$^{-}$, energetisch hohes HOMO: -5,0 eV) in ein Akzeptormaterial (**35H$_2$**$^{2+}$, niedriges LUMO: -4,7 eV) umgewandelt werden.

## 4.3 Untersuchungen zur Regioisomerie

Unpublizierte Ergebnisse: D. M. Gampe, S. Schramm, A. Darsen, P. Naumov, R. Beckert *Manuskript wird derzeit erstellt*

Nach der Deprotonierung von *N*-Phenylfluorubin (**35**) kann die entstandene negative Ladung leicht durch Zugabe von Elektrophilen abgefangen werden.[93] Die Delokalisierung der Ladung ermöglicht die Bildung von bis zu vier Regioisomeren (siehe Schema 11). Um die Löslichkeit zu erhöhen, war 1-Hexyliodid als Alkylierungsmittel eingesetzt worden. Nach beendeter Reaktion konnten die Regioisomere durch säulenchromatographische Aufarbeitung in drei Gruppen getrennt werden. Isomer **37A** wird rein erhalten, **37B** und **37C** werden über eine weitere präparative Dünnschichtchromatographie und die Derivate **37D** und **37E** mittels erneuter Säulenchromatographie isoliert. Da für einen vollständigen Reaktionsumsatz ein leichter Überschuss an Hexyliodid benötigt wurde (1,1 Äquivalente), fand am Zwitterion **37D** partiell eine Zweifachalkylierung unter Erhalt von **37E** statt. Die Substitutionsmuster der Isomere **37A** (1,9-Dihydro) und **B** (1,10-Dihydro) waren unserem Wissen nach bisher unbekannt. Während **37A** in hohen Ausbeuten aus **35** gewonnen wurde, konnten von den anderen Fluorubinen nur wenige Milligramm isoliert werden. Die geringen Substanzmengen waren für grundlegende photochemische Charakterisierungen ausreichend, jedoch wählten wir zusätzlich eine separate Syntheseroute zum Substitutionsmuster von **37B**, um weiterführende Untersuchungen durchführen zu können (siehe Kapitel „4.4 1,10-Disubstituierte Fluorubine“).

Alle Derivate bilden intensiv gefärbte Lösungen und zeigen die, für rigide Systeme typischen, schwingungsaufgelösten Absorptionsbanden im sichtbaren Bereich (siehe Abbildung 18).[94]

Schema 11: Synthese der Fluorubin-Regioisomere und Fotografie ihrer $CHCl_3$-Lösungen unter UV-Bestrahlung.

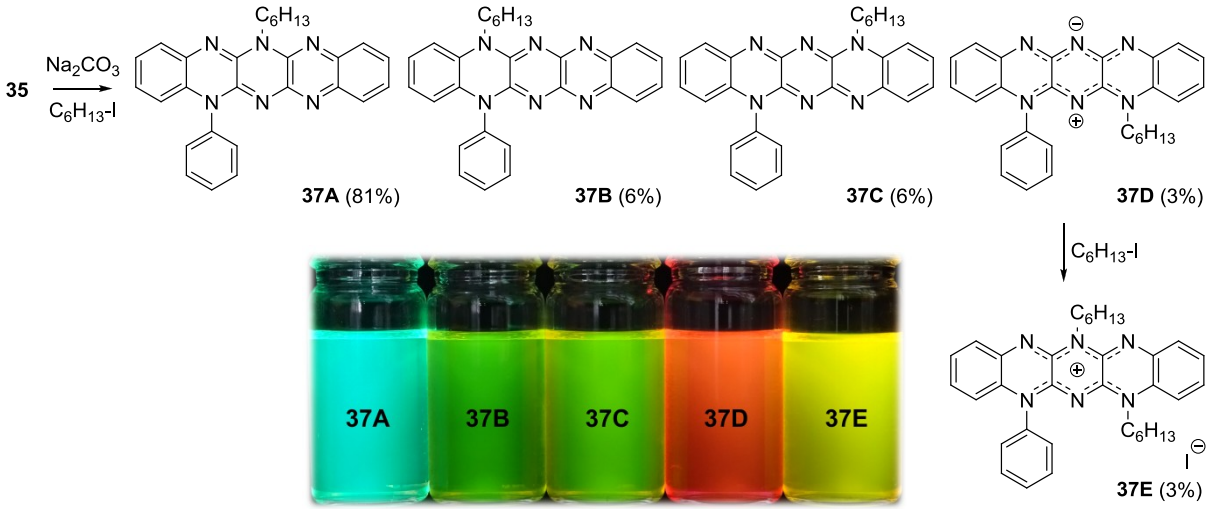

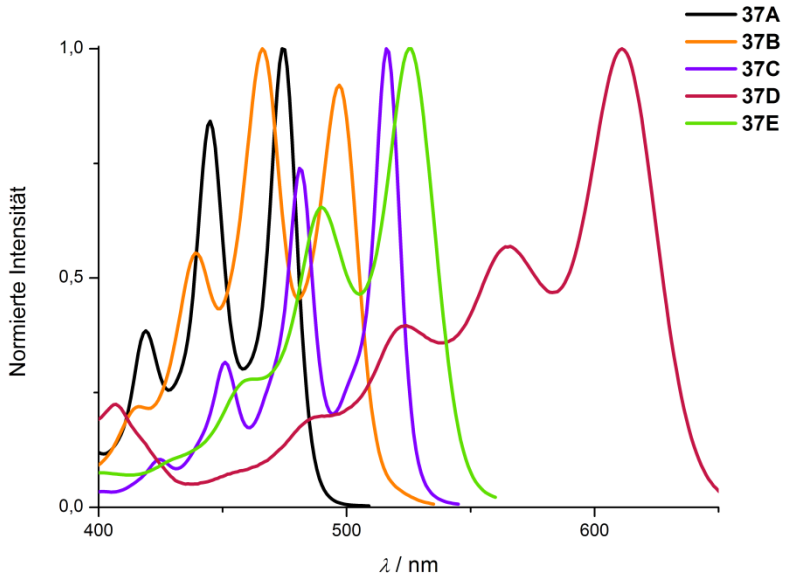


Abbildung 18: UV/Vis-Absorptionsspektren der Regioisomere und des zweifach hexylierten Kations **37E**.

**37C**, **D** und **E** verhalten sich photochemisch sehr ähnlich zu den von Fleischhauer entwickelten Fluorubinen (vergleiche Strukturen in Schema 2B und Abbildung 16). Dies beweist, dass physikalische Eigenschaften wie Schmelzverhalten, Morphologie in fester Phase und Löslichkeit über die Substituenten gesteuert werden können, ohne die photochemischen Eigenschaften zu beeinflussen. Alle Derivate besitzen hohe Extinktionskoeffizienten ($\log \varepsilon > 4{,}5$) und zeigen Fluoreszenzemissionen nach Stoke's Shifts von lediglich ~450 $cm^{-1}$. Abbildung 19 stellt die Fluoreszenzspektren der Regioisomere vergleichend dar. Derivat **37A** ist das stärkste Fluorophor ($\Phi_{FL} = 99\%$), gefolgt von **37C** ($\Phi_{FL} = 97\%$) sowie **37B** und **E** ($\Phi_{FL} = 70\%$). Zwitterion **37D** weist eine rote Emission mit einer Quantenausbeute von 22% auf.

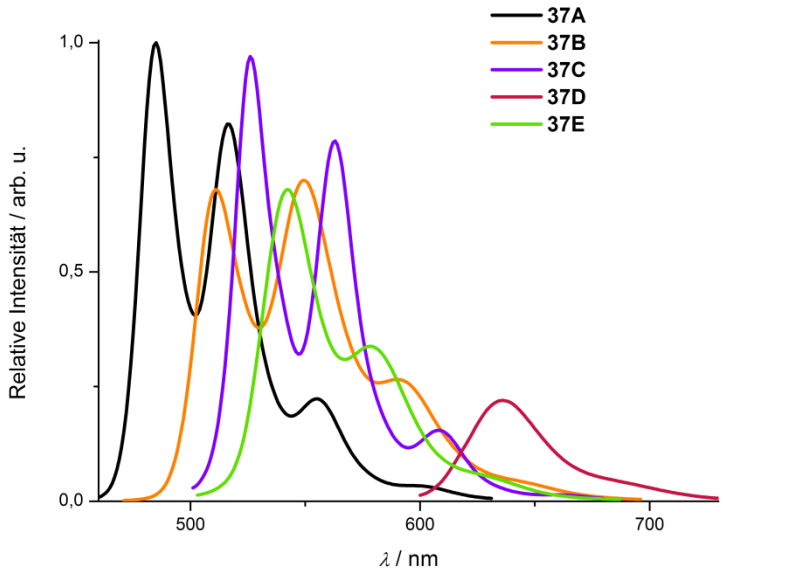


Abbildung 19: Darstellung der Fluoreszenzspektren, gemessen in $CHCl_3$.

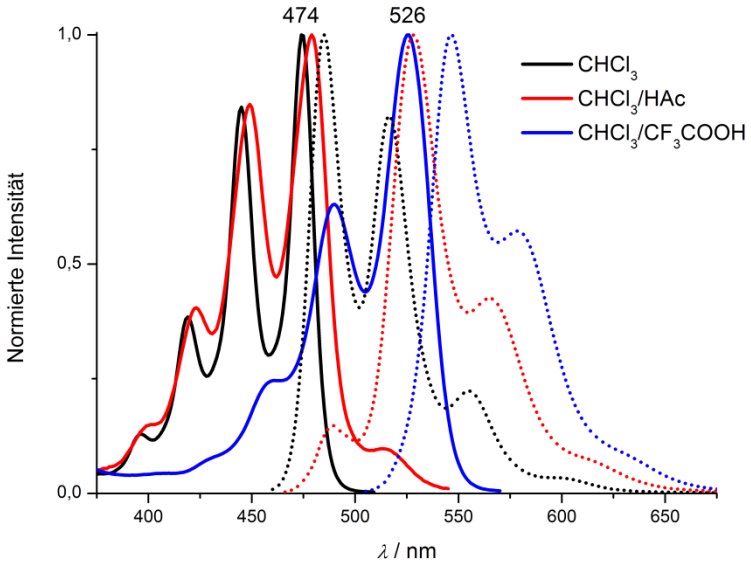


Abbildung 20: Acidochromie des Derivats **37A**; UV/Vis-Absorption (Linie) und Fluoreszenzemission (Punkte) bei verschiedenen pH-Werten.

Wie in Abbildung 20 dargestellt wird, können die photochemischen Eigenschaften von **37A** durch Säurezugabe gesteuert werden. Das Absorptionsmaximum verschiebt sich um 52 nm (≙ 0,26 eV) bathochrom, wodurch auch die optische Bandlücke um 0,24 auf 2,26 eV verringert wird. Von einer türkis-fluoreszenten Lösung kann zur gelben Fluoreszenz in Essigsäure ($\Phi_{FL}$ = 90%) oder zur orangenen Emission ($\Phi_{FL}$ = 90%) in Trifluoressigsäure gewechselt werden.

Über diese pH-Sensitivität wird das LUMO von Derivat **37A** herabgesetzt, was durch die Verschiebung der Reduktion zu höheren Potentialen sichtbar ist (siehe Abbildung 21). Das LUMO kann per Ansäuern von -3,2 (**37A**) über -4,0 (**37AH**$^+$) nach -4,3 eV (**37AH**$_2^{2+}$) variiert werden.

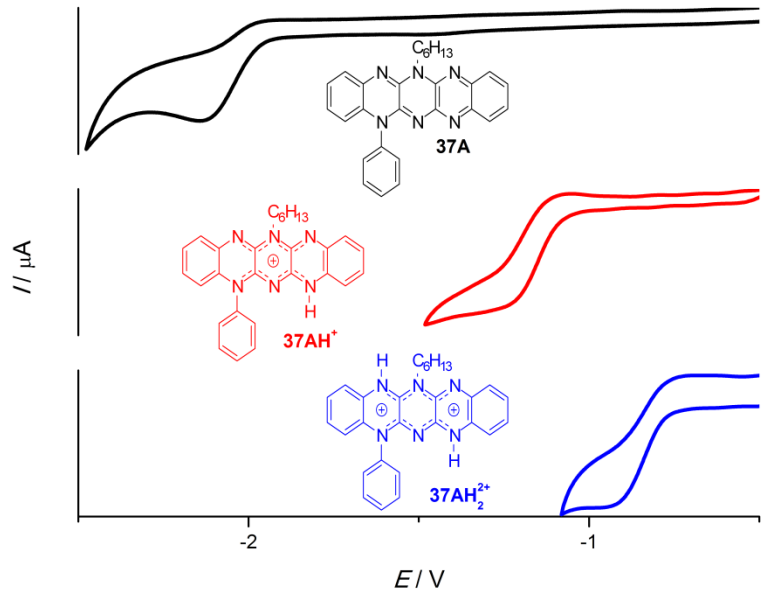


Abbildung 21: Reduktionszyklen der Cyclovoltammogramme von **37A** bei verschiedenen Protonierungsstufen.

Dank der simplen Alkylierungsreaktion von *N*-Phenylfluorubin können fast alle möglichen Regioisomere erzeugt werden. Diese beeindrucken vor allem durch ihre hohen Extinktionskoeffizienten und Fluoreszenzquantenausbeuten. Eine besonders spannende Eigenschaft stellt die pH-Sensitivität dar, wodurch die Eigenschaften gezielt variiert werden können. Da bei der Alkylierung vorrangig das bisher unbekannte Derivat **37A** entsteht, wurden dessen Eigenschaften intensiv studiert.

## 4.4 1,10-Disubstituierte Fluorubine

Teile dieses Kapitels sind publiziert in: D. M. Gampe, S. Schramm, S. Ziemann, M. Westerhausen, H. Görls, P. Naumov, R. Beckert, *J. Org. Chem.* **2017**, *82*, 6153-6162.

Über die in Schema 12 dargestellte Syntheseroute ist das letzte unbekannte Substitutionsmuster der Fluorubine zugänglich. Wir wollten Derivate erzeugen, welche die Grundeigenschaften der Fluorubine (hohe Stabilitäten, Extinktionskoeffizienten und Quantenausbeuten) mit tief liegenden LUMOs und besserer Löslichkeit vereinen. Weiterhin war es angedacht, partiell Donorgruppen einzuführen, um einen CT einhergehend mit einer Verringerung der Bandlücke hervorzurufen.

Die präsentierten Derivate sind über drei bzw. vier Stufen, ausgehend von kommerziell erhältlichen Ausgangsstoffen, zugänglich. Dabei wird durch die Synthese der *N*-funktionalisierten Phenylendiamine **40-42** das Substitutionsmuster der Zielverbindungen festgelegt. Die Substituenten an den Stickstoff-Atomen führen nicht nur zu einer Fixierung der Dihydro-Form, sondern steuern auch Eigenschaften wie Löslichkeit, Kristallisationsverhalten ($^t$Butyl) oder Donorcharakter (Methoxy).[95] Während die aliphatischen Reste via Amidierung von *o*-Phenylendiamin **36** mittels Pivaloylchlorid und anschließender Reduktion eingeführt werden konnten, wurden die Aryl-Einheiten per Buchwald-Hartwig Reaktion, ausgehend von *o*-Dibrombenzen **38**, installiert.

Schema 12: Synthese der 1,10-disubstituierten Fluorubine **46**-**48**.

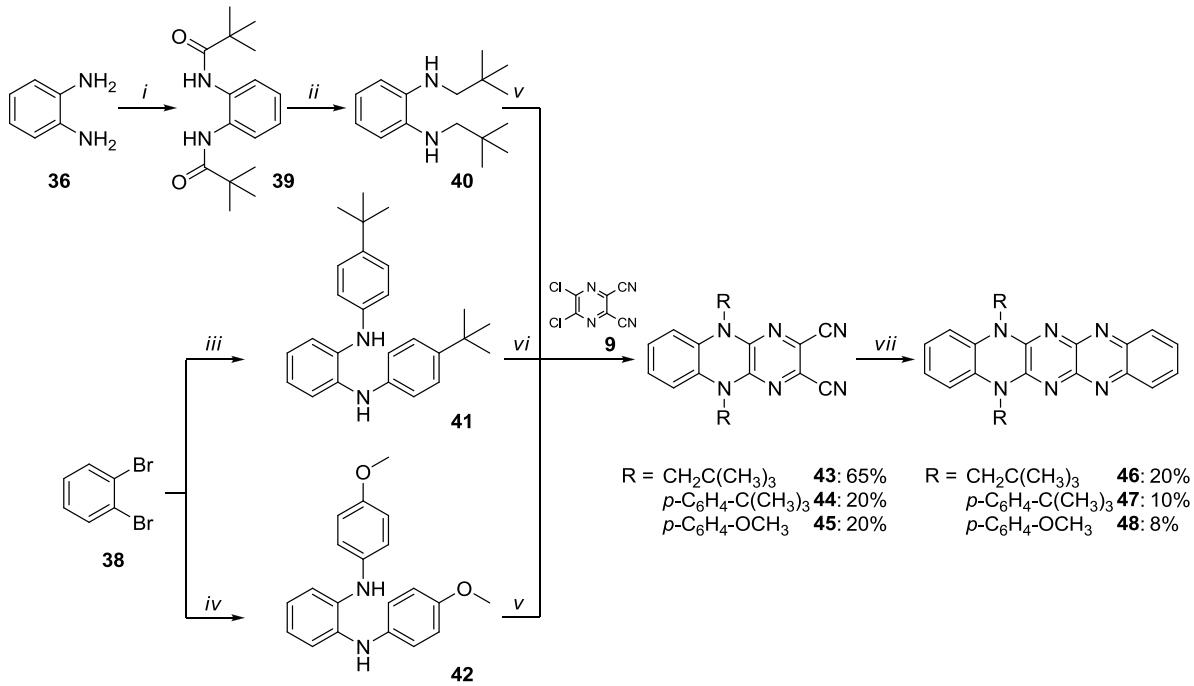


*i*) Pivaloylchlorid, THF, 88%.
*ii*) $LiAlH_4$, THF, $N_2$, 45%.
*iii*) *p*-$^t$Butyl-aminobenzen, $Pd(dba)_2$, SPhos, $KO^tBu$, Toluen, $N_2$, 85%.
*iv*) *p*-Anisidin, $Pd_2(dba)_3$, BINAP, $NaO^tBu$, Toluen, $N_2$, 95%.
*v*) **9**, Dioxan, $N_2$.
*vi*) **9**, $Pd(dba)_2$, RuPhos, Hünig-Base, Toluen, $N_2$.
*vii*) 1.: **36**, DMA, $N_2$; 2.: Oxidation durch Luftsauerstoff.

Anschließende Umsetzungen mit Dichloro-dicyano-pyrazin **9** erzeugte die Dihydro-Tetraazaanthracene **43**-**45**. Aufgrund des elektronenschiebenden Charakters der alkyl- und *para*-methoxy Substituenten reagierten die Diamine **43** und **45** über eine nucleophile Substitution unter Zyklisierung. Diamin **44** hingegen bedurfte einer Pd-katalysierten Buchwald-Hartwig Kreuzkupplung, um mit **9** zu zyklisieren. Die vicinale Dicyano-Substruktur der Anthracene erlaubte schließlich eine weitere Zyklisierung mit *o*-Phenylendiamine (**36**) zu den fünfkernigen Hexaaza-Derivaten **46**-**48**. Wie schon in 4.2 beschrieben, geschieht die Oxidation der intermediären und nicht isolierten Tetrahydro-Hexaazapentacene sofort durch Luftsauerstoff bei der Aufarbeitung und liefert die stark fluoreszierenden Zielstrukturen in annehmbaren Ausbeuten.

Röntgenkristallstrukturanalysen der Derivate **46** und **47** ließen den vergleichbar schmalen π-π-Abstand der Ebenen erkennen (siehe Abbildung 22). *neo*-Pentyl Fluorubin kristallisiert in Dimeren (π-π-Abstand 3,3 Å), welche über Wasserstoffbrückenbindungen verknüpft sind und ein Zickzackmuster bilden. Die eindimensionalen π-Stapel (π-π-Abstand 3,4 Å) des, aus Aceton kristallisierten, $^{t}$Butyl-Phenyl Derivats **47** sind über co-kristallisiertes Lösungsmittel verbunden und bilden ein gegeneinander verdrehtes Mauermotiv.

Unter neutralen pH-Bedingungen zeigen alle Derivate eine starke, schwingungsaufgelöste Absorption mit vier scharfen Banden im Bereich von λ = 400 - 520 nm. Dabei unterscheiden sich die photochemischen Eigenschaften der Fluorubine nur marginal, weshalb Abbildung 23 die Spektren von Derviat **46** beispielhaft darstellt. Die Absorption des *neo*-Pentyl Derivats **46** ist, gegenüber der von **47** und **48**, um 7 nm (≙ 0,03 eV) bathochrom verschoben. Durch die Torsion der Phenyl-Substituenten wird eine effektive π-Konjugation und damit die Erweiterung des chromophoren Systems verhindert. Der schwache elektronenschiebende Effekt der Alkyl-Gruppe ist hingegen Bindungswinkel unabhängig, was die leichte Rotverschiebung des Spektrums erklärt.

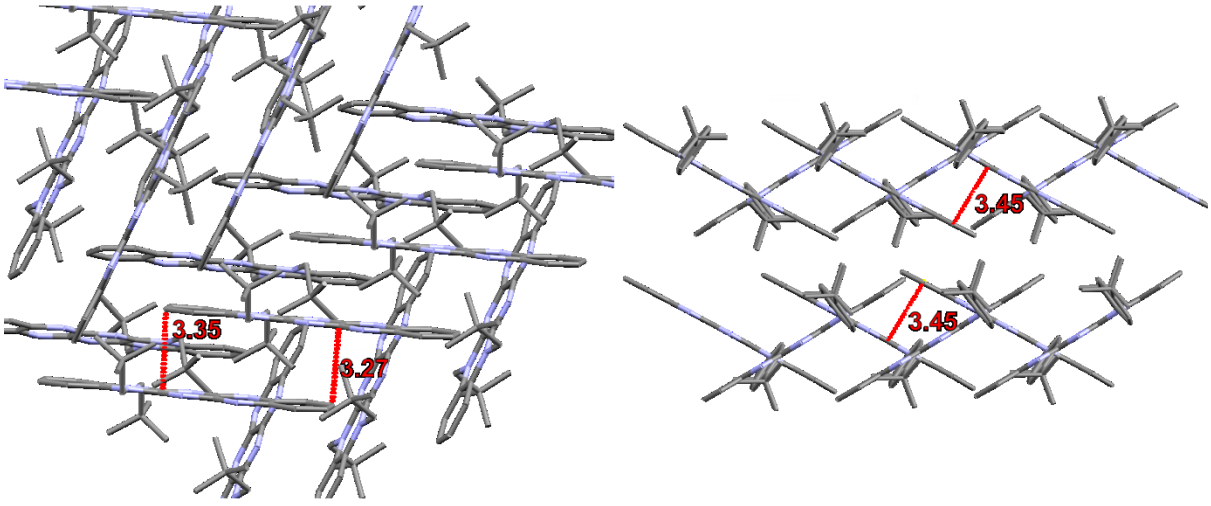


Abbildung 22: Anordnung der Moleküle im Kristall (links: **46**, rechts: **47**). Wasserstoffatome, Standardabweichung und Aceton-Moleküle sind übersichtlichkeitshalber vernachlässigt.

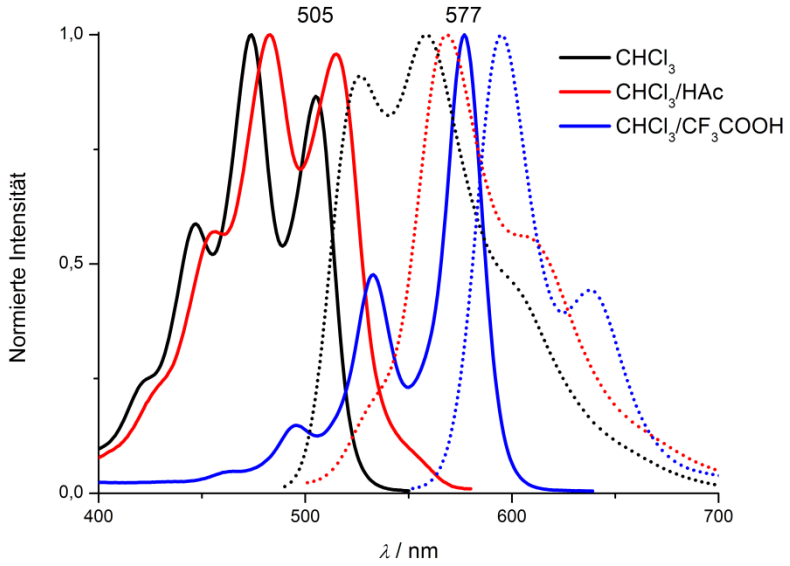


Abbildung 23: Acidochromie des Derivats **46**; Absorption (Linie), Emission (Punkte) verschiedener pH-Werte.

Zugabe von Essigsäure überführt die Derivate bei pH ≈ 3,5 in Amidinium-Salze (**46H**$^+$, **47H**$^+$, **48H**$^+$). Dies zieht drastische Geometrieänderungen innerhalb des Systems und folglich auch drastische Änderungen der Eigenschaften nach sich. So werden nicht nur die Bandlücken (um 0,1 eV zu $\Delta E_{opt}$ = 2,3 eV) verengt, wodurch sich die Absorptionsbanden leicht bathochrom verschieben, auch die Art der Banden wird stark beeinflusst (siehe Abbildung 23 zum Vergleich der Protonierungszustände). Beispielsweise sind die Schwingungsübergänge deutlich unschärfer, was auf Tautomerisierung und damit verbundenem Bindungsausgleich zurückführbar ist.

Wird der pH-Wert noch weiter erniedrigt (pH ≈ 0,5), ergeben sich doppelte Amidinium Salze mit völlig neuen Eigenschaften. Alle Derivate (**46H$_2$**$^{2+}$, **47H$_2$**$^{2+}$, **48H$_2$**$^{2+}$) absorbieren bis in den roten Spektralbereich und bilden drei scharfe, separierte Banden bei $\lambda_{max}$ = 500, 530 und 580 nm, mit bemerkenswerten Extinktionskoeffizienten von: $\varepsilon = 12\times10^4$ (**46H$_2$**$^{2+}$), $8\times10^4$ (**47H$_2$**$^{2+}$) bzw. $9\times10^4$ M$^{-1}$ cm$^{-1}$ (**48H$_2$**$^{2+}$) und optischen Bandlücken von $\Delta E_{opt}$ = 2,0 eV.

Die Fluoreszenzemission wird durch Verringerung des pH-Wertes gleichermaßen bathochrom verschoben, von einer grünen Emissionsfarbe über gelb nach rot. Dabei zeigt **48H$_2$**$^{2+}$ keine nennenswerte Fluoreszenzemission, jedoch besitzt *neo*-Pentyl Derivat **46H$_2$**$^{2+}$ eine (für eine rote Emission) außerordentlich hohe Quantenausbeute von 76%.[96]

Cyclovoltammetrische Experimente bei unterschiedlichen Protonierungsstufen zeigten die Variabilität der Grenzorbitallagen, sichtbar durch das Verschieben der Redoxpotentiale (siehe Publikation 6). Während die neutralen Spezies **46** - **48** je eine Ein-Elektronen-Reduktion aufweisen, sind die zweifach protonierten in der Lage, zwei Elektronen reversibel aufzunehmen. Die Elektronenaffinität steigt, einhergehend mit dem Absinken des LUMO auf bis zu -4,77 eV (**46H$_2$**$^{2+}$, **47H$_2$**$^{2+}$, **48H$_2$**$^{2+}$), mit der Protonierung stark an. Abbildung 24 stellt die Verschiebung der Molekülorbitale mit steigendem Protonierungsgrad, am Beispiel von Di-*neo*-pentyl-Fluorubin **46**, dar.

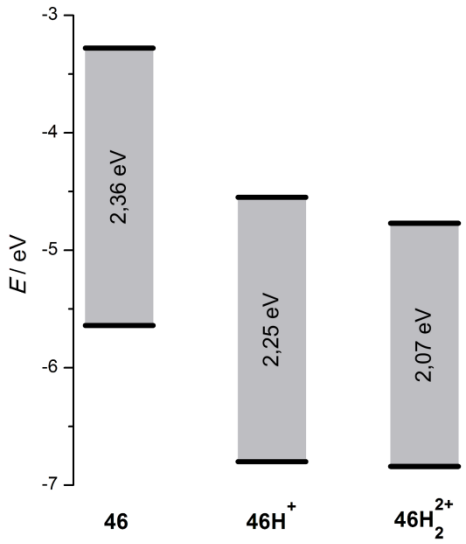


Abbildung 24: Veränderung der Grenzorbitallagen mit dem Protonierungsgrad des Derivats **46**.

Über die entwickelte Syntheseroute waren wir in der Lage, verschiedene Derivate der 1,10-disubstituierten Fluorubine herzustellen. Die Spezies zeichnen sich durch schmale π-π-Abstände in kristalliner Phase, hohe Stabilität und pH-Sensitivität aus. Durch Protonierung können Absorptions-, Emissions- und Redoxverhalten gezielt variiert werden.

# 5 Zusammenfassung und Ausblick

Ein großer und wichtiger Bestandteil dieser, auf der Chemie der Azaacene beruhenden, Promotion ist die Synthese von neuartigen funktionellen Derivaten. Hierfür stand zunächst die Erweiterung der synthetischen Zugangsmöglichkeiten im Vordergrund, woraus die als „Funktionelle Vorstufen“ benannten Strukturen hervorgingen (z.B. Nitro-Anthracen **7d** und bis-Thiazol **14** in Abbildung 25).

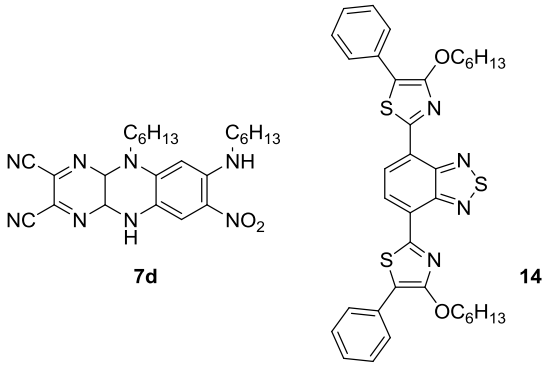


Abbildung 25: Wichtige Vertreter der „Funktionellen Vorstufen“ (bis-Hexyl-nitro-tetraazaanthracen **7d** und bis-Thiazolo-benzothiazol **14**).

Die Synthese von hochsubstituierten Dihydro-Tetraazaanthracenen (**7a-i**) gelang über ein konsekutives dreistufiges Herstellungsverfahren, ausgehend von preiswerten Edukten. Hinsichtlich der komplexen Struktur der Nitro-Derivate **7b-g** wurden sie auf ihre photo- und elektrochemischen Eigenschaften untersucht. Diese zeichneten sich durch starke Absorptionen bis in den roten Bereich des sichtbaren Lichts ($\log \varepsilon$ bis zu 4,5) und teilweise reversibler Redox-Aktivität aus. Aus den elektrochemischen Messungen ließen sich untypische Grenzorbitalenergien von -5,3 (HOMO) und -3,7 eV (LUMO) ableiten, welche im Vergleich zu literaturbekannten Azaacenen auf einen ambipolaren Charakter schließen lassen.

Studien an Benzothiadiazolen -„Piazthiolen“- offenbarten deren großes Potential als Vorstufen von *C*-substituierten Diaminen bzw. den daraus resultierenden Azaacenen. Durch die Synthese der Derivate **11**-**14** ließ sich beweisen, dass diese Bausteine extrem stabil gegenüber verschiedenster Reaktionstypen sind. Bei der Charakterisierung wurde der starke Donorcharakter der integrierten 4-Alkoxythiazole detektiert. Vor allem die dadurch hervorgerufene schmale Bandlücke von bis-Thiazol **14** ($\Delta E$ = 2 eV) ist bemerkenswert. Weiterhin sind seine starke Absorption ($\log \varepsilon$ = 4,5) und Fluoreszenz ($\Phi_{FL}$ = 30%) Eigenschaften, welche mit konventionellen Donor-Bt-Donor Systemen vergleichbar sind.[97] Besonders erwähnenswert ist dabei, dass keine teuren Kreuzkupplungsreaktionen zum Aufbau nötig waren, wie es beispielsweise bei Diarylamin- oder Thiophen-Donoren der Fall ist.[98]

Über Benzothiadiazole als Diamin-Precursor gelang schließlich die Synthese von *C*-funktionalisierten Tetraazaanthracenen (zum Beispiel **24** und **AntS** in Abbildung 26).

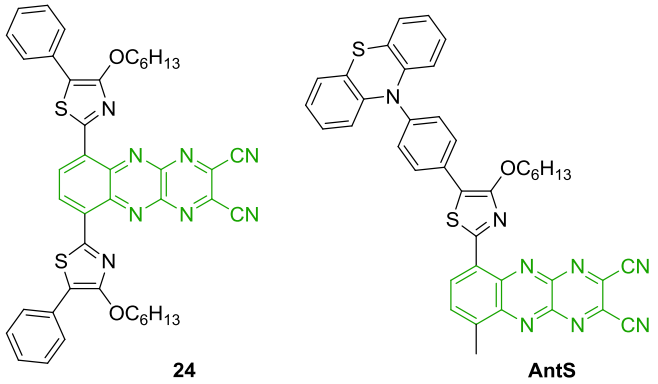


Abbildung 26: Tetraazaanthracen (grün) als Akzeptoreinheit, beispielhaft an bis-Thiazolo-anthracen **24** und D-A Farbstoff **AntS** dargestellt.

Die Kombination der elektronenarmen Tetraazaanthracene (grün hervorgehobene Struktur in Abbildung 26) mit Thiazolen, welche hervorragende Donoreigenschaften aufweisen, führte zu den NIR-absorbierenden Farbstoffen **21**-**24**. Durch ihre photo- und elektrochemische Charakterisierung konnte unter anderem die gegenüber den Piazthiolen (**11**-**14**) deutlich stärkere Elektronenaffinität der Tetraazaanthracene bestätigt werden. Die Bandlücken werden somit um 1-1,2 eV zu Werten von $\Delta E$ = 1-1,3 eV verringert, wodurch die Maxima der CT-Banden von Bt zu Anthracen einen bis zu 300 nm (≙ 0,8 eV von **14** zu **24**) betragenden Rot-Shift erfahren. Außerdem bewirkt die Verknüpfung von zwei Thiazol-Einheiten mit Tetraazaanthracen eine rekordverdächtig niedrige LUMO-Energie von -4,8 eV (**24**).

Im Folgenden war es durch die Installation von *para*-ständigen Brom-Substituenten am Phenyl-Rest der Thiazole gelungen, Diarylamine per Buchwald-Hartwig-Aminierung einzuführen. Um verschiedene Donor- bzw. Akzeptoreinheiten vergleichen zu können, waren je drei Bausteine getestet worden. Abhängig vom Akzeptorbaustein lässt sich die Absorption im blauen (Pyrazin, **PyrX**), orangenen (Benzothiadiazol, **BtX**) oder roten bis NIR-Bereich (Anthracen, **AntX**) detektieren. Dabei erscheinen die Absorptionsmaxima bei rund 395 (**PyrX**), 455 (**BtX**), bzw. 700 nm (**AntX**). Über die Reduktionspotentiale aus cyclovoltammetrischen Messungen konnten Akzeptor-abhängige LUMO-Energien von -3,1 (**PyrX**), -3,7 eV (**BtX**) und -4,7 eV (**AntX**) berechnet werden. Die Transformation der jeweiligen Bt-Einheit zu Tetraazaanthracenen führte somit zum stärksten der getesteten Akzeptorblöcke. Dass sich die Eigenschaften durch gezielte Kombination von Donor- und Akzeptoreinheit abstimmen lassen, zeigte die Integration von verschiedenen Diarylaminen. Carbazol (**PyrC**, **BtC**) und Phenoxazin (**PyrO**, **BtO**) führen zu hohen Fluoreszenzquantenausbeuten von 30-50% im Akzeptor-bedingten Spektralbereich, während die Absorptionen und Emissionen bei der Verwendung von Phenothiazin (**PyrS**, **BtS**) am weitesten rotverschoben sind. Die Ionisierbarkeit bzw. Oxidierbarkeit, welche mit dem HOMO korrelieren, hängen gänzlich von der Diarylamin-Substruktur ab. Phenoxa- und Phenothiazine zeigen je eine reversible Ein-Elektronen-Oxidation bei 0,3 V, woraus

die HOMO-Lagen von -5,4 eV abgeleitet werden konnten. Die Carbazole besitzen diese Eigenschaft nicht, weshalb die HOMO-Lagen von -6,0 (**PyrC**) bis -5,8 eV (**BtC**, **AntC**) variieren. Besonders beachtlich sind die schmalen HOMO-LUMO Abstände, welche durch die Verknüpfung von Phenoxa- oder Phenothiazin über den Phenyl-thiazolyl-Rest mit Tetraazaanthracen (**AntO**, **AntS**) hervorgerufen werden. Unserem Wissen nach wurde bisher noch nicht über derart schmale Bandlücken von 0,7 eV bei $\pi$-konjugierten Einzelmolekülen berichtet. Diese sind vergleichbar mit denen von Halbmetallen, wie Silicium oder Germanium.[99]

Durch die Synthese von Fluorubinen mit bisher unbekannten Substitutionsmustern (zum Beispiel **35**, **37A** oder **46** in Abbildung 27) konnten vielseitige Vertreter dieser Substanzklasse erschlossen werden. Ihre pH-abhängigen Eigenschaften wurden intensiv mittels UV/Vis-Absorptions- und Fluoreszenzemissionsspektroskopie sowie Cyclovoltammetrie untersucht.

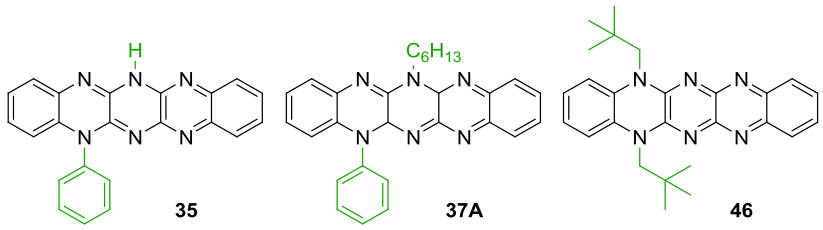


Abbildung 27: Darstellung der Fluorubin-Derivate **35**, **37A** und **46**. Zur Verdeutlichung der Substitutionsmuster, wurden die entsprechenden Reste grün markiert.

Unter Verwendung des *N*-substituierten Bausteins **7a** konnte erfolgreich erstmalig ein unsymmetrisch-*N*-substituiertes Fluorubin erhalten werden. *N*-Phenylfluorubin **35** besticht mit hervorragenden photochemischen Eigenschaften, wie starker Absorption (bis zu $\log \varepsilon = 4{,}6$) und Fluoreszenzemission ($\Phi_{FL} = 95\%$). Bei Basenzugabe unter Ausbildung des anionischen Amids $\mathbf{35}^-$, werden die Energien der Grenzorbitale um 1,4 eV erhöht und liegen im typischen Bereich eines BHJ-Donormaterials (z. B. P3HT). Absorption und Emission verschieben sich leicht bathochrom und $\mathbf{35}^-$ zeigt eine intensive gelbe Fluoreszenz ($\Phi_{FL} = 90\%$). Durch Überführung der Neutralspezies **35** in die kationischen Amidinium-Ionen $\mathbf{35H}^+$ bzw. $\mathbf{35H_2}^{2+}$ wird die Fluoreszenzemission ebenfalls bathochrom verschoben. Jedoch sinken die Quantenausbeuten auf 60 bzw. 20% aufgrund vermehrter Schwingungsdeaktivierung. Im Gegensatz dazu steigt die Elektronenaffinität mit dem Protonierungsgrad stark an, was mit der Verringerung der LUMO-Energien zu -4,3 ($\mathbf{35H}^+$) und sehr niedrigen -4,7 eV ($\mathbf{35H_2}^{2+}$) korreliert. Über diese pH-sensitiven Eigenschaften kann ausgehend von **35** vom Donormaterial ($\mathbf{35}^-$) bis zum Elektronenakzeptor ($\mathbf{35H_2}^{2+}$) variiert werden. Der präparativ einfache Zugang zum kristallinen Dihydrochlorid ($\mathbf{35H_2}^{2+}\cdot 2\mathrm{Cl}^-$) signalisiert überdies Anwendungspotential als n-Typ Halbleiter.

Beim Versuch das anionische Amid $\mathbf{35}^-$ mit Elektrophilen abzufangen, konnten fast alle möglichen zweifach substituierten Regioisomere (**37A-D**) über aufwendige Trennungsverfahren isoliert werden. Das Regioisomer mit der höchsten Ausbeute von 81% ist **37A**, welches gleichzeitig das erste

1,9-disubstituierte Fluorubin darstellt. Aufgrund seiner starken, pH-sensitiven Fluoreszenzemission ($\Phi_{FL}$ zwischen 90 und 99%) könnte dieses Derivat zur Bestimmung der Acidität organischer Lösungsmittel herangezogen werden.

Über drei- bzw. vierstufige Reaktionssequenzen konnten die 1,10-disubstituierten Fluorubine **46**-**48**, ausgehend von kommerziell erhältlichen Ausgangsmaterialien dargestellt werden. Diese zeichnen sich ebenfalls durch ihre pH-Schaltbarkeit aus, verbunden mit starker UV/Vis-Absorption ($\log \varepsilon = 4{,}4 – 5{,}1$) sowie Fluoreszenzquantenausbeuten zwischen 30 und 76%. Nennenswerter Spitzenreiter ist hierbei Derivat $\mathbf{46H_2^{2+}}$ ($\log \varepsilon = 5{,}1$, $\Phi_{FL}$ = 76%). Die Grenzorbitalenergien werden von -5,6 und -3,3 eV im Falle der Neutralformen **46**-**48** mittels zweifacher Protonierung auf niedrige -6,8 eV und -4,8 eV herabgesetzt.

Die lediglich als Zwischenstufen geplanten Stoffe - Tetraazaanthracene **7** und Benzothiadiazole **11**-**14** – zeigten überraschende Eigenschaften, welche sie zu vielversprechenden Materialien für elektronische oder optoelektronische Anwendungen machen. Weiterhin gelang es über diese Benzothiadiazole, Azaacene als Akzeptorpart in D-A Farbstoffe zu integrieren wodurch einzigartige Materialien (**24**, **AntO**, **AntS**) entstanden. Diese Transformation könnte auch auf bereits angewandte Bt-basierte Halbleiter übertragen werden, um die LUMO-Lagen herabzusetzen und Bandlücken zu verringern. Erfolgreich konnten Fluorubine (**35**, **37A**, **46**-**48**) mit bisher unbekannten Substitutionsmustern hergestellt werden. Während der Charakterisierung war unter anderem die pH-abhängige Variabilität der Grenzorbitalenergien von Bedeutung, welche auch bei neuartigen Vertretern beachtet werden sollte. Die präsentierten Eigenschaften lassen auf vielfältige Anwendungsmöglichkeiten schließen und weisen gleichzeitig auf neue Zielsetzungen, beispielsweise der Charakterisierung von **35**, **37A** und **46** in fester Phase und die damit einhergehende Untersuchung von Feld- oder photovoltaischen Effekten.

# 6 Conclusion and Outlook

This thesis deals with the azaacene chemistry and enhances the synthetic access to azaacenes. During the synthetic studies, the versatile dihydro-tetraazaanthracenes **7** and benzothiadiazoles **11**-**14** were found to be attractive materials (see Figure 1 for two examples of these substance classes).

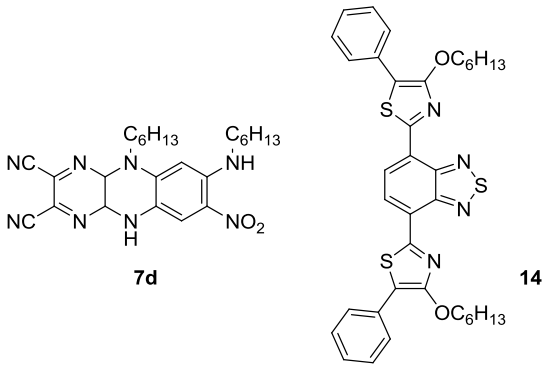


Figure 1: Derivatives of the "Functional Precursors". Left: bis-Hexyl-nitro-tetraazaanthracen **7d**; right: bis-thiazole **14**.

The synthesis of the highly substituted dihydro-tetraazaanthracenes (**7a-i**) succeeded via a consecutive three step procedure starting with commercially available starting materials. The sophisticated structures of nitro-derivatives **7b-g** were characterized with regard to their photo- and electrochemical behavior. The materials show intense absorption bands till the red region of visible light (log $\varepsilon$ up to 4.5) and reversible redox activity. Due to the electrochemical measurements, we estimated unusual frontier orbital energies to -5.3 (HOMO) and -3.7 eV (LUMO). Through the comparison to similar systems described in the literature, these frontier orbital energies point to an ambipolar behavior.

Benzothiadiazoles were found to be suitable *C*-substituted diamine and azaacene precursors, respectively. The synthesis of Bt-based dyes **11**-**14** elucidates the chemical stability of Bt against most reaction types. Spectroscopical and electrochemical characterization revealed the strong electron donating properties of thiazoles. Especially the narrow band gap of 2 eV, the strong absorption of up to log $\varepsilon$ = 4.5 and fluorescence ($\Phi_{FL}$ = 30%), which were evoked by combining two thiazoles with Bt to **14** are remarkable. The advantage of thiazole-Bt-thiazole derivative **14** with regard to other D-Bt-D derivatives bearing conventional donor moieties (e. g. diarylamines), is that **14** possesses similar properties[97] and can be synthesized without expensive transition metal catalysis, as in the case of diarylamines or thiophenes.[98]

Thanks to the easy transformation of the Bt substructure novel *C*-functionalized tetraazaanthracenes were prepared successfully (see Figure 2 for two examples).

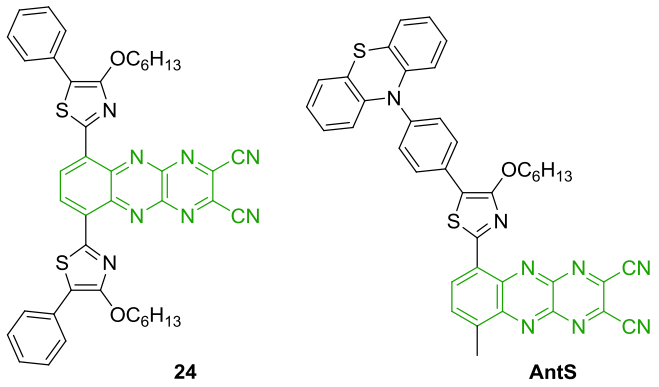


Figure 2: Tetraazaanthracene (green) as the electron accepting unit, exemplarily depicted on the structures of bis-thiazole **24** and D-A system **AntS**.

Combination of electron-deficient tetraazaanthracenes with the 4-alkoxythiazole donor motif lead to NIR-absorbing dyes **21**-**24**. The comparison of the absorption and redox activity of the new derivatives **21**-**24** and their Bt precursors revealed the much stronger electron affinity of the anthracenes. The band gaps are narrowed by 1 - 1.2 eV to $\Delta E = 1 - 1.3$ eV and the CT absorption bands entail a redshift by up to 300 nm (≙ 0.8 eV by comparing **14** with **24**). Furthermore the introduction of two thiazole-donor structures generates the highly electron-deficient derivative **24**, possessing a low LUMO energy of -4.8 eV.

To enhance the electron donating characteristic of thiazoles, *para*-brominated phenyl residues ready for the introduction of diarylamines via Buchwald-Hartwig cross coupling reactions were used. For comparison of donor and acceptor strengths, three different electron donor and acceptor moieties were tested during this study. Depending on the acceptor the absorption varies from the blue (pyrazines, **PyrX**) and orange (piazthiols, **BtX**) to the red and NIR region (anthracenes, **AntX**). The absorption maxima are located at approximately 395 (**PyrX**), 455 (**BtX**) and 700 nm (**AntX**). Cyclic voltammetry revealed the acceptor-dependent reduction potentials, which correlate to the LUMO levels of -3.1 (**PyrX**), -3.7 (**BtX**) and -4.7 eV (**AntX**). These properties lead to the assumption that tetraazaanthracene is the strongest of the involved acceptor units. The integration of different diarylamine donors, showed the possibility to tune the properties by the controlled combination of donor and acceptor units. While the carbazoles (**PyrC**, **BtC**) and phenoxazines (**PyrO**, **BtO**) possess high fluorescence quantum yields of 30-50% within the acceptor-dependent spectral region of about 490 (pyrazine) and 600 nm (Bt), the emissions of the phenothiazines (**PyrS**, **BtS**) are redshifted to 530 and 640 nm, respectively. The electrochemical measurements demonstrated donor-dependent HOMO levels. Phenoxazines and phenothiazines show reversible one electron oxidation steps at 0.3 V pointing to a consistent HOMO energy of -5.4 eV of these six derivatives (**PyrO**, **PyrS**, **BtO**, **BtS**, **AntO**, **AntS**). The decreased HOMO levels of carbazoles fluctuate between -6.0 (**PyrC**) and -5.8 eV (**BtC**, **AntC**). Remarkable are the narrow band gaps obtained by combining phenoxazine or phenothiazine with tetraazaanthracene (**AntO**, **AntS**). To our knowledge, there are no examples of

metal-free, $\pi$-conjugated small molecules possessing such small HOMO-LUMO differences of 0.7 eV, comparable with those of metalloids as Si or Ge.[99]

The synthesis of fluorubines with unknown substitution patterns (for example **35**, **37A** and **46** depicted in Figure 3) yielded versatile derivatives of this functional dye class. UV/Vis-absorption as well as fluorescence emission spectroscopy and cyclic voltammetry were carried out to investigate the pH-sensitive properties.

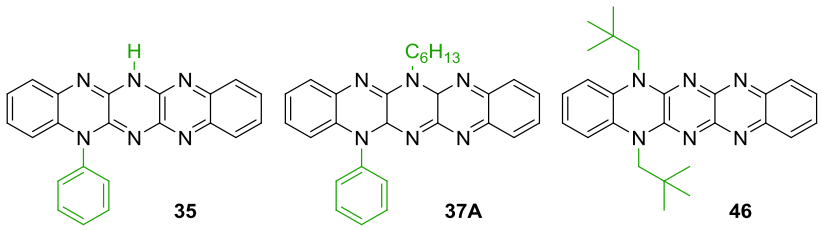


Figure 3: Depiction of fluorubine derivatives **35**, **37A** and **46** with marked residues.

Starting with dihydro-tetraazaanthracene **7a**, we synthesized to our best knowledge the first unsymmetrical *N*-substituted fluorubine. *N*-phenylfluorubine **35** is featured by high molar extinction coefficients (up to log $\varepsilon$ = 4.6) and fluorescence quantum yields ($\Phi_{FL}$ = 95%). The anionic amide $\mathbf{35}^-$ is observed in alkaline solutions. Thereby the frontier orbital energies rise from -6.6 to -5.0 eV (HOMO) and -4.0 to -2.7 eV (LUMO), respectively. While **35** shows a green fluorescence that of $\mathbf{35}^-$ is bright yellow with a quantum yield of 90%. Due to acidification, **35** is transformed to $\mathbf{35H}^+$ and $\mathbf{35H_2}^{2+}$. The fluorescence is shifted bathochromically, but protonation increases radiative deactivation and the quantum yields decrease linearly with the protonation state to 60 and 20%. Associated with protonation, the electron affinity is increased drastically and lead to decreased LUMO energies of -4.3 ($\mathbf{35H}^+$) and -4.7 eV ($\mathbf{35H_2}^{2+}$). Furthermore, we obtained the crystal structure of the double hydrochloride of **35**, which confirmed the access of $\mathbf{35H_2}^{2+}$ in solid state and promise an application of the latter as n-type semiconductor.

The reaction of $\mathbf{35}^-$ with electrophilic partners affords nearly all regioisomers of the disubstituted fluorubine core (**37A**-**D**). The separation was difficult but provided all isomers as pure substances. Derivative **37A** was obtained with a yield of 81% as main product and is the first 1,9-disubstituted fluorubine according to our research. Thanks to the strong pH-dependent fluorescence emission ($\Phi_{FL}$ = 90 - 99%) it could act as indicator in non-polar organic solvents, but the estimation of the p$K_a$ values needs further studies.

The 1,10-disubstituted fluorubines were synthesized via three (**47**, **48**) or four (**46**) consecutive reaction steps. Studies of the pH-dependent properties revealed outstanding features. It is possible to vary the strong absorption (log $\varepsilon$ = 4.4 – 5.1) and emission ($\Phi_{FL}$ = 30 – 76%) from green to red. Derivative $\mathbf{46H_2}^{2+}$ is particularly featured by high extinction coefficients (log $\varepsilon$ up to 5.1) and a quantum yield of 76% in the red region. The frontier orbital energies can be varied from -5.6 and -3.3 eV of the neutral species (**46**-**48**) to -6.8 and -4.8 eV upon double protonation ($\mathbf{46H_2}^{2+}$-$\mathbf{48H_2}^{2+}$).

As one part of our fundamental synthetic studies we found attractive azaacene precursor derivatives. The *N*-substituted tetraazaanthracenes **7** and Bt-derivatives **11-14** possess promising features for electronic and optoelectronic applications. Via these Bt-precursors we incorporated azaacenes as electron accepting moiety in D-A type dyes and obtained remarkable properties in particular for the low LUMO derivatives **24**, **AntO** and **AntS**. The transformation of Bt to tetraazaantracene via our synthetic protocol could be applied on established Bt systems to tune the LUMO energy and possibly obtain enhanced solar cell materials. Furthermore, the syntheses of fluorubines with literature unknown substitution patterns (**35**, **37A**, **46**-**48**) were described. The drastically changing properties (frontier orbital energies, absorption and emission) of these dyes upon protonation were studied intensively and should be noted during the future investigation of novel derivatives. Since the described properties of **35**, **37A** and **46** offer diverse application possibilities the next step should be their characterization in solid state.

# 7 Quellenverzeichnis


[1] a) M. Reimann, *Technologie des Anilins*, Springer-Verlag, **1866**; b) C. Meinel, *Angew. Chem.* **1992**, *104*, 1293-1309; c) O. Meth-Cohn, M. Smith, *J. Chem. Soc., Perkin Trans. 1* **1994**, 5-7; d) K. Hübner, *Chem. unserer Zeit* **2006**, *40*, 274-275.

[2] a) R. Leach, R. Pierce, *The Printing Ink Manual*, Springer-Verlag, **1999**; b) T. Gessner, U. Mayer, *Triarylmethane and Diarylmethane Dyes, In Ullmann's Encyclopedia of Industrial Chemistry*, Wiley-VCH, **2000**; c) K. Hunger, *Industrial Dyes - Chemistry, Properties, Application*, Wiley-VCH, **2002**.

[3] a) H. Zollinger, *Color chemistry : syntheses, properties, and applications of organic dyes and pigments*, Wiley-VCH, **1987**; b) J. Griffiths, *Chimia* **1991**, *45*, 304-307; c) J. Griffiths, *Chem. unserer Zeit* **1993**, *27*, 21-31.

[4] A. W. Hains, Z. Liang, M. A. Woodhouse, B. A. Gregg, *Chem. Rev.* **2010**, *110*, 6689-6735.

[5] A. Pron, P. Gawrys, M. Zagorska, D. Djurado, R. Demadrille, *Chem. Soc. Rev.* **2010**, *39*, 2577-2632.

[6] U. Mitschke, P. Bäuerle, *J. Mater. Chem.* **2000**, *10*, 1471-1507.

[7] M. O. Reese, S. A. Gevorgyan, M. Jørgensen, E. Bundgaard, S. R. Kurtz, D. S. Ginley, D. C. Olson, M. T. Lloyd, P. Morvillo, E. A. Katz, A. Elschner, O. Haillant, T. R. Currier, V. Shrotriya, M. Hermenau, M. Riede, K. R. Kirov, G. Trimmel, T. Rath, O. Inganäs, F. Zhang, M. Andersson, K. Tvingstedt, M. Lira-Cantu, D. Laird, C. McGuiness, S. Gowrisanker, M. Pannone, M. Xiao, J. Hauch, R. Steim, D. M. DeLongchamp, R. Rösch, H. Hoppe, N. Espinosa, A. Urbina, G. Yaman-Uzunoglu, J.-B. Bonekamp, A. J. J. M. van Breemen, C. Girotto, E. Voroshazi, F. C. Krebs, *Sol. Energy Mater. Sol. Cells* **2011**, *95*, 1253-1267.

[8] J. E. Anthony, *Chem. Rev.* **2006**, *106*, 5028-5048.

[9] J. E. Anthony, *Angew. Chem.* **2008**, *120*, 460-492.

[10] J. E. Anthony, A. Facchetti, M. Heeney, S. R. Marder, X. Zhan, *Adv. Mater.* **2010**, *22*, 3876-3892.

[11] a) G. J. Richards, J. P. Hill, T. Mori, K. Ariga, *Org. Biomol. Chem.* **2011**, *9*, 5005-5017; b) X. Shi, P. M. Burrezo, S. Lee, W. Zhang, B. Zheng, G. Dai, J. Chang, J. T. López Navarrete, K.-W. Huang, D. Kim, J. Casado, C. Chi, *Chem. Sci.* **2014**, *5*, 4490-4503; c) X. Shi, W. Kueh, B. Zheng, K. W. Huang, C. Chi, *Angew. Chem. Int. Ed.* **2015**, *54*, 14412-14416.

[12] U. H. Bunz, J. U. Engelhart, B. D. Lindner, M. Schaffroth, *Angew. Chem. Int. Ed.* **2013**, *52*, 3810-3821.

[13] E. H. O. Fischer, *Chem. Ber.* **1890**, *23*, 2789–2793.

[14] R. Nietzki, *Chem. Ber.* **1895**, *28*, 1357–1360.

[15] O. Hinsberg, *Liebigs Ann. Chem.* **1901**, *319*, 257–286

[16] O. Hinsberg, E. Schwantes, *Chem. Ber.* **1903**, *36*, 4039-4050.

[17] Q. Miao, *Adv. Mater.* **2014**, *26*, 5541-5549.

[18] Q. Miao, T.-Q. Nguyen, T. Someya, G. B. Blanchet, C. Nuckolls, *J. Am. Chem. Soc.* **2003**, *125*, 10284-10287.

[19] J. Nishida, N. Naraso, S. Murai, E. Fujiwara, H. Tada, M. Tomura, Y. Yamashita, *Org. Lett.* **2004**, *6*, 2007-2010.

[20] a) D. L. Z. He, R. Mao, Q. Tang, Q. Miao, *Org. Lett.* **2012**, *14*, 1050-1053; b) J. Jaung, K. Fukunishi, M. Matsuoka, *J. Heterocycl. Chem.* **1997**, *34*, 653-656; c) G. J. Richards, J. P. Hill, K. Okamoto, A. Shundo, M. Akada, M. R. Elsegood, T. Mori, K. Ariga, *Langmuir* **2009**, *25*, 8408-8413.

[21] F. Schramm, D. Walther, H. Görls, C. Käpplinger, R. Beckert, *Z. Naturforsch.* **2005**, *60b*, 843 - 852.

[22] J. Fleischhauer, R. Beckert, Y. Jüttke, D. Hornig, W. Günther, E. Birckner, U. W. Grummt, H. Görls, *Chem. Eur. J.* **2009**, *15*, 12799-12806.

[23] Y.-Y. Liu, C.-L. Song, W.-J. Zeng, K.-G. Zhou, Z.-F. Shi, C.-B. Ma, F. Yang, H.-L. Zhang, X. Gong, *J. Am. Chem. Soc.* **2010**, *132*, 16349-16351.

[24] U. H. Bunz, J. U. Engelhart, *Chem. Eur. J.* **2016**, *22*, 4680-4689.

[25] a) S. Miao, S. M. Brombosz, P. V. Schleyer, J. I. Wu, S. Barlow, S. R. Marder, K. I. Hardcastle, U. H. Bunz, *J. Am. Chem. Soc.* **2008**, *130*, 7339-7344; b) J. U. Engelhart, B. D. Lindner, O. Tverskoy, M. Schaffroth, F. Rominger, U. H. Bunz, *J. Org. Chem.* **2013**, *78*, 1249-1253; c) U. H. Bunz, *Acc. Chem. Res.* **2015**, *48*, 1676-1686.
[26] J. Li, Q. Zhang, *ACS Appl. Mater. Interfaces* **2015**, *7*, 28049-28062.
[27] a) B. D. Lindner, Y. Zhang, S. Höfle, N. Berger, C. Teusch, M. Jesper, K. I. Hardcastle, X. Qian, U. Lemmer, A. Colsmann, U. H. F. Bunz, M. Hamburger, *J. Mater. Chem. C* **2013**, *1*, 5718-5724; b) J. Zhao, G. Li, C. Wang, W. Chen, S. C. J. Loo, Q. Zhang, *RSC Adv.* **2013**, *3*, 9653; c) J. J. Bryant, Y. Zhang, B. D. Lindner, E. A. Davey, A. L. Appleton, X. Qian, U. H. Bunz, *J. Org. Chem.* **2012**, *77*, 7479-7486.
[28] F. A. Cotton, Z. Li, C. Y. Liu, C. A. Murillo, D. Villagrán, *Inorg. Chem.* **2006**, *45*, 767-778.
[29] V. Lami, D. Leibold, P. Fassl, Y. J. Hofstetter, D. Becker-Koch, P. Biegger, F. Paulus, P. E. Hopkinson, M. Adams, U. H. F. Bunz, S. Huettner, I. Howard, A. A. Bakulin, Y. Vaynzof, *Solar RRL* **2017**, *1*, 1700053.
[30] a) P. J. S. Foot, V. Montgomery, C. J. Rhodes, P. Spearman, *Mol. Cryst. Liq. Cryst. Sci. Technol., Sect. A* **1993**, *236*, 199-204; b) A. Mateo-Alonso, N. Kulisic, G. Valenti, M. Marcaccio, F. Paolucci, M. Prato, *Chem. Asian J.* **2010**, *5*, 482-485.
[31] a) K. Hutchinson, G. Srdanov, R. Hicks, H. Yu, F. Wudl, *J. Am. Chem. Soc.* **1998**, *120*, 2989-2990; b) P. Langer, A. Bodtke, N. N. Saleh, H. Görls, P. R. Schreiner, *Angew. Chem. Int. Ed.* **2005**, *44*, 5255-5259; c) S. A. P. Langer, A. Bodtke, N. N. R. Saleh, K. Weisz, H. Görls, P. R. Schreiner, *J. Org. Chem.* **2008**, *73*, 5048-5063.
[32] a) F. Stöckner, R. Beckert, D. Gleich, E. Birckner, W. Günther, H. Görls, G. Vaughan, *Eur. J. Org. Chem.* **2007**, *2007*, 1237-1243; b) S. Herzog, G. Buehrdel, R. Beckert, S. Klimas, E.-U. Würthwein, S. Grimme, H. Görls, *Synthesis* **2009**, *2009*, 4049-4057; c) J. Preßler, R. Beckert, S. Rau, R. Menzel, E. Birckner, W. Günther, H. Görls, *Z. Naturforsch.* **2012**, *67b*, 367-372; d) R. Strathausen, R. Beckert, J. Fleischhauer, D. Müller, H. Görls, *Z. Naturforsch.* **2014**, *69b*, 641-649.
[33] P. Biegger, M. Schaffroth, K. Brödner, O. Tverskoy, F. Rominger, U. H. F. Bunz, *Chem. Commun.* **2015**, *51*, 14844-14847.
[34] B. D. Lindner, J. U. Engelhart, M. Marken, O. Tverskoy, A. L. Appleton, F. Rominger, K. I. Hardcastle, M. Enders, U. H. Bunz, *Chem. Eur. J.* **2012**, *18*, 4627-4633.
[35] K. J. L. Sawtschenko, A. Neudeck, L. Dunsch, *Electrochim. Acta* **1996**, *41*, 123-131.
[36] G. T. W. Ried, *Liebigs Ann. Chem.* **1988**, 1197- 1199.
[37] G. J. Richards, J. P. Hill, N. K. Subbaiyan, F. D'Souza, P. A. Karr, M. R. Elsegood, S. J. Teat, T. Mori, K. Ariga, *J. Org. Chem.* **2009**, *74*, 8914-8923.
[38] S. Shanmugaraju, S. A. Joshi, P. S. Mukherjee, *J. Mater. Chem.* **2011**, *21*, 9130-9138.
[39] C. M. Cardona, W. Li, A. E. Kaifer, D. Stockdale, G. C. Bazan, *Adv. Mater.* **2011**, *23*, 2367-2371.
[40] Z. Liang, Q. Tang, J. Xu, Q. Miao, *Adv. Mater.* **2011**, *23*, 1535-1539.
[41] a) B. D. Lindner, F. Paulus, A. L. Appleton, M. Schaffroth, J. U. Engelhart, K. M. Schelkle, O. Tverskoy, F. Rominger, M. Hamburger, U. H. F. Bunz, *J. Mater. Chem. C* **2014**, *2*, 9609-9612; b) J. U. Engelhart, O. Tverskoy, U. H. Bunz, *J. Am. Chem. Soc.* **2014**, *136*, 15166-15169.
[42] B. A. D. Neto, A. A. M. Lapis, E. N. da Silva Júnior, J. Dupont, *Eur. J. Org. Chem.* **2013**, *2013*, 228-255.
[43] B. A. D. Neto, A. S. Lopes, M. Wüst, V. E. U. Costa, G. Ebeling, J. Dupont, *Tetrahedron Lett.* **2005**, *46*, 6843-6846.
[44] a) V. G. Pesin, V. A. Sergeev, *Khim. Geterotsikl. Soedin.* **1967**, *3*, 839-844; b) E. Perzon, X. Wang, S. Admassie, O. Inganäs, M. R. Andersson, *Polymer* **2006**, *47*, 4261-4268.
[45] a) R. Menzel, E. Täuscher, D. Weiß, R. Beckert, H. Görls, *Z. Anorg. Allg. Chem.* **2010**, *636*, 1380-1385; b) R. Menzel, A. Breul, C. Pietsch, J. Schäfer, C. Friebe, E. Täuscher, D. Weiß, B. Dietzek, J. Popp, R. Beckert, U. S. Schubert, *Macromol. Chem. Phys.* **2011**, *212*, 840-848; c) E. Täuscher, D. Weiß, R. Beckert, J. Fabian, A. Assumpção, H. Görls, *Tetrahedron Lett.* **2011**, *52*, 2292-2294; d) L. K. Calderón-Ortiz, E. Täuscher, E. Leite Bastos, H. Görls, D. Weiß, R. Beckert, *Eur. J. Org. Chem.* **2012**, *2012*, 2535-2541; e) S. H. Habenicht, S. Schramm, M. Zhu,

R. R. Freund, T. Langenstuck, R. Strathausen, D. Weiss, C. Biskup, R. Beckert, *Photochem. Photobiol. Sci.* **2015**, *14*, 2097-2107.

[46] a) K. M. Omer, S. Y. Ku, J. Z. Cheng, S. H. Chou, K. T. Wong, A. J. Bard, *J. Am. Chem. Soc.* **2011**, *133*, 5492-5499; b) T. Miyazaki, M. Shibahara, J. Fujishige, M. Watanabe, K. Goto, T. Shinmyozu, *J. Org. Chem.* **2014**, *79*, 11440-11453; c) D. Jiang, S. Chen, Z. Xue, Y. Li, H. Liu, W. Yang, Y. Li, *Dyes Pigm.* **2016**, *125*, 100-105.

[47] a) M. Jorgensen, Krebs, F. C., *J. Org. Chem.* **2005**, *70*, 6004-6017; b) J. C. Bijleveld, M. Shahid, J. Gilot, M. M. Wienk, R. A. J. Janssen, *Adv. Funct. Mater.* **2009**, *19*, 3262-3270; c) B. Wang, S. W. Tsang, W. Zhang, Y. Tao, M. S. Wong, *Chem. Commun.* **2011**, *47*, 9471-9473.

[48] Y. Lin, H. Fan, Y. Li, X. Zhan, *Adv. Mater.* **2012**, *24*, 3087-3106, 3081.

[49] R. Menzel, D. Ogermann, S. Kupfer, D. Weiß, H. Görls, K. Kleinermanns, L. González, R. Beckert, *Dyes Pigm.* **2012**, *94*, 512-524.

[50] E. Täuscher, R. Beckert, D. Weiß, H. Görls, *Synthesis* **2010**, *10*, 1603-1608.

[51] K. Pilgram, R. D. Skiles, *J. Heterocycl. Chem.* **1974**, *11*, 777-780.

[52] V. G. Pesin, S. A. D'yachenko, E. V. Golubeva, *Khim. Geterotsikl. Soedin.* **1969**, *5*, 619-622.

[53] a) E. Täuscher, L. Calderón-Ortiz, D. Weiß, R. Beckert, H. Görls, *Synthesis* **2011**, *14*, 2334-2339; b) L. Calderón Ortiz, H. Würfel, E. Täuscher, D. Weiß, E. Birckner, H. Görls, R. Beckert, *Synthesis* **2013**, *46*, 126-134.

[54] a) M. Paramasivam, A. Gupta, A. M. Raynor, S. V. Bhosale, K. Bhanuprakash, V. J. Rao, *RSC Adv.* **2014**, *4*, 35318-35331; b) R. Misra, P. Gautam, *Org. Biomol. Chem.* **2014**, *12*, 5448-5457.

[55] a) S. Fery-Forgues, D. Lavabre, *J. Chem. Educ.* **1999**, *76*, 1260-1264; b) A. M. Brouwer, *Pure Appl. Chem.* **2011**, *83*, 2213-2228.

[56] a) M. Grätzel, *Inorg. Chem.* **2005**, *44*, 6841-6851; b) J. E. Coughlin, Z. B. Henson, G. C. Welch, G. C. Bazan, *Acc. Chem. Res.* **2014**, *47*, 257-270.

[57] J.-L. Brédas, J. E. Norton, J. Cornil, V. Coropceanu, *Acc. Chem. Res.* **2009**, *42*, 1691-1699.

[58] a) N. Miki, *Liquid Encapsulation Technology for Microelectromechanical Systems, Advances in Micro/Nano Electromechanical Systems and Fabrication Technologies*, InTech; https://www.intechopen.com/books/advances-in-micro-nano-electromechanical-systems-and-fabrication-technologies/liquid-encapsulation-technology-for-microelectromechanical-systems, **2013**; b) A. Anctil, V. Fthenakis, *Life Cycle Assessment of Organic Photovoltaics, Third Generation Photovoltaics*, InTech; https://www.intechopen.com/books/third-generation-photovoltaics/life-cycle-assessment-of-organic-photovoltaics, **2012**.

[59] a) J. A. Mikroyannidis, D. V. Tsagkournos, S. S. Sharma, Y. K. Vijay, G. D. Sharma, *J. Mater. Chem.* **2011**, *21*, 4679; b) Y. Chen, X. Wan, G. Long, *Acc. Chem. Res.* **2013**, *46*, 2645-2655; c) B. Kan, M. Li, Q. Zhang, F. Liu, X. Wan, Y. Wang, W. Ni, G. Long, X. Yang, H. Feng, Y. Zuo, M. Zhang, F. Huang, Y. Cao, T. P. Russell, Y. Chen, *J. Am. Chem. Soc.* **2015**, *137*, 3886-3893.

[60] a) B. Kan, Q. Zhang, M. Li, X. Wan, W. Ni, G. Long, Y. Wang, X. Yang, H. Feng, Y. Chen, *J. Am. Chem. Soc.* **2014**, *136*, 15529-15532; b) M. Li, W. Ni, H. Feng, X. Wan, Y. Liu, Y. Zuo, B. Kan, Q. Zhang, Y. Chen, *Org. Electron.* **2015**, *24*, 89-95.

[61] C. B. Nielsen, S. Holliday, H. Y. Chen, S. J. Cryer, I. McCulloch, *Acc. Chem. Res.* **2015**, *48*, 2803-2812.

[62] Y. Lin, Y. Wang, J. Wang, J. Hou, Y. Li, D. Zhu, X. Zhan, *Adv. Mater.* **2014**, *26*, 5137-5142.

[63] D. Dang, Y. Zhi, X. Wang, B. Zhao, C. Gao, L. Meng, *Dyes Pigm.* **2017**, *137*, 43-49.

[64] H. Yao, Y. Chen, Y. Qin, R. Yu, Y. Cui, B. Yang, S. Li, K. Zhang, J. Hou, *Adv. Mater.* **2016**, *28*, 8283-8287.

[65] a) B. P. Rand, J. Genoe, P. Heremans, J. Poortmans, *Prog. Photov.* **2007**, *15*, 659-676; b) P. Bäuerle, A. Mishra, *Angew. Chem. Int. Ed.* **2012**, *51*, 2020-2067.

[66] a) A. Mishra, M. K. R. Fischer, P. Bäuerle, *Angew. Chem.* **2009**, *121*, 2510-2536; b) K. Kawabata, M. Saito, I. Osaka, K. Takimiya, *J. Am. Chem. Soc.* **2016**, *138*, 7725-7732.

[67] Y. Lin, X. Zhan, *Mater. Horiz.* **2014**, *1*, 470-488.

[68] P. Gawrys, T. Marszalek, E. Bartnik, M. Kucinska, J. Ulanski, M. Zagorska, *Org. Lett.* **2011**, *13*, 6090-6093.

[69] a) E. Wang, L. Hou, Z. Wang, S. Hellström, W. Mammo, F. Zhang, O. Inganäs, M. R. Andersson, *Org. Lett.* **2010**, *12*, 4470-4473; b) R. Wąsik, P. Wińska, J. Poznański, D. Shugar, *J. Phys. Chem. B* **2012**, *116*, 7259-7268.
[70] D. G. D. Patel, F. Feng, Y.-y. Ohnishi, K. A. Abboud, S. Hirata, K. S. Schanze, J. R. Reynolds, *J. Am. Chem. Soc.* **2012**, *134*, 2599-2612.
[71] C. Wetzel, A. Mishra, E. Mena-Osteritz, K. Walzer, M. Pfeiffer, P. Bäuerle, *J. Mater. Chem. C* **2016**, *4*, 3715-3725.
[72] D. M. de Leeuw, M. M. J. Simenon, A. R. Brown, R. E. F. Einerhand, *Synth. Met.* **1997**, *87*, 53-59.
[73] a) W. J. Beenken, F. Herrmann, M. Presselt, H. Hoppe, S. Shokhovets, G. Gobsch, E. Runge, *Phys. Chem. Chem. Phys.* **2013**, *15*, 16494-16502; b) S.-B. Li, Y.-A. Duan, Y. Geng, H.-B. Li, J.-Z. Zhang, H.-L. Xu, M. Zhang, Z.-M. Su, *Phys. Chem. Chem. Phys.* **2014**, *16*, 25799-25808.
[74] a) A. B. Padmaperuma, *Advances in Materials Physics and Chemistry* **2012**, *2*, 163-172; b) P. Hu, K. Du, F. Wei, H. Jiang, C. Kloc, *Cryst. Growth Des.* **2016**, *16*, 3019-3027.
[75] a) J. R. Huber, W. W. Mantulin, *J. Am. Chem. Soc.* **1972**, 3755-3760; b) M. Sonntag, P. Strohriegl, *Chem. Mater.* **2004**, *16*, 4736-4742; c) T. J. J. Müller, A. W. Franz, C. S. Barkschat, M. Sailer, K. Meerholz, D. Müller, A. Colsmann, U. Lemmer, *Macromol. Symp.* **2010**, *287*, 1-7; d) R. M. Pearson, C. H. Lim, B. G. McCarthy, C. B. Musgrave, G. M. Miyake, *J. Am. Chem. Soc.* **2016**, *138*, 11399-11407.
[76] a) S. Kato, T. Matsumoto, M. Shigeiwa, H. Gorohmaru, S. Maeda, T. Ishi-i, S. Mataka, *Chem. Eur. J.* **2006**, *12*, 2303-2317; b) J. Zhang, W. Chen, A. J. Rojas, E. V. Jucov, T. V. Timofeeva, T. C. Parker, S. Barlow, S. R. Marder, *J. Am. Chem. Soc.* **2013**, *135*, 16376-16379; c) T. C. Parker, D. G. D. Patel, K. Moudgil, S. Barlow, C. Risko, J.-L. Brédas, J. R. Reynolds, S. R. Marder, *Mater. Horiz.* **2015**, *2*, 22-36.
[77] a) Y. Liu, F. Zhang, C. He, D. Wu, X. Zhuang, M. Xue, Y. Liu, X. Feng, *Chem. Commun.* **2012**, *48*, 4166-4168; b) T. Takeda, J. Tsutsumi, T. Hasegawa, S.-I. Noro, T. Nakamura, T. Akutagawa, *J. Mater. Chem. C* **2015**, *3*, 3016-3022.
[78] J. T. Bloking, X. Han, A. T. Higgs, J. P. Kastrop, L. Pandey, J. E. Norton, C. Risko, C. E. Chen, J.-L. Brédas, M. D. McGehee, A. Sellinger, *Chem. Mater.* **2011**, *23*, 5484-5490.
[79] S. H. Habenicht, M. Siegmann, S. Kupfer, J. Kübel, D. Weiß, D. Cherek, U. Möller, B. Dietzek, S. Gräfe, R. Beckert, *Methods Appl. Fluoresc.* **2015**, *3*, 025005.
[80] a) G. Mann, J. F. Hartwig, *J. Am. Chem. Soc.* **1996**, *118*, 13109-13110; b) J. P. Wolfe, S. L. Buchwald, *J. Org. Chem.* **2000**, *65*, 1144-1157.
[81] J. F. Hartwig, *Acc. Chem. Res.* **2008**, *41*, 1534-1544.
[82] T. A. Halgren, *J. Comput. Chem.* **1996**, *17*, 490-519.
[83] T. Yanai, D. P. Tew, N. C. Handy, *Chem. Phys. Lett.* **2004**, *393*, 51-57.
[84] M. J. Frisch, G. W. Trucks, H. B. Schlegel, G. E. Scuseria, M. A. Robb, J. R. Cheeseman, G. Scalmani, V. Barone, B. Mennucci, G. A. Petersson, H. Nakatsuji, M. Caricato, X. Li, H. P. Hratchian, A. F. Izmaylov, J. Bloino, G. Zheng, J. L. Sonnenberg, M. Hada, M. Ehara, K. Toyota, R. Fukuda, J. Hasegawa, M. Ishida, T. Nakajima, Y. Honda, O. Kitao, H. Nakai, T. Vreven, J. A. Montgomery Jr., J. E. Peralta, F. Ogliaro, M. J. Bearpark, J. Heyd, E. N. Brothers, K. N. Kudin, V. N. Staroverov, R. Kobayashi, J. Normand, K. Raghavachari, A. P. Rendell, J. C. Burant, S. S. Iyengar, J. Tomasi, M. Cossi, N. Rega, N. J. Millam, M. Klene, J. E. Knox, J. B. Cross, V. Bakken, C. Adamo, J. Jaramillo, R. Gomperts, R. E. Stratmann, O. Yazyev, A. J. Austin, R. Cammi, C. Pomelli, J. W. Ochterski, R. L. Martin, K. Morokuma, V. G. Zakrzewski, G. A. Voth, P. Salvador, J. J. Dannenberg, S. Dapprich, A. D. Daniels, Ö. Farkas, J. B. Foresman, J. V. Ortiz, J. Cioslowski, D. J. Fox, *Gaussian 09, Revision A.02, Gaussian, Inc., Wallingford, CT* **2009**.
[85] R. Menzel, S. Kupfer, R. Mede, D. Weiß, H. Görls, L. González, R. Beckert, *Eur. J. Org. Chem.* **2012**, *2012*, 5231-5247.
[86] a) S. Admassie, O. Inganäs, W. Mammo, E. Perzon, M. R. Andersson, *Synth. Met.* **2006**, *156*, 614-623; b) W. Alhalasah, R. Holze, *J. Solid State Electrochem.* **2007**, *11*, 1605-1612.
[87] Y. Akimoto, *Bull. Chem. Soc. Jpn.* **1956**, *29*, 460-464.

[88] a) CIBA-SOCIETE, BE614457, **1962**; b) W. Deuschel, G. Riedel, DE1142981B1, **1963**; c) G. Riedel, W. Deuschel, GB970.472, **1964**; d) G. Riedel, W. Deuschel, GB970.471, **1964**; e) C. E. Foster, GB2.430.936A, **2005**.
[89] J. Fleischhauer, S. Zahn, R. Beckert, U.-W. Grummt, E. Birckner, H. Görls, *Chem. Eur. J.* **2012**, *18*, 4549 – 4557.
[90] Z. He, R. Mao, D. Liu, Q. Miao, *Org. Lett.* **2012**, *14*, 4190-4193.
[91] F. Paulus, B. D. Lindner, H. Reiß, F. Rominger, A. Leineweber, Y. Vaynzof, H. Sirringhaus, U. H. Bunz, *J. Mater. Chem. C* **2015**, *3*, 1604-1609.
[92] a) G. Li, Y. Wu, J. Gao, C. Wang, J. Li, H. Zhang, Y. Zhao, Y. Zhao, Q. Zhang, *J. Am. Chem. Soc.* **2012**, *134*, 20298-20301; b) G. J. Richards, S. Ishihara, J. Labuta, D. Miklik, T. Mori, S. Yamada, K. Ariga, J. P. Hill, *J. Mater. Chem. C* **2016**, *4*, 11514-11523.
[93] Q. Tang, J. Liu, H. S. Chan, Q. Miao, *Chemistry* **2009**, *15*, 3965-3969.
[94] M. Bendikov, F. Wudl, D. F. Perepichka, *Chem. Rev.* **2004**, *104*, 4891-4945.
[95] a) B. Kohl, F. Rominger, M. Mastalerz, *Org. Lett.* **2014**, *16*, 704-707; b) B. Kohl, F. Rominger, M. Mastalerz, *Angew. Chem. Int. Ed.* **2015**, *54*, 6051-6056.
[96] a) H. Maeda, T. Maeda, K. Mizuno, K. Fujimoto, H. Shimizu, M. Inouye, *Chem. Eur. J.* **2006**, *12*, 824-831; b) M. Ganschow, S. Koser, S. Hahn, F. Rominger, J. Freudenberg, U. H. Bunz, *Chem. Eur. J.* **2017**, *23*, 4415-4421.
[97] a) L. Wang, L. Yin, C. Ji, Y. Li, *Dyes Pigm.* **2015**, *118*, 37-44; b) P. Gautam, R. Maragani, R. Misra, *RSC Adv.* **2015**, *5*, 18288-18294.
[98] a) J.-Z. Cheng, C.-C. Lin, P.-T. Chou, A. Chaskar, K.-T. Wong, *Tetrahedron* **2011**, *67*, 734-739; b) Y. Jeon, T.-M. Kim, J.-J. Kim, J.-I. Hong, *New J. Chem.* **2015**, *39*, 9591-9595.
[99] T. C. McGill, D. A. Collins, *Semicond. Sci. Technol.* **1993**, *8*, S1-S5.

# Danksagung

Nun möchte ich allen, die mir zum Gelingen dieser Arbeit verholfen haben, meinen aufrichtigen Dank aussprechen.

An erster Stelle danke ich meinem Doktorvater Herrn Professor Dr. R. Beckert, für die Möglichkeit in seiner einzigartigen Arbeitsgruppe promovieren zu dürfen. Dabei durfte ich stets meine Ideen frei verfolgen und mich in diverse Richtungen entfalten. Außerdem danke ich ihm für die vielen konstruktiven und ermutigenden Diskussionen, auch fernab der Chemie.

Zu Dank bin ich der gesamten Arbeitsgruppe (vor allem Dr. Dieter, Dodo, Stefan, Kaufi, Anja und allen kurzzeitigen Mitgliedern) verschuldet, da ich immer eine fröhliche und familiäre Arbeits-, Pausen-, Wander-, Feieratmosphäre vorfand. Jedem wurde bei Problemen aller Art ein (vielleicht auch nicht immer ernst gemeinter) Rat zuteil und jeder durfte so sein wie er ist. Weiterhin will ich auch meinen Hiwi Veit G. Hänsch und meinen Bacheloranten Florian Nöller wegen ihrer erfolgsgekrönten Arbeit und tollen Charaktere erwähnen.

Der gesamten Analytikabteilung des IOMC/IAAC möchte ich für die Anfertigung der NMR- (Dr. Günter, Dr. Bellstedt, Fr. Sentis, Fr. Rambach, Fr. Pielenz) und MS-Spektren (Dr. Poppitz, Fr. Schönau, Fr. Heineck), sowie der EA (Fr. Köhn, Fr. Lentvogt) danken. Besonders möchte ich hierbei Herrn Dr. Görls hervorheben, der selbst aus den kleinsten Kristallen eine Kristallstrukturanalyse zauberte.

Außerdem geht ein großer Dank nach Abu Dhabi an Stefan Schramm und seinen Chef Dr. P. Naumov, durch die meine Veröffentlichungen auf ein höheres Niveau gehoben wurden und dadurch natürlich ihren Teil zum Gelingen dieser Arbeit beitrugen. Herrn Prof. Dr. M. Westerhausen und Steffen Ziemann möchte ich an dieser Stelle auch für die erfolgreiche Zusammenarbeit danken.

Der ehemaligen SG1 sowie allen anderen Freunden und Bekannten meiner Studien- und Promotionszeit gilt ein besonderer Dank, da sie die Zeit nicht nur durch teils hitzige Diskussionen oder Klatsch wie im Flug vergehen ließen, sondern immer für spaßige Abende und Urlaube zu haben waren.

Meinen Freunden aus der Heimat entrichte ich einen herzlichen Dank dafür, dass sie immer für mich da sind, mich verstehen und mir helfen eine Welt ohne Chemie aufrecht zu erhalten.

Zu guter Letzt möchte ich meiner Freundin Stephanie sowie unseren Familien, dabei vor allem meinen Eltern und meinem Bruder, danken für die bedingungslose Hilfsbereitschaft in jeder Lebenslage. Es gibt durchaus wichtigere Dinge als Studium, Promotion oder Forschung.

# Selbstständigkeitserklärung

Ich erkläre, dass ich die vorliegende Arbeit selbständig und nur unter Verwendung der angegebenen Hilfsmittel, persönlichen Mitteilungen und Quellen angefertigt habe.

Jena, der

_____

Dominique M. Gampe

# Anhang

Im Folgenden sind alle hier erwähnten Veröffentlichungen im Original dargestellt. Die Rechte des Nachdrucks wurden von allen Verlagen bezogen. Außerdem sind alle weiterführenden Informationen (Supporting information), sowie der Experimentalteil zu Kapitel 4.3, elektronisch (CD) angehängt.

**Publikation 1:**

„Stable and easily accessible functional dyes: dihydrotetraazaanthracenes as versatile precursors for higher acenes“

D. M. Gampe, M. Kaufmann, D. Jakobi, T. Sachse, M. Presselt, R. Beckert, H. Görls,

*Chem. Eur. J.* **2015**, *21*, 7571-7581.



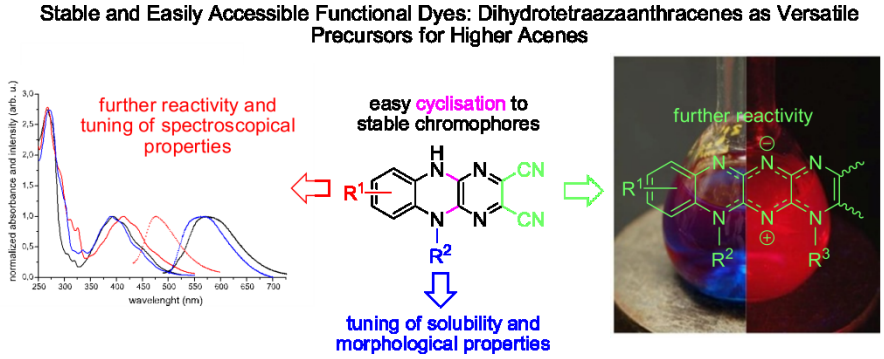

ChemPubSoc Europe DOI: 10.1002/chem.201500230 CHEMISTRY A European Journal Full Paper

Sensitizers

# Stable and Easily Accessible Functional Dyes: Dihydrotetraazaanthracenes as Versatile Precursors for Higher Acenes

Dominique Mario Gampe,[a] Martin Kaufmann,[a, b] Dörthe Jakobi,[a] Torsten Sachse,[b] Martin Presselt,[b] Rainer Beckert,*[a] and Helmar Görls[c]

**Abstract:** A series of new dihydrotetraazaanthracenes and one new dihydrotetraazatetracene as substances for applications in organoelectronic devices and as suitable building blocks for higher azaacenes was synthesised. The condensation of aromatic diamines with dichlorodicyanopyrazine led to these tricyclic/tetracyclic compounds. Syntheses of *N*-substituted phenylenediamines were developed to enable the introduction of multiple functional groups such as ester, amino, or nitro groups on the chromophoric system. Relationships between the structure and the spectroscopic properties could be derived from UV/Vis absorption and fluorescence spectroscopy, as well as by DFT and TD-DFT calculations of molecular and aggregate structures. The absorption spectra are dominated by $\pi$–$\pi^*$ transitions of the single molecules, whereas aggregation needs to be taken into account to obtain reasonable agreement between theory and experiment in certain cases. Single-crystal X-ray analyses were carried out to examine the morphology and solid packing effects. Finally, a dihydrotetraazaanthracene was used as a building-block to create a mesoionic octaazapentacene.

## Introduction

Significant progress is being made in the development of organic electronic and optoelectronic devices.[1] However, many of the recently developed material systems contain scarce or expensive materials, such as redox systems containing ruthenium or fullerenes as acceptor materials, respectively.[2] Generally, the use of expensive materials can negate the advantage of inexpensive, large-scale production of organic electronic devices.[3] Hence, there is huge demand for replacing such systems with stable organic dyes, for example, in solar cells.[4] Since the successful stabilisation of pentacene, linear-condensed acenes have found many applications as versatile organic semiconductors.[5] The replacement of CH by other atoms (mainly N or S) results in heteroacenes in which a different reactivity can be observed. The introduction of nitrogen atoms, particularly, leads to novel properties such as reduced HOMO-LUMO gaps, and especially to dramatically increased chemical stabilities.[6] Recent reviews[7] show that aza-substituted acenes are emerging in charge transport materials as well as in other functional materials. Among the azaacenes, linear systems, for example, **1** "Pyrazinacenes",[8] comprise by far the majority of derivatives. However, the synthesis of higher azaacenes remains challenging because of 1) limited access to appropriate diamines and the corresponding bis-electrophilic partners, 2) low yields of reactions with bis-electrophiles (classic conditions, partially Pd-catalysed), and 3) poor solubility of the azaacenes because of severe aggregation phenomena, which complicates characterisation and processing.

Most of the syntheses described use the condensation reaction of *vicinal* diamines **1** with partners **2** possessing vicinal leaving groups X, as depicted in Scheme 1, in which X = OH,[9] X = halogen: nucleophilic heteroaromatic substitution[10] or Pd-catalysis,[10c] X = CN,[11] diketones,[12] and quinone imines.[13] In all of these cases, the rings A and B themselves can be hetero-

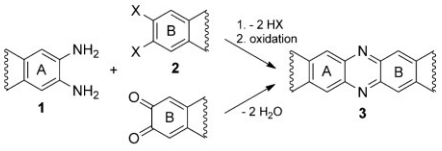


**Scheme 1.** Retrosynthetic approach to azaacenes.

[a] Dipl.-Chem. D. M. Gampe, Dipl.-Chem. M. Kaufmann, D. Jakobi, Prof. Dr. R. Beckert
Friedrich Schiller University Jena
Institute of Organic and Macromolecular Chemistry
Humboldtstraße 10, 07743 Jena (Germany)
E-mail: rainer.beckert@uni-jena.de

[b] Dipl.-Chem. M. Kaufmann, M. Sc. T. Sachse, Dr. M. Presselt
Friedrich Schiller University Jena
Institute of Physical Chemistry
Helmholtzweg 4, 07743 Jena (Germany)

[c] Dr. H. Görls
Friedrich Schiller University Jena
Institute of Inorganic and Analytical Chemistry
Humboldtstraße 8, 07743 Jena (Germany)

Supporting information for this article is available on the WWW under http://dx.doi.org/10.1002/chem.201500230.

ChemPubSoc Europe

CHEMISTRY A European Journal Full Paper

cycles and members of bi- and polycyclic compounds. Cycloadditions of quinodimethides generated in situ[6d,7d] and oxidative *ortho*-annulations,[14a] as well as special methods, for example, for hexaazaanthracenes[14b] and hexaazaacridines,[14c] are rather exceptional.

Tetraazaanthracenes were synthesised in 1988 by the condensation of phenylenediamines with 5,6-dichloro-2,3-dicyanopyrazine;[15] however, their first use as strong acceptors in the form of n-type FET devices was reported in 2004.[16] Miao and co-workers took advantage of these compounds as building blocks for the production of highly electron-deficient hexaazapentacenes and their dihydro precursors.[17]

In the present work, we focus on the synthesis and characterisation of new derivatives of dihydrotetraazaanthracenes **16** and **17** (Scheme 2), because they are easily accessible, starting from a functionalised diamine **10** and **12**, and 5,6-dichloro-2,3-dicyanopyrazine (**14**). We were particularly interested in the introduction of functional substructures R into diamines that are

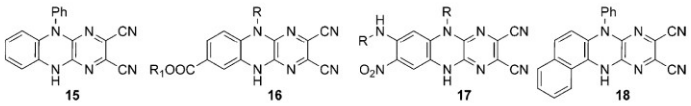


**Scheme 2.** Synthesised tetraaza-substituted dihydroanthracenes.

able to preserve the corresponding dihydroanthracene forms. The substitution at the amino group causes a "frozen" dihydro form and, consequently, prevents oxidation by air. There are examples that such dihydro derivatives show much higher stabilities[18] and intense fluorescence[7c,10a] compared with the fully aromatic species. The simple introduction of substituents enabled us to synthesise a multitude of different dihydroazaanthracenes. The reactions tolerate nearly all functionalities. Therefore, it is possible to introduce electron-withdrawing and electron-donating moieties and, furthermore, solubility-improving groups. Halogen atoms for further cross-coupling experiments and alkyl chains possessing ester groups as precursors for amphiphilic features can also be obtained. The nitro-substituted dihydrotetraazaanthracenes **17** are expected to allow access to higher azaacenes by reduction and subsequent condensation reactions, whereas compounds **16** offer the possibility of modifications to the ester group. In addition, they might serve as precursors for hexaazapentacenes by nucleophilic substitution of the cyano groups.[8,17] To study the properties of extended π-systems, derivative **15** and angular tetracene **18** were both integrated into the study. To investigate the interactions between substituents and dihydroazaacene chromophores, UV/Vis absorption and emission spectroscopy measurements were performed, both of which were supplemented by quantum chemical simulations of the spectral features and line-fit analyses of the experimental spectra.

## Results and Discussion

### Syntheses

Diamines **10** can be obtained in four steps, starting with 4-fluoro benzoic acid through nitration,[19a] followed by esterification,[19b] nucleophilic fluoride substitution and reduction (Scheme 3).[20] The vicinal diamines **12** were prepared starting with 1,5-dichloro-2,4-dinitrobenzene by aminolyses to give **8**.[21] Generally, the reduction of both nitro groups in **9** is possible; however, the tetramino derivatives of type **11** proved to be very sensitive to oxidation and tended to decompose rapidly. Naphthalene derivative **13** was synthesised by azo coupling of commercially available 2-phenylamino-naphthalene with diazotated aniline and subsequent reduction with sodium dithionite.[22]

The model substance **15** was synthesised by cyclisation of *N*-phenyl-*o*-phenylenediamine and **14** (Scheme 4). Triamines **12**, diamines **10**, and naphthalene derivative **13** were cyclised with **14** under the exclusion of oxygen. In all cases, dihydrotetraazaanthracenes **16** and **17** and the angularly fused dihydrotetraazatetracene **18** were isolated as the main products.

Nitro-substituted derivatives **17** and the tetracene **18** show

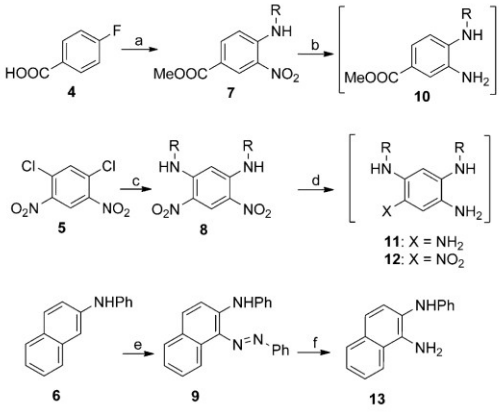


**Scheme 3.** Syntheses of vicinal diamines. Reagents and conditions: a) 1. $KNO_3$, $H_2SO_4$;[19a] 2. $SOCl_2$, MeOH;[19b] 3. R-$NH_2$: 36–99%; b) $H_2$,Pd/C, EtOH; c) EtOH, R-$NH_2$: 40–97%; d) Raney-Nickel, 30% $NH_2NH_2$, EtOH; e) Ph-$NH_2$, $NaNO_2$, EtOH/$H_2O$;[22a] f) $NaS_2O_4$, DMF.[22b]

an intense red colour in both the solid state and in solution, whereas derivatives of type **16** were obtained as orange crystals. All derivatives were fully characterised by means of elemental analysis (EA), MS and NMR experiments.

ChemPubSoc Europe
CHEMISTRY A European Journal Full Paper

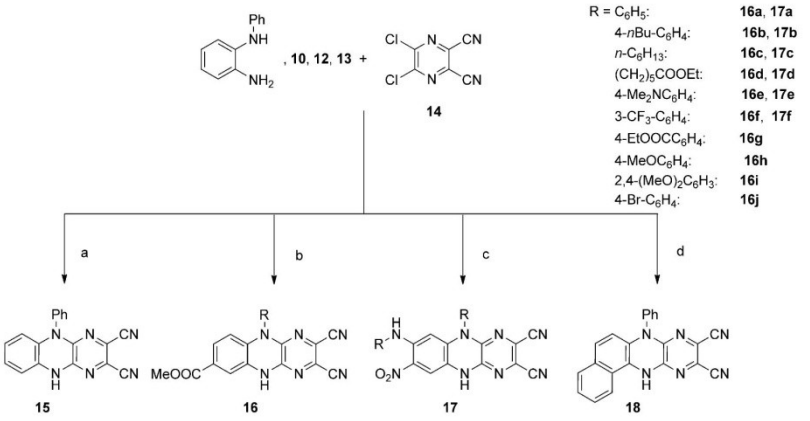


**Scheme 4.** Syntheses of dihydrotetraazaanthracenes **15**–**17** and dihydrotetraazatetracene **18**. Reagents and conditions: a) dioxane, 30 min reflux, 97%; b) EtOH, reflux, 18–65%; c) dioxane, 4 h reflux, overnight 80 °C, 18–35%; d) dioxane, DIPEA, 4 h reflux, 68%.

### Dihydrotetraazaanthracenes 16

Single crystals of **16h** and **16d** that were suitable for X-ray crystallographic analysis were grown by evaporating the solvent from solutions in acetonitrile (**16h**) or acetone (**16d**). The resulting crystal structures are illustrated in Figure 1. The 4-methoxyphenyl substructure in derivative **16h** is distorted with an angle of 78.09° (C4-N2-C11-C12) out of plane. The bond lengths C4–N2, N2–C3, C9–N3, and N3–C10 indicate the involvement of the lone pair of N2 and N3 in the conjugated system.

Contrary to expectations, π–π interactions of the neighbouring stacks of **16h** cannot be observed. As depicted in Figure 2, two molecules form a point symmetric dimer through H-bridges that connect to the next dimer due to the π–π interactions of the 4-methoxyphenyl groups, thus generating a chain-like supramolecule. Despite having a similar structure, derivative **16d** coordinates a solvent molecule at the cyclic NH group, which efficiently prevents the formation of dimers and allows the formation of the π–π-stacking framework.

All derivates of type **16** show a similar UV/Vis absorption behaviour. Typically, the spectra display a strong absorption at approximately 267–274 nm and a less intense absorption at 389–393 nm, indicating that the substituents have only a small electronic influence (Figure 3). The fluorescence spectra are characterised by relatively broad, plateau-like emissions from 552 to 572 nm.

Quantum chemical calculations were performed to identify the origins of the transitions in the visible spectral range utilising the range-corrected functional CAM-B3LYP together with Ahlrichs-pvdz douple-ζ basis set and Grimmes dispersion correction (for technical details, see the Supporting Information), which were shown to yield reliable geometries and UV/Vis absorption spectra at reasonable computational cost.[23–28] A comparison between theoretical and experimental spectra is shown in Figure 4 for **16e** as a representative derivative. The theoretical spectra are represented by a stick spectrum that is additionally broadened by simple Gaussians, with a full-width at half-maximum of 0.2 eV and redshifted by 0.8 eV. Results for those derivatives not shown are almost identical; thus, theory reproduces the experimental observation that exchanging the substituent R has little or no influence on the main chromo-

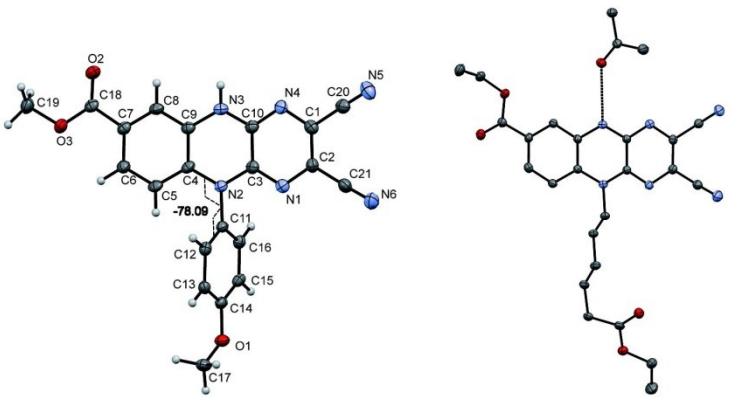


**Figure 1.** View of **16h** (left) and **16d** (right, H-atoms are omitted for clarity).[35]

ChemPubSoc Europe
CHEMISTRY A European Journal Full Paper

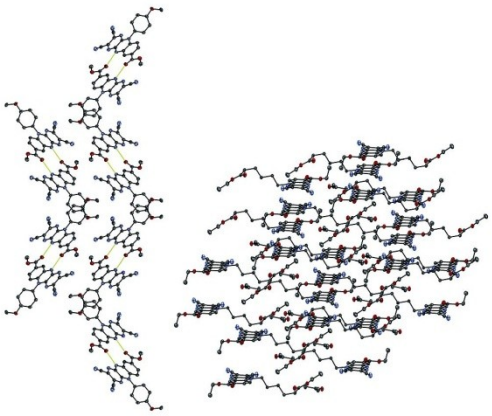

**Figure 2.** View of molecular packing **16h** (left) and **16d** (right).

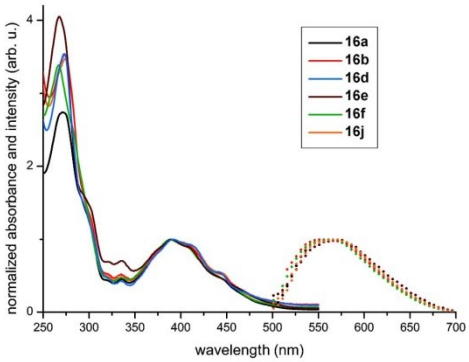


**Figure 3.** Normalised absorption (line) and emission (points) spectra of selected derivatives **16** in acetonitrile. $\lambda_{max}$ absorption/emission for **16a**: 389/562 nm; **16b**: 389/552 nm, **16d**: 391/567 nm, **16e**: 391/572 nm, **16f**: 389/565 nm, and **16j**: 388/552 nm.

phore. This is further substantiated by inspection of the optimised ground-state geometries, which were always characterised by a nearly perpendicular arrangement of the phenyl groups R with respect to the main chromophore, thus, decoupling the two (not shown).

The experimental absorption maximum at approximately 400 nm, which shows a vibrational progression, as well as the low-energy shoulder at approximately 500 nm are well reproduced by the TD-DFT calculations. The intense absorption at approximately 400 nm is largely dominated by a $\pi$–$\pi^*$ transition from the HOMO to the LUMO+1 (contribution to the total electronic transition: $C_i^2$ *100=87.6; the threshold for plotting transition arrows in figures is set at $C_i^2$ *100=20; arrow thicknesses in the transition schemes scale linearly with $C_i^2$), whereas the low-energy transition at approximately 500 nm is from HOMO to LUMO. Both transitions show a weak

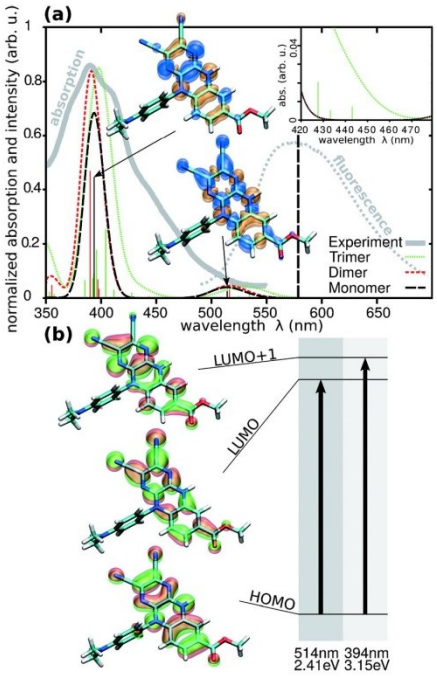


**Figure 4.** a) Broadened and shifted theoretical (monomer, dimer, trimer: dashed lines) and experimental (solid lines) UV/Vis absorption and fluorescence (right spectra, vertical dashed line in case of theory) spectra of derivative **16e**. Charge difference densities are shown for the most prominent monomer transitions. b) Scheme illustrating the orbital contributions to the energetically lowest two transitions of the monomer compound.

charge transfer towards the cyano substituents in addition to their $\pi$–$\pi^*$ character, as shown by the charge difference densities and canonical molecular orbitals in Figure 4a and b. It is notable that none of the substances **16** show any contribution around 450 nm, where the experimental spectrum exhibits a weak and broad shoulder, in their monomer form according to theory. However, progressing to higher aggregates, weak signals emerge in that spectral region, as shown in the inset in Figure 4a. Hence, theory supports the attribution of features around 450 nm to aggregate effects. As examples, the aggregate spectra of **16a**, **16e** and **16f** were calculated and are shown in the Supporting Information.

### Dihydrotetraazatetracenes: Influence of an extended $\pi$-system

We investigated the influence of an extended $\pi$-system or an additional ester group at the chromophoric system on the spectroscopic properties. The UV/Vis and fluorescence spectra of the three comparable compounds are depicted in Figure 5. As assumed, there is no significant difference between the absorption spectra of the tetraaza-substituted dihydroanthra-

ChemPubSoc Europe
CHEMISTRY A European Journal Full Paper

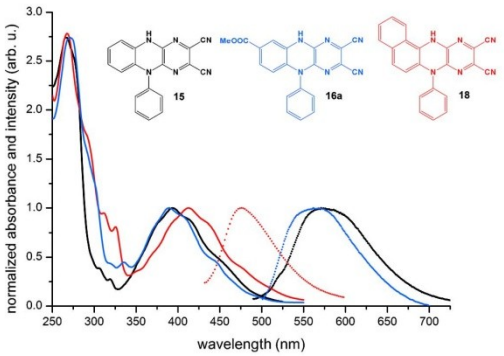


**Figure 5.** Comparison of the spectral data between the tetraaza-substituted dihydroanthracenes **15**, **16a** and dihydrotetracene **18** in acetonitrile (absorption = line; emission = points). $\lambda_{max}$ absorption/emission for **15**: 393/571 nm, **16a**: 389/562 nm, and **18**: 413/476 nm.

cenes of type **15**/**16a** and the dihydrotetracene derivative **18**. The enlarged π-system in **18**, compared with those in **15** and **16a**, means that all frontier molecular orbitals are spatially extended (Figure 6). Thus, the LUMO energy of **18** decreases slightly, whereas the energies of HOMO and LUMO+1 are increased slightly compared with those in **15**. As a consequence, the absorption bands are slightly shifted bathochromically, as seen in the experimental absorption spectra. Furthermore, the energy gap between the first two excited states increases due to the extension of the π-system from **15** to **18**.

In contrast to the rather small spectral differences between the absorption spectra of **15**, **16a** and **18**, a relatively strong deviance was observed in their fluorescence spectra. The tricyclic derivatives exhibit a large shift between the absorption maxima at approximately 390 nm and the fluorescence maxima of approximately 180 nm. However, the onset of the fluorescence spectra fit approximately to the low-energy absorptions at approximately 500 nm (Figure 6). If the low-energy transition is the origin of the fluorescence, the reorganisation energy would be expected to be rather small (energy of vertical transition to the lowest excited state is approximated as 2.49 eV; the 0–0 fluorescence transition energy is estimated at 2.25 eV; thus, the excited state reorganisation energy is approximately 240 meV). The energy difference between the TD-DFT-optimised $S^1$ state and the $S^0$ state at the same geometry of an isolated molecule **15** of 2.17 eV (572 nm) approximately match the energy of the experimental fluorescence spectrum (ca. 2.18 eV, ca. 570 nm).

In contrast to the tricyclic derivatives, the fluorescence of the tetracyclic analogue **18** reveals a much smaller shift between the absorption maximum at 413 nm and the fluorescence maximum at 476 nm of only 63 nm. Thus, the fluorescence appears to originate from the major π–π* excited state at 413 nm, even if our TD-DFT calculations again predict a low-energy absorption at 575 nm, but with very low intensity, and a fluorescence at 641 nm. We assume that the transition from the $S^2$ state to the low-energy $S^1$ state is either forbidden or occurs at a very low rate in **18**. A more detailed analysis of how the structural modifications from substance **15** to **18** change the excited state dynamics will be carried out in a subsequent work.

The aggregation behaviour of such polycyclic aromatic compounds is crucial for the electronic properties in the solid state or thin film. Therefore, we studied the intermolecular interactions by X-ray single-crystal analysis (see Figure 7). The crystals were grown by slowly evaporating the solvents from solutions of chloroform/ethanol (**15**) or acetonitrile (**18**).

Whereas **15** exhibits dimeric structures, **18** forms a step-like π-stacking network. The distance between those steps is an even 3.315 Å because of an effective interaction, and the polymeric stacks of **18** are connected to each other because of the solvent molecules. Every dihydrotetracene unit is linked by H-bonds to an acetonitrile molecule, which itself interacts with the neighbouring dihydrotetracene stack.

The dimeric structure in the case of **15** results in alternating distances between the planes in the packing; depending on the kind of interaction, they are 3.398 or 3.634 Å. The dimers are connected through H-bonds between the phenyl moieties and the nitrogen of the pyrazine unit from the neighbouring dihydroanthracene plane (3.634 Å). The substructure on the rear of each dimer is related through π-interactions to the next (3.398 Å).

### Nitro-substituted dihydrotetraazaanthracenes 17

Compared with derivatives of type **16**, nitro-substituted dihydrotetraazaanthracenes **17** give rise to complex absorption spectra. The strongest absorptions of **17a**–**d** are located at $\lambda =$ 367–376 nm. Whereas alkyl-substituted derivatives **17c** and **17d** show a further absorption at $\lambda \approx 448$ nm, those possessing aromatic residues show only a shoulder. All derivatives in the long-wavelength region exhibit two overlapping peaks between 504 and 550 nm. In the presence of a strong *para*-donor substituent (dimethylamino, **17e**), the spectrum differs from those discussed previously, particularly in the spectral range between 350 and 457 nm, where it features a single broad absorption band that is centred at approximately 430 nm. The absorption bands of derivatives **17a**–**d** between 350 and 457 nm appear to be slightly redshifted in the case of **17f**. In contrast to the other derivatives **17**, lower energetic absorption bands (cf. 475–600 nm) are unresolved for **17f**. Given that all derivatives **17** contain a nitro group, mesomerism is possible, in which the substituted nitrogen acts as an electron donor. This results in a quinoid substructure, in which the nitro group accepts the electron pair (see Scheme 5). Such a structure may be the reason for the strong bathochromically shifted absorbance compared with the other dihydroazaanthracenes described (**15** and **16**).

To enable a reliable interpretation of the peaks found in the absorption spectra of **17** (Figure 8), we performed line-fit analyses of the experimental spectra to deconvolute the electronic transitions from vibrational progression and we performed quantum chemical calculations to unravel the origin of the

ChemPubSoc Europe
CHEMISTRY A European Journal Full Paper

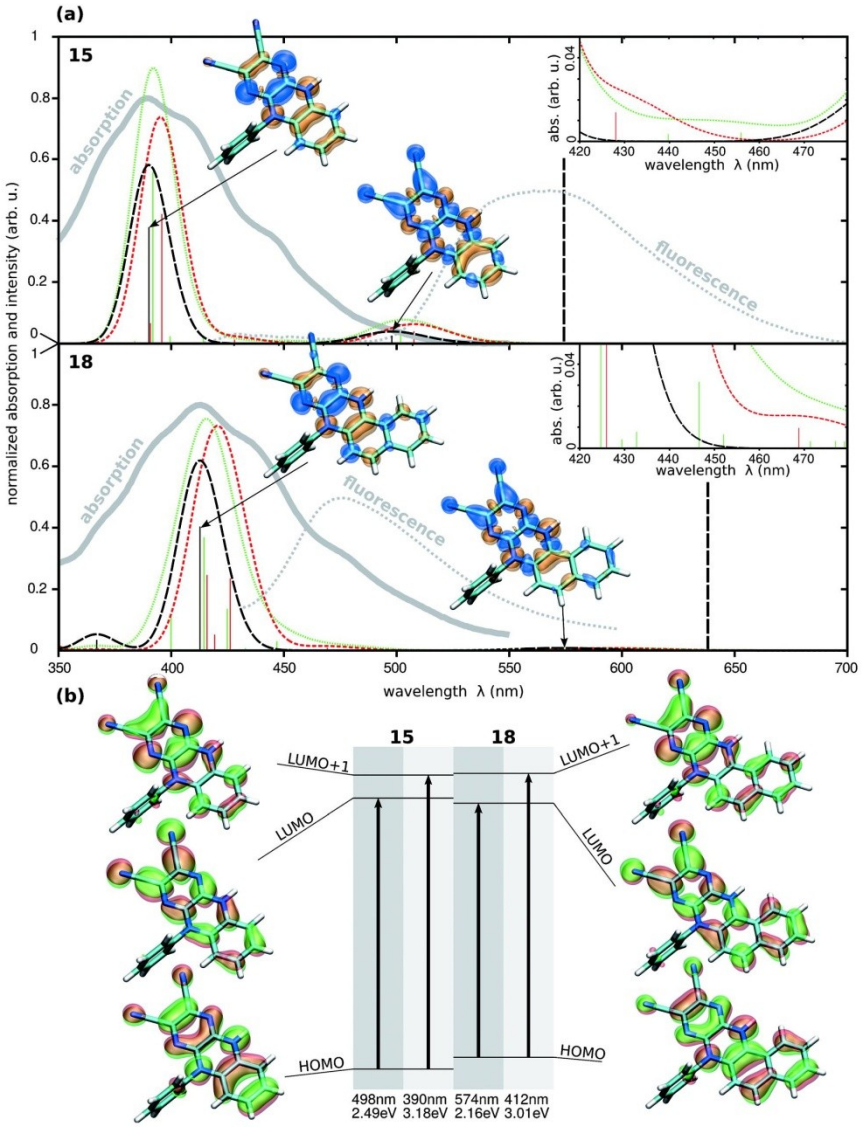


**Figure 6.** a) Broadened and shifted theoretical (monomer, dimer, trimer: dashed lines) and experimental (solid lines) UV/Vis absorption and fluorescence (right spectra, vertical dashed line in case of theory) spectra of derivatives **15** and **18**. Charge different densities that result instantaneously with photoexcitation are shown for the most prominent monomer transitions. b) Scheme illustrating the orbital contributions to the energetically lowest two transitions of **15** and **18**.

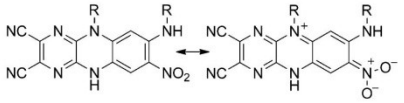

**Scheme 5.** Mesomeric structures of derivatives **17**.

electronic transitions. As examples, the results of these calculations are shown in Figure 9 for derivatives **17b**, **17d** and **17e**. In contrast to the spectra shown in Figure 4 and Figure 6, we found three prominent peak structures around 525, 425 and 360 nm in Figure 9 to be best described by each using an ordinary vibrational progression[29] (for details see the Supporting

ChemPubSoc Europe
CHEMISTRY A European Journal Full Paper

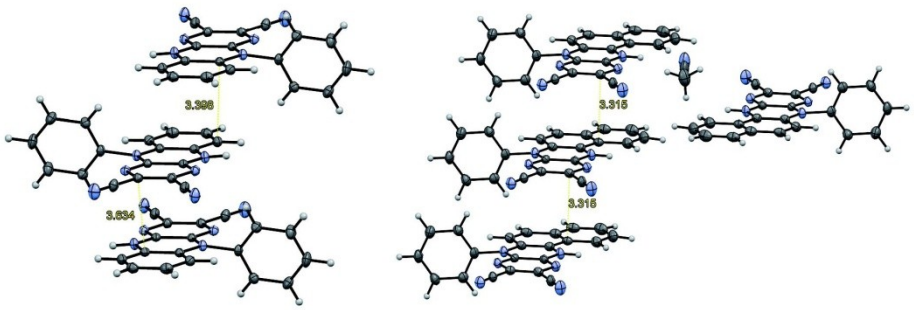


**Figure 7.** Comparison between the packing of **15** (left) and **18** (right). Yellow lines show the interaction between atoms.[35]

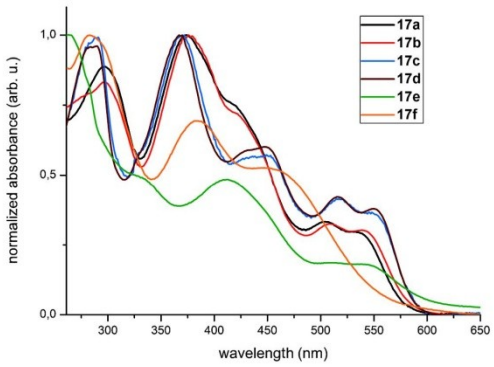


**Figure 8.** Normalised UV/Vis spectra of selected nitro-substituted dihydrotetraazaanthracenes of type **17** in acetonitrile. $\lambda_{max}$ absorption for **17a**: 372 nm, **17b**: 376 nm, **17c**: 370 nm, **17d**: 367 nm, **17e**: 413 nm, and **17f**: 382 nm.

Information). The vibrational progressions derived from the experimental spectra are applied to broaden the vertical pure electronic transitions derived from the TD-DFT calculations, as seen in Figure 9. In the TD-DFT calculations, we considered different conformers by means of a generalised rotamer search algorithm[30,31] with subsequent quantum chemical optimisation. We found the central absorptions between 350 and 500 nm of the conformers of any particular derivative **17** to differ significantly only if R contained a phenyl-ring, yielding two distinct conformers in each case: the two residuals pointing away from each other, that is, angular, and a face-to-face configuration of the rings. Alkyl chains turned out to have only a very weak impact on the resulting spectra, although the actual conformer geometries differed greatly.

Considering that the experimental absorption spectra of **17a** and **17b** are very similar (cf. Figure 8), we focus on the spectral features of our TD-DFT results regarding **17b** in the following. As shown in Figure 9, the experimental spectrum could be reproduced well by using a semiempirical approach; that is, by using absorption parameters derived ab initio together with those obtained from line-fits of the experimental spectra, particularly for the face-to-face conformer. The absorption features observed experimentally at 375, 425 and 525 nm originate basically from HOMO to LUMO+2, LUMO+1 and LUMO (in the latter case, the HOMO–LUMO excitation largely dominates the total electronic transition: $C_i^2$ *100=85) transitions, respectively. Whereas for the face-to-face conformer, only the peak at approximately 525 nm is underestimated in its relative oscillator strength by the TD-DFT calculations, both the peaks at 525 and 425 nm are underestimated for the angular conformer. In the case of the alkyl-substituted derivatives **17c** and **17d**, the experimental absorption spectra are very similar and we focus discussion of the particular features on **17d**. As in the case of **17b**, the simulated absorption spectrum of the **17d** face-to-face conformer (in the case of alkyl-substitution labelled as cisoidal), fits the experimental spectrum better than the simulated absorption spectrum of the angular conformer, as shown in Figure 9. The energy spacing between the three major electronic transitions is particularly large and the long-wavelength absorption at approximately 525 nm is significantly more intense in the case of the cisoidal conformer compared with the angular conformer.

In the case of the dimethyl-amino-phenylene-substituted derivative **17e**, the broad absorption at approximately 430 nm is reproduced basically by a single electronic transition for the angular conformer and by two superposed, similarly intense transitions for the face-to-face conformer. The low-energy absorption between 500 and 550 nm is again predicted to be too low for both conformers, whereas the face-to-face conformer shows significantly higher oscillator strength for this low-energy absorption.

In the case of **17f**, the semiempirical description of the absorption spectra presented above failed because of the lack of visible vibrational progression in the spectra. Furthermore, the theoretical spectra of **17f** could not reproduce the experimental findings at all and, instead, gave results that were qualitatively similar to those obtained with **17e**. This might be due to aggregation effects mediated by the spatially small residuals in the solution and will be subject to further investigation. It should be noted that, given the results shown in Figures 4 and

ChemPubSoc Europe
CHEMISTRY A European Journal Full Paper

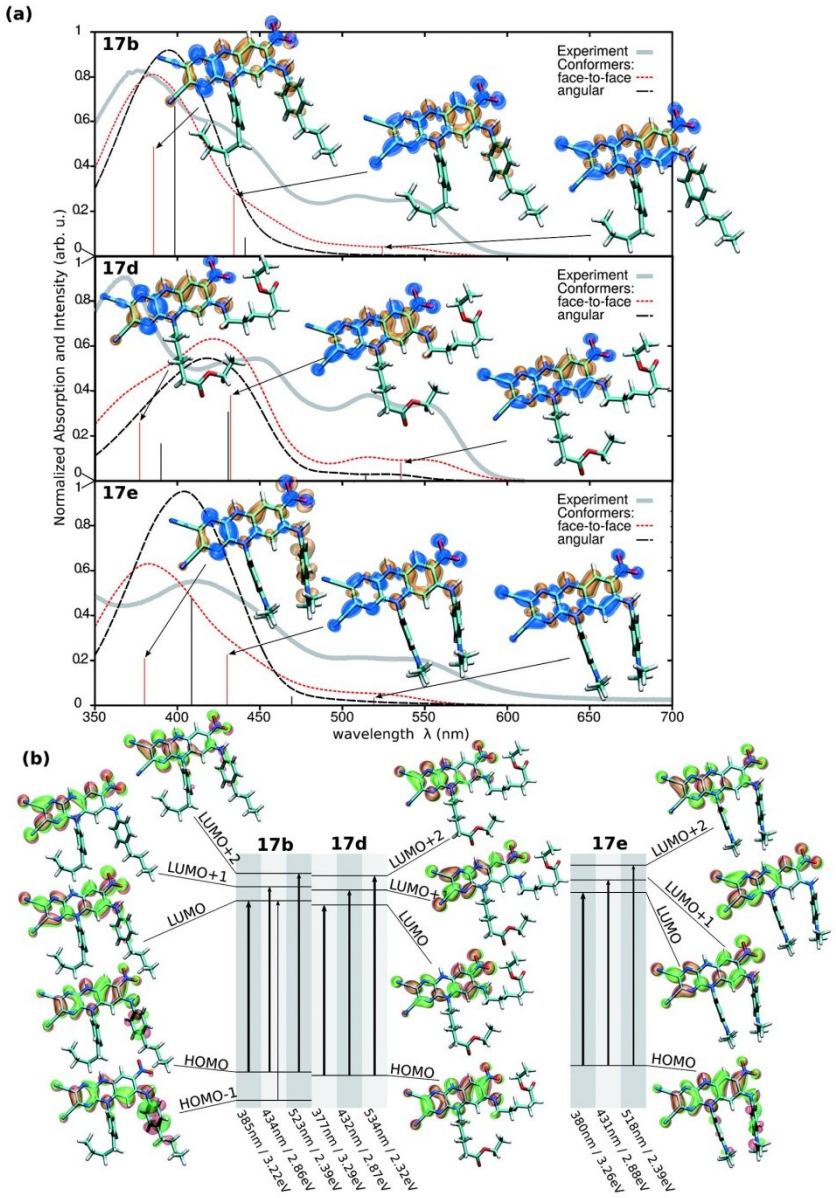


**Figure 9.** a) Broadened and shifted theoretical (monomer, dashed line) and experimental (solid line) UV/Vis absorption spectra of derivatives **17 b**, **17 d** and **17 e**. Transition densities are shown for the most prominent monomer. b) Scheme illustrating the orbital contributions to the lowest three transitions of the three substances.

6, agreement between theory and experiment is expected to improve if aggregates of derivates **17** are investigated.

Contrary to other dihydrotetraazaanthracenes presented here, none of the nitro derivatives **17** measured showed fluorescence. The changes in the absorption and emission behaviour compared with derivatives **15**, **16** and **18** can possibly be attributed to the presence of the nitro group. This functional group is well-known

ChemPubSoc Europe

CHEMISTRY A European Journal Full Paper

for its ability to act as a quencher of fluorescence in many cases.[32]

### Imidazodihydroanthracenes

In a first attempt to cyclise the tetramines **11** synthesised in situ with **14**, the yellow-fluorescent imidazodihydroanthracene derivatives **19** were isolated instead of the desired octaazapentacenes (Scheme 6). Most likely, the reason for the formation of

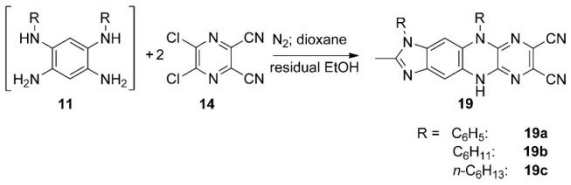


**Scheme 6.** Tetracyclic imidazoles **19** as unexpected cyclisation products (30–58%).

derivatives **19** is the oxidising capacity of the cyclisation partner **14**. Together with small amounts of ethanol, which was used as a solvent, acetic acid could be formed in the course of a redox reaction. In a subsequent cyclisation reaction, this reactive acid was able to easily transform one diamine part of **11** to yield the 2-methylimidazole derivatives of type **19**.

These novel imidazole derivatives **19** were isolated in the form of intense yellow-orange solids. Their solubilities increase, as expected, from the phenyl derivative **19a** through **19b** (cyclohexyl) to the long-chained **19c** (*n*-hexyl). The UV/Vis spectra reveal that the chemical nature of the R group does not exert any influence on the chromophoric system (Figure 10). All derivatives show a strong absorption band at 305 nm and a second broad band in the range around 410 nm. Larger differences arise from the fluorescence spectra: whereas derivative **19a** shows a substantial emission at $\lambda = 529$ nm, that of **19c** is bathochromically shifted by 32 nm.

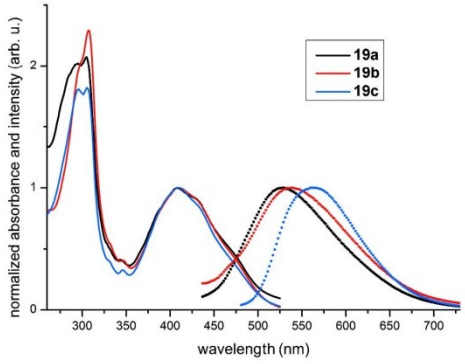


**Figure 10.** Normalised absorption (line) and emission (points) spectra of compounds **19** in acetonitrile. $\lambda_{max}$ absorption/emission for **19a**: 408/529 nm, **19b**: 409/539 nm, and **19c**: 409/561 nm.

The similar absorption behaviour of derivatives **19** could be explained by examining their X-ray structure. We succeeded in obtaining single crystals from **19a** and its X-ray crystal structure is depicted in Figure 11. The central tetranuclear unit is almost ideally planar, but the phenyl residues are twisted significantly, with torsion angles of 57.6° (C2-N1-C13-C14) and 68.2° (C4-N2-C19-C24) out of the plane. As a result of this twisting, there is no interaction between the π-electrons of the imidazodihydroanthracene unit and the phenyl moieties. Therefore, the chromophoric system does not seem to be enlarged (in **19a**) compared with the aliphatic substituted derivatives (**19b**, **19c**), which explains the almost identical absorption behaviour of the three derivatives.

A different approach to yield even larger azaacenes than discussed in the previous section was enabled by our development of derivatives **17**. Thus, we succeeded in synthesising derivatives of octaazapentacene of type **22d**, as illustrated in Scheme 7. We were recently successful in reducing the nitro group

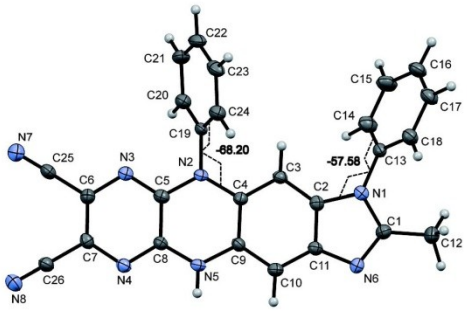


**Figure 11.** View of **19a** showing the atom-numbering scheme.[35]

in **17d** by means of Pd on activated charcoal and hydrogen gas, and obtained a green fluorescent diamine of type **20d**. This proved to be very sensitive to atmospheric oxygen and was, therefore, cyclised in situ with **14**. In our initial studies, we isolated derivative **22d** in yields of approximately 10% as a deep-blue solid with gold metallic luster. $^1$H NMR spectra and MS data indicate the presence of the expected derivative of octaazapentacene. It is noteworthy that the tetrahydro derivative **21d** formed primarily was immediately oxidised to the mesoionic azaacene (Scheme 7). It was nearly impossible to isolate the intermediate substance **21d**; the red solution very rapidly becomes blue with red emission (Scheme 7). Furthermore, we could not detect N–H signals in the $^1$H NMR spectrum. Additionally, the pentacene obtained shows similar spectroscopic properties to that of the mesoionic hexaazapentacene developed by Fleischhauer et al.,[33] particularly with respect to the broad-structured absorption behaviour in the orange to red region of the visible spectrum. However, the absorption is, perhaps due to the electron-withdrawing cyano residues, slightly redshifted by approximately 21 nm compared

ChemPubSoc Europe

CHEMISTRY A European Journal Full Paper

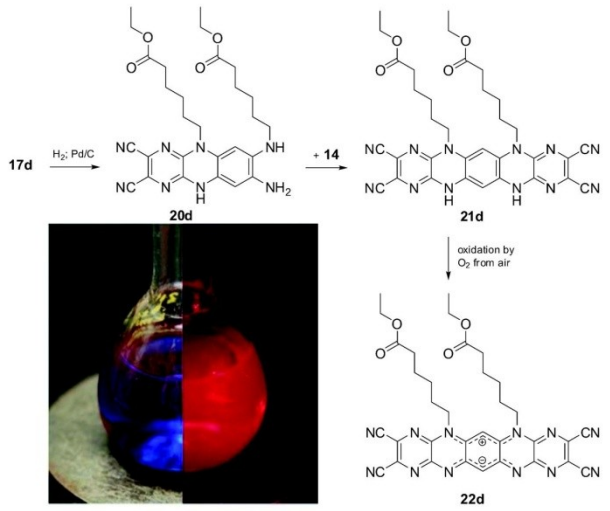


**Scheme 7.** Using the building block for synthesis of higher azaacenes; for example, derivative **17d**. Photographs of compound **22d** dissolved in $CH_2Cl_2$ in daylight (left) and under irradiation with $\lambda = 365$ nm (right).

with the hexaazapentacene described by Fleischhauer. In addition, the small Stokes shift of the red emission points to low energy loss after excitation, which is typical for rigid systems such as higher acenes.[34] The positions of residues in diamine **20d** mean that the pentacene has to be mirror symmetric, as depicted in derivative **21d**. Currently, we cannot provide any information concerning the electronic state; however, experimental data (ESR measurements) suggest a singlet and thus mesoionic state for molecule **22d**. This is consistent with the findings of other groups for hexaazaanthracenes[14b] and hexaazaacridines.[14c]

To our knowledge, the synthesised pyrazinacene **22d** represents the zwitterionic pentacene with the highest number of N atoms discovered to date.

## Conclusion

Our attempt to develop novel dihydrotetraazaanthracenes **16** and **17** as new materials for use in organic electronic devices has been realised by cyclisation reactions of *N*-substituted *o*-phenylenediamines with **14** in moderate yields. Analogously, 1-amino-2-phenylaminonaphthalene was successfully transformed into dihydrotetraazatetracene **18**. The presence of moieties such as bromine groups or ester substructures means that derivatives **16** provide opportunities to introduce further functional groups through cross-coupling or transesterification reactions. All new derivatives feature intense absorptions in the yellow-orange region of the visible spectrum. Donor/acceptor substituents at the peripheric phenyl moieties affect, in the case of derivatives **16**, their UV/Vis spectra only slightly. Whereas dihydrotetraazaanthracenes **16** and dihydrotetraazatetracene **18** show dramatically different shifted fluorescence, hence indicating slow relaxation from higher excited states to the $S^1$ state in **18**, none of the nitro derivatives of type **17** are fluorescent. An unexpected result was obtained by cyclisation of tetramines **10**, synthesised in situ, with **14**. Instead of tetrahydrooctaazapentacenes **21**, the yellow-fluorescent derivatives of imidazodihydroanthracenes **19** were isolated and fully characterised. All three groups of dihydrotetraazaacenes presented here possess the preconditions to serve as building-blocks for higher azaacenes (see Scheme 8). The nitro group of derivates **17** can be reduced to another vicinal diamine, which, in subsequent reactions, can be cyclised with a wide range of bis-electrophilic partners (e.g., with **14** to the mesoionic octaazapentacenes **22**). Additionally, all our dihydroazaacenes contain a vicinal dicyano substructure, which is suitable for further condensation reactions with diamines. Previously, this twofold extrusion of hydrogen cyanide formed the basis for the synthesis of a series of edge-sharing condensed oligopyrazine analogues.[8] By using both routes, we were already successful in the synthesis of higher azaacenes, which are redox switchable systems with interesting properties such as high photostability, large molar extinction coefficient and fluorescent quantum yield. We will report in a forthcoming paper on the use of derivatives **17** as starting material for the construction of derivatives of octaazapentacene and their redox behaviour, as well as on other unsymmetrical azaacenes, using **16**, and their application as functional dyes.

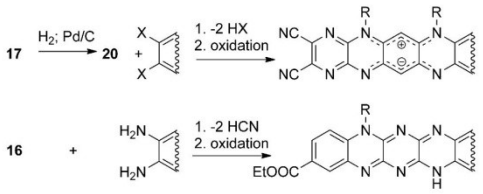


**Scheme 8.** Dihydroazaanthracenes as suitable building blocks for higher azaacenes.

## Experimental Section

Further details of the synthetic procedures, quantum chemical calculations, NMR spectra and single-crystal X-ray data can be found in the Supporting Information.

ChemPubSoc Europe

CHEMISTRY
A European Journal
Full Paper

### Acknowledgements

We thank Professor Todd Martínez and Julia Preiß for scientific exchange and support. Additionally, we thank Dr. Günther, G. Sentis and H. Heinecke from HKI Jena for measuring the NMR spectra, Mrs Schönau and Mrs Heineck for the measurement of the MS spectra. M.K., T.S. and M.P. gratefully acknowledge financial support from the "Bundesministerium für Bildung und Forschung" (FKZ: 03K3507). T.S. furthermore acknowledge financial support from the "Deutsche Bundesstiftung Umwelt".

**Keywords:** chromophores · cyclization · density functional calculations · nitrogen heterocycles · sensitizers

[1] a) M. A. Green, K. Emery, Y. Hishikawa, W. Warta, E. D. Dunlop, *Prog. Photovoltaics* **2014**, *22*, 1–9; b) J. You, L. Dou, K. Yoshimura, T. Kato, K. Ohya, T. Moriarty, K. Emery, C.-C. Chen, J. Gao, G. Li, Y. Yang, *Nat. Commun.* **2013**, *4*, 1446–1456; c) R. Fitzner, E. Mena-Osteritz, A. Mishra, G. Schulz, E. Reinold, M. Weil, C. Korner, H. Ziehlke, C. Elschner, K. Leo, M. Riede, M. Pfeiffer, C. Uhrich, P. Bäuerle, *J. Am. Chem. Soc.* **2012**, *134*, 11064–11067.

[2] a) M. Grätzel, *J. Photochem. Photobiol. C* **2003**, *4*, 145–153; b) P. Wang, S. M. Zakeeruddin, J. E. Moser, M. K. Nazeeruddin, T. Sekiguchi, M. Grätzel, *Nat. Mater.* **2003**, *2*, 402–407; c) M. Grätzel, *Acc. Chem. Res.* **2009**, *42*, 1788–1798; d) S. Tschierlei, M. Presselt, C. Kuhnt, A. Yartsev, T. Pascher, V. Sundström, M. Karnahl, M. Schwalbe, B. Schäfer, S. Rau, M. Schmitt, B. Dietzek, J. Popp, *Chem. Eur. J.* **2009**, *15*, 7678–7688; e) B. Schäfer, H. Görls, M. Presselt, M. Schmitt, J. Popp, W. Henry, J. G. Vos, S. Rau, *Dalton Trans.* **2006**, *18*, 2225–2231.

[3] a) N. Li, D. Baran, K. Forberich, F. Machui, T. Ameri, M. Turbiez, M. Carrasco-Orozco, M. Drees, A. Facchetti, F. C. Krebs, C. J. Brabec, *Energy Environ. Sci.* **2013**, *6*, 3407–3413; b) M. Grätzel, R. A. J. Janssen, D. B. Mitzi, E. H. Sargent, *Nature* **2012**, *488*, 304–312; c) H. Hoppe, N. S. Sariciftci, *J. Mater. Res.* **2004**, *19*, 1924–1945; d) M. Al-Ibrahim, H. K. Roth, U. Zhokhavets, G. Gobsch, S. Sensfuss, *Sol. Energy Mater. Sol. Cells* **2005**, *85*, 277; e) F. C. Krebs, *Sol. Energy Mater. Sol. Cells* **2009**, *93*, 465–475; f) L. Blankenburg, K. Schultheis, H. Schache, S. Sensfuss, M. Schroedner, *Sol. Energy Mater. Sol. Cells* **2009**, *93*, 476–483.

[4] F. C. Krebs, *Org. Electron.* **2009**, *10*, 761–768.

[5] a) A. R. Reddy, M. Bendikov, *Chem. Commun.* **2006**, 1179–1181; b) O. Berg, E. L. Chronister, T. Yamashita, G. W. Scott, R. M. Sweet, J. Calabrese, *J. Phys. Chem. A* **1999**, *103*, 2451–2459; c) J. E. Anthony, *Angew. Chem. Int. Ed.* **2008**, *47*, 452–483; *Angew. Chem.* **2008**, *120*, 460–492; d) L. B. Roberson, J. Kowalik, L. M. Tolbert, C. Kloc, R. Zeis, X. Chi, R. Fleming, C. Wilkins, *J. Am. Chem. Soc.* **2005**, *127*, 3069–3075; e) O. D. Jurchescu, M. Popinciuc, B. J. vanWees, T. T. M. Palstra, *Adv. Mater.* **2007**, *19*, 688–692; f) O. D. Jurchescu, J. Baas, T. T. M. Palstra, *Appl. Phys. Lett.* **2004**, *84*, 3061–3063; g) T. Minakata, Y. Natsume, *Synth. Met.* **2005**, *153*, 1–5; h) J. Takeya, C. Goldmann, S. Haas, K. P. Pernstich, B. Ketterer, B. Batlogg, *J. Appl. Phys.* **2003**, *94*, 5800–5804.

[6] a) P. J. S. Foot, V. Montgomery, C. J. Rhodes, P. Spearman, *Mol. Cryst. Liquid Cryst.* **1993**, *236*, 199–204; b) H.-Y. Chen, I. Chao, *ChemPhysChem* **2006**, *7*, 2003–2007; c) J. I. Wu, C. S. Wannere, Y. Mo, P. v. R. Schleyer, U. H. F. Bunz, *J. Org. Chem.* **2009**, *74*, 4343–4349; d) Y.-Y. Liu, C.-L. Song, W.-J. Zeng, K.-G. Zhou, Z.-F. Shi, C.-B. Ma, F. Yang, H.-L. Zhang, X. Gong, *J. Am. Chem. Soc.* **2010**, *132*, 16349–16351.

[7] a) S. Miao, A. L. Appleton, N. Berger, S. Barlow, S. R. Marder, K. I. Hardcastle, U. H. F. Bunz, *Chem. Eur. J.* **2009**, *15*, 4990–4993; b) U. H. F. Bunz, *Pure Appl. Chem.* **2010**, *82*, 953–968; c) G. J. Richards, J. P. Hill, T. Mori, K. Ariga, *Org. Biomol. Chem.* **2011**, *9*, 5005–5017; d) Q. Miao, *Synlett* **2012**, *23*, 326–336; e) U. H. F. Bunz, J. U. Engelhart, B. D. Lindner, M. Schaffroth, *Angew. Chem. Int. Ed.* **2013**, *52*, 3810–3821; *Angew. Chem.* **2013**, *125*, 3898–3910.

[8] G. J. Richards, J. P. Hill, N. K. Subbaiyan, F. D'Souza, P. A. Karr, M. R. J. Elsegood, S. J. Teat, T. Mori, K. Ariga, *J. Org. Chem.* **2009**, *74*, 8914–8923.

[9] a) C. Seillan, H. Brisset, O. Siri, *Org. Lett.* **2008**, *10*, 4013–4016; b) Z. He, D. Liu, R. Mao, Q. Tang, Q. Miao, *Org. Lett.* **2012**, *14*, 1050–1053.

[10] a) F. Stöckner, R. Beckert, D. Gleich, E. Birckner, W. Günther, H. Görls, G. Vaughan, *Eur. J. Org. Chem.* **2007**, 1237–1243; b) Z. He, R. Mao, D. Liu, Q. Miao, *Org. Lett.* **2012**, *14*, 4190–4193; c) J. U. Engelhart, B. D. Lindner, O. Tverskoy, F. Rominger, U. H. F. Bunz, *Org. Lett.* **2012**, *14*, 1008–1011.

[11] G. J. Richards, J. P. Hill, K. Okamoto, A. Shundo, M. Akada, M. R. J. Elsegood, T. Mori, K. Ariga, *Langmuir* **2009**, *25*, 8408–8413.

[12] a) Y. Fogel, M. Kastler, Z. Wang, D. Andrienko, G. J. Bodwell, K. Müllen, *J. Am. Chem. Soc.* **2007**, *129*, 11743–11749; b) S. Miao, S. M. Brombosz, P. v. R. Schleyer, J. I. Wu, S. Barlow, S. R. Marder, K. I. Hardcastle, U. H. F. Bunz, *J. Am. Chem. Soc.* **2008**, *130*, 7339–7344.

[13] F. Wudl, P. A. Koutentis, A. Weitz, B. Ma, T. Strassner, K. N. Houk, S. I. Khan, *Pure Appl. Chem.* **1999**, *71*, 295–302.

[14] a) J. Preßler, R. Beckert, S. Rau, R. Menzel, E. Birckner, W. Günther, H. Görls, *Z. Naturforsch.Sect. B* **2012**, *67*, 0367–0372; b) K. Hutchison, G. Srdanov, R. Hicks, H. Yu, F. Wudl, *J. Am. Chem. Soc.* **1998**, *120*, 2989–2990; c) P. Langer, A. Bodtke, N. N. R. Saleh, H. Görls, P. R. Schreiner, *Angew. Chem. Int. Ed.* **2005**, *44*, 5255–5259; *Angew. Chem.* **2005**, *117*, 5389–5393.

[15] G. T. W. Ried, *Liebigs Ann. Chem.* **1988**, 1197–1199.

[16] J. Nishida, N. Naraso, S. Murai, E. Fujiwara, H. Tada, M. Tomura, Y. Yamashita, *Org. Lett.* **2004**, *6*, 2007–2010.

[17] R. M. Z. He, R. Mao, D. Liu, Q. Miao, *Org. Lett.* **2012**, *14*, 4190–4193.

[18] a) E. Clar, *The Aromatic Sextet*, Wiley, New York, **1972**; b) Q. Miao, T. Q. Nguyen, T. Someya, G. B. Blanchet, C. Nuckolls, *J. Am. Chem. Soc.* **2003**, *125*, 10284–10287.

[19] a) K. Shang, J. Gallagher, N. M. Bie, F. Li, Q. Che, Y. Wang, Y. Jiang, *J. Org. Chem.* **2014**, *79*, 5134–5144; b) S. Munack, V. Leroux, K. Roderer, M. Ökvist, A. van Eerde, L.-L. Gundersen, U. Krengel, P. Kast, *Chem. Biodiversity* **2012**, *9*, 2507–2527.

[20] H. G. O. Becker, *Organikum*, 23rd ed., Wiley-VCH, Weinheim, **2009**.

[21] A. J. Boydston, C. S. Pecinovsky, S. T. Chao, C. W. Bielawski, *J. Am. Chem. Soc.* **2007**, *129*, 14550–14551.

[22] a) E. E. Kostyuchenko, V. F. Traven, R. A. Mkhitarov, B. I. Stepanov, *Zh. Org. Khim.* **1980**, *16*, 1702–1707; b) L. F. Tietze, Th. Eicher, Reaktionen und Synthesen im organisch-chemischen Praktikum und Forschungslaboratorium, 2nd ed., Thieme, Stuttgart, **1991**, 324.

[23] T. Yanai, D. P. Tew, N. C. Handy, *Chem. Phys. Lett.* **2004**, *393*, 51–57.

[24] A. Schäfer, H. Horn, R. Ahlrichs, *J. Chem. Phys.* **1992**, *97*, 2571–2576.

[25] S. Grimme, J. Antony, S. Ehrlich, H. Krieg, *J. Chem. Phys.* **2010**, *132*, 154104.

[26] S. Grimme, S. Ehrlich, L. Goerigk, *J. Comput. Chem.* **2011**, *32*, 1456–1465.

[27] W. J. D. Beenken, F. Herrmann, M. Presselt, H. Hoppe, S. Shokhovets, G. Gobsch, E. Runge, *Phys. Chem. Chem. Phys.* **2013**, *15*, 16494–16502.

[28] W. Beenken, M. Presselt, T. H. Ngo, W. Dehaen, W. Maes, M. Kruk, *J. Phys. Chem. A* **2014**, *118*, 862–871.

[29] S. T. Hoffmann, H. Bässler, A. Köhler, *J. Phys. Chem. B* **2010**, *114*, 17037–17048.

[30] N. M. O'Boyle, M. Banck, C. A. James, C. Morley, T. Vandermeersch, G. R. Hutchison, *J. Cheminf.* **2011**, *3*, 1–33.

[31] The Open Babel Package, version 2.3.0, http://openbabel.org, accessed February, **2014**.

[32] S. Shanmugaraju, S. A. Joshi, P. S. Mukherjee, *J. Mater. Chem.* **2011**, *21*, 9130–9138.

[33] J. Fleischhauer, S. Zahn, R. Beckert, U.-W. Grummt, E. Birckner, H. Görls, *Chem. Eur. J.* **2012**, *18*, 4549–4557.

[34] A. L. Appleton, S. Barlow, S. R. Marder, K. I. Hardcastle, U. H. F. Bunz, *Synlett* **2011**, *14*, 1983–1986.

[35] CCDC-1032655 (**15**), 1032659 (**16d**), 1032658 (**16h**), 1032660 (**18**) and 1032657 (**19b**) contain the supplementary crystallographic data for this paper. These data can be obtained free of charge from The Cambridge Crystallographic Data Centre via www.ccdc.cam.ac.uk/data_request/cif..

Received: January 19, 2015
Published online on April 7, 2015

 

**Publikation 2:**

„Surprising characteristics of D–A-type functional dyes by introducing 4-alkoxythiazoles as the donor-unit“

D. M. Gampe, F. Nöller, V. G. Hänsch, S. Schramm, A. Darsen, S. H. Habenicht, S. Ehrhardt, D. Weiß, H. Görls, R. Beckert,

*Tetrahedron* **2016**, *72*, 3232-3239.



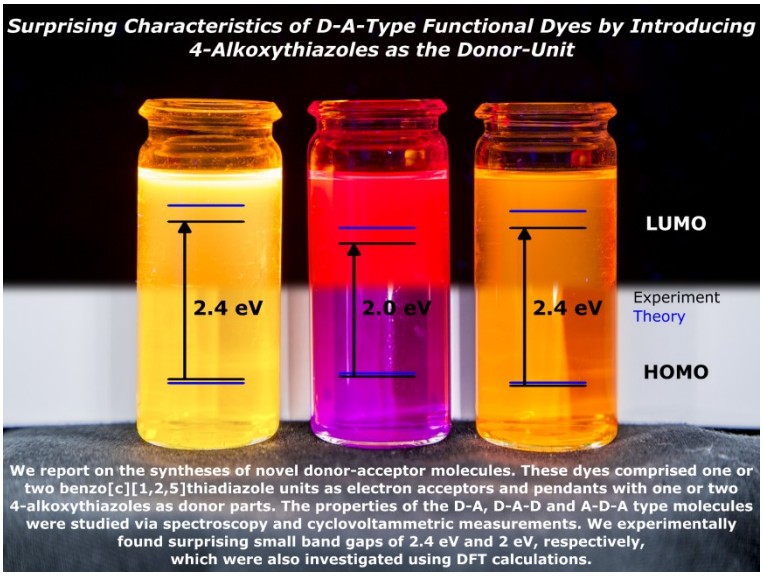

Tetrahedron 72 (2016) 3232–3239

Contents lists available at ScienceDirect

Tetrahedron

journal homepage: www.elsevier.com/locate/tet

# Surprising characteristics of D–A-type functional dyes by introducing 4-alkoxythiazoles as the donor-unit

D.M. Gampe [a], F. Nöller [a], V.G. Hänsch [a], S. Schramm [a], A. Darsen [a], S.H. Habenicht [a], S. Ehrhardt [a], D. Weiß [a], H. Görls [b], R. Beckert [a,*]

[a] Friedrich Schiller University Jena, Institute of Organic and Macromolecular Chemistry, Humboldtstraße 10, 07743 Jena, Germany
[b] Friedrich Schiller University Jena, Institute of Inorganic and Analytical Chemistry, Humboldtstraße 8, 07743 Jena, Germany

ARTICLE INFO

*Article history:*
Received 14 March 2016
Received in revised form 6 April 2016
Accepted 19 April 2016
Available online 20 April 2016

*Keywords:*
Synthesis
Chromophores
Fluorophores
D–A-type dyes
DFT calculations

ABSTRACT

In this study, we report on the syntheses of novel donor–acceptor molecules. These new dyes comprised benzo[*c*][1,2,5]thiadiazole and pendants with one or two 4-alkoxythiazoles as donor parts, which were introduced without Pd-catalyzed cross coupling reactions. The optical and electrochemical properties were studied via absorption, emission spectroscopy and cyclovoltammetric measurements. We experimentally found surprising small band gaps from HOMO to LUMO of 2.4 eV and 2 eV, respectively, which were also investigated using DFT calculations.



## 1. Introduction

Since the development of the organic photovoltaic (OPV) devices, there is a great interest in novel semiconductive materials, such as the light harvesting unit.[1–3] Thereby, the solar energy conversion is realized by two fundamental devices: heterojunctions (HJ) and dye sensitized solar cells (DSSCs). The active layer in the first case is realized via π-conjugated polymers or small molecules as the donor materials and mostly fullerenes as the acceptor.[4–8] The efficiencies of small molecule bulk-HJ (BHJ) have recently been raised significantly. Thus, novel small molecules became attractive because of their good reproducibility, charge carrier mobilities and monodispersity for usage in BHJ.[9–11] In comparison, OPVs working on the DSSC approach only use small molecules to convert light into electricity.[12–14] New semiconductive materials are also important for the development of organic field effect transistors. Therefore, high charge carrier mobilities and small reorganization energies are necessary.[15] In summary, such functional materials offer a wide range of possible applications. By using functional dyes as the active layer, such as merocyanines, squaraines or porphyrines, which are established in DSSC devices, they, furthermore, offer an utilization as the emitting unit in organic light emitting diodes.[16]

The band gap (energy difference between HOMO and LUMO) and specific energy level of these single molecules could be influenced very strongly using the donor–acceptor (D–A) approach.[17–19] Since the HOMO is mainly determined by the donor part, while the LUMO relies on the acceptor unit, their energy levels could be tuned by selecting the building blocks carefully. Moreover, D–A type dyes are often featured by intramolecular charge transfer (ICT) processes. The ICT not only lowers the band gap, but also enhances charge carrier mobility.

The greatest advantage of organic dyes regarding inorganic or polydispers semiconductors is the possibility of simple and manifold derivatization.[20] Furthermore, a good solubility and well-defined morphology could be realized easily and is important for receiving good processabilities.

The reactivity, derivatization and the usage of benzo[*c*][1,2,5]thiadiazole (BT) as an electron acceptor has been studied intensively over the last few years.[21–23] It is used in many different D–A type copolymers, but rather in D–A type small molecules[24–31] and especially in D–A–D type dyes showing two-photon absorption.[32,33] Thereby, the electron-donating units are mostly based on thiophene or triarylamine, which were introduced via Pd-catalyzed cross-coupling reactions.

We here present a D–A, D–A–D and an A–D–A type system (see Scheme 1), where 4-alkoxythiazoles are used as the electron-

* Corresponding author. E-mail address: rainer.beckert@uni-jena.de (R. Beckert).
*URL:* http://www.agbeckert.uni-jena.de/

http://dx.doi.org/10.1016/j.tet.2016.04.046
0040-4020/

donating moieties, while the established BTs are utilized as the electron-accepting units. Starting at BT, it is possible to synthesize these structures via five steps and without expensive Pd-catalyzed cross-coupling reactions. We obtained well-soluble functional dyes by fusing two kinds of established substructures, which could act as model substances for forthcoming studies.

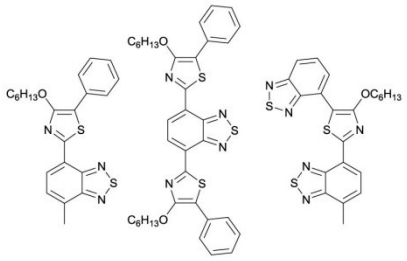


**Scheme 1.** Structures of the D–A type dyes **1**, **2** and **3**.

## 2. Results and discussion

### 2.1. Syntheses and structures

Knowing the synthesis and especially the purification of mono brominated BT is elaborate,[34] we decided to start with 4-methyl-BT **13**, which is easy accessible via sulphurisation of 3-methyl-1,2-phenylenediamine **15** (see Scheme 2).[24] Bromination of **13** gave the mono-brominated species **11** in good yields, and the treatment of BT (**14**) with an excess of bromine leads to 4,7-dibromo-BT **12**.[34]

The nitrile functions should be introduced via nucleophilic substitution of bromine. According to the literature,[35] the mono-nitrile **9** could be obtained in moderate yield. The synthesis of **10** occurred with more difficulty, but the dinitrile was accessible via the slightly optimised procedure of *Garo* et al.[36,37] The subsequent addition reactions between hydrogen sulphide and the nitriles **9** and **10** were realized via freshly prepared *O,O′*-diethyldithiophosphate, which is able to release $H_2S$.[38] For the preparation of target compound **3**, we also had to synthesize the cyclization partner **16**. This was realized beginning with the α-bromination of **13** by means of NBS.[39] Nucleophilic substitution of bromine (see compound **20**) by $CN^-$ was carried out subsequently,[40] followed by hydrolysis of the isolated nitrile to obtain the BT-substituted acetic acid **18**. After the esterification and renewed bromination of the α-carbon atom, the desired, racemic product **16** was obtained as yellowish oil in moderate yield. Hantzsch cyclization was carried out via, by our group, optimized reaction conditions to introduce the thiazole substructures.[41–43] The thioamides **7**, **8** on addition of ethyl α-bromophenylacetate **21** or compound **16**, respectively, gave the 4-hydroxythiazoles **4**, **5** and **6** under alkaline conditions. Williamson type etherifications were carried out to introduce the hexyl side chains and gave the desired well-soluble products.

The structures were determined by elemental analysis, mass spectrometry and NMR experiments. We were also able to obtain single crystals suitable for single crystal X-ray analysis via slow evaporation of a solution of **1** in a mixture of *n*-heptane and chloroform. It is noteworthy that 0.5 molecules of $CHCl_3$ co-crystallized in the packing of compound **1**. Due to this, we obtained an alternating packing of two kinds of structures in the single crystal analysis (as depicted in Fig. 1). While one molecule of thiazole **1** appears strictly planar and interacts via H-bonds to the neighboring molecules (molecule distance of about 3.4 Å), the phenyl residue of the other kind is, due to the interaction to $CHCl_3$ (distance of about 3.6 Å), twisted by about 27° relative to the BT-thiazole plane.

### 2.2. Photophysical and electrochemical properties

The UV–vis absorption and fluorescence spectra of BT-thiazoles **1**, **2** and **3** are depicted in Fig. 2. All derivatives show intense absorption in the visible region and two strong bands. In the case of **1**, the maxima of the absorption are located at $\lambda_{max}$=316 nm and 452 nm. Due to the second electron donating moiety in **2**, the absorption bands entail a significant bathochromic shift to $\lambda_{max}$=365 nm and 545 nm. The UV–vis absorption spectrum of derivative **3**, compared to that of compound **1**, is only slightly bathochromic shifted, but the A–D–A type dye **3** exhibits a more intense absorption with maxima at $\lambda_{max}$=315 nm and 470 nm. The absorption spectra of all dyes are low structured with broad absorption bands, but all compounds exhibit high oscillator strengths with log ε between 4.0 and 4.5. All donor–acceptor dyes possess high Stoke's shifts of about $\upsilon$=5500 $cm^{-1}$ (**1**), $\upsilon$=3600 $cm^{-1}$ (**2**) and $\upsilon$=4900 $cm^{-1}$ (**3**) as the maxima of the fluorescence spectra appear, after excitation at the appropriate absorption maximum, in the orange and red region of visible light at $\lambda$=602 nm for **1**, $\lambda$=667 nm for **2** and $\lambda$=609 nm for **3**, respectively.

Fluorescence measurements in different solvents showed a positive fluorescence solvatochromism (see SI, Figs. 1–3). Thus, the change from nonpolar (cyclohexane) to polar solvents, such as aceton, leads to a bathochromic shift of the fluorescence maxima (**1**: $\Delta\lambda$=55 nm ≙ 1580 $cm^{-1}$; **2**: $\Delta\lambda$=34 nm ≙ 793 $cm^{-1}$; **3**: $\Delta\lambda$=51 nm ≙ 1430 $cm^{-1}$). Furthermore, we examined the fluorescence quantum yields in cyclohexane to $\Phi_F$=0.5 E·$mol^{-1}$ for **1**, $\Phi_F$=0.3 E·$mol^{-1}$ for **2** and $\Phi_F$=0.1 E·$mol^{-1}$ for **3**, respectively.[44,45]

Cyclic voltammetry was performed to investigate the redox potential; the voltammograms are depicted in Fig. 3. Thiazole **1** exhibits a reduction at a potential of $E_{1/2}$=−1.8 V and an irreversible oxidation at $E$=0.82 V. Thus, we determined the HOMO and LUMO energy via the onset potential of the oxidation and reduction. The band gap is $E_{Gap}^{CV}$=2.44 eV, which is in good agreement with $E_{Gap}^{opt}$=2.35 eV, ascertained via the energy of the longest wavelength absorption band at 10% intensity. We achieved different results in case of bis-thiazole **2**, which could be oxidized twice, while the first step at $E_{1/2}$=0.67 V seems to be reversible, the second one at $E$=0.93 V is irreversible. A reversible reduction step is located at $E_{1/2}$=−1.5 V at the reduction wave. Through this, the reduction of our dyes relies, as expected, on the BT unit and the oxidation takes place at the thiazole moiety, since bis-thiazole **2** could be oxidized twice. Furthermore, it is remarkable that the introduction of a second thiazole moiety leads to a significantly lowered LUMO energy of about 0.4 eV (**2**, see Table 1), in comparison to the structure containing only one donating unit (**1**), while the HOMO is nearly unaffected. This results in a smaller band gap for **2** of $E_{Gap}^{CV}$=2.06 eV, which correlates well with the optical band gap, examined via absorption spectroscopy, of $E_{Gap}^{opt}$=1.97 eV. Derivative **3** exhibits a similar behavior like the D–A type dye **1**. The A–D–A dye **3** is featured by an irreversible oxidation at a potential of: $E$=1.25 V and a reversible reduction at $E_{1/2}$=−1.8 V, with respect to the limit of cyclic voltammetry measurements in THF. Due to the second BT unit compound **3** should be able to accept two electrons, but possibly the second reduction occurs at a potential beyond the limits of the appropriate solvents. However, we were able to examine the energies of HOMO and LUMO which lead to a band gap of $E_{Gap}^{CV}$=2.44 eV that concurs to the optical gap of $E_{Gap}^{opt}$=2.28 eV.

In order to gain more detailed insight into the electronic characteristics of the herein presented target compounds density functional theory (DFT) calculations have been performed. The effects of solvation (THF) have been addressed for ground properties

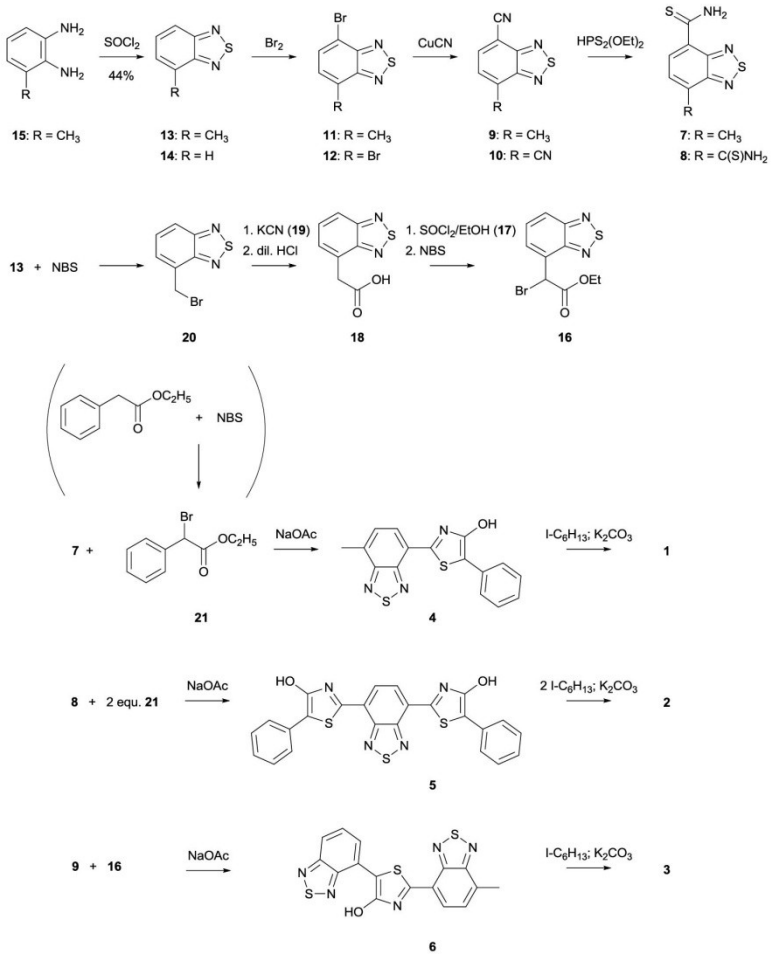


**Scheme 2.** Syntheses of D–A type dye **1**, D–A–D derivative **2** and A–D–A type dye **3**.

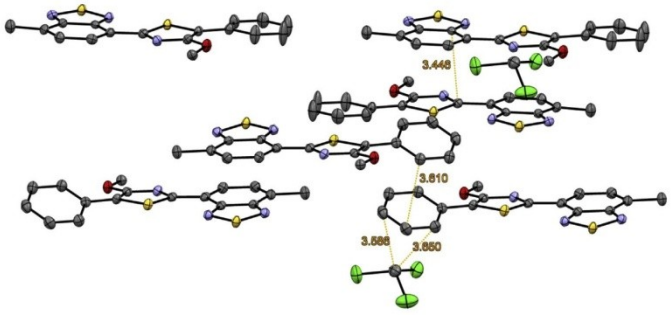


**Fig. 1.** ORTEP view of the packing and molecule distances of compound **1**, hydrogen atoms and the hexyl side chains are hided for clarity.

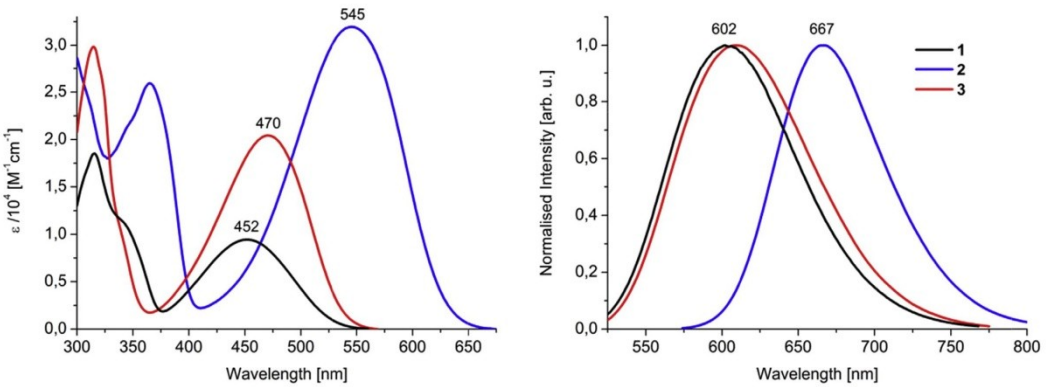


**Fig. 2.** UV–vis absorption and fluorescence emission spectra of derivatives **1** (black line), **2** (red line) and **3** (blue line).

by means of a polarizable continuum model.[46] After an initial systematic conformational search with MMFF,[47] the best geometries were optimized at the CAM-B3LYP/6-31+G(d,p)[48] level of theory as implemented in Gaussian 09.[49] After the ground state optimization and its validation via frequency calculation, the HOMO and LUMO energies where calculated at B3LYP/6-31d+G(d,p) level of theory. The frontier orbitals of **1**, **2** and **3** are depicted in Fig. 4.

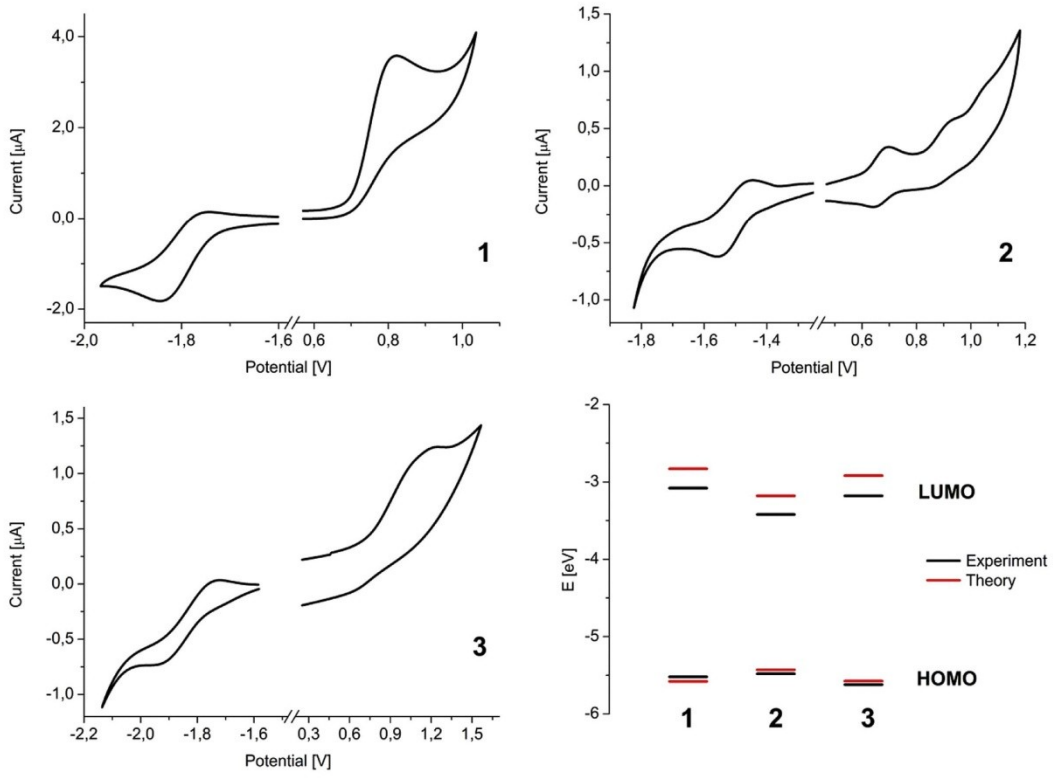


**Fig. 3.** Cyclic voltammetry of compounds **1** (top left), **2** (top right) and **3** (bottom left). The spectra were calibrated externally against $E_{1/2}(Fc/Fc^{+})$. Scheme of the experimental and theoretical examined orbital energies (bottom right).

**Table 1**
Spectroscopic and calculated data of the target structures **1**, **2** and **3**

| | $\lambda_{Abs}$[a]/nm [$\varepsilon/10^4$ $M^{-1}$ $cm^{-1}$] | $\lambda_F$[a] ($\lambda_{exc.}$)/nm | Stokes S.[b] $\upsilon/cm^{-1}$ | $\Phi$/%[c] | $E^{ox}_{onset}$[d]/V | $E^{red}_{onset}$[d]/V | HOMO[e]/eV | LUMO[e]/eV | $E^{CV}_{Gap}$[f]/eV | $E^{opt}_{Gap}$[g]/eV | $E^{DFT}_{Gap}$[h] |
|---|---|---|---|---|---|---|---|---|---|---|---|
| 1 | 316 [1.9]; 452 [0.9] | 602 (470) | 5510 | 52 | 0.72 | −1.72 | −5.52 | −3.08 | 2.44 | 2.35 | 2.74 |
| 2 | 365 [2.6]; 545 [3.2] | 667 (470) | 3556 | 28 | 0.68 | −1.38 | −5.48 | −3.42 | 2.06 | 1.97 | 2.25 |
| 3 | 315 [3.0]; 470 [2.0] | 609 (510) | 4856 | 9 | 0.82 | −1.62 | −5.62 | −3.18 | 2.44 | 2.28 | 2.66 |

[a] Measured in THF.
[b] Relative to the maximum of the absorption band.
[c] Measured in cyclohexane, relative to rhodamine 6G ($\Phi$=0.95) and fluorescein ($\Phi$=0.91).[44]
[d] Recorded by cyclic voltammetry in 0.1 M solution of $TBAPF_6$ in THF, versus $E_{onset}(Fc/Fc^+)$.
[e] Calculated via $E_{HOMO}=-[E_{onset}(Ox)-E_{onset}(Fc/Fc^+)]-4.8$ eV and $E_{Lumo}=-[E_{onset}(Red)-E_{onset}(Fc/Fc^+)]-4.8$ eV.
[f] $E_{Gap}=-(E_{HOMO}-E_{LUMO})$.
[g] Calculated from the onset (10%) of the absorption spectra.
[h] Calculated energies at B3LYP/6-31+G(d,p) level of theory based on a CAM-B3LYP/6-31+G(d,p) optimized ground state geometry.

The HOMO and LUMO are both nearly identically delocalized throughout the whole $\pi$-System of the molecules. This leads to the assumption that there is no big CT involved into the transition from the HOMO to the LUMO. The error of the calculated-to the experimental values anyway adjudges within the 0.3 eV margin that is typical of DFT calculations[50,51] and especially for thiazole-based chromophores[52] like fireflyoxyluciferin.[53] These findings are in very good agreement with the experimentally determined HOMO/LUMO energies (see Fig. 3, bottom right). All spectroscopic, electrochemical and calculated results are summarized in Table 1.

## 3. Conclusion

In conclusion, we were able to synthesize three novel D–A type functional dyes based on the known BT as the accepting and 4-hexyloxythiazoles as the donating units. We obtained the substances **1**, **2** and **3** via five, six and seven reaction steps, respectively, and without expensive Pd-catalyzed cross-coupling reactions, starting from simple and commercially available starting materials.

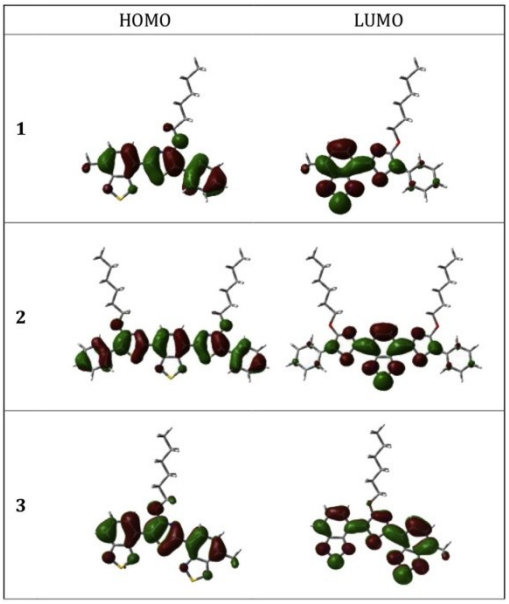


**Fig. 4.** Frontier orbitals of target compounds **1**, **2** and **3**.

All intermediates were obtained in moderate to good yields and only the synthesis of benzothiadiazole-4,7-dicarbonitrile **10** needs further optimization. The well-soluble dyes show strong absorbance in the visible region, a fluorescence emission with moderate quantum yields and Stoke's shifts of $\upsilon$=5500 $cm^{-1}$ (**1**), $\upsilon$=3600 $cm^{-1}$ (**2**) and $\upsilon$=4900 $cm^{-1}$ (**3**), respectively. Spectroscopically and electrochemically examined band gaps of about 2.4 eV (**1**, **3**) and 2 eV (**2**) are surprisingly small compared to the molecular weight and number of conjugated units in our compounds. The small gap and strong absorption of bis-thiazole **2** in the region of about 550 nm show especial promise as an application as the donor material in small molecule BHJ solar cells. We will report about the usage of our materials and increasing the donor strength of the thiazole unit, e.g., by introducing diarylamine substituents, in a forthcoming publication.

## 4. Experimental section

### 4.1. General methods

Solvents for UV–vis and emission spectroscopy were of analytical grade and bought from Sigma–Aldrich. $^1H$ and $^{13}C$ NMR spectra were recorded on Bruker AC-250 (250 MHz), AC-300 (300 MHz) and AC-400 (400 MHz) spectrometers. Chemical shifts ($\delta$) are given relative to solvents. UV–vis data for the compounds were collected with a PerkinElmer LAMBDA 45 UV–vis spectrometer and emission spectra were measured with a Jasco FP 6500 instrument. Mass spectra were measured either with a Finnigan MAT SSQ 710 (EI) or a MAZ 95 XL (ESI) system. Elemental analysis was carried out on a Leco-CHNS-932. TLC materials were from Merck (Polygram SIL G/UV254, aluminum oxide 60 F254). The material for column chromatography was also obtained from Merck (silica gel 60, 0.04–0.063 mm). The fluorescence quantum yields were measured in the perpendicular excitation-emission geometry, while the absorbance was adjusted between 0.04–0.05 at the chosen excitation wavelength (see $\lambda_{exc.}$ in Table 1). Afterwards the calculation was done via the following equation: $\Phi = \frac{I}{I_r}\frac{A_r}{A}\frac{n^2}{n_r^2}\Phi_r$, were $I$ is the corrected integrated emission intensity, $A$ is the absorbance at the excitation wavelength, $n$ is the refractive index of the solvent (measured at a Müller Abbe Refractometer AR-4) and $\Phi$ is the quantum yield. The subscript $r$ refers to the reference fluorophore of known quantum yield, we used rhodamine 6G ($\Phi_F$=0.95 E $mol^{-1}$ in EtOH) and fluorescein ($\Phi_F$=0.91 E $mol^{-1}$ in 0.1 M NaOH solution) as the fluorescence standards.[44] The cyclovoltammetric measurements were performed at a Metrohm Autolab PGSTAT30 potentiostat. in 0.1 M solution of $TBAPF_6$ in THF (concentration of compounds: **1**: $1\times10^{-3}$ M; **2** and **3**: $1\times10^{-5}$ M) on a graphite working electrode with a scanning speed of 50 mV $s^{-1}$, platinum was used as counter and Ag/AgCl as the reference electrode. The data were calibrated externally versus ferrocen/ferrocenium.

### 4.2. Syntheses

*4.2.1. 7-Methylbenzo[c][1,2,5]thiadiazole-4-carbonitrile (**9**).* To a solution of **11** (2.6 g, 11.4 mmol) in NMP (20 mL) CuCN (1.2 g, 13.7 mmol, 1.2 equiv) was added portion wise under stirring at 80 °C. After heating the mixture to 150 °C for 2 h, TLC (silica; toluene) showed only a small amount of the desired product, and an additional portion of CuCN (800 mg, 9 mmol, 0.8 equiv) was added. The resulting dark reaction mixture was heated for additional 3 h at 150 °C and stirred at 80 °C overnight. After cooling to room temperature aqueous $NH_3$ (40 mL, 15%) was added and stirred for 1 h. The resulting precipitate was filtrated. The filtrate was extracted three times with $CH_2Cl_2$, while the precipitate was rinsed intensively with $CH_2Cl_2$. The combined $CH_2Cl_2$ phases were washed with brine, dried over $Na_2SO_4$ and evaporated to dryness. Purification by column chromatography (silica; toluene) supplied the nitrile (**9**; $R_f \approx 0.5$; 1.5 g, 8.5 mmol, 74%) as white powder. Mp: 177 °C; $^1$H NMR (250 MHz, $CDCl_3$): $\delta$=7.95 (d, $J$=7.1 Hz, 1H), 7.45 (d, $J$=7.1 Hz, 1H), 2.83 (s, 3H) ppm; $^{13}$C NMR (63 MHz, $CDCl_3$): $\delta$=154.89, 152.93, 138.61, 136.25, 127.51, 115.70, 103.46, 77.16, 18.59 ppm; MS (EI): $m/z$=175 [$M^+$], 148 [$(M-CN)^+$]; EA calcd for $C_8H_5N_3S$: C, 54.84; H, 2.88; N, 23.98; found: C, 55.09; H, 2.79; N, 23.71.

*4.2.2. Benzo[c][1,2,5]thiadiazole-4,7-dicarbonitrile (**10**).* A mixture of **12** (1 g, 3.4 mmol), 0.55 mL of pyridine (6.9 mmol, 2 equiv) and sodium iodide (0.03 mmol, 0.01 equiv) in 10 mL of DMF was degassed with nitrogen over 15 min. Under $N_2$, CuCN (1.2 g, 13.7 mmol, 4 equiv) was added and the suspension was heated to reflux for 20 h, as indicated by TLC (silica; $CH_2Cl_2$). The mixture was allowed to cool to room temperature and cold aqueous $NH_3$ (20 mL, 15%) was added. The resulting dark suspension was stirred for an additional hour and the precipitate was filtrated and rinsed intensively with $CH_2Cl_2$. The resulting organic layer was washed with water, dried over $MgSO_4$ and evaporated to dryness to obtain the crude product. Purification by column chromatography (silica; $CH_2Cl_2$) supplied **10** ($R_f \approx 0.8$, 350 mg, 1.9 mmol, 56%) as pale yellow powder. Mp: 183 °C; $^1$H NMR (300 MHz, $CDCl_3$): $\delta$=8.13 (s, 2H) ppm; $^{13}$C NMR (63 MHz, $CDCl_3$): $\delta$=152.41, 134.42, 113.82, 110.67 ppm; MS (EI): $m/z$=186 [$M^+$]; EA calcd for $C_8H_2N_4S$: C, 51.61; H, 1.08; N, 30.09; found: C, 51.92; H, 1.10; N, 29.91.

*4.2.3. 7-Methylbenzo[c][1,2,5]thiadiazole-4-carbothioamide (**7**).* A mixture of **9** (1.5 g, 8.6 mmol), *O,O′*-diethyldithiophosphate (1.55 mL, 9.7 mmol, 1.1 equiv) and 1 mL of THF was heated to 80 °C for 6 h. The reaction was quenched by diluting the mixture with 40 mL of saturated $NaHCO_3$-solution and stirred for an additional hour. The resulting yellow precipitate was filtrated and washed with water and small amount of ethanol. The orange, crystalline product (**7**; 1.5 g, 7.2 mmol, 84%) was obtained after recrystallization from cyclohexane/$CHCl_3$ (1:1). Mp: 191–193 °C (dec); $^1$H NMR (400 MHz, $CDCl_3$): $\delta$=10.47 (s, 1H), 9.03 (d, $J$=7.4 Hz, 1H), 8.16 (s, 1H), 7.51 (d, $J$=7.4 Hz, 1H), 2.79 (s, 3H) ppm; $^{13}$C NMR (101 MHz, $CDCl_3$): $\delta$=196.33, 155.77, 151.22, 138.70, 137.28, 128.53, 125.25, 18.37 ppm; MS (EI): $m/z$=209 [$M^+$], 176 [$(M-HS)^+$]; EA calcd for $C_8H_7N_3S_2$: C, 45.91; H, 3.37; N, 20.08; found: C, 46.23; H, 3.24; N, 20.36.

*4.2.4. Benzo[c][1,2,5]thiadiazole-4,7-bis(carbothioamide) (**8**).* To phosphorus pentasulfide (600 mg, 2.7 mmol, 2.5 equiv) ethanol was added very carefully under vigorous stirring, until a clear solution accrued. To this freshly prepared *O,O′*-diethyldithiophosphate, compound **10** (200 mg, 1.1 mmol) was added in small portions. The reaction was heated to reflux. After 4 h the mixture was allowed to cool down and diluted with saturated $NaHCO_3$-solution (20 mL) and stirred for an additional hour. The precipitate was filtrated and washed with water. The crude product was purified by hot filtration of an ethanol suspension to obtain **8** as orange powder (170 mg, 0.7 mmol, 62%). Mp: 255 °C; $^1$H NMR (250 MHz, DMSO): $\delta$=10.52 (s, 2H), 9.95 (s. 2H), 8.28 (s, 2H) ppm; $^{13}$C NMR (63 MHz, DMSO): $\delta$=195.61, 150.15, 133.59, 130.61 ppm; MS (EI): $m/z$=254 [$M^+$], 221 [$(M-HS)^+$]; EA calcd for $C_8H_6N_4S_3$: C, 37.78; H, 2.38; N, 22.03; found: C, 37.97; H, 2.26; N, 22.41.

*4.2.5. Ethyl 2-(benzo[c][1,2,5]thiadiazol-4-yl)acetate (**17**).* 3 g (15 mmol)of **18** were dissolved in 40 mL of ethanol and 1.3 mL (17 mmol, 1.1 equiv) of thionyl chloride were added drop wise. After stirring under refluxing conditions over 3 h, as indicated by TLC (silica; toluene:ethyl acetate/20:1), the reaction was quenched by adding 5 mL of water. The reaction mixture was concentrated under reduced pressure and diluted with water and diethyl ether. The organic phase was separated and extracted with brine, dried over $MgSO_4$ and evaporated to dryness. The product (2.7 g, 12 mmol, 80%) was obtained as colorless oil after purification by column chromatography (silica; toluene:ethyl acetate/20:1). $^1$H NMR (250 MHz, Acetone): $\delta$=7.95 (d, $J$=8.6 Hz, 1H), 7.73–7.65 (m, 1H), 7.61 (d, $J$=6.7 Hz, 1H), 4.17 (s, 2H), 4.16–4.08 (m, 2H), 1.20 (t, $J$=7.1 Hz, 3H); $^{13}$C NMR (63 MHz, Acetone): $\delta$=170.96, 155.76, 130.64, 130.37, 129.24, 121.04, 61.29, 37.67, 29.84, 14.47; MS (EI): $m/z$=222 [$M^+$], 149 [$(M-HCO_2Et)^+$]; EA calcd for $C_{10}H_{10}N_2O_2S$: C, 54.04; H, 4.53; N, 12.60; found: C, 53.71; H, 4.61; N, 12.74.

*4.2.6. Ethyl 2-(benzo[c][1,2,5]thiadiazol-4-yl)-2-bromoacetate (**16**).* To a mixture of 2.7 g (12 mmol) of **17** and 2.27 g of *N*-bromosuccinimide (13 mmol, 1.05 equiv) in 150 mL tetrachloroethylen, 3 droplets of hydrobromic acid (62%) were added and the resulting suspension was stirred over 12 h under reflux. As indicated by TLC (silica; toluene) the reaction turnover stops at about 50%, so the reaction was quenched by adding a saturated $Na_2S_2O_3$-solution. The organic phase was separated and extracted twice with $Na_2CO_3$-solution and water. After drying over $MgSO_4$, the mixture was evaporated and a yellow oil was obtained. The product/educt (1/0.7) mixture was used as obtained for further reaction steps (2.5 g mixture: 1.5 g, 5 mmol, 42%). $^1$H NMR (250 MHz, Acetone): $\delta$=8.09 (dd, $J$=8.8, 0.9 Hz, 1H), 8.02 (d, $J$=6.9 Hz, 1H), 7.79 (dd, $J$=8.8, 7.0 Hz, 1H), 6.39 (s, 1H), 4.25 (q, $J$=7.1 Hz, 2H), 1.21 (t, $J$=5.6 Hz, 3H) ppm; MS (EI): $m/z$=300 [$M^+$], 302 [$(M+2)^+$], 221 [$(M-Br)^+$].

*4.2.7. 2-(7-Methylbenzo[c][1,2,5]thiadiazol-4-yl)-5-phenylthiazol-4-ol (**4**).* A suspension of **7** (720 mg, 3.5 mmol), 0.78 mL of ethyl-2-bromo-2-phenylacetate (**21**; 4.5 mmol, 1.3 equiv) and sodium acetate (710 mg, 8.6 mmol, 2.5 equiv) in 10 mL of ethanol was heated to reflux. After 6 h the red reaction mixture was allowed to cool to room temperature and water was added. The red precipitate was filtrated and rinsed with water, ethanol, $CHCl_3$ and pentane. After drying under reduce pressure the product was obtained as red powder (590 mg, 1.8 mmol, 53%). Mp: 325 °C (dec); $^1$H NMR (400 MHz, DMSO): $\delta$=11.28 (s, 1H), 8.37 (d, $J$=7.4 Hz, 1H), 7.81 (d, $J$=7.5 Hz, 2H), 7.67 (d, $J$=7.3 Hz, 1H), 7.42 (t, $J$=7.8 Hz, 2H), 7.25 (t, $J$=7.4 Hz, 1H), 2.76 (s, 3H) ppm; $^{13}$C NMR could not be measured due to bad solubility; MS (EI): $m/z$=325 [$M^+$]; EA calcd for $C_{16}H_{11}N_3OS_2$: C, 59.06; H, 3.41; N, 12.91; found: C, 59.45; H, 3.35; N, 12.72.

*4.2.8. 4-(4-(Hexyloxy)-5-phenylthiazol-2-yl)-7-methylbenzo[c][1,2,5]thiadiazole (**1**).* To a stirred suspension of **4** (580 mg, 1.8 mmol) and 250 mg potassium carbonate (1.8 mmol) in acetone (20 mL), 1-iodohexane (0.34 mL, 2.3 mmol, 1.3 equiv) was added and the resulting mixture was heated to reflux. After 7 h the mixture was allowed to cool down and water was added, while an orange precipitate was formed. The mixture was filtrated and the crude product was rinsed with water. Purification was done by recrystallization from ethanol to afford compound **1** (495 mg,

1.2 mmol, 68%) as orange plates. Mp: 96–98 °C; $^1$H NMR (300 MHz, $CDCl_3$): $\delta$=8.46 (d, $J$=7.3 Hz, 1H), 7.87 (d, $J$=7.4 Hz, 2H), 7.48 (d, $J$=7.3 Hz, 1H), 7.39 (t, $J$=7.7 Hz, 2H), 7.26 (s, 1H), 4.57 (t, $J$=6.6 Hz, 2H), 2.79 (s, 3H), 1.95–1.84 (m, 2H), 1.60–1.51 (m, 2H), 1.44–1.32 (m, 4H), 0.92 (t, $J$=6.9 Hz, 3H) ppm; $^{13}$C NMR (63 MHz, $CDCl_3$): $\delta$=159.20, 155.71, 151.54, 132.65, 132.03, 129.98, 128.60, 128.42, 126.74, 126.48, 126.42, 123.91, 114.33, 70.54, 31.56, 29.55, 25.78, 22.60, 18.13, 14.01 ppm. MS (EI): $m/z$=409 [$M^+$]; HRMS (ESI): calcd for M+$Na^+$: 432.1180, found: 432.1174; EA calcd for $C_{22}H_{23}N_3OS_2$: C, 64.52; H, 5.66; N, 10.26; found: C, 64.21; H, 5.74; N, 10.01. UV–vis (THF): $\lambda_{max}$ (log $\varepsilon$)=316 nm (4.3), 452 nm (3.9).

*4.2.9. 2,2′-(Benzo[c][1,2,5]thiadiazole-4,7-diyl)bis(5-phenylthiazol-4-ol) (**5**).* A mixture of **8** (610 mg, 2.4 mmol), 1.7 mL of ethyl-2-bromo-2-phenylacetate (**21**; 9.7 mmol, 4 equiv) and 1 g of sodium acetate (12.2 mmol, 5 equiv) was diluted with 10 mL of ethanol. The suspension was heated to reflux with stirring. After 6 h the reaction was stopped and allowed to cool to room temperature. To the black slurry water was added and the resulting dark mixture was filtrated and rinsed with water, hot ethanol, $CHCl_3$ and ethyl acetate. After drying under reduced pressure, the dark blue powder was obtained (490 mg, 1 mmol, 42%). NMR experiments were not possible due to the bad solubility. Melting point (decomposition) could not be measured, due to the dark color of the product. MS (EI): $m/z$=486 [$M^+$]; EA calcd for $C_{24}H_{14}N_4O_2S_3$: C, 59.24; H, 2.90; N, 11.51; found: C, 58.71; H, 2.95; N, 11.83.

*4.2.10. 4,7-Bis(4-(hexyloxy)-5-phenylthiazol-2-yl)benzo[c][1,2,5]thiadiazole (**2**).* To a mixture of **5** (450 mg, 0.9 mmol) and potassium carbonate (250 mg, 1.8 mmol, 2 equiv) in acetone (50 mL), 1-iodohexane (0.3 mL, 2.3 mmol, 2.5 equiv) was added. The resulting blue slurry was heated to reflux with stirring. After 6 h the reaction was allowed to cool to room temperature and quenched with water. The precipitate was filtrated and washed with water and a small amount of cold ethanol. By rinsing with $CHCl_3$ the product was dissolved. After evaporating the $CHCl_3$ phase, the product was purified by column chromatography (silica; toluene/$n$-heptane 1:1, $R_f \approx 0.8$). The dark blue powder with metallic luster was obtained after drying under reduced pressure (97 mg, 0.15 mmol, 16%). Mp: 219 °C; $^1$H NMR (400 MHz, $CDCl_3$): $\delta$=8.61 (s, 2H), 7.88 (d, $J$=7.6 Hz, 4H), 7.40 (t, $J$=7.7 Hz, 4H), 7.29–7.23 (m, 2H), 4.58 (t, $J$=6.6 Hz, 4H), 1.96–1.87 (m, 4H), 1.60–1.50 (m, 4H), 1.44–1.35 (m, 8H), 0.93 (t, $J$=7.0 Hz, 6H) ppm; $^{13}$C NMR (101 MHz, $CDCl_3$): $\delta$=159.86, 153.58, 151.97, 132.02, 128.83, 126.98, 126.87, 126.31, 126.02, 116.05, 77.16, 70.80, 31.74, 29.69, 25.96, 22.78, 14.20 ppm; MS (EI): $m/z$=654 [$M^+$]; HRMS (EI): calcd: 654.2157, found: 654.2162; EA calcd for $C_{36}H_{38}N_4O_2S_3$: C, 66.02; H, 5.85; N, 8.55; found: C, 65.61; H, 5.94; N, 8.69. UV–vis (THF): $\lambda_{max}$ (log $\varepsilon$)=365 nm (4.4), 545 nm (4.5).

*4.2.11. 5-(Benzo[c][1,2,5]thiadiazol-4-yl)-2-(7-methylbenzo[c][1,2,5]thiadiazol-4-yl)thiazol-4-ol (**6**).* A mixture of **7** (1.15 g, 6.5 mmol), **16** (2.9 g, 6.6 mmol, 1.05 equiv) and sodium acetate (1.1 g, 13 mmol, 2 equiv) in 100 mL of ethanol was stirred under reflux until everything of **7** was consumed, as indicated by TLC (silica; toluene). After 8 h the hot reaction mixture was filtrated rapidly and the brown precipitate was washed with additional 100 mL of hot ethanol. Rinsing with $n$-pentane afforded the desired orange product, after drying under reduced pressure, in yields of 76% (1.9 g, 5 mmol). NMR experiments were not possible due to the bad solubility. Mp: >340 °C; MS (EI): $m/z$=383 [$M^+$]; EA calcd for $C_{16}H_9N_5OS_3$: C, 50.11; H, 2.37; N, 18.26; found: C, 50.45; H, 2.41; N, 18.05.

*4.2.12. 4-(5-(Benzo[c][1,2,5]thiadiazol-4-yl)-4-(hexyloxy)thiazol-2-yl)-7-methylbenzo[c][1,2,5]thiadiazole (**3**).* 1.9 g (4.9 mmol) of **6** and 1.05 g (10 mmol, 2 equiv) of sodium carbonate were suspended in 80 mL of an acetone/DMSO mixture (7:1). To the stirred suspension 1-iodohexane (8 mL, 5.5 mmol, 1.1 equiv) was added and heated to reflux. After 16 h, an orange fluorescence was obtained and the mixture was filtrated. The precipitate was washed with water and hot ethanol. Recrystallization from $CHCl_3$ afforded the product as red microcrystals (1.7 g, 3.6 mmol, 74%). Mp: 186–188 °C; $^1$H NMR (250 MHz, $CDCl_3$): $\delta$=8.49 (t, $J$=6.8 Hz, 2H), 7.83 (d, $J$=8.6 Hz, 1H), 7.65 (dd, $J$=8.6, 7.4 Hz, 1H), 7.45 (d, $J$=7.3 Hz, 1H), 4.67 (t, $J$=6.6 Hz, 2H), 2.79 (s, $J$=7.5 Hz, 3H), 2.01–1.88 (m, 2H), 1.65–1.54 (m, 2H), 1.49–1.33 (m, 4H), 0.93 (t, $J$=7.0 Hz, 3H) ppm; $^{13}$C NMR (63 MHz, $CDCl_3$): $\delta$=162.05, 158.57, 155.87, 155.25, 152.49, 151.76, 133.09, 130.25, 128.54, 126.94, 126.00, 125.64, 124.31, 118.74, 109.72, 77.16, 70.87, 31.73, 29.70, 26.01, 22.77, 18.33, 14.18 ppm; MS (EI): $m/z$=467 [$M^+$]; HRMS (ESI): calcd for M+$Na^+$: 490.0806, found: 490.0831; EA calcd for $C_{22}H_{21}N_5OS_3$: C, 56.51; H, 4.53; N, 14.98; found: C, 56.25; H, 4.45; N, 15.13. UV–vis (THF): $\lambda_{max}$ (log $\varepsilon$)=315 nm (4.5), 470 nm (4.3).

## Supplementary data

Supplementary data (syntheses of starting materials, solvatochromism measurements, X-Ray and analytical data) associated with this article can be found in the online version, at http://dx.doi.org/10.1016/j.tet.2016.04.046.

CCDC 1446811 (**1**) contains the supplementary crystallographic data for this publication. Data can be obtained free of charge from The Cambridge Crystallographic Data Centre via www.ccdc.cam.ac.uk/data_request/cif.

## References and notes


1. Dhanabalan, A.; van Duren, J. K. J.; van Hal, P. A.; van Dongen, J. L. J.; Janssen, R. A. J. *Adv. Funct. Mat.* **2001**, *11*, 255–262.
2. Kan, B.; Zhang, Q.; Li, M.; Wan, X.; Ni, W.; Long, G.; Wang, Y.; Yang, X.; Feng, H.; Chen, Y. *J. Am. Chem. Soc.* **2014**, *136*, 15529–15532.
3. Wang, B.; Tsang, S. W.; Zhang, W.; Tao, Y.; Wong, M. *S. Chem. Commun.* **2011**, 9471–9473.
4. Chen, H.-Y.; Hou, J.; Zhang, S.; Liang, Y.; Yang, G.; Yang, Y.; Yu, L.; Wu, Y.; Li, G. *Nat. Phot.* **2009**, *3*, 649–653.
5. Dong, Y.; Cai, W.; Hu, X.; Zhong, C.; Huang, F.; Cao, Y. *Polymer* **2012**, *53*, 1465–1472.
6. Lin, Y.; Li, Y.; Zhan, X. *Chem. Soc. Rev.* **2012**, *41*, 4245–4272.
7. Wang, L.; Yin, L.; Ji, C.; Li, Y. *Dyes Pigm.* **2015**, *118*, 37–44.
8. Yuan, J.; Zhai, Z.; Dong, H.; Li, J.; Jiang, Z.; Li, Y.; Ma, W. *Adv. Funct. Mater.* **2013**, *23*, 885–892.
9. Hulea, I. N.; Fratini, S.; Xie, H.; Mulder, C. L.; Iossad, N. N.; Rastelli, G.; Ciuchi, S.; Morpurgo, A. F. *Nat. Mater.* **2006**, *5*, 982–986.
10. Mikroyannidis, J. A.; Tsagkournos, D. V.; Sharma, S. S.; Vijay, Y. K.; Sharma, G. D. *J. Mater. Chem.* **2011**, *21*, 4679–4688.
11. Zhou, J.; Zuo, Y.; Wan, X.; Long, G.; Zhang, Q.; Ni, W.; Liu, Y.; Li, Z.; He, G.; Li, C.; Kan, B.; Li, M.; Chen, Y. *J. Am. Chem. Soc.* **2013**, *135*, 8484–8487.
12. Chen, L.; Li, X.; Ying, W.; Zhang, X.; Guo, F.; Li, J.; Hua, J. *Eur. J. Org. Chem.* **2013**, *2013*, 1770–1780.
13. Zhang, X.; Chen, L.; Li, X.; Mao, J.; Wu, W.; Ågren, H.; Hua, J. *J. Mater. Chem. C* **2014**, *2*, 4063–4072.
14. Duan, T.; Hsiao, T.-Y.; Chi, Y.; Chen, X.; He, Y.; Zhong, C. *Dyes Pigm.* **2016**, *124*, 45–52.
15. Newman, C. R.; Frisbie, C. D.; da Silva Filho, D. A.; Brédas, J.-L.; Ewbank, P. C.; Mann, K. R. *Chem. Mater.* **2004**, *16*, 4436–4451.
16. Mitschke, U.; Baeuerle, P. *J. Mater. Chem.* **2000**, *10*, 1471–1507.
17. Li, Y. *Acc. Chem. Res.* **2012**, *45*, 723–733.
18. Misra, R.; Gautam, P. *Org. Biomol. Chem.* **2014**, *12*, 5448–5457.
19. Zeng, S.; Yin, L.; Jiang, X.; Li, Y.; Li, K. *Dyes Pigm.* **2012**, *95*, 229–235.
20. Chen, Y.; Wan, X.; Long, G. *Acc. Chem. Res.* **2013**, *46*, 2645–2655.
21. Knochel, P.; Zimdars, S.; Langhals, H. *Synthesis* **2011**, *2011*, 1302–1308.
22. Neto, B. A. D.; Lapis, A. A. M.; da Silva Júnior, E. N.; Dupont, J. *Eur. J. Org. Chem.* **2013**, *2013*, 228–255.
23. Zhang, X.; Han, S.; Pan, Q.; He, C.-Y. *Synlett* **2015**, 2175–2179.
24. Bijleveld, J. C.; Shahid, M.; Gilot, J.; Wienk, M. M.; Janssen, R. A. J. *Adv. Funct. Mater.* **2009**, *19*, 3262–3270.
25. Bloking, J. T.; Han, X.; Higgs, A. T.; Kastrop, J. P.; Pandey, L.; Norton, J. E.; Risko, C.; Chen, C. E.; Brédas, J.-L.; McGehee, M. D.; Sellinger, A. *Chem. Mater.* **2011**, *23*, 5484–5490.
26. Jorgensen, M.; Krebs, F. C. *J. Org. Chem.* **2005**, *70*, 6004–6017.
27. Misra, R.; Gautam, P.; Mobin, S. M. *J. Org. Chem.* **2013**, *78*, 12440–12452.

28. Miyazaki, T.; Shibahara, M.; Fujishige, J.; Watanabe, M.; Goto, K.; Shinmyozu, T. *J. Org. Chem.* **2014**, *79*, 11440–11453.
29. Omer, K. M.; Ku, S. Y.; Cheng, J. Z.; Chou, S. H.; Wong, K. T.; Bard, A. J. *J. Am. Chem. Soc.* **2011**, *133*, 5492–5499.
30. Jiang, D.; Chen, S.; Xue, Z.; Li, Y.; Liu, H.; Yang, W.; Li, Y. *Dyes Pigm.* **2016**, *125*, 100–105.
31. Gautam, P.; Maragani, R.; Misra, R. *RSC Adv.* **2015**, *5*, 18288–18294.
32. Cheng, J.-Z.; Lin, C.-C.; Chou, P.-T.; Chaskar, A.; Wong, K.-T. *Tetrahedron* **2011**, *67*, 734–739.
33. Kato, S.; Matsumoto, T.; Shigeiwa, M.; Gorohmaru, H.; Maeda, S.; Ishi-i, T.; Mataka, S. *Chem.—Eur. J.* **2006**, *12*, 2303–2317.
34. Pilgram, K.; Zupan, M.; Skiles, R. *J. Heterocycl. Chem.* **1970**, *7*, 629–633.
35. Hernández, A. R.; Kool, E. T. *Org. Lett.* **2011**, *13*, 676–679.
36. Garo, F.; Häner, R. *Eur. J. Org. Chem.* **2012**, *2012*, 2801–2808.
37. Pilgram, K.; Skiles, R. D. *J. Heterocycl. Chem.* **1974**, *11*, 777–780.
38. Habenicht, S. H.; Siegmann, M.; Kupfer, S.; Kübel, J.; Weiß, D.; Cherek, D.; Möller, U.; Dietzek, B.; Gräfe, S.; Beckert, R. *Methods Appl. Fluoresc.* **2015**, *3*, 025005.
39. Jonas, R.; Prücher, H.; Wurziger, H. *Eur. J. Med. Chem.* **1993**, *28*, 141–148.
40. Pesin, V. G.; D'yachenko, S. A.; Golubeva, E. V. *Khim. Geterotsikl. Soedin.* **1969**, *5*, 619–622.
41. Täuscher, E.; Beckert, R.; Weiß, D.; Görls, H. *Synthesis* **2010**, *10*, 1603–1608.
42. Täuscher, E.; Weiß, D.; Beckert, R.; Fabian, J.; Assumpção, A.; Görls, H. *Tetrahedron Lett.* **2011**, *52*, 2292–2294.
43. Täuscher, E.; Calderón-Ortiz, L.; Weiß, D.; Beckert, R.; Görls, H. *Synthesis* **2011**, *14*, 2334–2339.
44. Brouwer, A. M. *Pure Appl. Chem.* **2011**, *83*, 2213–2228.
45. Fery-Forgues, S.; Lavabre, D. *J. Chem. Educ.* **1999**, *76*, 1260–1264.
46. Tomasi, J.; Mennucci, B.; Cammi, R. *Chem. Rev.* **2005**, *105*, 2999–3093.
47. Halgren, T. A. *J. Comput. Chem.* **1996**, *17*, 490–519.
48. Yanai, T.; Tew, D. P.; Handy, N. C. *Chem. Phys. Lett.* **2004**, *393*, 51–57.
49. Frisch, M. J.; Trucks, G. W.; Schlegel, H. B.; Scuseria, G. E.; Robb, M. A.; Cheeseman, J. R.; Scalmani, G.; Barone, V.; Mennucci, B.; Petersson, G. A.; Nakatsuji, H.; Caricato, M.; Li, X.; Hratchian, H. P.; Izmaylov, A. F.; Bloino, J.; Zheng, G.; Sonnenberg, J. L.; Hada, M.; Ehara, M.; Toyota, K.; Fukuda, R.; Hasegawa, J.; Ishida, M.; Nakajima, T.; Honda, Y.; Kitao, O.; Nakai, H.; Vreven, T.; Montgomery, J. A., Jr.; Peralta, J. E.; Ogliaro, F.; Bearpark, M. J.; Heyd, J.; Brothers, E. N.; Kudin, K. N.; Staroverov, V. N.; Kobayashi, R.; Normand, J.; Raghavachari, K.; Rendell, A. P.; Burant, J. C.; Iyengar, S. S.; Tomasi, J.; Cossi, M.; Rega, N.; Millam, N. J.; Klene, M.; Knox, J. E.; Cross, J. B.; Bakken, V.; Adamo, C.; Jaramillo, J.; Gomperts, R.; Stratmann, R. E.; Yazyev, O.; Austin, A. J.; Cammi, R.; Pomelli, C.; Ochterski, J. W.; Martin, R. L.; Morokuma, K.; Zakrzewski, V. G.; Voth, G. A.; Salvador, P.; Dannenberg, J. J.; Dapprich, S.; Daniels, A. D.; Farkas, Ö.; Foresman, J. B.; Ortiz, J. V.; Cioslowski, J.; Fox, D. J. *Gaussian 09*; Gaussian: Wallingford, CT, USA, 2009.
50. Jacquemin, D.; Wathelet, V.; Perpète, E. A.; Adamo, C. *J. Chem. Theory Comput.* **2009**, *5*, 2420–2435.
51. Jacquemin, D.; Perpète, E. A.; Ciofini, I.; Adamo, C. *Theor. Chem. Acc.* **2010**, *128*, 127–136.
52. Habenicht, S. H.; Schramm, S.; Zhu, M.; Freund, R. R.; Langenstuck, T.; Strathausen, R.; Weiss, D.; Biskup, C.; Beckert, R. *Photochem Photobiol. Sci.* **2015**, *14*, 2097–2107.
53. Pinto da Silva, L.; Esteves da Silva, J. C. G. *Int. J. Quantum Chem.* **2013**, *113*, 45–51.

**Publikation 3:**

„Pushing to the Low Limits: Tetraazaanthracenes with Very Low-Lying LUMO Levels and Near-Infrared Absorption"

D. M. Gampe, S. Schramm, F. Nöller, D. Weiß, H. Görls, P. Naumov, R. Beckert,

*Chem. Commun.* **2017**, *53*, 10220-10223.



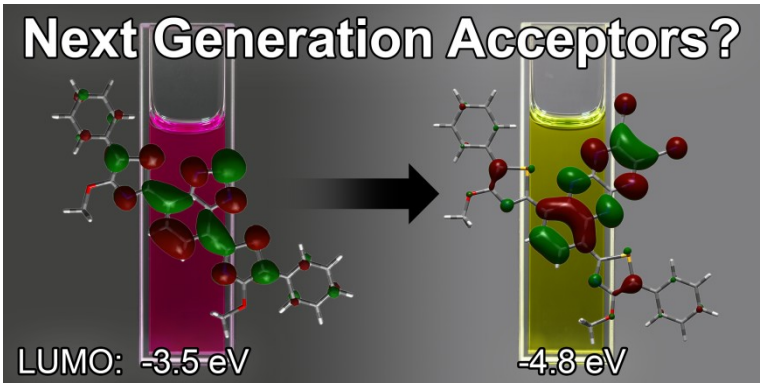

ChemComm

COMMUNICATION

View Article Online
View Journal | View Issue



Cite this: *Chem. Commun.*, 2017, 53, 10220

Received 6th July 2017,
Accepted 23rd August 2017

DOI: 10.1039/c7cc05224c

rsc.li/chemcomm

# Pushing to the low limits: tetraazaanthracenes with very low-lying LUMO levels and near-infrared absorption†

Dominique Mario Gampe,‡[a] Stefan Schramm, ‡[ab] Florian Nöller,[a] Dieter Weiß,[a] Helmar Görls,[c] Panče Naumov [b] and Rainer Beckert ⋆[a]

**Here we propose the combination of the 4-alkoxythiazole donor motif with highly photostable tetraazaanthracenes as electron-acceptor units. The segregated frontier orbitals in these dyes afford optical band gaps of 1.4–1.1 eV. Cyclic voltammetry confirmed the very low-lying LUMO levels that are attributed to the highly electron-deficient tetraazaanthracene moiety.**

The recent advances in organic photovoltaics owe greatly to the continual efforts to improve bulk heterojunction solar cells (BHJ).[1] A vast number of both polymers[2] and small molecules[3] have been designed and investigated with regard to their electron-donating properties towards fullerene-based acceptors,[4] especially the phenyl-$C_{61}$-butyric acid methyl ester ($PC_{61}BM$), which is reaching its performance limit.[5] Small-molecule acceptors are now generally thought to be advantageous relative to the conventional fullerene derivatives due to their processability from solution,[6] cost-effective synthesis,[7] tunable frontier orbital energies[8] and improved efficiency of light harvesting.[9] Since the recent results have indicated superior performance of BHJs based on small molecule acceptors relative to the traditional fullerene-based devices,[10] this line of pursuit calls for new acceptor materials and manifold donor–acceptor pairs as an alternative to the design of new potential donor species.

Long-wavelength absorbing small molecules are typically designed by using the charge transfer (CT) in donor–acceptor (D–A) type dyes.[11] Since the highest occupied molecular orbital (HOMO) and the lowest unoccupied molecular orbital (LUMO) are determined by the respective electron-donating and electron-accepting moieties, the energy levels of a D–A type dye can be tuned by incorporating the appropriate building blocks by applying simple molecular design principles.[12] In that regard, 4-alkoxythiazoles are known to excel with their photochemical properties[13] and the propensity to donate electrons to the benzo[1,2,5]thiadiazole (Bt) acceptor moieties.[14] The Bt-based acceptor structures are easily functionalized[15] and have been already applied to construct D–A systems.[16] As it has been demonstrated recently tetraazaanthracenes can easily be obtained from Bt substructures, whereby the LUMO energy is drastically decreased to levels that are applicable to electron-accepting materials.[17] Here we present that combination of 4-alkoxythiazole donors and tetraazaanthracene acceptor moieties fulfill these requirements and are viable candidates for advanced solar cell applications.

Chart 1 depicts the designed target structures, which were prepared *via* the synthetic route shown in Scheme 1. Hantzsch cyclization between the appropriate α-bromoethylphenylacetate (**20**, **21**) and the carbothioamides (**17**, **18**, **19**) afforded the 4-hydroxythiazoles **14**, **15** and **16**.[18] These Bt derivatives were transformed into the 4-$^n$hexyloxythiazoles **11**, **12** and **13** *via* Williamson-type etherifications with iodohexane. Reductive desulfurization of the Bt-thiazoles (**11**, **12**, **13**) with sodium borohydride afforded the *o*-phenylenediamine substructures, which due to their instability against oxygen were used as obtained after a short work-up procedure (for further details

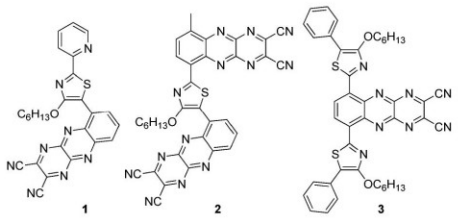


Chart 1 Structures of the target molecules.

[a] *Friedrich Schiller University Jena, Institute of Organic and Macromolecular Chemistry, Humboldtstraße 10, 07743 Jena, Germany. E-mail: rainer.beckert@uni-jena.de*
[b] *New York University Abu Dhabi, P.O. Box 129188, Abu Dhabi, United Arab Emirates*
[c] *Friedrich Schiller University Jena, Institute of Inorganic and Analytical Chemistry, Humboldtstraße 8, 07743 Jena, Germany*

† Electronic supplementary information (ESI) available: Experimental and computational details, CV, characterization of **11**, crystallography of **11**. CCDC 1554777. For ESI and crystallographic data in CIF or other electronic format see DOI: 10.1039/c7cc05224c

‡ These authors are contributed equally.

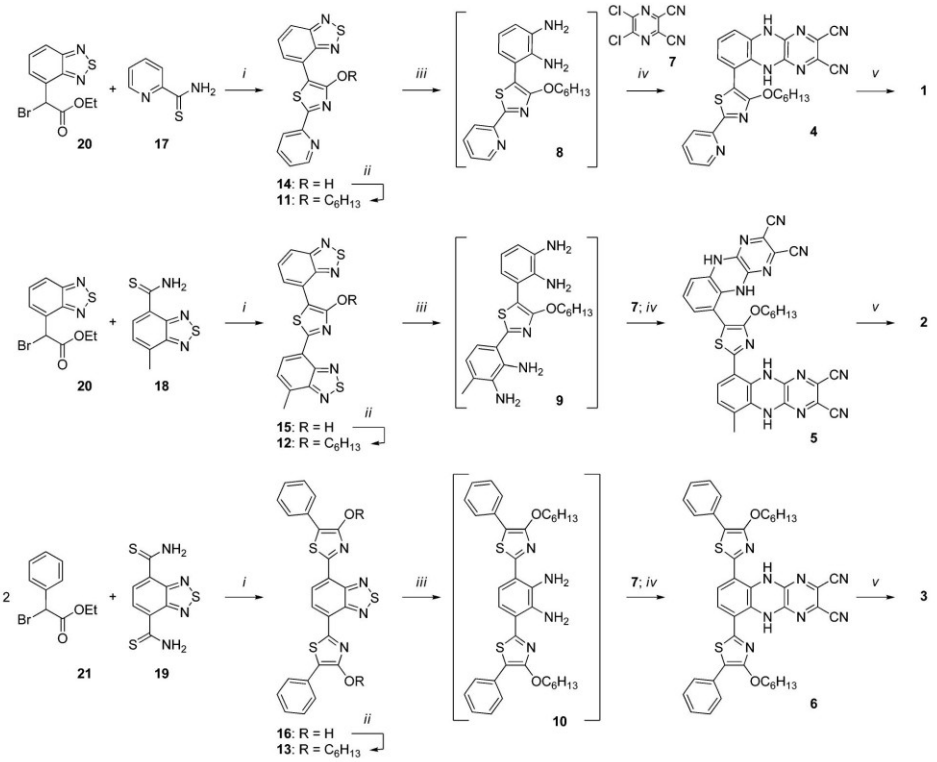


Scheme 1 Synthetic route to the target compounds **1**, **2** and **3**. (i) NaAc, EtOH, 80 °C, **14**: 63%, **15**: 76%, **16**: 48%; (ii) I-$C_6H_{13}$, $K_2CO_3$, acetone, 70 °C, **11**: 85%, **12**: 74%; **13**: 28%; (iii) $NaBH_4$, $CoCl_2$ (cat.), EtOH/THF, $N_2$, short work-up, **8**, **9**, **10**: quant.; (iv) 5,6-dichloro-2,3-dicyanopyrazine (**7**), dioxane, $N_2$, 110 °C, **4**: 32%, **5**: 58%, **6**: 33%; (v) DDQ, THF, $N_2$, **1**: 91%, **2**: 57%, **3**: 90%.

see the ESI†).[19] The following cyclizations with dichlorodicyanopyrazine (**7**) provided the dihydrotetraazaanthracenes **4**, **6** and the thiazol-bridged bis-dihydrotetraazaanthracene **5**. To obtain the D–A derivatives **1**, **2** and **3**, the dihydrospecies were oxidized with dichlorodicyanobenzoquinone. Utilizing this synthetic protocol, Bt derivatives (**11**, **12**, **13**) are easily transformed into tetraazaanthracenes in two steps and 30% yield. The target materials were fully characterized and showed good photostability under laboratory conditions in solution (such as THF, toluene, benzene) and in the solid state. When heated in protic solvents, such as methanol, they are reduced back to their dihydro precursors (**4**, **5**, **6**). This behavior is known for azaacenes, but the mechanism remains unexplored and obscure.[20] All derivatives form deep-colored solutions—the pyridyl derivative **1** displays blue-green, the bis-anthracene **2** green and the bis-thiazole **3** dark yellow solutions. Strong π–π* transition bands in the UV and blue regions dominate the electronic absorption spectra of all compounds (Fig. 1A). Molar extinction coefficients ($\varepsilon$) of 2.14 (**1**), 3.82 (**2**) and 3.63 × $10^4$ $M^{-1}$ $cm^{-1}$ (**3**) were determined at the respective maxima of 349 (**1**), 353 (**2**) and 446 nm (**3**). Broad CT bands extend over the whole visible and the near-infrared (NIR) region. Both A–D–A type dyes **1** and **2** show long-wavelength absorption to 900 nm, which is related to optical band gaps of 1.45 (**1**) and 1.42 eV (**2**). Comparison with their corresponding Bt precursors **11** and **12** points to the acceptor strength of the anthracenes, as the optical gaps are decreased by 1 and 0.9 eV, respectively (Table 1). In the case of the absorption spectra of D–A–D molecules **13** to **3**, a strong bathochromic shift of ~300 nm (≙ 0.8 eV) was observed. The CT band of **3** extends between 550 and 1100 nm, with a maximum at 839 nm ($\varepsilon$ = 6350 $M^{-1}$ $cm^{-1}$) and a narrow band gap of 1.13 eV was estimated. These long-wavelength absorptions seem remarkable, since in contrast to the fullerene-based materials they provide significant overlap with the solar spectrum of up to about 1100 nm.[21]

The redox activity of the molecules was examined using cyclic voltammetry (Fig. 1B). All derivatives (**1**, **2**, **3**) possess an irreversible oxidation step at 0.8 V (against $Fc/Fc^+$), which is typical for 4-alkoxythiazoles (Fig. S3–S5, ESI†).[14] As expected, the bis-thiazole **3** can be oxidized twice, hence the irreversible oxidation at 1 V. Two reversible one-electron reduction steps were

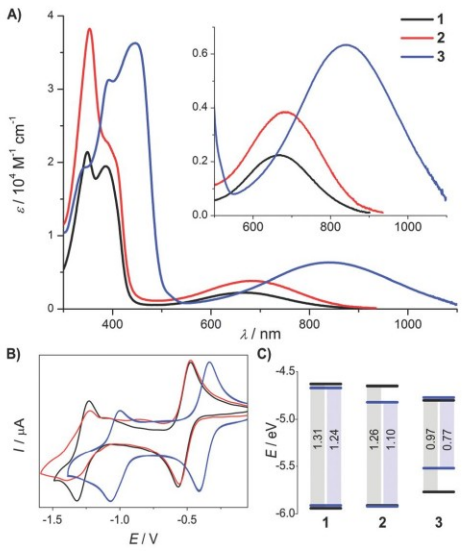


Fig. 1 (A) UV/Vis absorption spectra (THF) of anthracene derivatives **1**, **2** and **3**; (B) reduction cycles of the target molecules, measured in 1 M solution of $TBAPF_6$ in THF, calibrated externally against $Fc/Fc^+$; (C) graphical depiction of the comparison between the experimental (black lines) and theoretical (blue lines) obtained frontier orbital energies.

detected that are attributed to the tetraazaanthracene substructure, which forms a stable radical anion and dianion. **1** and **2** are reduced at half-wave potentials of $E_{1/2} = -0.52$ and $-1.3$ V (against $Fc/Fc^+$). The D–A–D molecule **3** has an extraordinary high electron affinity, as reflected in the reductions at $-0.37$ and $-1.00$ V. These high reduction potentials (**1**, **2**: ~0 V/**3**: 0.16 V against SCE) secure electrochemical stability against water and oxygen.[22] The electrochemical LUMO levels were calculated to $-4.6$ eV (**1**, **2**) and $-4.7$ (**1**)/$-4.8$ eV (**2**) by means of DFT/TD-DFT, respectively (Table 1, Fig. 1C and ESI†). These low levels seem remarkable by comparison with conventional acceptor materials, such as $PC_{61}BM$ ($E_{LUMO} = -3.75$ eV),[23] $PC_{71}BM$ ($-4.30$ eV)[24] or tetracyano-*p*-quinodimethane (TCNQ: $-4.23$ eV).[25] Furthermore, they are in the range of Wang's 4CN-4Cl-perylenediimide that has an "ultra-low LUMO level" of $-4.64$ eV.[26] Notably, a record-breaking low LUMO for non-fluorinated materials was determined by CV and DFT to $-4.8$ eV for bis-thiazole **3**. To our knowledge, only three- and four-fold fluorinated TCNQ derivatives deploy such low LUMOs ($-5.24$ eV in F4TCNQ).[25,27] Electrochemical band gaps of $\Delta E^{CV} = 1.3$ (**1**, **2**) and 1 eV (**3**) were estimated *via* the HOMO levels of $-5.9$ (**1**, **2**) and $-5.8$ eV (**3**), respectively, and are in very good agreement with the optical gaps. The slightly narrower $\Delta E^{CV}$ (see Table 1) can be explained by molecular torsion that is associated with an ineffective π-conjugation of π-systems in solution (increasing $\Delta E^{opt}$ from UV/Vis absorption).

Comparison between the energy levels of the anthracene derivatives and the Bt precursors (**11**, **12**, **13**) confirm the high electron deficiency of the tetraazaanthracenes. While the HOMO layers of **11** and **1**, **12** and **2** as well as **13** and **3** remain constant (see Table 1), as they are located at the thiazole donor part, the LUMOs decrease drastically. The reduction waves of **1**, **2** and **3** are shifted by 1.3 V to higher potentials relative to the appropriate Bt precursor **11**, **12** or **13**; consequently the LUMO levels and band gaps are decreased by ~1.2 eV. Bt substituents are applied frequently as strong electron-accepting unit in D–A materials.[28] However the synthetic effort to prepare the tetraazaanthracenes seems worthwhile considering the narrow band gaps and low-lying LUMOs.

In summary, this work describes successful combination of the 4-alkoxythiazole donor and tetraazaanthracene acceptor building block. The derivatives were synthesized without expensive

Table 1 Summary of the photochemical data and the estimated frontier orbital energies

| | **11** | **1** | **12**[14] | **2** | **13**[14] | **3** |
|---|---|---|---|---|---|---|
| $\lambda_{max}$[a]/nm [log ε] | 433 [4.3]; 242 [4.4] | 664 [3.4]; 349 [4.3] | 470 [4.3]; 315 [4.5] | 685 [3.6]; 353 [4.6] | 545 [4.5]; 365 [4.4] | 839 [3.8]; 446 [4.6] |
| **$\Delta E^{opt}$[b]/eV** | **2.52** | **1.45** | **2.28** | **1.42** | **1.97** | **1.13** |
| $E_{HOMO}$[c]/eV | −5.83 | −5.94 | −5.62[f] | −5.91 | −5.48[f] | −5.77 |
| $E_{LUMO}$[c]/eV | −3.28 | −4.63 | −3.18[f] | −4.65 | −3.42[f] | −4.80 |
| **$\Delta E^{CV}$[d]/eV** | **2.55** | **1.31** | **2.44** | **1.26** | **2.06** | **0.97** |
| $E_{HOMO}$[e]/eV (error) | −5.66 (0.17) | −5.91 (0.03) | −5.58 (0.04) | −5.92 (0.01) | −5.43 (0.05) | −5.52 (0.25) |
| $E_{LUMO}$[f]/eV (error) | −3.34 (0.06) | −4.67 (0.04) | −2.92 (0.26) | −4.82 (0.17) | −3.18 (0.24) | −4.77 (0.03) |
| **$\Delta E^{DFT}$[d]/eV (error)** | **2.32 (0.23)** | **1.24 (0.07)** | **2.66 (0.22)** | **1.10 (0.16)** | **2.25 (0.19)** | **0.77 (0.22)** |

[a] Measured in THF. [b] Calculated *via* the onset (10%) of the absorption spectra. [c] Recorded by cyclic voltammetry in 0.1 M solution of $TBAPF_6$ in THF, calculated *via* $E_{HOMO} = -[E_{onset}(ox\ vs.\ Fc^+/Fc) + 5.1\ eV]$ and $E_{LUMO} = -[E_{onset}(red\ vs.\ Fc^+/Fc) + 5.1\ eV]$. [d] $\Delta E = -(E_{HOMO} - E_{LUMO})$. [e] Calculated energies at B3LYP/6-31+G(d,p) level of theory based on a B3LYP/6-31+G(d,p) PCM THF optimized ground state geometry, HOMO energies resulted from B3LYP/6-31+G(d,p) calculations, LUMO energies resulted from PBE/6-31+G(d,p) calculations,[29] 'error' stands for the difference between the experimental and theoretical estimated values. [f] Frontier orbital energies were calculated *via* the outdated equations: $E_{HOMO} = -[E_{onset}(ox) - E_{onset}(Fc/Fc^+)] - 4.8$ eV and $E_{LUMO} = -[E_{onset}(red) - E_{onset}(Fc/Fc^+)] - 4.8$ eV.

 

transition metal catalysis and are fully spectroscopically characterized. Broad absorption bands were observed over the whole visible to the NIR region. Utilization of tetraazaanthracene as electron-accepting moiety results in narrow band gaps and record-breaking low LUMOs which becomes evident by comparison with their Bt-acceptor bearing precursors. Due to good solubility in common organic solvents, such as chloroform or dichlorobenzene, and easy accessibility, the bis-thiazole **3** is particularly promising for application in organic electronics.

We thank Dr P. Commins for proofreading the manuscript and Anja Darsen for the synthesis of some starting materials. The computations were carried out on the High-Performance Computing resources (Dalma) at New York University Abu Dhabi.

## Conflicts of interest

There are no conflicts to declare.

## References

1 (*a*) B. P. Rand, J. Genoe, P. Heremans and J. Poortmans, *Prog. Photovoltaics*, 2007, **15**, 659; (*b*) Y.-W. Su, S.-C. Lan and K.-H. Wei, *Mater. Today*, 2012, **15**, 554; (*c*) P. Bäuerle and A. Mishra, *Angew. Chem., Int. Ed.*, 2012, **51**, 2020; (*d*) Y. Li, *Acc. Chem. Res.*, 2012, **45**, 723.
2 (*a*) G. Li, R. Zhu and Y. Yang, *Nat. Photonics*, 2012, **6**, 153; (*b*) J. Yan and B. R. Saunders, *RSC Adv.*, 2014, **4**, 43286; (*c*) L. Lu, T. Zheng, Q. Wu, A. M. Schneider, D. Zhao and L. Yu, *Chem. Rev.*, 2015, **115**, 12666.
3 (*a*) Y. Lin, Y. Li and X. Zhan, *Chem. Soc. Rev.*, 2012, **41**, 4245; (*b*) Y. Chen, X. Wan and G. Long, *Acc. Chem. Res.*, 2013, **46**, 2645.
4 C. Zhan and J. Yao, *Chem. Mater.*, 2016, **28**, 1948.
5 (*a*) L. Dou, J. You, Z. Hong, Z. Xu, G. Li, R. A. Street and Y. Yang, *Adv. Mater.*, 2013, **25**, 6642; (*b*) N. Kaur, M. Singh, D. Pathak, T. Wagner and J. M. Nunzi, *Synth. Met.*, 2014, **190**, 20.
6 C. B. Nielsen, S. Holliday, H. Y. Chen, S. J. Cryer and I. McCulloch, *Acc. Chem. Res.*, 2015, **48**, 2803.
7 D. Dang, Y. Zhi, X. Wang, B. Zhao, C. Gao and L. Meng, *Dyes Pigm.*, 2017, **137**, 43.
8 (*a*) H. Yao, Y. Chen, Y. Qin, R. Yu, Y. Cui, B. Yang, S. Li, K. Zhang and J. Hou, *Adv. Mater.*, 2016, **28**, 8283; (*b*) D. M. Gampe, S. Schramm, M. Kaufmann, H. Görls and R. Beckert, *New J. Chem.*, 2016, **40**, 10100; (*c*) D. M. Gampe, S. Schramm, S. Ziemann, M. Westerhausen, H. Gorls, P. Naumov and R. Beckert, *J. Org. Chem.*, 2017, **82**, 6153.
9 Y. Lin, Y. Wang, J. Wang, J. Hou, Y. Li, D. Zhu and X. Zhan, *Adv. Mater.*, 2014, **26**, 5137.
10 (*a*) J. W. Jung and W. H. Jo, *Chem. Mater.*, 2015, **27**, 6038; (*b*) Y. Yu, F. Yang, Y. Ji, Y. Wu, A. Zhang, C. Li and W. Li, *J. Mater. Chem. C*, 2016, **4**, 4134; (*c*) Y. Lin, F. Zhao, Q. He, L. Huo, Y. Wu, T. C. Parker, W. Ma, Y. Sun, C. Wang, D. Zhu, A. J. Heeger, S. R. Marder and X. Zhan, *J. Am. Chem. Soc.*, 2016, **138**, 4955.
11 (*a*) J. Fabian, H. Nakazumi and M. Matsuoka, *Chem. Rev.*, 1992, **92**, 1197; (*b*) A. Mishra, M. K. R. Fischer and P. Bäuerle, *Angew. Chem.*, 2009, **121**, 2510.
12 (*a*) D. F. Perepichka and M. R. Bryce, *Angew. Chem., Int. Ed. Engl.*, 2005, **44**, 5370; (*b*) A. Pron, P. Gawrys, M. Zagorska, D. Djurado and R. Demadrille, *Chem. Soc. Rev.*, 2010, **39**, 2577.
13 (*a*) R. Menzel, D. Ogermann, S. Kupfer, D. Weiß, H. Görls, K. Kleinermanns, L. González and R. Beckert, *Dyes Pigm.*, 2012, **94**, 512; (*b*) R. Menzel, S. Kupfer, R. Mede, D. Weiß, H. Görls, L. González and R. Beckert, *Eur. J. Org. Chem.*, 2012, 5231.
14 D. M. Gampe, F. Nöller, V. G. Hänsch, S. Schramm, A. Darsen, S. H. Habenicht, S. Ehrhardt, D. Weiß, H. Görls and R. Beckert, *Tetrahedron*, 2016, **72**, 3232.
15 B. A. D. Neto, A. A. M. Lapis, E. N. da Silva Júnior and J. Dupont, *Eur. J. Org. Chem.*, 2013, 228.
16 (*a*) K. M. Omer, S. Y. Ku, J. Z. Cheng, S. H. Chou, K. T. Wong and A. J. Bard, *J. Am. Chem. Soc.*, 2011, **133**, 5492; (*b*) J. T. Bloking, X. Han, A. T. Higgs, J. P. Kastrop, L. Pandey, J. E. Norton, C. Risko, C. E. Chen, J.-L. Brédas, M. D. McGehee and A. Sellinger, *Chem. Mater.*, 2011, **23**, 5484; (*c*) R. Misra, P. Gautam, T. Jadhav and S. M. Mobin, *J. Org. Chem.*, 2013, **78**, 4940; (*d*) L. Wang, L. Yin, C. Ji and Y. Li, *Dyes Pigm.*, 2015, **118**, 37.
17 (*a*) J. Nishida, N. Naraso, S. Murai, E. Fujiwara, H. Tada, M. Tomura and Y. Yamashita, *Org. Lett.*, 2004, **6**, 2007; (*b*) Y. Liu, F. Zhang, C. He, D. Wu, X. Zhuang, M. Xue, Y. Liu and X. Feng, *Chem. Commun.*, 2012, **48**, 4166; (*c*) D. M. Gampe, V. G. Hänsch, S. Schramm, R. Menzel, D. Weiß and R. Beckert, *Eur. J. Org. Chem.*, 2017, 1369.
18 E. Täuscher, R. Beckert, D. Weiß and H. Görls, *Synthesis*, 2010, 1603.
19 D. M. Gampe, M. Kaufmann, D. Jakobi, T. Sachse, M. Presselt, R. Beckert and H. Görls, *Chem. – Eur. J.*, 2015, **21**, 7571.
20 (*a*) O. Hinsberg and J. Pollak, *Chem. Ber.*, 1896, **29**, 784; (*b*) B. D. Lindner, J. U. Engelhart, O. Tverskoy, A. L. Appleton, F. Rominger, A. Peters, H. J. Himmel and U. H. Bunz, *Angew. Chem., Int. Ed.*, 2011, **50**, 8588; (*c*) R. M. Z. He, D. Liu and Q. Miao, *Org. Lett.*, 2012, **14**, 4190.
21 ASTM G173-03(2012), Standard Tables for Reference Solar Spectral Irradiances: Direct Normal and Hemispherical on 37° Tilted Surface, ASTM International, West Conshohocken, PA, 2012.
22 D. M. de Leeuw, M. M. J. Simenon, A. R. Brown and R. E. F. Einerhand, *Synth. Met.*, 1997, **87**, 53.
23 W. J. Beenken, F. Herrmann, M. Presselt, H. Hoppe, S. Shokhovets, G. Gobsch and E. Runge, *Phys. Chem. Chem. Phys.*, 2013, **15**, 16494.
24 S.-B. Li, Y.-A. Duan, Y. Geng, H.-B. Li, J.-Z. Zhang, H.-L. Xu, M. Zhang and Z.-M. Su, *Phys. Chem. Chem. Phys.*, 2014, **16**, 25799.
25 P. Hu, K. Du, F. Wei, H. Jiang and C. Kloc, *Cryst. Growth Des.*, 2016, **16**, 3019.
26 J. Gao, C. Xiao, W. Jiang and Z. Wang, *Org. Lett.*, 2014, **16**, 394.
27 A. B. Padmaperuma, *Adv. Mater. Phys. Chem.*, 2012, **2**, 163.
28 J. E. Coughlin, Z. B. Henson, G. C. Welch and G. C. Bazan, *Acc. Chem. Res.*, 2014, **47**, 257.
29 J. Tomasi, B. Mennucci and R. Cammi, *Chem. Rev.*, 2005, **105**, 2999.

**Publikation 4:**

„Mixing Chromophores: Novel D-A-type Dyes with low lying LUMOs and narrow Bandgaps by Connecting 4-Alkoxythiazoles and Azaacenes“

D. M. Gampe, V. G. Hänsch, S. Schramm, R. Menzel, D. Weiß, R. Beckert,

*Eur. J. Org. Chem.* **2017**, *2017*, 1369-1379.



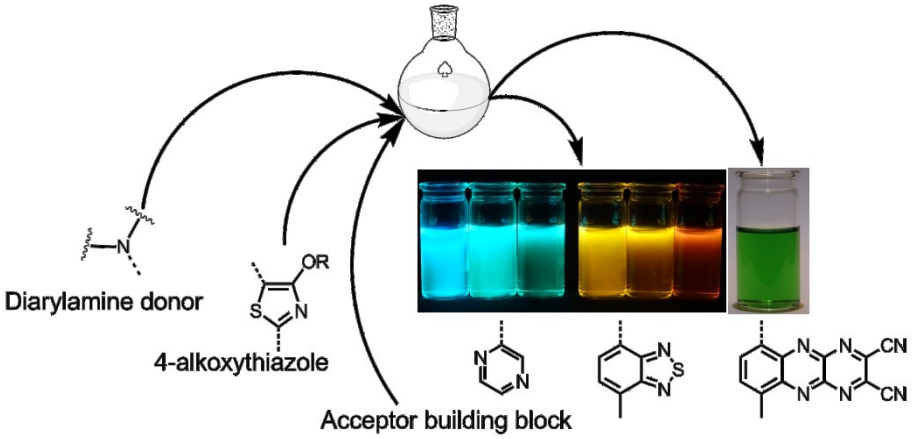

ChemPubSoc Europe
DOI: 10.1002/ejoc.201601521
EurJOC European Journal of Organic Chemistry
Full Paper

Donor–Acceptor Systems

# Mixing Chromophores: Donor–Acceptor Dyes with Low-Lying LUMOs and Narrow Band Gaps by Connecting 4-Alkoxythiazoles and Azaacenes

Dominique Mario Gampe,[a] Veit Georg Hänsch,[a] Stefan Schramm,[a,b] Roberto Menzel,[a,c] Dieter Weiß,[a] and Rainer Beckert*[a]

*Dedicated to the memory of Professor Dr. Ernst Anders[‡]*

**Abstract:** The synthesis and characterization of novel donor–acceptor (D–A) type functional dyes is presented. The materials studied are based on the 4-alkoxythiazole structure containing one of three arylamine donor units and one of three acceptor building blocks. The nine dyes were characterized with respect to their photo- and electrochemical properties based on UV/Vis absorption and fluorescence emission spectroscopy, as well as cyclic voltammetry. Density functional theory calculations were carried out to support these investigations. The building blocks used brought their characteristics into the final target structures: the reversible oxidation and electron-donating properties of diarylamines, the high fluorescence quantum yields of 4-alkoxythiazoles, and the low-lying LUMOs of tetraazaanthracenes. Furthermore, by introducing tetraazaanthracenes as the acceptor moiety, very narrow band gaps of 1.1 and 0.7 eV were estimated electrochemically.

## Introduction

Monodisperse metal-free molecules that are based on the donor–acceptor (D–A) approach are increasingly being employed in devices such as dye-sensitized solar cells (DSSCs) or bulk heterojunction solar cells (BHJs) to convert sunlight into electricity.[1] The charge-transfer (CT) character of such D–A-type small molecules lowers the band gap [energetic distance from the highest occupied molecular orbital (HOMO) to the lowest unoccupied molecular orbital (LUMO)], leading to a bathochromic shift of the associated absorption, and thereby enabling favourable near-infrared (NIR) absorption to be utilised.[2]

We recently reported the application of 4-alkoxythiazoles as the electron-donating unit in D–A type molecules.[3] 4-alkoxythiazoles are a well-known and well-studied class of heterocycles.[4] Many derivatives have been designed and studied intensively with regard to their superior photo- and electrochemical properties, during the last decade,[5] and a wide range of applications have been developed based on the high extinction coefficients, quantum yields and simple derivatisation reactions.[6] They can be incorporated as dyes in blue fluorescent polymers as the emitting species[7] or as a Förster resonance energy transfer donors in terpolymers,[8] and their use as a fluoride ion sensor[9] or as a sensitizer in DSSCs[10] has been realised. Furthermore, solvatochromic, long-wavelength-absorbing dyes of small molecular weight were constructed by tuning the D–A units on the thiazole scaffold.[11]

We have now successfully introduced diarylamine substituents into the thiazole-based D–A dyes, which were described recently,[3] to enhance the electron-donating character. Diarylamines, which are known to be outstanding electron-donating units,[12] excel through their nonlinear optical[13] and p-type semiconducting properties,[14] and are able to form stable radical cations.[15]

In this study, we used three cyclic diarylamines as electron-donating moieties, carbazole, phenoxazine and phenothiazine, and we tested three kinds of electron-accepting units to compare the D–A combinations. Pyrazine was used as a weak electron acceptor, piazthiole (Bt) as a strong and well-known accepting unit,[16] and tetraazaanthracene as a novel building block for D–A materials.

Tetraazaanthracenes are known for their high electron deficiency[17] because of their low-lying LUMO levels, and they were found to be suitable n-type semiconductors in organic field-effect transistors (OFETs).[18] High stability, interesting photochemical properties and versatile derivatisation possibilities made them a promising target structure for optoelectronic applications.[19]

Novel D–A type molecules possessing deep LUMO energies and narrow band gaps were designed by mixing these three kinds of building blocks (thiazoles, diarylamines, tetraazaanthracenes).

[a] Friedrich Schiller University Jena, Institute of Organic and Macromolecular Chemistry,
Humboldtstraße 10, 07743 Jena, Germany
E-mail: rainer.beckert@uni-jena.de
http://www.agbeckert.uni-jena.de/
[b] NYU Abu Dhabi, Saadiyat Campus, Experimental Research Building (C1), P. O. Box 129188, Abu Dhabi, United Arab Emirates
[c] Sartorius Stedim Biotech,
August-Spindler-Strasse 11, 37079 Göttingen, Germany
[‡] January 3, 1942 – December 27, 2016
Supporting information for this article is available on the WWW under http://dx.doi.org/10.1002/ejoc.201601521.

ChemPubSoc Europe
EurJOC European Journal of Organic Chemistry
Full Paper

Given their economical synthesis, as well as tuneable frontier orbital energies and morphologies, such electron-accepting materials have been studied and tested intensively, with the intent of replacing fullerenes in organic devices.[20] Recent results indicate that fullerene-free organic solar cells can compete with traditional fullerene-based systems.[21]

Based on the building blocks described herein, nine compounds bearing the D–A motif were synthesised and characterised. Scheme 1 shows the general structure of the novel dyes, which are based on 4-alkoxythiazoles as the central unit. The substitution pattern of the central core, with an electron-withdrawing unit on the 2-position and an electron-donating moiety on the 5-position of the thiazole, favours a strong CT character, as ascertained by our group.[22]

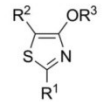

$R^1$ = electron-withdrawing group
$R^2$ = electron-donating group
$R^3$ = solubilizing group

Scheme 1. General motif of the synthesized D–A dyes.

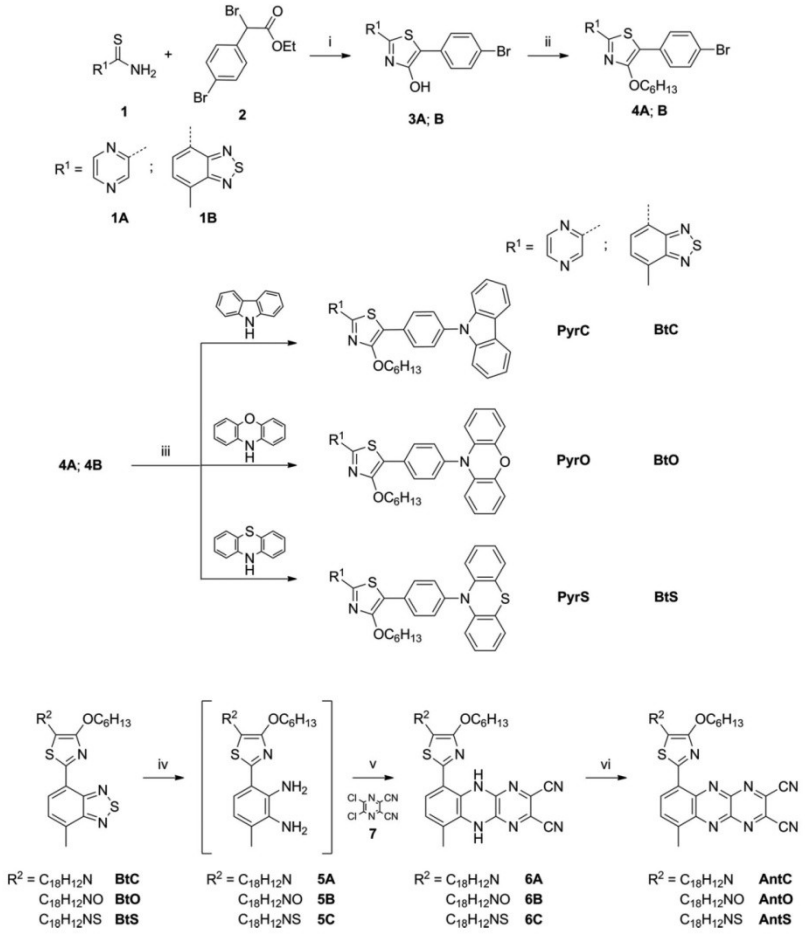


Scheme 2. Synthesis of *para*-brominated 4-alkoxythiazoles **4A** and **4B**. Buchwald–Hartwig cross-coupling reactions between the brominated thiazoles **4A** and **4B** with diarylamines carbazole, phenoxazine and phenothiazine. Synthesis of the tetraazaanthracene-derivatives AntC, AntO and AntS. Reagents and conditions: (i) EtOH, NaAc, 80 °C, **3A**: 25 %, **3B**: 87 %; (ii) acetone, I-$C_6H_{13}$, 60 °C, **4A**: 80 %, **4B**: 72 %; (iii) $Pd(dba)_2$, SPHOS, KO*t*Bu, toluene, 110 °C, $N_2$, PyrC: 53 %, PyrO: 46 %, PyrS: 35 %, BtC: 83 %, BtO: 95 %, BtS: 80 %; (iv) EtOH/THF, $N_2$, $NaBH_4$, $CoCl_2$ (cat.); (v) dioxane, $N_2$, **6A**: 54 %, **6B**: 30 %, **6C**: 45 %; (vi) THF, $N_2$, DDQ (1.1 equiv.), AntC: 53 %, AntO: 57 %, AntS: 58 %.

ChemPubSoc Europe
EurJOC European Journal of Organic Chemistry
Full Paper

## Results and Discussion

### Synthesis

The central thiazole moieties could be obtained through Hantzsch cyclisation reactions between carbothioamides **1A** and **1B**, and ethyl 2-bromo-(4-phenyl)acetate (**2**) under alkaline conditions (see Scheme 2).[22] These condensation reactions afforded 4-hydroxythiazoles, bearing *para*-bromo-phenyl substituents (**3A**, **3B**), in variable yields. Williamson-type etherification was carried out to incorporate solubilising groups, such as *n*-hexyl side chains (**4A**, **4B**). As depicted in Scheme 2, the diarylamine substituents were introduced through Buchwald–Hartwig cross-coupling reactions. As established by Menzel et al., we synthesised the D–A molecules by using $Pd(dba)_2$ as the precatalyst, SPHOS as the ligand and KO*t*Bu as the base in degassed toluene.[6] These cross-coupling reactions between **4A** or **4B**, respectively, and diarylamines carbazole, phenoxazine and phenothiazine afforded six D–A dyes: pyrazine-substituted compounds PyrC, PyrO and PyrS, in moderate yield, and Bt-substituted dyes BtC, BtO and BtS, in very good yields.

Although the Bt acceptor dyes BtC, BtO and BtS represent target structures, they can also be converted through reduction into the corresponding *o*-phenylenediamine and subsequent cyclisation. Thus, a variety of acceptor blocks are available; for example, condensation with *o*-quinones affords quinoxaline derivatives, which are also favoured acceptor structures.[23] In contrast, we wanted to establish a stronger electron-accepting building block. After desulfurization of the Bt by means of sodium borohydride, the corresponding diamine **5** was converted into dihydro-tetraazaanthracene **6** through cyclisation with dichloro-dicyano-pyrazine **7** (see Scheme 2). Dichloro-dicyano-benzoquinone was used as oxidant to obtain the target deep-green tetraazaanthracenes AntC, AntO and AntS, in moderate yields.

The structures of all the new D–A dyes were fully characterised based on elemental analysis, mass spectrometric and NMR spectroscopic analysis.

### Photochemical Properties

UV/Vis absorption spectroscopy was carried out to investigate the photochemical properties of the D–A molecules. All derivatives show at least two broad absorption bands in their UV/Vis spectrum (see Figure 1). The bands located at $\lambda \approx 250$ nm possess high extinction coefficients of $\varepsilon = 3.9–5.4 \times 10^4$ $M^{-1}$ $cm^{-1}$, which can be attributed to the $\pi$–$\pi^*$ transitions of the arylamine donor systems. These transitions are independent of the respective acceptor and are part of the spectra of all the dyes.

As described previously, the absorption of visible light is achieved through CT within the thiazole-based D–A molecules.[6,10,24] In the case of pyrazine-substituted chromophores of PyrC, PyrO and PyrS, these absorption bands are located in the blue region of the spectrum, at $\lambda_{max} \approx 395$ nm with high extinction coefficients of $\varepsilon = 1.9–2.5 \times 10^4$ $M^{-1}$ $cm^{-1}$. The optical band gaps of the three pyrazine acceptor molecules could be estimated to be $\Delta E_{opt} \approx 2.7$ eV based on the onset of the UV/Vis spectra.

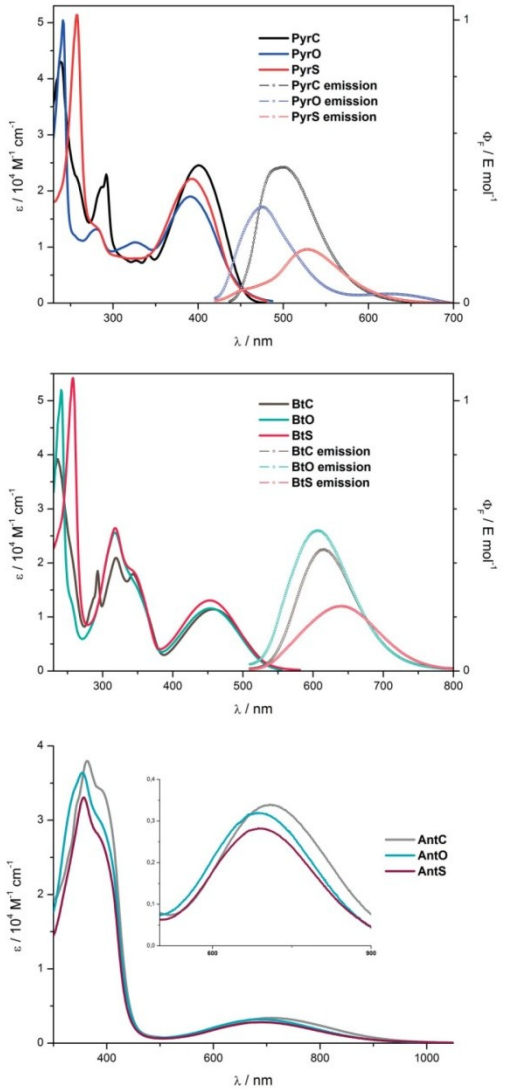


Figure 1. UV/Vis absorption spectra of all compounds in THF. For the pyrazine (PyrC, PyrO and PyrS) and the Bt (BtC, BtO and BtS) derivatives the fluorescence spectra, normalized against the fluorescence quantum yields, are also given in dotted lines.

The three orange Bt-substituted chromophores BtC, BtO and BtS show remarkably strong CT character. The lowest energy transitions show a very broad absorption band, with maxima located at $\lambda \approx 455$ nm with $\varepsilon \approx 1.3 \times 10^4$ $M^{-1}$ $cm^{-1}$. Additionally, another absorption band located at $\lambda \approx 318$ nm appears in the UV/Vis spectra of all the piazthioles, which could be assigned

ChemPubSoc Europe
EurJOC European Journal of Organic Chemistry
Full Paper

Table 1. Summary of the photochemical properties of the D–thiazole–A dyes.

| | PyrC | PyrO | PyrS | BtC | BtO | BtS | AntC | AntO | AntS |
|---|---|---|---|---|---|---|---|---|---|
| $\lambda_{max}$ [nm] (log $\varepsilon$)[a] | 401 (4.39) | 391 (4.28) | 393 (4.35) | 458 (4.06) | 453 (4.06) | 453 (4.12) | 709 (3.53) | 687 (3.51) | 694 (3.45) |
| | 238 (4.63) | 241 (4.70) | 257 (4.71) | 319 (4.32) | 317 (4.41) | 318 (4.42) | 363 (4.58) | 354 (4.56) | 357 (4.52) |
| | | | | 236 (4.59) | 241 (4.72) | 258 (4.73) | | | |
| $\lambda_F$ [nm][a] | 501 | 477 | 530 | 616 | 607 | 641 | – | – | – |
| Stokes-shift $\upsilon$ [eV][b] | 0.62 | 0.57 | 0.75 | 0.69 | 0.69 | 0.80 | – | – | – |
| $\Phi_F$[c] | 0.48 | 0.34 | 0.19 | 0.45 | 0.52 | 0.24 | – | – | – |
| $E_{gap}^{opt}$ [eV][d] | 2.74 | 2.71 | 2.73 | 2.31 | 2.33 | 2.32 | 1.30 | 1.34 | 1.33 |

[a] Measured in THF. [b] Relative to the maximum of the absorption band. [c] Measured in cyclohexane, relative to quinine sulfate ($\lambda_{exc}$ = 366 nm; $\Phi$ = 0.53), rhodamine 6G ($\lambda_{exc}$ = 470 nm; $\Phi$ = 0.94) or fluorescein ($\lambda_{exc}$ = 470 nm; $\Phi$ = 0.91).[27] [d] Calculated based on the onset (10 %) of the absorption spectra.

to a HOMO-1 to LUMO transition. The optical band gaps are decreased to $\Delta E_{opt} \approx 2.3$ eV, which also points to a much stronger CT character of the Bt-substituted dyes than the pyrazine compounds, which means a much stronger electron-accepting moiety.

Considering the spectra of the tetraazaanthracene-substituted dyes, both large bathochromic and hyperchromic shifts were observed. On the one hand, the HOMO-1 to LUMO transition is redshifted by 42 nm compared with that of the piazthioles to $\lambda \approx 360$ nm, with higher extinction coefficients of $\varepsilon$ = 3.3–3.8 × $10^4$ $M^{-1}$ $cm^{-1}$. On the other hand, the broad absorption band in the visible region is shifted to $\lambda_{max}$ = 709 (AntC), 687 (AntO) and 694 nm (AntS), respectively. This leads to the assumption that a strong CT character is involved and, thus, the tetraazaanthracene acceptor is much stronger than Bt. The deep-green colour of these derivatives in solution could be explained by the appearance of such broad absorption bands (absorption over the range of $\lambda$ = 500 – 900 nm). Such broad and far redshifted absorption is rarely observed in the case of monodispers, metal-free materials, excluding the well-established functional dyes such as squaraines, porphyrines or phthalocyanines.[25] Regarding the optical properties, the tetraazaanthracenes represent promising candidates for application in small molecule BHJ or DSSC.[26] Furthermore, the onset values of the lowest energy transition of $\lambda$ = 950 nm (AntC), 922 nm (AntO) and 935 nm (AntS) lead to narrow optical band gaps of $\Delta E_{opt} \approx 1.3$ eV.

The properties of our derivatives were studied after excitation at the appropriate absorption maximum by means of fluorescence emission spectroscopy. The pyrazine-substituted derivatives show broad, less structured emission bands with maxima at $\lambda_F$ = 501 nm (PyrC), $\lambda_F$ = 477 nm (PyrO) and $\lambda_F$ = 530 nm (PyrS) in tetrahydrofuran (THF). Notably, PyrO shows a shoulder to higher wavelengths and PyrS possesses a shoulder in the lower wavelength region. The energy loss after photonic excitation, the Stokes shifts, amount to $\upsilon$ = 0.62 (PyrC), 0.57 (PyrO) and 0.75 eV (PyrS), respectively. Fluorescence spectroscopy in different solvents revealed strong solvatochromic behaviour (see Figure S1–S8 in the Supporting Information). For example, the maximum of the emission of PyrC shifts from $\lambda_F$ = 478 nm in cyclohexane to $\lambda_F$ = 551 nm in methanol ($\Delta E$ = 0.35 eV; PyrO: $\Delta E$ = 0.41 eV; PyrS: $\Delta E$ = 0.38 eV).

The orange to red fluorescence emission of the Bt-substituted thiazoles occurs with large Stokes shifts of $\upsilon$ = 0.69 (BtC, BtO) and 0.80 eV (BtS), at $\lambda_F$ = 616 nm (BtC), $\lambda_F$ = 607 nm (BtO) and $\lambda_F$ = 641 nm (BtS). A positive solvatochromism of the fluorescence emission was also obtained in the case of the piazthioles, the maxima fluctuate depending on the solvent by about $\Delta\lambda_F \approx 50$ nm (BtC/BtO: $\Delta E$ = 0.17 eV; BtS: $\Delta E$ = 0.12 eV).

Fluorescence quantum yields were measured in cyclohexane relative to fluorescence standards, as described by Brouwer.[27] Moderate quantum yields were obtained in the case of the blue to green fluorescence emission of the pyrazine-substituted molecules: $\Phi_F$ = 0.48 (PyrC), $\Phi_F$ = 0.34 (PyrO) and $\Phi_F$ = 0.19 (PyrS). Because of the emission in the orange to red region of visible light and coincident relatively small molecular weight, the quantum yields of the piazthioles are remarkable, with $\Phi_F$ = 0.45 (BtC), $\Phi_F$ = 0.52 (BtO) and $\Phi_F$ = 0.24 (BtS). The fluorescence quantum yields typically range from moderate to good, which is an outstanding feature of 4-alkoxythiazoles. Indeed, the phenothiazine donor bearing systems PyrS and BtS show the most redshifted emission within their class of acceptors, but also the weakest emission, which could be assigned to the additional sulfur atom. Sulfur is known for promoting intersystem crossing through spin-orbit coupling, which contributes energetic deactivation.[28]

All three tetraazaanthracene-substituted D–A dyes (AntC, AntO and AntS) showed, with respect to the limits of the spectrometer, no fluorescence until $\lambda$ = 900 nm after photonic excitation at different wavelengths. Some important results of the photochemical measurements are summarised in Table 1.

### Electrochemical Properties

The electrochemical properties of our new dyes, the electron affinity and ionisation energies, were studied by means of cyclic voltammetry (see Figure 2, and Figure S9, S10 and Table S1 in the Supporting Information). The oxidation waves were characterised by the appropriate arylamine donor. Thus, phenoxazines PyrO, BtO and AntO, and phenothiazines PyrS, BtS and AntS exhibit a reversible single-electron oxidation step at approximately 0.3 V against $Fc/Fc^+$, which leads to nearly constant HOMO energies of approximately $E_{HOMO}$ = −5.4 eV for all phenoxazine- and phenothiazine-substituted dyes {estimated from $E_{HOMO} = -[E_{onset}$ (Ox vs. $Fc/Fc^+$) + 5.1 eV]}.[29] This typical reversible oxidation of diarylamines was not detected in the cyclic voltammograms of the carbazoles within the limits of the solvent used (THF) and, consequently, the carbazole-substituted molecules PyrC, BtC and AntC show only the irreversible oxidation of the thiazole moiety. This irreversible oxidation occurs in the voltammograms of all dyes, but is influenced by

 

ChemPubSoc Europe
EurJOC European Journal of Organic Chemistry
Full Paper

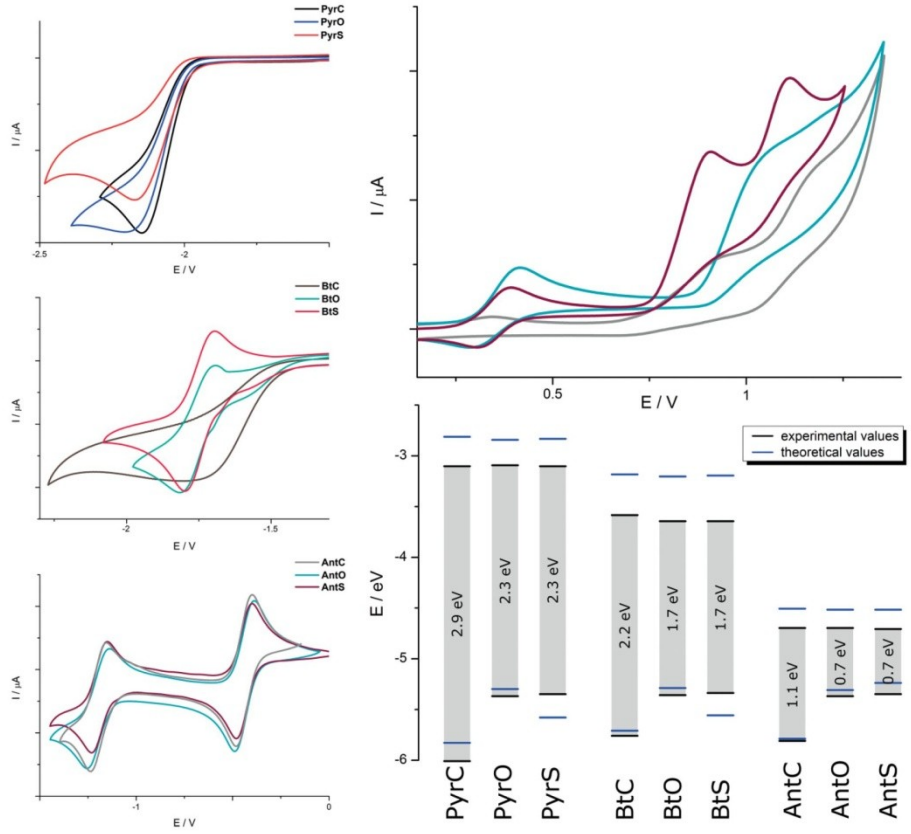


Figure 2. Depiction of the reduction waves of all derivatives (left) and typical oxidation waves (right top) of AntC (grey), AntO (cyan) and AntS (red). Graphical depiction of the experimental and theoretical estimated HOMO and LUMO levels (right bottom).

the donor as well as the acceptor units. Thereby, the oxidation potential fluctuates between $E$ = 0.94 V (BtC) and $E$ = 1.17 V (PyrS) (see Figure 2 and Table S1 and Figure S9, S10 in the Supporting Information).

Reductions of the D–A dyes described seem to take place at the appropriate acceptor and are not influenced by the whole π-system, because the reduction potentials vary only with the kind of acceptor itself. Whereas the pyrazine units show an irreversible reduction at $E \approx -2.2$ V, the piazthioles form reversible reduction waves at $E_{1/2} = -1.75$ V (except for BtC, which is irreversible at $E = -1.80$ V). These reduction potentials lead to LUMO energies for the pyrazine acceptors of $E_{LUMO} = -3.1$ eV, whereas the LUMO energies of the piazthioles are decreased by 0.5 eV to $E_{LUMO} = -3.6$ eV (see Table 2). The band gap of BtC could be estimated with the HOMO energy of $E_{HOMO} = -5.8$ eV to $\Delta E_{CV} = 2.2$ eV, which is comparable to other carbazole-π-Bt systems described.[30] In contrast, the band gaps of BtO and BtS are narrower, because of the easier ionizability of phenoxazine and phenothiazine, and could be estimated to $\Delta E_{CV} = 1.7$ eV; they are able to compete with the band gaps of Bt-based D–A copolymers[31] or Bt-based small molecules bearing two donor units.[32] Concluding, the energy levels of the frontier orbitals of our Bt-based materials (BtC: –5.8 to –3.6 eV; BtO, BtS: –5.4 to –3.7 eV, see Table 2) appear to be suitable for application as donor materials in BHJs, because the HOMO–LUMO levels are comparable to levels of other materials that have been reported recently.[33]

The use of tetrazaanthracene as the electron-accepting unit leads to drastically lowered LUMO energies at $E_{LUMO} = -4.7$ eV. The strong electron affinity of derivatives AntC, AntO and AntS is manifested in the two-step one-electron reduction at potentials of $E_{1/2} = -0.44$ V and $E_{1/2} = -1.20$ V, which is comparable to that of the widely used oxidant chloranil.[18] Associated with energetically decreased LUMO energies, the band gaps are, compared with the Bt-substituted derivatives, also markedly narrowed by 1 eV. As depicted in Figure 3 and described earlier, the HOMO levels are heavily affected by the donor group, which explains the strong CT character of these materials. The

 

ChemPubSoc Europe
EurJOC European Journal of Organic Chemistry
Full Paper

Table 2. Summary of the experimental and theoretical estimated frontier orbital energies.

| | PyrC | PyrO | PyrS | BtC | BtO | BtS | AntC | AntO | AntS |
|---|---|---|---|---|---|---|---|---|---|
| $E_{HOMO}$ [eV][a] | –6.01 | –5.36 | –5.38 | –5.77 | –5.36 | –5.35 | –5.83 | –5.39 | –5.38 |
| $E_{LUMO}$ [eV][a] | –3.11 | –3.11 | –3.12 | –3.61 | –3.66 | –3.66 | –4.73 | –4.72 | –4.73 |
| $E_{gap}$ [eV][b] | 2.90 | 2.25 | 2.26 | 2.16 | 1.70 | 1.69 | 1.10 | 0.67 | 0.65 |
| $E_{HOMO}$ [eV][c] | –5.61 | –5.08 | –5.36 | –5.49 | –5.07 | –5.34 | –5.57 | –5.09 | –5.02 |
| $E_{LUMO}$ [eV][c] | –2.60 | –2.63 | –2.62 | –2.97 | –2.99 | –2.98 | –4.29 | –4.30 | –4.30 |
| $E_{gap}$ [eV][c] | 3.01 | 2.46 | 2.74 | 2.52 | 2.09 | 2.36 | 1.28 | 0.78 | 0.72 |

[a] Recorded by cyclic voltammetry in 0.1 M solution of $TBAPF_6$ in THF, calculated from $E_{HOMO} = -[E_{onset}$ (ox vs. $Fc/Fc^+) + 5.1$ eV] and $E_{LUMO} = -[E_{onset}$ (red vs. $Fc/Fc^+) + 5.1$ eV]. [b] $E_{Gap} = -(E_{HOMO} - E_{LUMO})$. [c] Calculated energies at B3LYP/6-31+G(d,p) level of theory based on a CAM B3LYP/6-31+G(d,p) PCM THF optimised ground-state geometry.

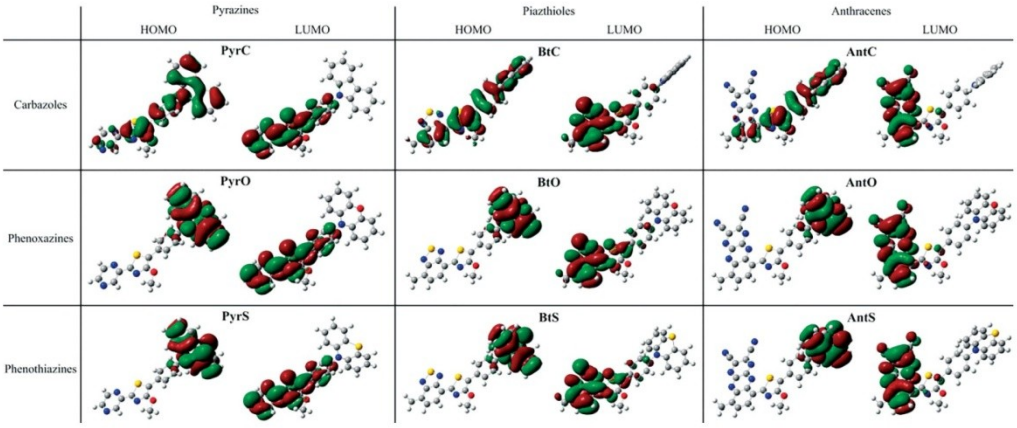


Figure 3. Frontier orbitals of the D–A dyes.

HOMO energies are $E_{HOMO} = -5.8$ eV (AntC) and –5.4 eV (AntO, AntS), which lead to band gaps of $\Delta E_{CV} = 1.1$ eV (AntC) and 0.7 eV (AntO, AntS), respectively. To our knowledge, such narrow band gaps have not been estimated for metal-free small molecules and are in the region of those of Si, Ge or GaSb, respectively.[34] The low-lying LUMOs, combined with the narrow band gaps, are promising properties for application as n-type semiconducting materials in OFETs, or for the replacement of fullerenes as accepting material in BHJs, because they surpass the LUMO levels of conventional acceptors such as $PC_{61}BM$, $PC_{71}BM$ or perylenebisimide ($E_{LUMO}$ = –3.7 to –4.3 eV).[35]

Density functional theory (DFT) and time-dependent density functional theory (TD-DFT) have been applied to verify the electronic characteristics of the target compounds presented herein. Effects of solvation (THF) have been addressed for ground-state properties by utilising the polarisable continuum model.[36] An initial systematic conformational search with the Merck molecular force field[37] followed by optimization at the CAM B3LYP/6-31+G(d,p)48 level of theory,[38] as implemented in the Gaussian 09 software package,[39] afforded the best geometries that were used for further calculations. The HOMO and LUMO energies were calculated at the B3LYP/6-31d+G(d,p) level of theory after ground-state optimization and validation of the ground state through frequency calculations. Graphical representations of the frontier orbitals of all derivatives are depicted in Figure 3, and the corresponding energies are summarised in Table 2. As shown in Figure 3, the separation of HOMO and LUMO increases from pyrazine to tetraazaanthracene, as well as from carbazole to the phenothiazine, which lead to stronger CT characters. Furthermore, analysis of the frontier orbitals explains the electrochemical behaviour. The LUMOs are only affected by the appropriate acceptor unit; they have the same extension within the class of acceptor, which leads to similar LUMO energy levels. Whereas the frontier orbitals of all phenoxazine- (PyrO, BtO, AntO) and phenothiazine- (PyrS, BtS, AntS) bearing D–A systems are well separated from each other, the HOMOs of the carbazole-donor dyes (PyrC, BtC, AntC) are extended over nearly the whole π-system and show an overlap with the appropriate LUMO, which leads to slightly enhanced band gaps. The theoretically estimated energy levels of the dyes described herein are consistent with those estimated experimentally. All energies calculated slightly overestimate (except for the HOMO of PyrS and BtS) the values of HOMO and LUMO estimated experimentally, which is typical for DFT calculations with B3LYP/6-31d+G(d,p).[40]

Only the errors of the calculated with respect to the experimental values of the LUMO energies of the Bt-substituted dyes

 

ChemPubSoc Europe

EurJOC European Journal of Organic Chemistry
Full Paper

are outside the 0.3 eV margin, which is characteristic for DFT calculations.[41] Indeed, together, the calculations reveal the tendency of the energy levels. Especially in the case of the tetraazaanthracene-substituted materials (AntC, AntO, AntS), both the HOMO and the LUMO energies are in very good agreement with the experimental values, with mean errors of 0.02–0.19 eV.

## Conclusions

We synthesised and characterised nine D–A molecules based on 4-alkoxythiazoles. These novel dyes are accessible over a simple, straightforward synthetic route and were identified by elemental analysis, NMR and MS experiments.

Variation of the diarylamine donor moiety influences the optical and electrochemical properties significantly. The use of carbazole and phenoxazine as electron-donating units (PyrC, PyrO, BtC, BtO) leads to high fluorescence quantum yields of the derivatives, whereas phenothiazine (PyrS, BtS), as a stronger-donating unit, leads to large Stokes shifts, because the fluorescence emission entails a bathochromic shift. In the case of the electrochemical properties, phenoxazine (PyrO, BtO, AntO) and phenothiazine (PyrS, BtS, AntS) gave remarkable results; these derivatives possess reversible one-electron oxidations at low potentials ($E_{1/2}$ = 0.3 V).

Through variation of the electron-accepting unit, the properties can be influenced more strongly. Pyrazines PyrC, PyrO, PyrS show strong blue to green fluorescence emission combined with a wide solvatochromism, whereas Bt-substituted molecules BtC, BtO, BtS possess an orange to red emission colour. All six D–A compounds have the potential for application as emitting species in organic light-emitting diodes because of their high fluorescence quantum yields ($\Phi$ = 0.2–0.5 $E$ mol$^{-1}$), good solubility and stability.

The band gaps decrease by 0.5 eV with the use of the stronger acceptor Bt compared with pyrazine. These small band gaps ($\Delta E$ = 2.2 eV for BtC, $\Delta E$ = 1.7 eV for BtO and BtS), optimal HOMO levels (–5.8 eV for BtC, –5.4 eV for BtO and BtS) and strong absorption (log $\varepsilon \approx$ 4.1 at $\lambda$ = 455 nm) in the visible region of our piazthioles are promising features for an application as donor material in BHJ solar cells.

Tetraazaanthracene was introduced as an electron-accepting unit in D–A materials for the first time. Associated with the strong electron deficiency of this building block, the LUMO levels of our tetraazaanthracenes (AntC, AntO, AntS) are decreased by 1 eV in comparison to those of the Bt-based D–A dyes to $E_{LUMO}$ = –4.7 eV. Given that the HOMO levels only depend on the kind of donor, the band gaps are also decreased by 1 eV in comparison to the appropriate Bt-based species, which leads to very narrow (AntC: 1.1 eV) and record-breaking band gaps of 0.7 eV (AntO, AntS), respectively. Low-lying LUMO levels, narrow band gaps and absorptions in the NIR region of light suggest the suitability of these compounds as acceptor materials in fullerene-free BHJ solar cells.

Our forthcoming studies will focus on the introduction of these novel compounds into optoelectronic devices. In addition, a wider range of donor moieties, such as diphenyl-, dianisidylamine or acridone, will be introduced in our D–A dyes.

## Experimental Section

Solvents for UV/Vis and emission spectroscopy were of analytical grade and purchased from Sigma–Aldrich. $^1$H and $^{13}$C NMR spectra were recorded with Bruker AC-250 (250 MHz), AC-300 (300 MHz) and AC-400 (400 MHz) spectrometers. Chemical shifts ($\delta$) are given relative to solvents. UV/Vis data for the compounds were collected with a PerkinElmer LAMBDA 45 UV/Vis spectrometer and emission spectra were measured with a Jasco FP 6500 instrument. Elemental analysis was carried out with a Leco CHNS-932 instrument. Mass spectra were measured either with a Finnigan MAT SSQ 710 (EI) or a MAZ 95 XL (ESI) system. TLC materials were purchased from Merck (Polygram SIL G/UV254, aluminum oxide 60 F254). The material for column chromatography was also obtained from Merck (silica gel 60, 0.04–0.063 mm). The fluorescence quantum yields were measured in cyclohexane against quinine sulfate ($\lambda_{exc}$ = 366 nm; $\Phi$ = 0.53), rhodamine 6G ($\lambda_{exc}$ = 470 nm; $\Phi$ = 0.94) or fluorescein ($\lambda_{exc}$ = 470 nm; $\Phi$ = 0.91) as fluorescence standards.[27,42] The cyclovoltammetric measurements were performed with a Metrohm Autolab PGSTAT30 potentiostat in 0.1 M solution of $TBAPF_6$ in THF (concentration of compounds: 1 × 10$^{-5}$ M) on a graphite working electrode with a scanning speed of 50 mV s$^{-1}$; platinum was used as counter and Ag/AgCl as the reference electrode. The data were calibrated externally vs. ferrocen/ferrocenium. Details of the analytical data are provided in the Supporting Information.

Pyrazine-2-carbothioamide (**1A**),[4a] 7-methylbenzo[*c*][1,2,5]thiadiazole-4-carbothioamide (**1B**),[3] ethyl 2-bromo-2-(4-bromophenyl)acetate (**2**)[43] and 5,6-dichloro-2,3-dicyanopyrazine (**7**)[44] were synthesized according to reported procedures. All other chemicals used were reagent grade and purchased from commercial sources. Solvents were purified by standard procedures.

**5-(4-Bromophenyl)-2-(pyrazin-2-yl)thiazol-4-ol (3A):** Pyrazine-2-carbothioamide (**1A**; 1 g, 7 mmol), ethyl 2-bromo-2-(4-bromophenyl)acetate (**2**; 2.8 g, 8.8 mmol) and sodium acetate (1.5 g, 18 mmol) were dissolved in ethanol (40 mL). The suspension was stirred and heated to reflux for 3 h. The yellow precipitate was filtered and washed with water, ethanol and *n*-pentane. Recrystallisation from ethanol/DMF afforded the product (0.6 g, 1.8 mmol, 25 %) as yellow crystals; m.p. 318–320 °C (dec.). $^1$H NMR (400 MHz, DMSO): $\delta$ = 11.78 (s, 1 H), 9.20 (s, 1 H), 8.70 (d, $J$ = 8.7 Hz, 2 H), 7.75 (d, $J$ = 8.5 Hz, 2 H), 7.61 (d, $J$ = 8.1 Hz, 2 H) ppm. $^{13}$C NMR could not be measured due to low solubility; MS (EI): $m/z$ = 333 [M$^{+}$], 335 [(M + 2)$^{+}$]. $C_{13}H_8BrN_3OS$ (334.19): calcd. C 46.72, H 2.41, N 12.57; found C 47.01, H 2.55, N 12.31.

**5-(4-Bromophenyl)-2-(7-methylbenzo[*c*][1,2,5]thiadiazol-4-yl)-thiazol-4-ol (3B):** 7-Methylbenzo[*c*][1,2,5]thiadiazole-4-carbothioamide (**1B**; 1.2 g, 5.7 mmol), sodium acetate (1.3 g, 16 mmol) and ethyl 2-bromo-2-(4-bromophenyl)acetate (**2**; 3 g, 9 mmol) were diluted with ethanol (45 mL). The resulting suspension was stirred and heated to reflux for 5 h. The reaction was quenched with water and the brown precipitate was filtered, washed with water and cold ethanol to afford **3B** (2 g, 5 mmol, 86 %); m.p. 290 °C (dec.); $^1$H NMR (400 MHz, DMSO): $\delta$ = 11.68–11.33 (m, 1 H), 8.38 (d, $J$ = 7.2 Hz, 1 H), 7.76 (d, $J$ = 8.5 Hz, 2 H), 7.68 (s, 1 H), 7.59 (d, $J$ = 8.5 Hz, 2 H), 2.76 (s, 3 H) ppm. $^{13}$C NMR could not be measured due to low solubility; MS (EI): $m/z$ = 403 [M$^{+}$], 405 [(M + 2)$^{+}$]. $C_{16}H_{10}BrN_3OS_2$ (404.30): calcd. C 47.53, H 2.49, N 10.39; found C 48.01, H 2.80, N 10.12.

**5-(4-Bromophenyl)-4-(hexyloxy)-2-(pyrazin-2-yl)thiazole (4A):** Compound **3A** (500 mg, 1.5 mmol) and $K_2CO_3$ (420 mg, 3 mmol) were dissolved in acetone (30 mL) and 1-iodohexane (240 µL, 1.65 mmol, 1.1 equiv.) was added. The resulting reaction mixture

 

ChemPubSoc Europe
EurJOC European Journal of Organic Chemistry
Full Paper

was heated to reflux with stirring for 10 h. The mixture was diluted with water and extracted three times with $CHCl_3$. The combined organic layers were dried with $MgSO_4$, filtered and the solvents evaporated to dryness. Recrystallisation from methanol/$CHCl_3$ afforded the product (500 mg, 1.2 mmol, 80 %) as yellow crystals; m.p. 76 °C. $^1$H NMR (250 MHz, $CDCl_3$): $\delta$ = 9.33 (d, $J$ = 1.4 Hz, 1 H), 8.56 (d, $J$ = 2.5 Hz, 1 H), 8.52 (dd, $J$ = 2.4, 1.6 Hz, 1 H), 7.67 (d, $J$ = 8.7 Hz, 2 H), 7.51 (d, $J$ = 8.7 Hz, 2 H), 4.53 (t, $J$ = 6.6 Hz, 2 H), 1.92–1.80 (m, 2 H), 1.55–1.45 (m, 2 H), 1.43–1.31 (m, 4 H), 0.92 (t, $J$ = 6.9 Hz, 3 H) ppm. $^{13}$C NMR (63 MHz, $CDCl_3$): $\delta$ = 160.29, 157.88, 146.80, 144.86, 144.01, 141.16, 131.99, 130.62, 128.55, 120.91, 114.55, 77.16, 71.15, 31.66, 29.59, 25.86, 22.73, 14.15 ppm. MS (EI): $m/z$ = 417 [$M^{+\cdot}$], 419 [$(M + 2)^{+\cdot}$], 333 [$(M - C_6H_{13})^{+}$]. $C_{19}H_{20}BrN_3OS$ (418.35): calcd. C 54.55, H 4.82, N 10.04; found C 54.87, H 4.76, N 10.43.

**4-[5-(4-Bromophenyl)-4-(hexyloxy)thiazol-2-yl]-7-methylbenzo[*c*][1,2,5]thiadiazole (4B):** Compound **3B** (2 g, 5 mmol) and $K_2CO_3$ (1.4 g, 10 mmol) were dissolved in acetone (50 mL) and 1-iodohexane (820 µL, 5.5 mmol, 1.1 equiv.) was added. The resulting reaction mixture was heated to reflux with stirring for 7 h. The mixture was diluted with water and extracted three times with $CHCl_3$. The combined organic layers were dried with $MgSO_4$, filtered and the solvents evaporated to dryness. Recrystallisation from ethanol/$CHCl_3$ afforded the product (1.8 g, 3.6 mmol, 72 %) as orange crystals; m.p. 125 °C. $^1$H NMR (250 MHz, $CDCl_3$): $\delta$ = 8.41 (d, $J$ = 7.3 Hz, 1 H), 7.70 (d, $J$ = 8.6 Hz, 2 H), 7.55–7.36 (m, 3 H), 4.54 (t, $J$ = 6.6 Hz, 2 H), 2.77 (s, 3 H), 1.95–1.79 (m, 2 H), 1.60–1.46 (m, 2 H), 1.38 (dd, $J$ = 8.8, 5.2 Hz, 4 H), 0.93 (t, $J$ = 6.8 Hz, 3 H) ppm. $^{13}$C NMR (63 MHz, $CDCl_3$): $\delta$ = 159.40, 155.63, 154.69, 151.43, 132.89, 131.62, 131.05, 128.36, 128.03, 126.59, 123.66, 119.91, 112.93, 70.60, 31.55, 29.51, 25.78, 22.60, 18.15, 14.03 ppm. MS (EI): $m/z$ = 487 [$M^{+\cdot}$], 489 [$(M + 2)^{+\cdot}$], 403 [$(M - C_6H_{13})^{+\cdot}$]. $C_{22}H_{22}BrN_3OS_2$ (488.46): calcd. C 54.10, H 4.54, N 8.60; found C 54.45, H 4.61, N 8.47.

**General Procedure for the Hartwig–Buchwald Coupling Reactions:** A solution of **4A**/**4B** (1 equiv.), diarylamine (1.1 equiv.) and KO*t*Bu (1.2 equiv.) in anhydrous toluene (10 mL) was degassed over 15 min with nitrogen. $Pd(dba)_2$ (0.04 equiv.) and SPHOS (0.08 equiv.) were added and the resulting dark solution was stirred and heated to reflux for 8 h. The mixture was diluted with $CHCl_3$ (50 mL) and extracted three times with water. The organic layer was dried with $Na_2SO_4$, filtered and the solvents evaporated to dryness.

**5-[4-(9*H*-Carbazol-9-yl)phenyl]-4-(hexyloxy)-2-(pyrazin-2-yl)thiazole (PyrC):** Synthesised according to the general procedure from **4A** (150 mg, 0.36 mmol) and carbazole (67 mg, 0.39 mmol, 1.1 equiv.). The crude product was recrystallised from EtOH/$CHCl_3$ to give PyrC (96 mg, 0.19 mmol, 53 %) as yellow crystals; m.p. 121 °C. $^1$H NMR (250 MHz, $CDCl_3$): $\delta$ = 9.38 (d, $J$ = 1.4 Hz, 1 H), 8.58 (d, $J$ = 2.5 Hz, 1 H), 8.56–8.53 (m, 1 H), 8.16 (d, $J$ = 7.6 Hz, 2 H), 8.05 (d, $J$ = 8.6 Hz, 2 H), 7.61 (d, $J$ = 8.6 Hz, 2 H), 7.50–7.39 (m, 4 H), 7.34–7.27 (m, 2 H), 4.61 (t, $J$ = 6.6 Hz, 2 H), 2.00–1.87 (m, 2 H), 1.59–1.49 (m, 2 H), 1.47–1.34 (m, 4 H), 0.93 (t, $J$ = 7.0 Hz, 3 H) ppm. $^{13}$C NMR (63 MHz, $CDCl_3$): $\delta$ = 160.38, 157.92, 146.85, 144.85, 144.02, 141.20, 140.88, 136.44, 130.78, 128.41, 127.36, 126.13, 123.62, 120.47, 120.20, 114.92, 109.98, 77.16, 71.22, 31.68, 29.64, 25.90, 22.75, 14.16 ppm. MS (ESI, +): $m/z$ = 527.3 [$(M + Na)^{+}$]. HRMS (ESI, +): $m/z$ calcd. 527.1882; found 527.1892; $C_{31}H_{28}N_4OS$ calcd.: C, 73.78; H, 5.59; N, 11.10; found C, 73.91; H, 5.63; N, 10.91.

**10-{4-[4-(Hexyloxy)-2-(pyrazin-2-yl)thiazol-5-yl]phenyl}-10*H*-phenoxazine (PyrO):** Synthesised according to the general procedure from **4A** (150 mg, 0.36 mmol) and phenoxazine (73 mg, 0.39 mmol, 1.1 equiv.). The crude product was recrystallised from EtOH/$CHCl_3$ to give PyrO (85 mg, 0.16 mmol, 46 %) as a pale-yellow powder; m.p. 101 °C. $^1$H NMR (250 MHz, $CDCl_3$): $\delta$ = 9.37 (d, $J$ = 1.4 Hz, 1 H), 8.58 (d, $J$ = 2.5 Hz, 1 H), 8.56–8.53 (m, 1 H), 8.03 (d, $J$ = 8.6 Hz, 2 H), 7.37 (d, $J$ = 8.6 Hz, 2 H), 6.72–6.57 (m, 6 H), 6.01 (dd, $J$ = 7.5, 1.7 Hz, 2 H), 4.59 (t, $J$ = 6.6 Hz, 2 H), 1.98–1.84 (m, 2 H), 1.58–1.46 (m, 2 H), 1.45–1.31 (m, 4 H), 0.92 (t, $J$ = 7.0 Hz, 3 H) ppm. $^{13}$C NMR (63 MHz, $CDCl_3$): $\delta$ = 160.49, 158.21, 146.80, 144.93, 144.12, 144.04, 141.21, 137.59, 134.42, 131.94, 131.29, 129.48, 123.39, 121.53, 115.61, 114.63, 113.46, 77.16, 71.22, 31.66, 29.61, 25.90, 22.74, 14.16 ppm. MS (ESI, +): $m/z$ = 543.2 [$(M + Na)^{+}$]; HRMS (ESI, +): $m/z$ calcd. 543.1831; found 543.1838. $C_{31}H_{28}N_4O_2S$ (520.65): calcd. C 71.51, H 5.42, N 10.76; found C 71.27, H 5.35, N 10.87.

**10-{4-[4-(Hexyloxy)-2-(pyrazin-2-yl)thiazol-5-yl]phenyl}-10*H*-phenothiazine (PyrS):** Synthesised according to the general procedure from **4A** (150 mg, 0.36 mmol) and phenothiazine (79 mg, 0.39 mmol, 1.1 equiv.). The crude product was recrystallised from EtOH/$CHCl_3$ to give PyrS (65 mg, 0.12 mmol, 35 %) as orange cubes; m.p. 133 °C. $^1$H NMR (250 MHz, $CDCl_3$): $\delta$ = 9.37 (d, $J$ = 1.3 Hz, 1 H), 8.58 (d, $J$ = 2.5 Hz, 1 H), 8.56–8.52 (m, 1 H), 8.02 (d, $J$ = 8.6 Hz, 2 H), 7.40 (d, $J$ = 8.6 Hz, 2 H), 7.05 (dd, $J$ = 7.2, 1.9 Hz, 2 H), 6.93–6.80 (m, 4 H), 6.36 (dd, $J$ = 7.8, 1.4 Hz, 2 H), 4.59 (t, $J$ = 6.6 Hz, 2 H), 1.98–1.85 (m, 2 H), 1.58–1.48 (m, 2 H), 1.46–1.32 (m, 4 H), 0.91 (t, $J$ = 7.0 Hz, 3 H) ppm. $^{13}$C NMR (63 MHz, $CDCl_3$): $\delta$ = 160.41, 158.03, 146.83, 144.88, 144.18, 144.03, 141.20, 139.98, 131.26, 130.49, 129.13, 127.03, 122.88, 121.22, 116.86, 114.80, 77.16, 71.21, 31.67, 29.62, 25.90, 22.74, 14.16 ppm. MS (ESI, +): $m/z$ = 559.2 [$(M + Na)^{+}$]; HRMS (ESI, +): $m/z$ calcd. 559.1602; found 559.1595. $C_{31}H_{28}N_4OS_2$ (536.71): calcd. C 69.37, H 5.26, N 10.44; found C 69.51, H 5.34; N, 10.58.

**4-{5-[4-(9*H*-carbazol-9-yl)phenyl]-4-(hexyloxy)thiazol-2-yl}-7-methylbenzo[*c*][1,2,5]thiadiazole (BtC):** Synthesised according to the general procedure from **4B** (500 mg, 1.03 mmol) and carbazole (190 mg, 1.13 mmol, 1.1 equiv.). The crude product was recrystallised from MeOH/toluene to give BtC (490 mg, 0.85 mmol, 83 %) as orange needles; m.p. 200 °C; $^1$H NMR (250 MHz, $CDCl_3$): $\delta$ = 8.49 (d, $J$ = 7.3 Hz, 1 H), 8.16 (d, $J$ = 7.7 Hz, 2 H), 8.11 (d, $J$ = 8.5 Hz, 2 H), 7.60 (d, $J$ = 8.5 Hz, 2 H), 7.54–7.38 (m, 5 H), 7.30 (t, $J$ = 7.3 Hz, 2 H), 4.64 (t, $J$ = 6.6 Hz, 2 H), 2.81 (s, 3 H), 2.05–1.85 (m, 2 H), 1.62–1.50 (m, 2 H), 1.49–1.30 (m, 4 H), 0.93 (t, $J$ = 7.0 Hz, 3 H) ppm. $^{13}$C NMR (63 MHz, $CDCl_3$): $\delta$ = 159.70, 155.87, 155.04, 151.69, 140.99, 135.77, 133.09, 131.49, 128.58, 128.07, 127.32, 126.81, 126.09, 123.94, 123.56, 120.44, 120.09, 113.53, 110.02, 77.16, 70.88, 31.73, 29.74, 25.98, 22.78, 18.33, 14.19 ppm. MS (EI): $m/z$ = 574 [$M^{+\cdot}$], 490 [$(M - C_6H_{13})^{+\cdot}$]; HRMS (EI): $m/z$ calcd. 574.1861; found 574.1868. $C_{34}H_{30}N_4OS_2$ (574.76): calcd. C 71.05, H 5.26, N 9.75; found C 71.43, H 5.32, N 9.64.

**10-{4-[4-(Hexyloxy)-2-(7-methylbenzo[*c*][1,2,5]thiadiazol-4-yl)-thiazol-5-yl]phenyl}-10*H*-phenoxazine (BtO):** Synthesised according to the general procedure from **4B** (500 mg, 1.03 mmol) and phenoxazine (210 mg, 1.14 mmol, 1.1 equiv.). The crude product was recrystallised from EtOH/$CHCl_3$ to give BtO (550 mg, 0.93 mmol, 90 %) as an orange powder; m.p. 203 °C. $^1$H NMR (400 MHz, $CDCl_3$): $\delta$ = 8.49 (d, $J$ = 7.3 Hz, 1 H), 8.09 (d, $J$ = 8.4 Hz, 2 H), 7.49 (d, $J$ = 7.3 Hz, 1 H), 7.36 (d, $J$ = 8.4 Hz, 2 H), 6.72–6.58 (m, 6 H), 6.05 (dd, $J$ = 7.6, 1.4 Hz, 2 H), 4.63 (t, $J$ = 6.6 Hz, 2 H), 2.82 (s, 3 H), 1.98–1.89 (m, 2 H), 1.62–1.53 (m, 2 H), 1.45–1.36 (m, 4 H), 0.93 (t, $J$ = 7.0 Hz, 3 H) ppm. $^{13}$C NMR (101 MHz, $CDCl_3$): $\delta$ = 159.89, 155.98, 155.44, 151.81, 144.29, 137.16, 134.65, 133.26, 132.66, 131.15, 129.23, 128.57, 126.93, 124.07, 123.44, 121.49, 115.62, 113.60, 113.48, 77.16, 70.96, 31.76, 29.79, 26.01, 22.77, 18.27, 14.14 ppm. MS (EI): $m/z$ = 590 [$M^{+\cdot}$], 506 [$(M - C_6H_{13})^{+\cdot}$]. HRMS (EI): $m/z$ calcd. 590.1810; found 590.1785. $C_{34}H_{30}N_4O_2S_2$ (590.76): calcd. C 69.13, H 5.12, N 9.48; found C 69.51, H 5.19, N 9.32.

ChemPubSoc Europe
EurJOC European Journal of Organic Chemistry
Full Paper

**10-{4-[4-(Hexyloxy)-2-(7-methylbenzo[*c*][1,2,5]thiadiazol-4-yl)-thiazol-5-yl]phenyl}-10*H*-phenothiazine (BtS):** Synthesised according to the general procedure from **4B** (500 mg, 1.03 mmol) and phenothiazine (225 mg, 1.13 mmol, 1.1 equiv.). The crude product was recrystallised from EtOH/$CHCl_3$ to give BtS (500 mg, 0.83 mmol, 80 %) as red crystals; m.p. 192 °C. $^1$H NMR (250 MHz, $CDCl_3$): $\delta$ = 8.49 (d, $J$ = 7.3 Hz, 1 H), 8.09 (d, $J$ = 8.5 Hz, 2 H), 7.49 (d, $J$ = 7.4 Hz, 1 H), 7.41 (d, $J$ = 8.5 Hz, 2 H), 7.03 (dd, $J$ = 7.2, 1.8 Hz, 2 H), 6.92–6.79 (m, 4 H), 6.34 (d, $J$ = 8.0 Hz, 2 H), 4.62 (t, $J$ = 6.6 Hz, 2 H), 2.81 (s, 3 H), 2.01–1.87 (m, 2 H), 1.57 (p, $J$ = 7.1 Hz, 3 H), 1.45–1.34 (m, 4 H), 0.92 (t, $J$ = 7.0 Hz, 3 H) ppm. $^{13}$C NMR (63 MHz, $CDCl_3$): $\delta$ = 159.76, 155.86, 155.22, 151.68, 144.38, 139.06, 133.16, 132.20, 130.97, 128.84, 128.56, 127.02, 126.89, 123.90, 122.66, 120.54, 116.41, 113.34, 77.16, 70.87, 31.72, 29.71, 25.97, 22.77, 18.34, 14.19 ppm. MS (EI): $m/z$ = 606 [$M^+$], 522 [$(M - C_6H_{13})^+$]; HRMS (EI): $m/z$ calcd. 606.1582; found 606.1584. $C_{34}H_{30}N_4OS_3$ (606.82): calcd. C 67.30, H 4.98, N 9.23; found C 67.06, H 5.09, N 9.41.

**General Procedure for the Desulfurization and Cyclization Reactions:** A degassed solution of piazthiole BtC, BtO or BtS (1 equiv.) and sodium borohydride (9 equiv.) in a mixture of EtOH/THF (3:1, 10 mL) was treated with a spatula of $CoCl_2$ and heated to reflux under nitrogen. The dark reaction mixture was stirred until all of the starting material (Bt) was desulfurized (evolving $H_2S$!) to give the corresponding diamine **5**, recognisable through the bright-green fluorescence (TLC: silica; toluene; $R_{f,Bt} \approx 0.7$, $R_{f,5} \approx 0.2$). The resulting mixture was evaporated and the residue was diluted with diethyl ether and water. The organic phase was washed with water three times and the combined aqueous phases were extracted with diethyl ether. After combining, drying and evaporating of the organic layers, the residue was dissolved in anhydrous dioxane (20 mL) and 5,6-dichloro-2,3-dicyanopyrazine (**7**; 1 equiv.) was added. The mixture was stirred under nitrogen at 80 °C overnight and heated to reflux for an additional 3 h, during which an orange precipitate formed. The reaction mixture was cooled to room temperature and the precipitate was filtered. The filtride was washed with EtOH and *n*-pentane to obtain the desired products as orange microcrystals.

**6-{5-[4-(9*H*-Carbazol-9-yl)phenyl]-4-(hexyloxy)thiazol-2-yl}-9-methyl-5,10-dihydropyrazino[2,3-*b*]quinoxaline-2,3-dicarbonitrile (6A):** According to the general procedure, the intermediate diamine **5A** was synthesised through desulfurization of BtC (150 mg, 0.26 mmol) by means of sodium borohydride (90 mg, 2.37 mmol). After a short work-up, crude diamine **5A** was dissolved in dioxane and **7** (50 mg, 0.26 mmol) was added. As described in the general procedure, **6A** (95 mg, 0.14 mmol, 54 %) was obtained as an orange microcrystalline solid; m.p. 347 °C (dec.). $^1$H NMR (400 MHz, THF): $\delta$ = 11.18 (s, 1 H), 8.61 (s, 1 H), 8.12 (d, $J$ = 7.7 Hz, 2 H), 8.02 (d, $J$ = 8.4 Hz, 2 H), 7.63 (d, $J$ = 8.3 Hz, 2 H), 7.42 (d, $J$ = 8.0 Hz, 2 H), 7.36 (t, $J$ = 7.5 Hz, 2 H), 7.23 (t, $J$ = 7.3 Hz, 2 H), 7.06 (d, $J$ = 8.2 Hz, 1 H), 6.62 (d, $J$ = 8.1 Hz, 1 H), 4.53 (t, $J$ = 6.9 Hz, 2 H), 2.12 (s, 3 H), 1.98–1.92 (m, 2 H), 1.61–1.56 (m, 2 H), 1.44–1.37 (m, 4 H), 0.92 (t, $J$ = 6.9 Hz, 3 H) ppm. $^{13}$C NMR could not be measured due to low solubility; MS (EI): $m/z$ = 672 [$M^+$], 588 [$(M - C_6H_{13})^+$]. $C_{40}H_{32}N_8OS$ (672.81): calcd. C 71.41, H 4.79, N 16.65; found C 71.73, H 4.87, N 16.97.

**6-{5-[4-(10*H*-Phenoxazin-10-yl)phenyl]-4-(hexyloxy)thiazol-2-yl}-9-methyl-5,10-dihydropyrazino[2,3-*b*]quinoxaline-2,3-dicarbonitrile (6B):** According to the general procedure, the intermediate diamine **5B** was synthesised through desulfurization of BtO (200 mg, 0.34 mmol) by means of sodium borohydride (110 mg, 3.05 mmol). After a short work-up, the crude diamine **5B** was dissolved in dioxane and **7** (68 mg, 0.34 mmol) was added. As described in the general procedure, **6B** (71 mg, 0.10 mmol, 30 %) was obtained as an orange microcrystalline solid; m.p. 310 °C (dec.). $^1$H NMR (250 MHz, THF): $\delta$ = 11.21 (s, 1 H), 8.79 (s, 1 H), 8.01 (d, $J$ = 8.4 Hz, 2 H), 7.39 (d, $J$ = 8.4 Hz, 2 H), 7.06 (d, $J$ = 8.3 Hz, 1 H), 6.69–6.50 (m, 7 H), 5.98 (dd, $J$ = 7.4, 1.7 Hz, 2 H), 4.49 (t, $J$ = 6.9 Hz, 2 H), 2.11 (s, 3 H), 1.98–1.85 (m, 2 H), 1.60–1.51 (m, 1 H), 1.44–1.36 (m, 4 H), 0.91 (t, $J$ = 6.6 Hz, 3 H) ppm. $^{13}$C NMR could not be measured due to low solubility; MS (EI): $m/z$ = 688 [$M^+$], 604 [$(M - C_6H_{13})^+$]. $C_{40}H_{32}N_8O_2S$ (688.81): calcd. C 69.75, H 4.68, N 16.27; found C 70.31, H 4.82, N 16.09.

**6-{5-[4-(10*H*-Phenothiazin-10-yl)phenyl]-4-(hexyloxy)thiazol-2-yl}-9-methyl-5,10-dihydropyrazino[2,3-*b*]quinoxaline-2,3-dicarbonitrile (6C):** According to the general procedure, the intermediate diamine **5C** was synthesised through desulfurization of BtS (200 mg, 0.33 mmol) by means of sodium borohydride (115 mg, 3.02 mmol). After a short work-up, the crude diamine **5C** was dissolved in dioxane and **7** (68 mg, 0.34 mmol) was added. As described in the general procedure, **6B** (104 mg, 0.15 mmol, 45 %) was obtained as an orange microcrystalline solid; m.p. 265 °C (dec.). $^1$H NMR (250 MHz, THF): $\delta$ = 11.23 (s, 1 H), 8.78 (s, 1 H), 7.97 (d, $J$ = 8.5 Hz, 2 H), 7.40 (d, $J$ = 8.5 Hz, 2 H), 7.08–6.99 (m, 3 H), 6.90–6.79 (m, 4 H), 6.60 (d, $J$ = 8.3 Hz, 1 H), 6.36 (dd, $J$ = 7.8, 1.2 Hz, 2 H), 4.47 (t, $J$ = 6.9 Hz, 2 H), 2.10 (s, 3 H), 1.95–1.85 (m, 2 H), 1.60–1.52 (m, 2 H), 1.44–1.36 (m, 4 H), 0.91 (t, $J$ = 5.9 Hz, 3 H) ppm. $^{13}$C NMR could not be measured due to low solubility; MS (EI): $m/z$ = 704 [$M^+$], 620 [$(M - C_6H_{13})^+$]. $C_{40}H_{32}N_8OS_2$ (704.87): calcd. C 68.16, H 4.58, N 15.90; found C 68.82, H 4.76, N 15.45.

**General Procedure for the Oxidation of the Dihydro-tetraaza-anthracenes (6):** Dihydrotetraazaanthracene **6A**, **6B** or **6C** (1 equiv.) was dissolved in anhydrous THF (10 mL) and the solution was degassed over 15 min. Under nitrogen flow, 2,3-dichloro-5,6-dicyano-1,4-benzoquinone (DDQ; 1.2 equiv.) was added and the resulting dark reaction mixture was stirred for 20 h at room temperature. After the reaction was quenched with water, the dark precipitate was filtered and rinsed with water and EtOH. Recrystallisation from THF/water afforded the pure products AntC, AntO and AntS as dark-blue to green crystals.

**6-{5-[4-(9*H*-Carbazol-9-yl)phenyl]-4-(hexyloxy)thiazol-2-yl}-9-methylpyrazino[2,3-*b*]quinoxaline-2,3-dicarbonitrile (AntC):** According to the general procedure, AntC was synthesised through oxidation of **6A** (86 mg, 0.13 mmol) by means of DDQ (35 mg, 0.15 mmol) and was obtained as blue crystalline solid (46 mg, 0.07 mmol, 53 %); m.p. 255 °C. $^1$H NMR (400 MHz, THF): $\delta$ = 9.06 (s, 1 H), 8.31 (d, $J$ = 8.4 Hz, 2 H), 8.14 (s, 1 H), 7.94 (d, $J$ = 7.5 Hz, 2 H), 7.80 (d, $J$ = 8.3 Hz, 2 H), 7.37 (d, $J$ = 8.1 Hz, 2 H), 7.28 (t, $J$ = 7.5 Hz, 2 H), 7.11 (t, $J$ = 7.3 Hz, 2 H), 4.69 (t, $J$ = 6.6 Hz, 2 H), 3.03 (s, 3 H), 2.01–1.95 (m, 2 H), 1.65–1.59 (m, 2 H), 1.46–1.38 (m, 4 H), 0.93 (t, $J$ = 6.9 Hz, 3 H) ppm. $^{13}$C NMR (101 MHz, THF): $\delta$ = 160.69, 144.82, 141.69, 141.29, 136.91, 135.13, 132.56, 129.10, 128.55, 127.03, 126.93, 123.92, 121.04, 120.89, 116.59, 110.78, 110.72, 71.42, 67.57, 32.74, 30.80, 30.68, 26.98, 23.70, 14.56 ppm. MS (EI): $m/z$ = 670 [$M^+$]; 586 [$(M - C_6H_{13})^+$]; HRMS (EI): $m/z$ calcd. 670.2263; found 670.2256. $C_{40}H_{30}N_8OS$ (670.79): calcd. C 71.62, H 4.51, N 16.70; found C 71.86, H 4.62, N 16.54.

**6-{5-[4-(10*H*-Phenoxazin-10-yl)phenyl]-4-(hexyloxy)thiazol-2-yl}-9-methylpyrazino[2,3-*b*]quinoxaline-2,3-dicarbonitrile (AntO):** According to the general procedure, AntO was synthesised through oxidation of **6B** (59 mg, 0.09 mmol) by means of DDQ (25 mg, 0.11 mmol) and was obtained as a green microcrystalline solid (34 mg, 0.05 mmol, 57 %); m.p. 230 °C. $^1$H NMR (400 MHz, THF): $\delta$ = 9.04 (s, 1 H), 8.25 (d, $J$ = 8.4 Hz, 2 H), 8.09 (s, 1 H), 7.51 (d, $J$ = 8.4 Hz, 2 H), 6.51 (dd, $J$ = 11.6, 7.5 Hz, 4 H), 6.48–6.42 (m, 2 H),

ChemPubSoc Europe

EurJOC European Journal of Organic Chemistry
Full Paper

5.97 (dd, $J$ = 5.9, 3.5 Hz, 2 H), 4.66 (t, $J$ = 6.6 Hz, 2 H), 3.02 (s, $J$ = 17.7 Hz, 3 H), 1.99–1.91 (m, 2 H), 1.64–1.56 (m, 2 H), 1.47–1.35 (m, 4 H), 0.92 (t, $J$ = 7.0 Hz, 3 H) ppm. $^{13}$C NMR (101 MHz, THF): $\delta$ = 160.73, 153.98, 148.28, 145.25, 143.76, 141.44, 137.59, 136.19, 135.87, 135.06, 134.57, 133.79, 133.25, 132.33, 131.21, 130.11, 124.56, 122.23, 116.10, 115.96, 114.53, 114.32, 71.39, 67.57, 32.72, 30.63, 26.96, 23.67, 18.08, 14.54 ppm. MS (EI): $m/z$ = 686 [$M^+$], 602 [$(M - C_6H_{13})^+$]; HRMS (EI): $m/z$ calcd. 686.2212; found 686.2236. $C_{40}H_{30}N_8O_2S$ (686.79): calcd. C 69.95, H 4.40, N 16.32; found C 70.29, H 4.56, N 16.10.

**6-{5-[4-(10*H*-Phenothiazin-10-yl)phenyl]-4-(hexyloxy)thiazol-2-yl}-9-methylpyrazino[2,3-*b*]quinoxaline-2,3-dicarbonitrile (AntS):** According to the general procedure, AntS was synthesised through oxidation of **6C** (87 mg, 0.12 mmol) by means of DDQ (34 mg, 0.15 mmol) and was obtained as a green crystalline solid (50 mg, 0.07 mmol, 58 %); m.p. 220 °C. $^1$H NMR (400 MHz, THF): $\delta$ = 9.09 (s, 1 H), 8.20 (d, $J$ = 8.5 Hz, 2 H), 8.14 (s, 1 H), 7.48 (d, $J$ = 8.5 Hz, 2 H), 6.99 (dd, $J$ = 7.5, 1.6 Hz, 2 H), 6.87 (td, $J$ = 7.8, 1.6 Hz, 2 H), 6.80 (td, $J$ = 7.4, 1.2 Hz, 2 H), 6.39 (dd, $J$ = 8.2, 1.1 Hz, 2 H), 4.69 (t, $J$ = 6.6 Hz, 2 H), 3.03 (s, 3 H), 2.01–1.94 (m, 2 H), 1.67–1.59 (m, 2 H), 1.49–1.40 (m, 4 H), 0.95 (t, $J$ = 7.1 Hz, 3 H) ppm. $^{13}$C NMR (101 MHz, THF): $\delta$ = 160.65, 153.94, 148.28, 145.46, 144.91, 141.35, 140.54, 136.64, 135.16, 133.33, 133.01, 131.83, 131.18, 129.99, 127.88, 127.41, 123.46, 121.24, 117.40, 116.40, 114.61, 71.43, 67.57, 32.73, 30.64, 26.98, 23.69, 18.04, 14.56 ppm. MS (EI): $m/z$ = 702 [$M^+$], 618 [$(M - C_6H_{13})^+$]; HRMS (EI): $m/z$ calcd. 702.1984; found 702.1992. $C_{40}H_{30}N_8OS_2$ (702.85): calcd. C 68.35, H 4.30, N 15.94; found C 68.71, H 4.39, N 16.09.

**Keywords:** Donor–acceptor systems · Dyes · Pigments · Density functional calculations · Azaacenes · Electrochemistry

[1] a) B. P. Rand, J. Genoe, P. Heremans, J. Poortmans, *Prog. Photovoltaics* **2007**, *15*, 659–676; b) A. Hagfeldt, G. Boschloo, L. Sun, L. Kloo, H. Pettersson, *Chem. Rev.* **2010**, *110*, 6595–6663; c) P. Bäuerle, A. Mishra, *Angew. Chem. Int. Ed.* **2012**, *51*, 2020–2067; *Angew. Chem.* **2012**, *124*, 2060; d) Y. Sun, G. C. Welch, W. L. Leong, C. J. Takacs, G. C. Bazan, A. J. Heeger, *Nat. Mater.* **2012**, *11*, 44–48; e) T. Duan, T.-Y. Hsiao, Y. Chi, X. Chen, Y. He, C. Zhong, *Dyes Pigm.* **2016**, *124*, 45–52.

[2] a) A. Mishra, M. K. R. Fischer, P. Bäuerle, *Angew. Chem. Int. Ed.* **2009**, *48*, 2474–2499; *Angew. Chem.* **2009**, *121*, 2510–2536; b) A. W. Hains, Z. Liang, M. A. Woodhouse, B. A. Gregg, *Chem. Rev.* **2010**, *110*, 6689–6735; c) H. Zhou, L. Yang, W. You, *Macromolecules* **2012**, *45*, 607–632; d) K. Kawabata, M. Saito, I. Osaka, K. Takimiya, *J. Am. Chem. Soc.* **2016**, *138*, 7725–7732.

[3] D. M. Gampe, F. Nöller, V. G. Hänsch, S. Schramm, A. Darsen, S. H. Habenicht, S. Ehrhardt, D. Weiß, H. Görls, R. Beckert, *Tetrahedron* **2016**, *72*, 3232–3239.

[4] a) E. Täuscher, R. Beckert, D. Weiß, H. Görls, *Synthesis* **2010**, 1603–1608; b) R. Menzel, E. Täuscher, D. Weiß, R. Beckert, H. Görls, *Z. Anorg. Allg. Chem.* **2010**, *636*, 1380–1385; c) E. Täuscher, L. Calderón-Ortiz, D. Weiß, R. Beckert, H. Görls, *Synthesis* **2011**, 2334–2339.

[5] a) R. Menzel, D. Weiß, E. Täuscher, R. Beckert, H. Görls, *Inorg. Chem. Commun.* **2012**, *18*, 65–68; b) R. Beckert, D. Weiß, L. Calderón Ortiz, H. Würfel, E. Täuscher, E. Birckner, H. Görls, *Synthesis* **2013**, *46*, 126–134; c) S. H. Habenicht, S. Schramm, S. Fischer, T. Sachse, F. Herrmann-Westendorf, A. Bellmann, B. Dietzek, M. Presselt, D. Weiß, R. Beckert, H. Görls, *J. Mater. Chem. C* **2016**, *4*, 958–971; d) S. Schramm, I. Navizet, P. Naumov, N. K. Nath, R. Berraud-Pache, P. Oesau, D. Weiss, R. Beckert, *Eur. J. Org. Chem.* **2016**, 678–681.

[6] R. Menzel, S. Kupfer, R. Mede, D. Weiß, H. Görls, L. González, R. Beckert, *Eur. J. Org. Chem.* **2012**, 5231–5247.

[7] R. Menzel, A. Breul, C. Pietsch, J. Schäfer, C. Friebe, E. Täuscher, D. Weiß, B. Dietzek, J. Popp, R. Beckert, U. S. Schubert, *Macromol. Chem. Phys.* **2011**, *212*, 840–848.

[8] a) J. Schäfer, R. Menzel, D. Weiß, B. Dietzek, R. Beckert, J. Popp, *J. Lumin.* **2011**, *131*, 1149–1153; b) A. M. Breul, I. Rabelo de Moraes, R. Menzel, M. Pfeffer, A. Winter, M. D. Hager, S. Rau, B. Dietzek, R. Beckert, U. S. Schubert, *Polym. Chem.* **2014**, *5*, 2715.

[9] L. K. Calderón-Ortiz, E. Täuscher, E. Leite Bastos, H. Görls, D. Weiß, R. Beckert, *Eur. J. Org. Chem.* **2012**, 2535–2541.

[10] R. Menzel, D. Ogermann, S. Kupfer, D. Weiß, H. Görls, K. Kleinermanns, L. González, R. Beckert, *Dyes Pigm.* **2012**, *94*, 512–524.

[11] A. Schade, R. Menzel, H. Görls, S. Spange, R. Beckert, *Asian J. Org. Chem.* **2013**, *2*, 498–503.

[12] a) M. Sonntag, P. Strohriegl, *Chem. Mater.* **2004**, *16*, 4736–4742; b) P. Li, Y. Cui, C. Song, H. Zhang, *Dyes Pigm.* **2017**, *137*, 12–23.

[13] a) J. R. Huber, W. W. Mantulin, *J. Am. Chem. Soc.* **1972**, *94*, 3755–3760; b) M. Thelakkat, C. Schmitz, C. Hohle, P. Strohriegl, H.-W. Schmidt, U. Hofmann, S. Schloter, D. Haarer, *Phys. Chem. Chem. Phys.* **1999**, *1*, 1693–1698; c) D. Jiang, S. Chen, Z. Xue, Y. Li, H. Liu, W. Yang, Y. Li, *Dyes Pigm.* **2016**, *125*, 100–105.

[14] a) T. J. J. Müller, A. W. Franz, C. S. Barkschat, M. Sailer, K. Meerholz, D. Müller, A. Colsmann, U. Lemmer, *Macromol. Symp.* **2010**, *287*, 1–7; b) I. S. Pereteanu, T. J. J. Müller, *Org. Biomol. Chem.* **2013**, *11*, 5127–5135; c) M. Reig, C. Gozálvez, R. Bujaldón, G. Bagdziunas, K. Ivaniuk, N. Kostiv, D. Volyniuk, J. V. Grazulevicius, D. Velasco, *Dyes Pigm.* **2017**, *137*, 24–35.

[15] a) T. J. J. Müller, L. Levi, S. Scheuren, *Synthesis* **2014**, *46*, 3059–3066; b) R. M. Pearson, C. H. Lim, B. G. McCarthy, C. B. Musgrave, G. M. Miyake, *J. Am. Chem. Soc.* **2016**, *138*, 11399–11407.

[16] a) S. Kato, T. Matsumoto, M. Shigeiwa, H. Gorohmaru, S. Maeda, T. Ishi-i, S. Mataka, *Chem. Eur. J.* **2006**, *12*, 2303–2317; b) B. A. D. Neto, A. A. M. Lapis, E. N. da Silva Júnior, J. Dupont, *Eur. J. Org. Chem.* **2013**, 228–255; c) J. Zhang, W. Chen, A. J. Rojas, E. V. Jucov, T. V. Timofeeva, T. C. Parker, S. Barlow, S. R. Marder, *J. Am. Chem. Soc.* **2013**, *135*, 16376–16379; d) T. C. Parker, D. G. D. Patel, K. Moudgil, S. Barlow, C. Risko, J.-L. Brédas, J. R. Reynolds, S. R. Marder, *Mater. Horiz.* **2015**, *2*, 22–37.

[17] a) T. M. P. Gawrys, E. Bartnik, M. Kucinska, J. Ulanski, M. Zagorska, *Org. Lett.* **2011**, *13*, 6090–6093; b) Y. Liu, F. Zhang, C. He, D. Wu, X. Zhuang, M. Xue, Y. Liu, X. Feng, *Chem. Commun.* **2012**, *48*, 4166–4168; c) T. Takeda, J. Tsutsumi, T. Hasegawa, S.-I. Noro, T. Nakamura, T. Akutagawa, *J. Mater. Chem. C* **2015**, *3*, 3016–3022.

[18] J. Nishida, N. Naraso, S. Murai, E. Fujiwara, H. Tada, M. Tomura, Y. Yamashita, *Org. Lett.* **2004**, *6*, 2007–2010.

[19] D. M. Gampe, M. Kaufmann, D. Jakobi, T. Sachse, M. Presselt, R. Beckert, H. Görls, *Chem. Eur. J.* **2015**, *21*, 7571–7581.

[20] a) J. T. Bloking, X. Han, A. T. Higgs, J. P. Kastrop, L. Pandey, J. E. Norton, C. Risko, C. E. Chen, J.-L. Brédas, M. D. McGehee, A. Sellinger, *Chem. Mater.* **2011**, *23*, 5484–5490; b) Y. Chen, X. Wan, G. Long, *Acc. Chem. Res.* **2013**, *46*, 2645–2655; c) J. W. Jung, W. H. Jo, *Chem. Mater.* **2015**, *27*, 6038–6043.

[21] a) H. Yao, Y. Chen, Y. Qin, R. Yu, Y. Cui, B. Yang, S. Li, K. Zhang, J. Hou, *Adv. Mater.* **2016**, *28*, 8283–8287; b) D. Dang, Y. Zhi, X. Wang, B. Zhao, C. Gao, L. Meng, *Dyes Pigm.* **2017**, *137*, 43–49.

[22] E. Täuscher, D. Weiß, R. Beckert, J. Fabian, A. Assumpção, H. Görls, *Tetrahedron Lett.* **2011**, *52*, 2292–2294.

[23] a) B. D. Lindner, Y. Zhang, S. Höfle, N. Berger, C. Teusch, M. Jesper, K. I. Hardcastle, X. Qian, U. Lemmer, A. Colsmann, U. H. F. Bunz, M. Hamburger, *J. Mater. Chem. C* **2013**, *1*, 5718–5724; b) B. D. Lindner, F. Paulus, A. L. Appleton, M. Schaffroth, J. U. Engelhart, K. M. Schelkle, O. Tverskoy, F. Rominger, M. Hamburger, U. H. F. Bunz, *J. Mater. Chem. C* **2014**, *2*, 9609–9612; c) see ref. [16d]; d) P.-Y. Gu, J. Zhang, G. Long, Z. Wang, Q. Zhang, *J. Mater. Chem. C* **2016**, *4*, 3809–3814.

[24] S. H. Habenicht, M. Siegmann, S. Kupfer, J. Kübel, D. Weiß, D. Cherek, U. Möller, B. Dietzek, S. Gräfe, R. Beckert, *Methods Appl. Fluoresc.* **2015**, *3*, 025005.

[25] a) J. Fabian, H. Nakazumi, M. Matsuoka, *Chem. Rev.* **1992**, *92*, 1197–1226; b) L. Macor, F. Fungo, T. Tempesti, E. N. Durantini, L. Otero, E. M. Barea, F. Fabregat-Santiago, J. Bisquert, *Energy Environ. Sci.* **2009**, *2*, 529; c) U. Mayerhöffer, K. Deing, K. Gruss, H. Braunschweig, K. Meerholz, F. Wurthner, *Angew. Chem. Int. Ed.* **2009**, *48*, 8776–8779; *Angew. Chem.* **2009**, *121*, 8934; d) T. Maeda, Y. Hamamura, K. Miyanaga, N. Shima, S. Yagi, H. Nakazumi, *Org. Lett.* **2011**, *13*, 5994–5997; e) Ö. Kurt, İ. Özçeşmeci, A. Koca, A. Gül, M. B. Koçak, *Dyes Pigm.* **2017**, *137*, 236–243.

[26] a) M. Grätzel, *J. Photochem. Photobiol. C* **2003**, *4*, 145–153; b) B. E. Hardin, H. J. Snaith, M. D. McGehee, *Nat. Photonics* **2012**, *6*, 162–169; c) M. Li, W.

 

ChemPubSoc Europe

EurJOC European Journal of Organic Chemistry
Full Paper

Ni, H. Feng, X. Wan, Y. Liu, Y. Zuo, B. Kan, Q. Zhang, Y. Chen, *Org. Electron.* **2015**, *24*, 89–95; d) F. Liu, H. Fan, Z. Zhang, X. Zhu, *ACS Appl. Mater. Interfaces* **2016**, *8*, 3661–3668.

[27] A. M. Brouwer, *Pure Appl. Chem.* **2011**, *83*, 2213–2228.

[28] S. H. Habenicht, S. Schramm, M. Zhu, R. R. Freund, T. Langenstuck, R. Strathausen, D. Weiss, C. Biskup, R. Beckert, *Photochem. Photobiol. Sci.* **2015**, *14*, 2097–2107.

[29] C. M. Cardona, W. Li, A. E. Kaifer, D. Stockdale, G. C. Bazan, *Adv. Mater.* **2011**, *23*, 2367–2371.

[30] R. Misra, P. Gautam, *Org. Biomol. Chem.* **2014**, *12*, 5448–5457.

[31] a) A. Dhanabalan, J. K. J. van Duren, P. A. van Hal, J. L. j. van Dongen, R. A. J. Janssen, *Adv. Funct. Mater.* **2001**, *11*, 255–262; b) J. C. Bijleveld, M. Shahid, J. Gilot, M. M. Wienk, R. A. J. Janssen, *Adv. Funct. Mater.* **2009**, *19*, 3262–3270; c) B. Wang, S. W. Tsang, W. Zhang, Y. Tao, M. S. Wong, *Chem. Commun.* **2011**, *47*, 9471–9473.

[32] a) S. Zeng, L. Yin, X. Jiang, Y. Li, K. Li, *Dyes Pigm.* **2012**, *95*, 229–235; b) L. Wang, L. Yin, C. Ji, Y. Li, *Dyes Pigm.* **2015**, *118*, 37–44; c) P. Gautam, R. Maragani, R. Misra, *RSC Adv.* **2015**, *5*, 18288–18294.

[33] a) Y. Lin, Y. Li, X. Zhan, *Chem. Soc. Rev.* **2012**, *41*, 4245–4272; b) M. Paramasivam, A. Gupta, A. M. Raynor, S. V. Bhosale, K. Bhanuprakash, V. J. Rao, *RSC Adv.* **2014**, *4*, 35318–35331; c) Y. Jeon, T.-M. Kim, J.-J. Kim, J.-I. Hong, *New J. Chem.* **2015**, *39*, 9591–9595.

[34] T. C. McGill, D. A. Collins, *Semicond. Sci. Technol.* **1993**, *8*, S1–S5.

[35] a) W. J. Beenken, F. Herrmann, M. Presselt, H. Hoppe, S. Shokhovets, G. Gobsch, E. Runge, *Phys. Chem. Chem. Phys.* **2013**, *15*, 16494–16502; b) J. Singh, M. R. Naragyan, *Nanosci. Technol.* **2014**, *1*, 8–15; c) S. More, R. Bhosale, A. Mateo-Alonso, *Chem. Eur. J.* **2014**, *20*, 10626–10631.

[36] J. Tomasi, B. Mennucci, R. Cammi, *Chem. Rev.* **2005**, *105*, 2999–3093.

[37] T. A. Halgren, *J. Comput. Chem.* **1996**, *17*, 490–519.

[38] T. Yanai, D. P. Tew, N. C. Handy, *Chem. Phys. Lett.* **2004**, *393*, 51–57.

[39] *Gaussian 09, Revision A.02*, M. J. Frisch, G. W. Trucks, H. B. Schlegel, G. E. Scuseria, M. A. Robb, J. R. Cheeseman, G. Scalmani, V. Barone, B. Mennucci, G. A. Petersson, H. Nakatsuji, M. Caricato, X. Li, H. P. Hratchian, A. F. Izmaylov, J. Bloino, G. Zheng, J. L. Sonnenberg, M. Hada, M. Ehara, K. Toyota, R. Fukuda, J. Hasegawa, M. Ishida, T. Nakajima, Y. Honda, O. Kitao, H. Nakai, T. Vreven, J. A. Montgomery Jr., J. E. Peralta, F. Ogliaro, M. Bearpark, J. J. Heyd, E. Brothers, K. N. Kudin, V. N. Staroverov, R. Kobayashi, J. Normand, K. Raghavachari, A. Rendell, J. C. Burant, S. S. Iyengar, J. Tomasi, M. Cossi, N. Rega, J. M. Millam, M. Klene, J. E. Knox, J. B. Cross, V. Bakken, C. Adamo, J. Jaramillo, R. Gomperts, R. E. Stratmann, O. Yazyev, A. J. Austin, R. Cammi, C. Pomelli, J. W. Ochterski, R. L. Martin, K. Morokuma, V. G. Zakrzewski, G. A. Voth, P. Salvador, J. J. Dannenberg, S. Dapprich, A. D. Daniels, Ö. Farkas, J. B. Foresman, J. V. Ortiz, J. Cioslowski, D. J. Fox, *Gaussian, Inc., Wallingford, CT* **2009**.

[40] D. M. Gampe, S. Schramm, M. Kaufmann, H. Görls, R. Beckert, *New J. Chem.* **2016**, *40*, 10100–10107.

[41] a) D. Jacquemin, V. Wathelet, E. A. Perpète, C. Adamo, *J. Chem. Theory Comput.* **2009**, *5*, 2420–2435; b) D. Jacquemin, E. A. Perpète, I. Ciofini, C. Adamo, *Theor. Chem. Acc.* **2011**, *128*, 127–136.

[42] S. Fery-Forgues, D. Lavabre, *J. Chem. Educ.* **1999**, *76*, 1260–1264.

[43] D. Cież, J. Svetlik, *Synlett* **2011**, 315–318.

[44] F. Stöckner, R. Beckert, D. Gleich, E. Birckner, W. Günther, H. Görls, G. Vaughan, *Eur. J. Org. Chem.* **2007**, 1237–1243.

Received: February 1, 2016

 

**Publikation 5:**

„*N*-Phenylfluorubine: one functional dye - chromophor, fluorophor, electron-acceptor and more“

D. M. Gampe, S. Schramm, M. Kaufmann, H. Görls, R. Beckert,

*New J. Chem.* **2016**, *40*, 10100-10107.



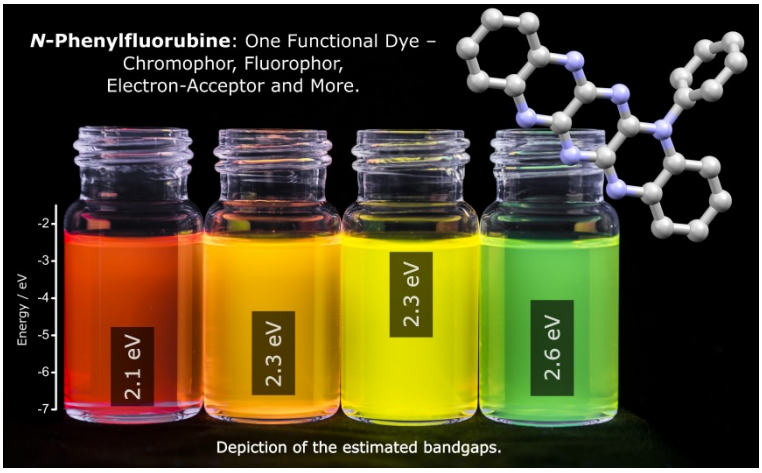

NJC

PAPER

Cite this: *New J. Chem.*, 2016, **40**, 10100

# *N*-Phenylfluorubine: one functional dye – chromophor, fluorophor, electron-acceptor and more†

D. M. Gampe,[a] S. Schramm,[a] M. Kaufmann,[a] H. Görls[b] and R. Beckert*[a]

Received (in Montpellier, France) 15th August 2016,
Accepted 24th October 2016

DOI: 10.1039/c6nj02544g

www.rsc.org/njc

We are presenting a new derivative of the fluorubine family which exhibits highly fluorescent activity. 5-Phenyl-dihydro[5,6,7,12,13,14]-hexaazapentacene was synthesized *via* two subsequent cyclization reactions starting from commercially available starting materials. Its properties were studied intensively *via* UV-vis and fluorescence spectroscopy, as well as cyclic voltammetry and quantum chemical calculations. Furthermore, we found a strong pH-sensitivity, which influences the photo- and electrochemical properties heavily. Thereby, it is possible to tune its properties from an electron-rich donor to a highly electron-deficient acceptor material.

## 1. Introduction

Paramount progress has occurred in developing organic electronic and optoelectronic devices over the last few years.[1–4] Hence, functional organic materials have become attractive from the industrial and academic point of view, but, so far, only expensive redox active systems, such as transition metal complexes, or *via* cross coupling synthesized polymers are used as an active layer in organic photovoltaic (OPV) devices.[5–9] A cheap, effective and consistent batch-to-batch fabrication of π-conjugated systems is desirable for the industrial fabrication of organic electronics.[10,11] Recent studies suggested that small molecules are able to challenge these demands and the efficiencies of OPVs based on them rose significantly.[12–14] Because of their easily tuneable morphology and energy levels, and their varied process abilities, monodisperse organic materials are on the spot.[15]

One of the most challenging aspects of such small molecules is their stability under working conditions.[16–19] One approach is concerned principally with the introduction of functional dyes into organic optoelectronic devices, such as merocyanines, squaraines, diketopyrrolopyrroles or porphyrines, which are established systems, for example in dye sensitized solar cells.[8,20] This indicates that stable functional materials are in great demand and the search for new innovative dyes has led us, among others, to acenes.[21]

Pentacene, for example, is used as a p-type semiconductor and, since its successful stabilization *via* steric residues at the reactive positions[22] or *via* substitution of CH by nitrogen[23] or sulphur[24,25] atoms, its derivatives are desirable target structures. In the case of substitution by heteroatoms, different reactivity as well as significantly changed properties were observed.[26] Azaacenes, which result *via* the introduction of nitrogen atoms into the acene backbone, are known for their high electron deficiency[27,28] and promising charge transport properties.[29,30] Furthermore, they exhibit great chemical and photostability,[31–34] as well as superior spectroscopic properties and were used successfully as sensors for both anions and metal ions.[35,36] Comprising, the properties of azaacenes offer a broad range of possible applications beyond semiconductors in field effect transistors like Li and Zhang described in 2015.[37] Using Cu-catalyzed Ullmann-Domino-reaction,[38] exemplarily, diaryldihydrophenazines with versatile emissive properties could be obtained, as they exhibit solvatochromic and thermochromic behaviour an application in organic light-emitting diodes is possible.[39] However, until recently, the synthesis, isolation and characterization of new azaacenes has been problematic due to instable intermediates and poor solubility of target compounds.[40–42]

An interesting approach concerning new synthetic strategies is the introduction of vicinale dinitriles and subsequent nucleophilic substitution by phenylenediamines, as developed by Richards *et al.*[43] The consecutive cyclization sequences lead to azaacenes with a high number of nitrogen atoms. Miao and co-workers used this strategy to generate hexaazapentacenes and investigated the redox system between the latter and their dihydro forms (also named fluorubines).[44] Both groups used

[a] *Institute of Organic and Macromolecular Chemistry, Friedrich Schiller University Jena, Humboldtstraße 10, 07743 Jena, Germany. E-mail: rainer.beckert@uni-jena.de; Web: http://www.agbeckert.uni-jena.de/*
[b] *Institute of Inorganic and Analytical Chemistry, Friedrich Schiller University Jena, Humboldtstraße 8, 07743 Jena, Germany*

† Electronic supplementary information (ESI) available: Solvatochromism/titration/CV measurements, X-ray, results of DFT calculations and analytical data. CCDC 1497236 ($3H_2^{2+}.2Cl^-$). For ESI and crystallographic data in CIF or other electronic format see DOI: 10.1039/c6nj02544g

 

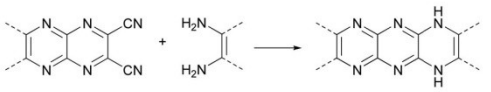

Scheme 1 General synthetic procedure for the substitution of the carbonitrile groups with diamines.

the oxidized azaacene-dicarbonitriles, which possess high reactivity against nucleophilic nitrile substitution, to synthesize their higher azaacenes (see Scheme 1).

Our group is interested in the more stable[45] and highly fluorescent dihydro-azapentacenes,[46,47] and furthermore, such materials were also recently tested successfully as semiconductive layers in thin film transistors.[34,48] Consequently, we used the 5-phenyl-5,10-dihydro-[1,4,5,10]-tetraazaanthracene **1**, which possesses a fixed dihydro form, as starting material for the further cyclization reaction. We obtained a versatile fluorubine derivative, which is accessible over two reaction steps and was synthesized *via* simple cyclization reactions using commercially available starting materials (see Scheme 2). Fluorubines are well-known for their high stability, and our compound **3** represents the first unsymmetrical derivative of the fluorubine family. It shows interesting features, such as high oscillator strengths, quantum yields and a strong pH sensitivity, as the properties are tuneable by simply adding acid or base, which are good attributes for application in organic electronic devices.

## 2. Results and discussion

### 2.1 Synthesis and structural characterization

Anthracene derivative **1** could be obtained after the reaction between *N*-phenyl-1,2-phenylenediamine and 2,3-dichloro-5,6-dicyanopyrazine in high yields.[40] We used the dicyano-substituted pyrazine instead of tetrachloropyrazine[49] as the first building block, because it generates the isolable anthracene **1**, which offers a route to unsymmetrical higher azaacenes. The subsequent cyclization between **1** and *o*-phenylenediamine gives the target compound **3** after oxidation of **3a** by oxygen during the purification. Due to the dihydro form of derivative **1**, the anthracene occurs with a lower reactivity against nucleophilic substitution compared to the oxidized azaacene structures of Richard's and Miao's groups. Thus, the second cyclization needs harsh conditions and long reaction times (>72 h) for a complete reaction turnover; however, this indicates the high chemical stability of our target structure **3**.

Table 1 Results of test reactions and one bigger charging stock

| Entry **1** | Solvent | Base | Time (h) | Yield |
|---|---|---|---|---|
| 100 mg (0.3 mmol) | 10 mL DMF | $Na_2CO_3$ | >100 | 14 mg (12%) |
| 100 mg (0.3 mmol) | 10 mL DMF | $Cs_2CO_3$ | >100 | 14 mg (12%) |
| 100 mg (0.3 mmol) | 10 mL DMSO | $Na_2CO_3$ | 72 | 10 mg (9%) |
| 100 mg (0.3 mmol) | 10 mL DMA | $Na_2CO_3$ | 84 | 16 mg (14%) |
| 7 g (22.6 mmol) | 80 mL DMA | $Na_2CO_3$ | 96 | 750 mg (9%) |

We tested different reaction conditions for this cyclization (see Table 1) based on the conditions publicized by Richard's and Miao's groups. Using boiling DMF as reaction medium, the turnover needs over 100 h, but affords **3** in 12% isolated yield. The role of the base used within the cyclization is to quench the emerging prussic acid, thus the base has no influence on the reaction itself. Using DMSO as solvent (at 180 °C) leads to a faster consumption of starting material **1**, but the isolated yield of **3** is smaller (9%) compared to that by using DMF. Due to the instability of DMSO, more side reactions take place. DMA is more stable than DMSO and possesses a higher boiling point than DMF, which leads to a faster reaction turnover (84 h) and higher yield (14%). Furthermore we tested this cyclization reaction using a bigger batch (entry: 7 g of **1**) in boiling DMA as reaction medium, but due to the lack of solubility of **3** the purification is more difficult (see Experimental section for detailed information) and affords **3** in only 9% yield.

We obtained single crystals suitable for single-crystal X-ray analysis, by slow evaporation of a hydrochloric acid/acetone solution of **3**. The resulting structure of **3** is depicted in Fig. 1. It is noteworthy, that pentacene **3** crystallized in the double protonated form (hereinafter referred to as $\mathbf{3H_2}^{2+}$), as the nitrogen atoms N4 and N5 are protonated. Thus, the pentacene backbone occurs as double cationic, where the charges are delocalized between the three pyrazine units. The lengths of the C–N bonds concerned are shortened and occur similar to typical C–N double bonds (about 1.33 Å), while C1–N1, C6–N2, C14–N5 and C9–N4 are longer and possess only partial double bond character (about 1.39 Å).[50] The bond lengths of C7–C16 (1.467(3)) and C8–C15 (1.461(3)) are enlarged because of the repulsion of the charges. As expected, the phenyl residue is twisted out of the almost planar fluorubine plane, with a torsion angle of about 88° (C1–N1–C17–C18). Thus, the phenyl moiety does not seem to be involved in the chromophoric π-system of the dye, but it fixes the dihydro-form of the pentacene backbone.

A characteristic image detail of the packing in the single crystals of compound $\mathbf{3H_2}^{2+}\cdot\mathbf{2Cl}^{-}$ is depicted in Fig. 2. The double

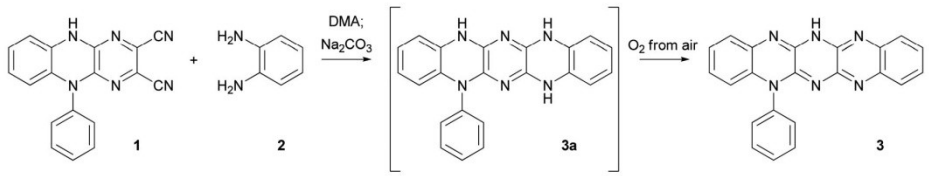


Scheme 2 Synthesis of target compound **3**.

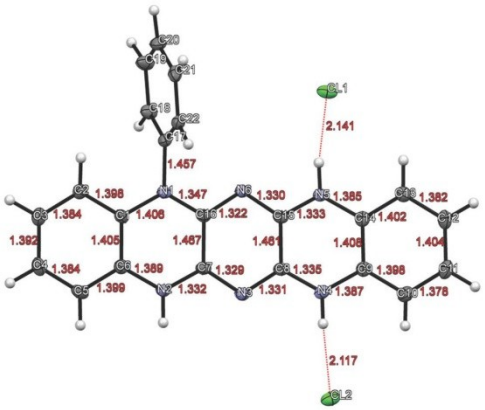


Fig. 1 ORTEP view of $3H_2^{2+}\cdot 2Cl^-$, showing the atom numbering scheme and the atom distances of the pentacene backbone. The s.u. are omitted for the sake of clarity.

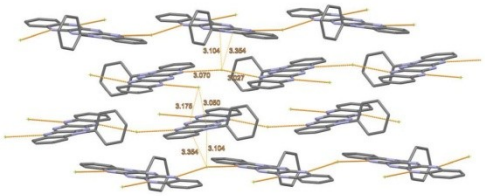


Fig. 2 View of the packing of compound $3H_2^{2+}\cdot 2Cl^-$. Some contacts are depicted and distances are given, all hydrogen atoms and the s.u. are omitted for clarity.

chlorine salt of the pentacene crystallizes in a chain-like structure, where the acenes are connected by hydrogen bonds going out from the chlorine atoms with distances of about 3.05 Å. Furthermore, the chain-like substructures are also connected to each other *via* the chlorine atoms. These interactions to the neighbouring azapentacene backbone within the adjacent chain system occur over distances of about 3.2 and 3.1 Å, and so the chlorine atoms are surrounded by azapentacene units.

### 2.2 Photochemical properties

The spectroscopic properties of fluorubine **3** were studied *via* UV-vis absorption and fluorescence emission spectroscopy. Some results are depicted in Fig. 3. *N*-Phenylfluorubine **3** shows vibronic structured absorption spectra, which are typical for such rigid systems.[51] Thus, the UV-vis absorption spectrum of **3** in methanol shows three substantial absorption bands at wavelengths of $\lambda_{max}$ = 418, 443 and 472 nm. An additional shoulder at $\lambda$ = 497 nm arises through autoprotolysis of **3** in polar solvents, as this shoulder does not appear in the spectra of **3** in non-polar solvents such as toluene (see Fig. S1 in the ESI†). Due to earlier experiences with fluorubine dyes,[49] we also measured our derivative at different pH-values in methanol. The properties of compound **3** change significantly upon protonation and deprotonation. By adding acetic acid to the methanolic solution of **3**, the system is transformed into an ammonium salt, which is due to the cationic charge in the fluorubine backbone more electron-deficient and possesses a decreased HOMO–LUMO gap. The spectrum of the protonated form $3H^+$ (see Scheme 3 for the acid–base equilibriums) is bathochromical shifted of $\Delta\lambda$ = 38 nm ≙ 1580 $cm^{-1}$ in comparison to **3**, but exhibits a nearly identical vibronic structure. In the case of adding the stronger hydrochloric acid, fluorubine **3** is double protonated ($3H_2^{2+}$), which is associated with a higher electron-deficiency, a significant bathochromic shift in the UV-vis absorption spectrum and a decreased band gap ($E_{Gap}^{opt}$ = 2.13 eV). The absorption bands of $3H_2^{2+}$ are shifted by $\Delta\lambda$ = 89 nm ≙ 3360 $cm^{-1}$ compared to **3**, to $\lambda_{max}$ = 483, 519 and 561 nm. All three protonation species (**3**, $3H^+$, $3H_2^{2+}$) are featured by high oscillator strengths with $\log\varepsilon \approx 4.6$ at the corresponding absorption maximum. Deprotonation of azapentacene **3** leads to an anionic dye and the absorption spectrum of $3^-$ entails a bathochromic shift of $\Delta\lambda$ = 46 nm ≙ 1880 $cm^{-1}$. The spectrum occurs lower structured and, in contrast to the protonated species, $3^-$ also exhibits lower extinction coefficients with a $\log\varepsilon \approx 4.2$ at

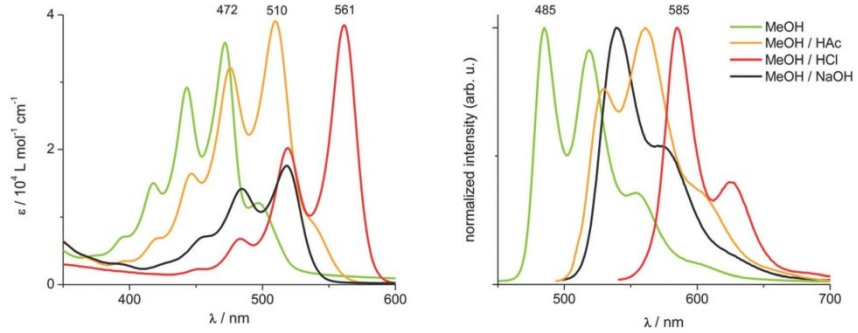


Fig. 3 pH-Dependent UV-vis absorption (left) and fluorescence emission (right) spectra of **3** in methanol.

 

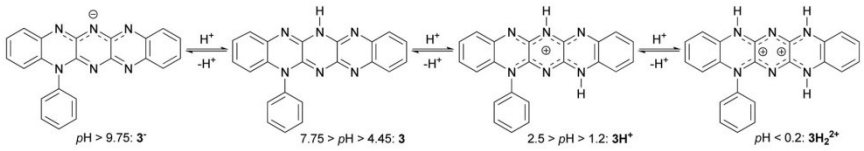


Scheme 3 Acidochromic behaviour of fluorubine dye **3**, the pH values are also given to obtain the corresponding species.

$\lambda_{max}$ = 518 nm. Furthermore, UV-vis titration was performed in MeOH/$H_2O$ 1 : 2 solutions (see Fig. S3 and S5 in the ESI†), where three points of change could be found and two relevant p$K_a$ were estimated to 8.2 ± 0.18 for the neutral to the deprotonated species (**3** to $\mathbf{3}^-$) and 3.04 ± 0.03 for the neutral to the monoprotonated form (**3** to $\mathbf{3H}^+$).

Additionally, we measured the fluorescence emission spectra after excitation at the appropriate absorption maximum (see Fig. 3, right graph), which also show the typical vibronic structure for acenes. The slight photonic energy loss between excitation and emission, recognizable by the small Stoke's shifts of about $\nu$ = 568 $cm^{-1}$ (**3**), $\nu$ = 740 $cm^{-1}$ ($\mathbf{3H}^+$), $\nu$ = 731 $cm^{-1}$ ($\mathbf{3H_2}^{2+}$) and $\nu$ = 752 $cm^{-1}$ ($\mathbf{3}^-$), is typical for such rigid systems.[52] Furthermore, we examined the fluorescence quantum yields of all four species.[53] In the case of the neutral form **3**, we obtained a quantum yield of $\Phi_F \approx 0.95$ E $mol^{-1}$ in methanol, which is within the experimental error comparable with fluorescein.[54] The sodium salt of anion $\mathbf{3}^-$ is also featured by a strong fluorescence emission ($\Phi_F \approx 0.9$ E $mol^{-1}$), but protonation seems to open more non-radiative deactivation pathways, as the quantum yields for $\mathbf{3H}^+$ ($\Phi_F \approx 0.6$ E $mol^{-1}$) and $\mathbf{3H_2}^{2+}$ ($\Phi_F \approx 0.2$ E $mol^{-1}$) decrease nearly linear to the protonation state. Some important spectroscopic results are summarized in Table 2.

In order to gain a more detailed insight into the electronic structure and the tautomerism of the molecule studied, sophisticated density functional theory/time-dependent density functional theory (DFT/TDDFT) calculations were carried out. The electronic transitions between the ground state and excited states for the tautomers studied here were carried out in order to correlate them to the values determined experimentally (Table 3).

Based on B3LYP/6-31+G(d,p) optimized geometries,[55–57] the absorption characteristics were investigated within the Frank–Condon region for the first six excited singlet states. Insights into the fluorescence emission were gained by applying TDDFT B3LYP/6-31+G(d,p) optimizations on the first excited state. Under linear-responsive consideration of the solvent (PCM: MeOH),[58] very good agreement to the experimental values could be reached by using the protonated structures as depicted in Scheme 3. Consequently, the mean error of our calculation is significantly below the typical error for TDDFT calculations (0.3 eV).[59] The reason for the error still resulting can be attributed mostly to the imperfect consideration of the solvent and the method used (DFT/TDDFT B3LYP/6-31+G(d,p), PCM: MeOH) itself. State-specific consideration of the solvent gave no better values than those with linear-responsive consideration of the solvent. Systematically better values may be achieved *via* the application of various other post-Hartree–Fock methods, such as CASSCF. However, this would increase the cost of the calculation tremendously by several orders of magnitude due to the extended π-system of the studied molecule and big molecule size overall. Considering this, it can be concluded that the values obtained here are a good compromise between the cost of calculation and accuracy.

Table 3 Comparison of the experimental and theoretical determined absorption (left) and fluorescence emission (right) maxima

| | $\lambda_{abs\,exp}$ [eV] | $\lambda_{abs\,calc}$ [eV] | $\Delta\lambda_{abs}$ [eV] | $\lambda_{F\,exp}$ [eV] | $\lambda_{F\,calc}$ [eV] | $\Delta\lambda_F$ [eV] |
|---|---|---|---|---|---|---|
| **3** | 2.49 | 2.79 | 0.29 | 2.24 | 2.25 | 0.01 |
| $\mathbf{3H}^+$ | 2.42 | 2.53 | 0.10 | 2.21 | 2.09 | 0.11 |
| $\mathbf{3H_2}^+$ | 2.20 | 2.30 | 0.10 | 1.98 | 1.85 | 0.13 |
| $\mathbf{3}^-$ | 2.39 | 2.50 | 0.11 | 2.17 | 2.01 | 0.15 |

As depicted in Fig. 4, both the HOMO and the LUMO are delocalized over the whole azaacene backbone, which leads to the assumption that there is no change of the dipole moment during the excitation of the molecule and no charge transfer is involved in the transition. Furthermore, the very small Stoke's shift as well as the negligible solvatochromism (see Fig. S1 in the ESI†), which means no stabilization *via* solvent dipolar

Table 2 Summary of the photochemical data

| | $\lambda_{abs}$/nm [$\varepsilon/10^4$ $M^{-1}$ $cm^{-1}$][a] | $\lambda_{F;max}$[a]/nm | Stokes $S{\cdot}\nu$[b]/$cm^{-1}$ | $\Phi$[c]/E $mol^{-1}$ | $E_{Gap}^{opt}$[d]/eV |
|---|---|---|---|---|---|
| **3** | 472 [3.58]; 443 [2.92]; 418 [1.50] | **485**; 519; 553 | 568 | 0.95 | 2.58 |
| $\mathbf{3H}^+$ | 510 [3.91]; 476 [3.21]; 447 [1.64] | 530; **561** | 740 | 0.63 | 2.25 |
| $\mathbf{3H_2}^{2+}$ | 561 [3.85]; 519 [2.02]; 483 [0.68] | **585**; 624 | 731 | 0.24 | 2.13 |
| $\mathbf{3}^-$ | 518 [1.76]; 484 [1.42] | **539**; 571 | 752 | 0.88 | 2.29 |

[a] Measured in MeOH for neutral fluorubine **3**, MeOH/acetic acid 1 : 1 for $\mathbf{3H}^+$, MeOH/hydrochloric acid 1 : 1 for $\mathbf{3H_2}^{2+}$ and MeOH/1 M NaOH solution 1 : 1 for $\mathbf{3}^-$. [b] Relative to the maximum of the absorption band. [c] Measured in solutions like footnote *a* with an absorbance below 0.05 at the appropriate excitation wavelength, relative to rhodamine 6G at $\lambda_{exc}$ = 510 nm ($\Phi$ = 0.95 in EtOH) and fluorescein at $\lambda_{exc}$ = 470 nm ($\Phi$ = 0.91 in 0.1 M NaOH).[54] [d] Calculated from the onset (10%) of the absorption spectra.

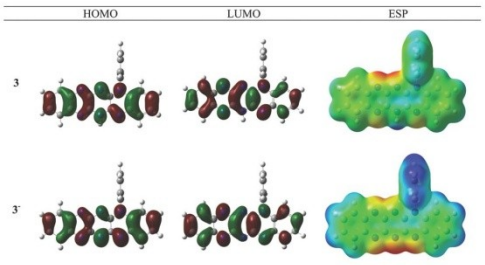


Fig. 4 Frontier orbitals of **3** and the deprotonated species $\mathbf{3}^-$ and the corresponding electrostatic potential (ESP, right; negative polarized parts are red/positive polarized parts: blue) on the van-der-Waals surface.

relaxation is induced, could be explained. The proton in compound **3** is very strongly polarized, which could be seen from the ESP and, consequently, it is easy to deprotonate the system.

### 2.3 Electrochemical properties

Cyclic voltammetry was performed in order to investigate the electrochemical properties (see Fig. 5 and Fig. S7–S10 in the ESI†). Fluorubine **3** exhibits a reversible reduction at a potential of $E_{1/2} = -0.95$ V, which leads to energy of the LUMO of $E_{LUMO} = -4$ eV (calculated *via*: $E_{Lumo} = [E_{onset}(red) - E_{onset}(Fc/Fc^+)] - 4.8$ eV) and, according to the optical gap, to a HOMO level at $E_{HOMO} = -6.6$ eV. The oxidation of **3** at a potential of $E = 0.4$ V seems to be irreversible (see Fig. S7 in the ESI†). Dunsch and co-workers[60] obtained similar results in the case of homofluorindine, and postulated a mechanism where the hydro form of the azapentacene loses one proton after oxidation and generates a radical (see Scheme 4). The oxidation step is irreversible in solution, because the proton drifts away and is not available for

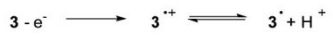


Scheme 4 Oxidation reaction of compound **3**.

the reverse reduction to the pristine fluorubine **3**. Due to follow-up reactions after the oxidation, new reduction (at $E = -0.25$ V) and oxidation steps ($E = 0.02$ V) appear.

By increasing the acidity and the protonation step, **3** is converted into $\mathbf{3H}^+$ or $\mathbf{3H_2}^{2+}$, respectively. Due to the protonation, the system is converted into a highly electron-deficient one, which could be made evident by the comparison of the appropriate reduction waves in the cyclic voltammetry measurements. The mono-protonated species $\mathbf{3H}^+$ shows two reversible reduction steps at potentials of $E_{1/2} = -0.68$ V and $E_{1/2} = -0.84$ V, and consequently, the energy of the LUMO is lowered by about 0.3 eV to $E_{LUMO} = -4.3$ eV. According to the band gap, estimated *via* absorption spectroscopy, the HOMO is nearly unaffected compared to the neutral form. The double protonated species $\mathbf{3H_2}^{2+}$ exhibits two well-separated reduction steps at $E_{1/2} = -0.26$ V and $E_{1/2} = -0.53$ V. Thus, the LUMO of the species ($\mathbf{3H_2}^{2+}$) is lowered significantly by about 0.7 eV in comparison to the neutral form **3**. The energy for the LUMO lies at: $E_{LUMO} = -4.7$ eV, which is, to the best of our knowledge, one of the lowest LUMO levels mentioned for heteroacenes. Such low LUMO energies ($-4.3$ eV for $\mathbf{3H}^+$ and $-4.7$ eV for $\mathbf{3H_2}^{2+}$) are promising characteristics for application as n-type semiconductors, as they surpass the established systems, such as PCBM or perylenediimides ($E_{LUMO} = -3.7$ eV).[62]

We obtained completely different results in the case of the anionic fluorubine dye $\mathbf{3}^-$. The reduction occurs, as expected for an electron-rich system, at $E = -2.15$ V, a much lower potential than for **3**, which leads to a significantly raised LUMO level to $E_{LUMO} = -2.7$ eV. The energy of the HOMO could be estimated to $E_{HOMO} = -5$ eV, where the optical band gap ($E_{Gap}^{opt} = 2.3$ eV) was used. This leads to high-lying energy levels for the corresponding frontier orbitals, which are comparable to the

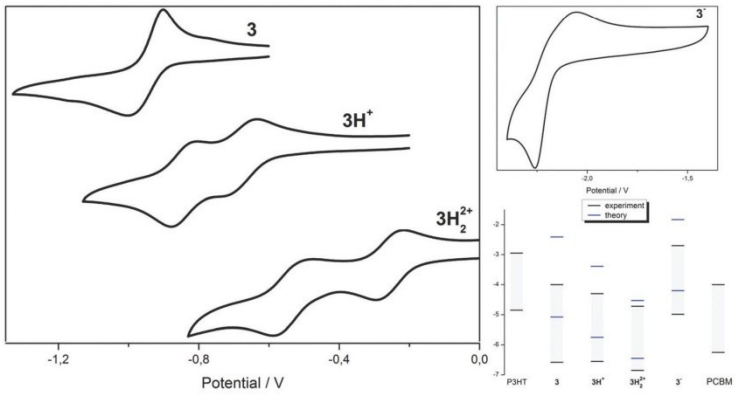


Fig. 5 Reduction waves of the cyclo voltammetry of fluorubine derivative **3**, the corresponding protonated species ($\mathbf{3H}^+$; $\mathbf{3H_2}^{2+}$) and the deprotonated form $\mathbf{3}^-$ (the spectra were calibrated externally against $E_{1/2}(Fc/Fc^+)$). Comparison of the experimental and theoretical examined orbital energies with poly(3-hexylthiophene) (P3HT) and phenyl-$C_{61}$-butyric acid methyl ester (PCBM).[61]

 

Table 4 Summary of the frontier orbital energies

| | $E_{onset}^{red}$ [a]/V | LUMO[b]/eV | HOMO[c]/eV | HOMO$^{DFT}$ [d]/eV | LUMO$^{DFT}$ [d]/eV | $E_{Gap}^{DFT}$ [d]/eV |
|---|---|---|---|---|---|---|
| **3** | −0.8 | −4.00 | −6.58 | −5.08 | −2.41 | 2.67 |
| $\mathbf{3H}^+$ | −0.5 | −4.30 | −6.55 | −5.75 | −3.39 | 2.36 |
| $\mathbf{3H_2}^{2+}$ | −0.1 | −4.72 | −6.85 | −6.45 | −4.53 | 1.92 |
| $\mathbf{3}^-$ | −2.1 | −2.70 | −4.99 | −4.20 | −1.83 | 2.37 |

[a] Recorded by cyclic voltammetry in 0.1 M solution of $TBAPF_6$ in THF at a scan rate of 50 mV $s^{-1}$ (THF + 1 drop of Tfa for $\mathbf{3H}^+$, THF/Tfa: 5 : 1 for $\mathbf{3H_2}^{2+}$ and DMF + 1 spatula NaH), *vs.* $E_{onset}(Fc/Fc^+)$. [b] Calculated *via* $E_{Lumo} = -[E_{onset}(red) - E_{onset}(Fc/Fc^+)] - 4.8$ eV. [c] $E_{HOMO} = E_{LUMO} - E_{Gap}^{opt}$. [d] HOMO: PBE/6-31+G(d,p), LUMO: PBE0/6-31+G(d,p), solvent: PCM MeOH.

established electron donor material P3HT ($E_{HOMO} = -5$ eV; $E_{LUMO} = -3$ eV).

To calculate the HOMO/LUMO energies of the molecule studied different widely used functionals were applied (B3LYP CAM-B3LYP, PBE, PBE0, B3PLYP, wB97XD). None of them gave values that are in perfect agreement with the experiment. Some of them typically underestimated the energy of the HOMO, such as B2PLYP, wB97XD or CAM-B3LYP, and others, such as B3LYP, PBE and PBE0, typically overestimated their energy. The best HOMO energies in terms of error compared to the experimental value are the results from the PBE calculations. The description of the LUMO energies is generally, as expected with all functionals, much worse than their HOMO counterparts. All functionals used showed a mean error of more than 0.3 eV compared to the experimental value. B2PLYP, wB97XD and CAM-B3LYP performed worst with 1.8 to 2.3 eV mean errors. PBE0 performed best with a mean error of 0.34 eV. This justifies the use of PBE for HOMO and PBE0 for LUMO energies. Surprisingly small errors for the band gap from HOMO to LUMO ranging from −0.21 to 0.11 eV could be obtained by applying this mixed functional method (see Table 4 for the important results and ESI† for all calculation values).

## 3. Conclusions

We were able to synthesize a new versatile derivative of the fluorubine family. 5-Phenyl-dihydro[5,6,7,12,13,14]-hexaazapentacene **3** is accessible through two simple cyclization reactions using commercially available materials. The isolated dye **3** exhibits high oscillator strength ($\log \varepsilon = 4.6$), high quantum yield of the green fluorescence ($\Phi = 0.95$ E $mol^{-1}$) and a strong pH-dependence, which influences its properties heavily. Thereby, we found three points of change and estimated two $pK_a$ values to $pK_a = 8.2$ and $pK_a = 3.0$, *via* UV-vis titration, which are located in the biologically relevant region.

By generating the anionic dye $\mathbf{3}^-$, an electron-rich system with energetic high-lying frontier orbitals at $E_{HOMO} = -4.99$ eV and $E_{LUMO} = -2.7$ eV is generated and a high quantum yield of $\Phi = 0.9$ E $mol^{-1}$ could be observed. By contrast, double protonation of **3** leads to highly electron-deficient $\mathbf{3H_2}^{2+}$, which exhibits a strong extinction coefficient ($\log \varepsilon = 4.6$) and a small band gap of $\Delta E = 2.1$ eV. With energetically very low-lying frontier orbitals at $E_{HOMO} = -6.85$ eV and $E_{LUMO} = -4.72$ eV, it surpasses the electron affinity of the established electron acceptor systems (*e.g.* PCBM).

In conclusion, fluorubine derivative **3** possesses promising properties for application in electronic and optoelectronic devices. Its adjustable properties and economical synthesis are especially very interesting and unique. In solution it could be turned from an electron donor ($\mathbf{3}^-$) into a strong electron acceptor ($\mathbf{3H_2}^{2+}$), thereby the fluorescence could be tuned from strong green over yellow and orange to red. Concluding, **3** could be used in a wide range either as electron donor, comparable to the established P3HT, or as a strong electron acceptor, depending on the required HOMO and LUMO energies.

## 4. Experimental part

### 4.1 Methods and Instrumentation

Solvents for UV-vis and emission spectroscopy were of analytical grade and bought from Sigma-Aldrich. $^1H$ and $^{13}C$ NMR and the corresponding correlation spectra were recorded on Bruker AC-250 (250 MHz), AC-300 (300 MHz) and AC-400 (400 MHz) spectrometers. Chemical shifts ($\delta$) are given relative to solvents. UV-vis data for the compounds were collected with a PerkinElmer LAMBDA 45 UV-vis spectrometer and emission spectra were measured with a Jasco FP 6500 instrument. Elemental analysis was carried out with a Leco CHNS-932 instrument. Mass spectra were measured either with a Finnigan MAT SSQ 710 (EI) or a MAZ 95 XL (ESI) system. Crystal structure determination: the intensity data were collected on a Nonius KappaCCD diffractometer, using graphite-monochromated Mo-K$\alpha$ radiation. Data were corrected for Lorentz and polarization effects; absorption was taken into account on a semi-empirical basis using multiple-scans.[63,64] The structure was solved by direct methods (SHELXS[65]) and refined by full-matrix least squares techniques against $F_o^2$ (SHELXL-97[65]). All hydrogen atoms were located by difference Fourier synthesis and refined isotropically. MERCURY was used for structure representations.[66] TLC materials were from Merck (Polygram SIL G/$UV_{254}$, aluminum oxide 60 $F_{254}$). The material for column chromatography was also obtained from Merck (silica gel 60, 0.04–0.063 mm). The quantum yields were measured against fluorescein ($\Phi_F = 0.91$ E $mol^{-1}$ in 1 M NaOH solution) and rhodamine 6G ($\Phi_F = 0.95$ E $mol^{-1}$ in EtOH) as the fluorescence standards.[53,54] The pH values of the UV-vis titration experiments were measured with a VWR pHenomenal MU6100H. The cyclovoltammetric measurements were performed at a Metrohm Autolab PGSTAT30 potentiostat. in 0.1 M solution of $TBAPF_6$ in THF (**3**), THF + 1 drop of Tfa (pH ≈ 2.5) for $\mathbf{3H}^+$, THF/Tfa: 5 : 1 for $\mathbf{3H_2}^{2+}$ and DMF + 1 spatula NaH for $\mathbf{3}^-$

(concentrations: $1 \times 10^{-4}$ M) on a graphite working electrode with a scanning speed of 50 mV $s^{-1}$, platinum was used as counter and Ag/AgCl as the reference electrode. The data were calibrated externally *versus* ferrocene/ferrocenium.

### 4.2 Synthesis

*N*-Phenyl-1,2-phenylenediamine and 1,2-phenylenediamine were used as purchased without further purification. 2,3-Dichloro-5,6-dicyanopyrazine could be purchased, but was synthesized as described in the literature.[46] 5-Phenyl-5,10-dihydropyrazino-[2,3-*b*]quinoxaline-2,3-dicarbonitrile **1** was also synthesized as described.[40]

Anthracene derivative **1** (100 mg, 0.32 mmol), 3 equiv. of 1,2-phenylenediamine (105 mg, 0.97 mmol) and 6 equiv. of sodium carbonate (205 mg, 1.93 mmol) were heated under reflux and stirring in 10 mL of purged DMA. The reaction was stopped when everything of anthracene **1** was consumed (TLC: silica; $CHCl_3$/acetone 95 : 5, $R_{f;1} \approx 0.8$; $R_{f;3} \approx 0.3$). The reaction mixture was diluted with the triple volume of water and extracted with ethyl acetate ($4 \times 50$ mL). The combined organic phases were extracted three times with 50 mL of 2 M hydrochloric acid (strong orange fluorescence of the aqueous phase). The aqueous phases were treated with sodium hydroxide to obtain pH $\approx$ 5 and extracted with $CHCl_3$ ($4 \times 50$ mL). After drying of the combined $CHCl_3$ phases, the solvent was removed under reduced pressure and the crude product was purified by a short column chromatography (silica; $CHCl_3$/acetone 95 : 5) to obtain the orange target compound **3**.

Purification of bigger reaction batches (at least 2 g of anthracene **1**):

After everything of **1** was consumed, the mixture was poured in 1 L of water and the precipitate was filtrated. After rinsing with water, the water phase was extracted with ethyl acetate ($3 \times 100$ mL) and the black precipitate was filled in a Soxhlet extractor and extracted with acetone. After approximately ten flow paths, the dark acetone solution was combined with the ethyl acetate phases and evaporated under reduced pressure. The crude product was purified by hot filtration of an ethanol suspension (approximately 50% of the total yield). The residual product in the Soxhlet extractor was then extracted with acetone/acetic acid (recognizable through the strong orange fluorescence in the Soxhlet extractor). After one day the extraction was stopped, the solution was evaporated to dryness and the residue was purified by column chromatography (silica; $CHCl_3$/acetone 95 : 5) to obtain the rest of the product (app. 50% of the total yield). m.p.: >350 °C; $^1$H NMR (400 MHz, DMSO): $\delta$ = 8.26 (s, 1H), 7.70 (t, $J$ = 7.5 Hz, 2H), 7.61 (t, $J$ = 7.2 Hz, 1H), 7.54 (d, $J$ = 7.8 Hz, 1H), 7.50 (d, $J$ = 9.0 Hz, 1H), 7.47 (d, $J$ = 7.2 Hz, 2H), 7.44–7.39 (m, 1H), 7.39–7.34 (m, 1H), 7.25 (d, $J$ = 7.6 Hz, 1H), 7.08 (t, $J$ = 7.2 Hz, 1H), 6.98 (t, $J$ = 7.8 Hz, 1H), 6.21 (d, $J$ = 7.6 Hz, 1H) ppm; $^{13}$C NMR (101 MHz, $CDCl_3$): $\delta$ = 147.70, 145.43, 144.21, 133.93, 131.63, 131.29, 131.12, 130.62, 129.88, 126.75, 126.26, 122.92, 122.45, 120.96, 118.82, 118.63, 116.39, 115.99, 113.15, 110.32 ppm; MS (EI): $m/z$ = 362 [$M^+$]; MS (ESI-neg): $m/z$ = 361.2 [$(M - H)^-$]; MS (ESI-pos): $m/z$ = 385.1 [$(M + Na)^+$]; HRMS (ESI-pos): calc.: 385.1178, found: 385.1180; EA calc. for $C_{22}H_{14}N_6$: C, 72.92; H, 3.89; N, 23.19; found: C, 73.14; H, 3.78; N, 23.07.

## References


1 L. Dou, J. You, Z. Hong, Z. Xu, G. Li, R. A. Street and Y. Yang, *Adv. Mater.*, 2013, **25**, 6642–6671.
2 Y.-W. Su, S.-C. Lan and K.-H. Wei, *Mater. Today*, 2012, **15**, 554–562.
3 P. Baeuerle and A. Mishra, *Angew. Chem., Int. Ed.*, 2012, **51**, 2020–2067.
4 A. Pron, P. Gawrys, M. Zagorska, D. Djurado and R. Demadrille, *Chem. Soc. Rev.*, 2010, **39**, 2577–2632.
5 B. P. Rand, J. Genoe, P. Heremans and J. Poortmans, *Prog. Photovoltaics*, 2007, **15**, 659–676.
6 H. Zhou, L. Yang and W. You, *Macromolecules*, 2012, **45**, 607–632.
7 Y. Ooyama and Y. Harima, *Eur. J. Org. Chem.*, 2009, 2903–2934.
8 A. Hagfeldt, G. Boschloo, L. Sun, L. Kloo and H. Pettersson, *Chem. Rev.*, 2010, **110**, 6595–6663.
9 N. Kaur, M. Singh, D. Pathak, T. Wagner and J. M. Nunzi, *Synth. Met.*, 2014, **190**, 20–26.
10 K. Okamoto, J. Zhang, J. B. Housekeeper, S. R. Marder and C. K. Luscombe, *Macromolecules*, 2013, **46**, 8059–8078.
11 R. Po and J. Roncali, *J. Mater. Chem. C*, 2016, **4**, 3677–3685.
12 Y. Lin, Y. Li and X. Zhan, *Chem. Soc. Rev.*, 2012, **41**, 4245–4272.
13 Y. Chen, X. Wan and G. Long, *Acc. Chem. Res.*, 2013, **46**, 2645–2655.
14 B. Kan, Q. Zhang, M. Li, X. Wan, W. Ni, G. Long, Y. Wang, X. Yang, H. Feng and Y. Chen, *J. Am. Chem. Soc.*, 2014, **136**, 15529–15532.
15 B. Kan, M. Li, Q. Zhang, F. Liu, X. Wan, Y. Wang, W. Ni, G. Long, X. Yang, H. Feng, Y. Zuo, M. Zhang, F. Huang, Y. Cao, T. P. Russell and Y. Chen, *J. Am. Chem. Soc.*, 2015, **137**, 3886–3893.
16 M. Jørgensen, K. Norrman and F. C. Krebs, *Sol. Energy Mater. Sol. Cells*, 2008, **92**, 686–714.
17 H.-L. Yip and A. K. Y. Jen, *Energy Environ. Sci.*, 2012, **5**, 5994.
18 Q. L. Song, F. Y. Li, H. Yang, H. R. Wu, X. Z. Wang, W. Zhou, J. M. Zhao, X. M. Ding, C. H. Huang and X. Y. Hou, *Chem. Phys. Lett.*, 2005, **416**, 42–46.
19 M. O. Reese, S. A. Gevorgyan, M. Jørgensen, E. Bundgaard, S. R. Kurtz, D. S. Ginley, D. C. Olson, M. T. Lloyd, P. Morvillo, E. A. Katz, A. Elschner, O. Haillant, T. R. Currier, V. Shrotriya, M. Hermenau, M. Riede, K. R. Kirov, G. Trimmel, T. Rath, O. Inganäs, F. Zhang, M. Andersson, K. Tvingstedt, M. Lira-Cantu, D. Laird, C. McGuiness, S. Gowrisanker, M. Pannone, M. Xiao, J. Hauch, R. Steim, D. M. DeLongchamp, R. Rösch, H. Hoppe, N. Espinosa, A. Urbina, G. Yaman-Uzunoglu, J.-B. Bonekamp, A. J. J. M. van Breemen, C. Girotto, E. Voroshazi and F. C. Krebs, *Sol. Energy Mater. Sol. Cells*, 2011, **95**, 1253–1267.
20 A. Mishra, M. K. R. Fischer and P. Bäuerle, *Angew. Chem.*, 2009, **121**, 2510–2536.
21 J. E. Anthony, *Chem. Rev.*, 2006, **106**, 5028–5048.


 

22 J. E. Anthony, *Angew. Chem.*, 2008, **120**, 460–492.
23 G. J. Richards, J. P. Hill, T. Mori and K. Ariga, *Org. Biomol. Chem.*, 2011, **9**, 5005–5017.
24 X. Shi, P. M. Burrezo, S. Lee, W. Zhang, B. Zheng, G. Dai, J. Chang, J. T. López Navarrete, K.-W. Huang, D. Kim, J. Casado and C. Chi, *Chem. Sci.*, 2014, **5**, 4490–4503.
25 X. Shi, W. Kueh, B. Zheng, K. W. Huang and C. Chi, *Angew. Chem., Int. Ed.*, 2015, **54**, 14412–14416.
26 U. H. Bunz, J. U. Engelhart, B. D. Lindner and M. Schaffroth, *Angew. Chem., Int. Ed.*, 2013, **52**, 3810–3821.
27 U. H. F. Bunz, *Pure Appl. Chem.*, 2010, **82**, 953–968.
28 Q. Tang, Z. Liang, J. Liu, J. Xu and Q. Miao, *Chem. Commun.*, 2010, **46**, 2977–2979.
29 A. L. Appleton, S. M. Brombosz, S. Barlow, J. S. Sears, J.-L. Brédas, S. R. Marder and U. H. Bunz, *Nat. Commun.*, 2010, **1**, 91.
30 Q. Miao, *Synlett*, 2012, 326–336.
31 G. Li, Y. Wu, J. Gao, C. Wang, J. Li, H. Zhang, Y. Zhao, Y. Zhao and Q. Zhang, *J. Am. Chem. Soc.*, 2012, **134**, 20298–20301.
32 A. Mateo-Alonso, N. Kulisic, G. Valenti, M. Marcaccio, F. Paolucci and M. Prato, *Chem. – Asian J.*, 2010, **5**, 482–485.
33 B. D. Lindner, J. U. Engelhart, O. Tverskoy, A. L. Appleton, F. Rominger, A. Peters, H. J. Himmel and U. H. Bunz, *Angew. Chem., Int. Ed.*, 2011, **50**, 8588–8591.
34 T.-Q. N. Q. Miao, T. Someya, G. B. Blanchet and C. Nuckolls, *J. Am. Chem. Soc.*, 2003, **125**, 10284–10287.
35 J. Zhao, G. Li, C. Wang, W. Chen, S. C. J. Loo and Q. Zhang, *RSC Adv.*, 2013, **3**, 9653.
36 B. Shi, P. Zhang, T. Wei, H. Yao, Q. Lin, J. Liu and Y. Zhang, *Tetrahedron*, 2013, **69**, 7981–7987.
37 J. Li and Q. Zhang, *ACS Appl. Mater. Interfaces*, 2015, **7**, 28049–28062.
38 H. Wang, Z. Zhang, H. Zhou, T. Wang, J. Su, X. Tong and H. Tian, *Chem. Commun.*, 2016, **52**, 5459–5462.
39 Z. Zhang, Y. S. Wu, K. C. Tang, C. L. Chen, J. W. Ho, J. Su, H. Tian and P. T. Chou, *J. Am. Chem. Soc.*, 2015, **137**, 8509–8520.
40 D. M. Gampe, M. Kaufmann, D. Jakobi, T. Sachse, M. Presselt, R. Beckert and H. Görls, *Chem. – Eur. J.*, 2015, **21**, 7571–7581.
41 U. Bunz, A. Appleton, S. Barlow, S. Marder and K. Hardcastle, *Synlett*, 2011, 1983–1986.
42 N. Kulisic, S. More and A. Mateo-Alonso, *Chem. Commun.*, 2011, **47**, 514–516.
43 G. J. Richards, J. P. Hill, N. K. Subbaiyan, F. D'Souza, P. A. Karr, M. R. Elsegood, S. J. Teat, T. Mori and K. Ariga, *J. Org. Chem.*, 2009, **74**, 8914–8923.
44 R. M. Z. He, D. Liu and Q. Miao, *Org. Lett.*, 2012, **14**, 4190–4193.
45 U. H. Bunz, *Acc. Chem. Res.*, 2015, **48**, 1676–1686.
46 F. Stöckner, R. Beckert, D. Gleich, E. Birckner, W. Günther, H. Görls and G. Vaughan, *Eur. J. Org. Chem.*, 2007, 1237–1243.
47 J. Fleischhauer, R. Beckert, Y. Juttke, D. Hornig, W. Gunther, E. Birckner, U. W. Grummt and H. Görls, *Chem. – Eur. J.*, 2009, **15**, 12799–12806.
48 F. Paulus, B. D. Lindner, H. Reiß, F. Rominger, A. Leineweber, Y. Vaynzof, H. Sirringhaus and U. H. Bunz, *J. Mater. Chem. C*, 2015, **3**, 1604–1609.
49 S. Z. J. Fleischhauer, R. Beckert, U.-W. Grummt, E. Birckner and H. Görls, *Chem. – Eur. J.*, 2012, **18**, 4549–4557.
50 N. A. Lange, *Lange's Handbook of Chemistry*, McGraw-Hill, Inc., New York, 15th edn, 1999.
51 M. Bendikov, F. Wudl and D. F. Perepichka, *Chem. Rev.*, 2004, **104**, 4891–4945.
52 R. Strathausen, R. Beckert, J. Fleischhauer, D. Müller and H. Görls, *Z. Naturforsch.*, 2014, **69b**, 641–649.
53 S. Fery-Forgues and D. Lavabre, *J. Chem. Educ.*, 1999, **76**, 1260–1264.
54 A. M. Brouwer, *Pure Appl. Chem.*, 2011, **83**, 2213–2228.
55 T. A. Halgren, *J. Comput. Chem.*, 1996, **17**, 490–519.
56 T. Yanai, D. P. Tew and N. C. Handy, *Chem. Phys. Lett.*, 2004, **393**, 51–57.
57 M. J. Frisch, G. W. Trucks, H. B. Schlegel, G. E. Scuseria, M. A. Robb, J. R. Cheeseman, G. Scalmani, V. Barone, B. Mennucci, G. A. Petersson, H. Nakatsuji, M. Caricato, X. Li, H. P. Hratchian, A. F. Izmaylov, J. Bloino, G. Zheng, J. L. Sonnenberg, M. Hada, M. Ehara, K. Toyota, R. Fukuda, J. Hasegawa, M. Ishida, T. Nakajima, Y. Honda, O. Kitao, H. Nakai, T. Vreven, J. A. Montgomery Jr., J. E. Peralta, F. Ogliaro, M. J. Bearpark, J. Heyd, E. N. Brothers, K. N. Kudin, V. N. Staroverov, R. Kobayashi, J. Normand, K. Raghavachari, A. P. Rendell, J. C. Burant, S. S. Iyengar, J. Tomasi, M. Cossi, N. Rega, N. J. Millam, M. Klene, J. E. Knox, J. B. Cross, V. Bakken, C. Adamo, J. Jaramillo, R. Gomperts, R. E. Stratmann, O. Yazyev, A. J. Austin, R. Cammi, C. Pomelli, J. W. Ochterski, R. L. Martin, K. Morokuma, V. G. Zakrzewski, G. A. Voth, P. Salvador, J. J. Dannenberg, S. Dapprich, A. D. Daniels, Ö. Farkas, J. B. Foresman, J. V. Ortiz, J. Cioslowski and D. J. Fox, *Gaussian 09, Revision A.02*, Gaussian, Inc., Wallingford, CT, 2009.
58 J. Tomasi, B. Mennucci and R. Cammi, *Chem. Rev.*, 2005, **105**, 2999–3093.
59 S. H. Habenicht, S. Schramm, S. Fischer, T. Sachse, F. Herrmann-Westendorf, A. Bellmann, B. Dietzek, M. Presselt, D. Weiß, R. Beckert and H. Görls, *J. Mater. Chem. C*, 2016, **4**, 958–971.
60 K. J. L. Sawtschenko, A. Neudeck and L. Dunsch, *Electrochim. Acta*, 1996, **41**, 123–131.
61 W. J. Beenken, F. Herrmann, M. Presselt, H. Hoppe, S. Shokhovets, G. Gobsch and E. Runge, *Phys. Chem. Chem. Phys.*, 2013, **15**, 16494–16502.
62 S. More, R. Bhosale and A. Mateo-Alonso, *Chem. – Eur. J.*, 2014, **20**, 10626–10631.
63 R. Hooft, *Collect: Data collection software*, Nonius BV, Delft, The Netherlands, 1998.
64 Z. Otwinowski and W. Minor, in *Methods Enzymol.*, ed. C. W. Carter Jr., 1997, vol. 276, pp. 307–326.
65 G. Sheldrick, *Acta Crystallogr., Sect. A: Found. Crystallogr.*, 2008, **64**, 112–122.
66 C. F. Macrae, P. R. Edgington, P. McCabe, E. Pidcock, G. P. Shields, R. Taylor, M. Towler and J. van de Streek, *J. Appl. Crystallogr.*, 2006, **39**, 453–457.

**Publikation 6:**

„From Highly Fluorescent Donors to Strongly Absorbing Acceptors: The Tunable Properties of Fluorubines“

D. M. Gampe, S. Schramm, S. Ziemann, M. Westerhausen, H. Gorls, P. Naumov, R. Beckert, *J. Org. Chem.* **2017**, *82*, 6153-6162.



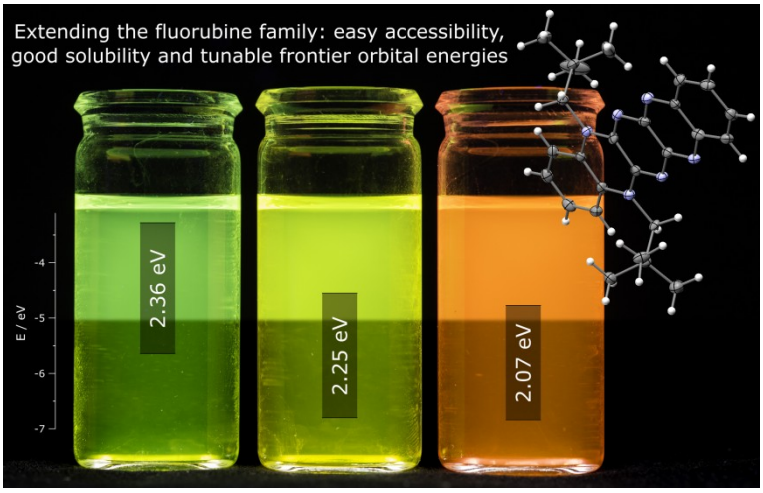

JOC The Journal of Organic Chemistry

Article

pubs.acs.org/joc

# From Highly Fluorescent Donors to Strongly Absorbing Acceptors: The Tunable Properties of Fluorubines

Dominique Mario Gampe,[†] Stefan Schramm,[†,§] Steffen Ziemann,[‡] Matthias Westerhausen,[‡] Helmar Görls,[‡] Panče Naumov,[§] and Rainer Beckert*[,†,⊥]

[†]Friedrich Schiller University Jena, Institute for Organic Chemistry und Macromolecular Chemistry, Humboldtstr. 10, Jena 07743, Germany

[‡]Friedrich Schiller University Jena, Institute for Inorganic und Analytical Chemistry, Humboldtstr. 8, Jena 07743, Germany

[§]New York University Abu Dhabi, P.O. Box 129188, Abu Dhabi, United Arab Emirates

Supporting Information

**ABSTRACT:** The synthesis and characterization of three novel fluorubine derivatives is reported via three to four simple reaction steps with isolatable intermediates. The functional dyes are characterized by their strong absorption peaks in the visible region and their high fluorescence quantum yields. A significant and useful feature is that the properties can be tuned over a wide range by changing the pH. Transformation of the dyes into protonated amidinium salts leads to narrower band gaps and to drastically lower LUMO energies. Further reduction of the pH results in the doubly protonated species with a high electron-deficiency and LUMO energies of −4.8 eV, bathochromic shifts, and a strong intensity increase of up to $\varepsilon$ = 120 000 $M^{-1}$ $cm^{-1}$.

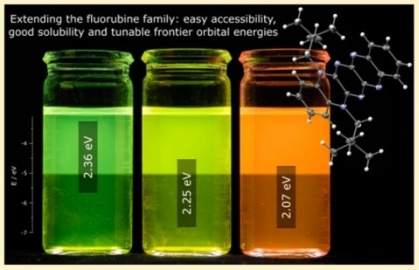


## INTRODUCTION

The application of acenes, especially pentacene, in organic thin-film transistors (OTFTs),[1−3] associated with the demand of its stabilization and derivatization,[4−6] has led to a renaissance in the research on azaacenes.[7] Even though most acenes are very reactive and undergo oxidations and photoinduced dimerizations,[8] azaacenes have been proven attractive because of their chemical and photochemical stability.[9,10] During the last two decades, many studies using a wide variety of structures and quantity of nitrogen atoms have been reported.[11−15] Consequently, some derivatives were introduced successfully as semiconductive components in OTFTs.[16−19] The main advantage of the azaacenes over other functional dyes is their long-term stability,[20,21] which leads to a broad range of applications, such as being the emitting species in organic light-emitting diodes (OLEDs)[22,23] and being the sensitizers in organic photovoltaics (OPVs).[24,25] Other studies have demonstrated the ability of certain azaacene derivatives to function as sensors for anions and metals[26,27] or as sensitizers in chemiluminescence reactions.[28,29]

Recently, we described different methods for the synthesis of dihydroazaacenes, particularly fluorubines.[30−32] These dihydrohexaazapentacene derivatives have excellent stability and remarkable optical properties. The first synthesis of the unsubstituted fluorubine core was accomplished in 1903 by Hinsberg and Schwantes (**1**, Scheme 1).[33] In their study, they found that this material is insoluble in most common solvents and exhibits a strong fluorescence emission, which can be tuned from green in alkaline solutions, to red by acidification. The most-challenging aspects of the azaacene chemistry proved to be their poor solubility and the difficulties with the isolation of the desired product because of the formation of many insoluble

**Scheme 1. Structures of Important Fluorubine Derivatives Reported in the Literature and Structures of the New Dyes (4, 5, 6)**

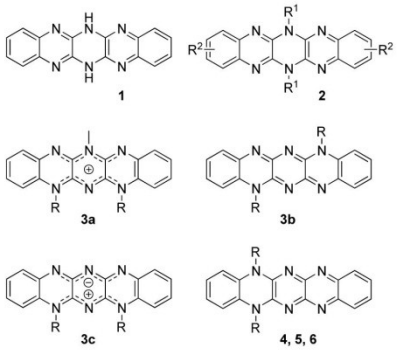


Received: March 31, 2017
Published: May 18, 2017





DOI: 10.1021/acs.joc.7b00676
J. Org. Chem. 2017, 82, 6153−6162

The Journal of Organic Chemistry Article

**Scheme 2. Synthetic Route to the Target Compounds 4, 5, and 6**[a]

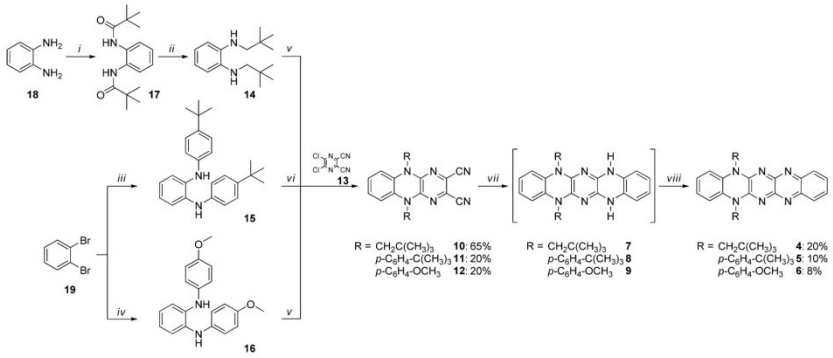


[a](*i*) pivaloyl chloride, THF, 88%; (*ii*) $LiAlH_4$, THF, $N_2$, 45%; (*iii*) *p*-$^t$butyl-aminobenzene, $Pd(dba)_2$, 2-dicyclohexylphosphino-2′,6′-dimethoxybiphenyl, KO$^t$Bu, toluene, $N_2$, 85%; (*iv*) *p*-anisidine, $Pd_2(dba)_3$, BINAP, NaO$^t$Bu, toluene, $N_2$, 95%; (*v*) **13**, dioxane, $N_2$; (*vi*) **13**, $Pd(dba)_2$, 2-dicyclohexylphosphino-2′,6′-diisopropoxybiphenyl, Hünig's base, toluene, $N_2$; (*vii*) **18**, DMA, $N_2$; (*viii*) [O].

side products (mostly polyaniline derivatives), which are probably the reasons why these materials have been underexplored. In 1955, Akimoto was the first to succeed in spectroscopic characterization of fluorubine,[34] and since then many patents exploring the synthesis, derivatization, and application of fluorubine dyes (**2**) have been filed.[35−39] While studying the decomposition of 1,2-diazetidines, we serendipitously isolated the first cationic fluorubine dye (**3a**, Scheme 1).[30] The compound displayed several interesting properties and we designed a synthetic route to functionalize new derivatives (**3b**). We obtained, based on the substitution pattern, the first zwitterionic derivative (**3c**).[40] Although some scientists have discussed the pH-dependent properties of azaacenes,[41−43] there are only a few publications quantifying this feature, and the electrochemical changes in particular have remained unexplored.[40,44] As we described recently,[45] the LUMO of such systems can be drastically decreased to levels that are required for n-type semiconductor applications or as electron-acceptors in fullerene-free bulk heterojunction (BHJ) solar cells.[46−48]

In this study, we have designed a synthetic procedure to introduce a new substitution pattern into fluorubines, as shown in compounds **4**, **5**, and **6**. Our aim was to combine the positive properties of known fluorubines (stability, strong absorption, and high quantum yields) with low-lying LUMO energies and enhanced solubility. Furthermore, we incorporated electron-donating moieties into the molecules to decrease the band gaps resulting from enhanced charge-transfer character of the compounds.

## ■ RESULTS AND DISCUSSION

**Synthesis and Structural Characterization.** The derivatives described here are accessible via three or four reaction steps starting from commercially available starting materials. The first reaction step, the synthesis of the *N*-functionalized phenylenediamines **14**−**16** (Scheme 2), defines the substitution pattern of the target compound. An *N*-functionalization not only fixes the dihydro form of the azaacene but also provides an opportunity to control the compound's physical properties, such as solubility, crystallinity, and the electron-donating character. We selected *neo*-pentyl (**14**) and *p*-$^t$butylphenyl functional groups (**15**) to increase solubility and to improve the propensity for crystallization. We also selected *p*-anisidyl (**16**) as an electron-donating moiety.[49,50] Even though the aliphatic residues (structure **14**) could be introduced via amidation of *o*-phenylenediamine **18** with pivaloyl chloride and subsequent reduction with $LiAlH_4$, the aromatic moieties (**15**, **16**) were implemented by using Buchwald−Hartwig coupling reactions, starting with dibromobenzene (**19**) and the appropriate aniline.[51] Subsequent cyclization reactions were carried out between the diamines and dichlorodicyanopyrazine (**13**) to obtain the dihydrotetraazaanthracenes (**10**, **11**, **12**). The cyclizations proceeded under normal substitution conditions because of the electron-donating character of the alkyl and *p*-anisidyl substituents of diamines **14** and **16**. However, the diamine **15** reacted only by using a Pd-catalysis with **13**, yielding **11**.[10] On the basis of the vicinal dicyano substructure in the anthracenes (**10**, **11**, **12**), further cyclization reactions with *o*-phenylenediamine (**18**) were conducted to obtain the target products **4**−**6**. In the consequences of the dihydro form being associated with the electron-donating character of these N atoms (**10**, **11**, **12**), very harsh conditions (reflux DMA, >72 h) were needed for this nucleophilic substitution to higher acenes, as established by Richards et al.[15] The intermediate tetrahydro-pentacenes (**7**, **8**, **9**) were not isolated because the molecules immediately oxidize in the presence of oxygen to form the final products **4**−**6** during the workup procedure.

Slow evaporation of saturated solutions of **4** ($EtOH/CHCl_3$) and **5** (acetone) afforded crystals suitable for X-ray diffraction experiments, and their crystal structures were determined (Figure 1). The $^t$butyl groups of the *neo*-pentyl derivative **4** are positioned above and below the fluorubine backbone with angles of 118.7(3)° and 117.6(3)°. The nitrogen atoms within the dihydropyrazine ring should be singly bonded to the adjacent carbon atoms (N3—C5/N4—C12), but with bond lengths of approximately 1.38 Å, they fit perfectly in the row of long (N3—C5:1.377(5)/N4—C12:1.379(5) Å), short (C5—N2:1.302(5)/C12—N5:1.296(5) Å), long (N2—C4:1.372(5)/N5—C13:1.373(5) Å), short (C4—N1:1.317(5)/C13—N6:1.314(5) Å), long (N1—C3:1.368(5)/N6—C14:1.373(5)



DOI: 10.1021/acs.joc.7b00676
J. Org. Chem. 2017, 82, 6153−6162

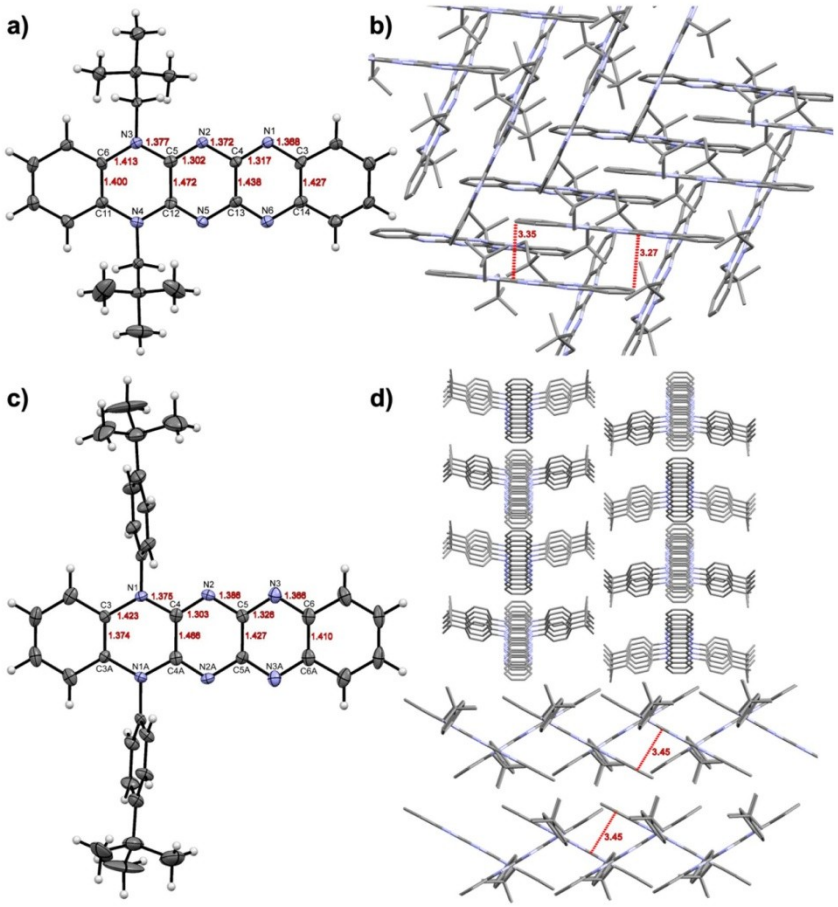


**Figure 1.** ORTEP view of the X-ray crystal structure of dyes **4** (a) and **5** (c), atom labeling and selected bond lengths. The packing of the dyes (**4**: b; **5**: d, viewed along the crystallographic *c* axis (d, top) and along the *b* axis (d, bottom)) are also shown. The hydrogen atoms (b, d), the s.u. and (in the case of **5**) acetone molecules are omitted for clarity.

Å), which is typical for conjugated $\pi$-systems in heteroaromatics.[52] There is a repulsive effect of the lone pairs of the N atoms in the dihydropyrazine. This manifests in an increased bonding distance between the C5—C12 carbons to 1.472(5) Å and coincides with our previous results.[45] Di-*neo*-pentylfluorubine **4** packs in a column-like structure with $\pi$—$\pi$ distances of the planar fluorubine molecules of about 3.3 Å. The single $\pi$-stacks are associated via weak hydrogen bonds (~2.6 Å; C−H···N) to the adjacent stack, forming a zigzag motif.

In the case of derivative **5**, the phenyl residues are twisted out of the fluorubine plane by torsion angles of about 80°, which impairs an effective $\pi$-conjugation over the whole system, because of the orthogonally positioned $\pi$-orbitals of phenyl and fluorubine. Surprisingly, both of the $^t$butylphenyl residues are angled by about 20° in the same direction against the backbone. Comparable to derivative **4**, the bond lengths within the dihydropyrazine ring are in the range of aromatic lengths (N1—C4/N1A—C4A; 1.375(6) Å), which points to an effective $\pi$−conjugation over the dihydro subunit. The adjacent bond of C4—C4A (1.466(10) Å) of derivative **5** is, similar to the one in **4**, enlarged because of the lone pair repulsion of the nitrogen atoms (N1 and N1A). Fluorubine **5** packs in one-dimensional stacks with $\pi$—$\pi$ distances of 3.4 Å. Such $\pi$-stacks are one property that may provide high conductivity and an application in OTFTs.[53] The stacks are connected to each other via weak hydrogen bonds (~2.7 Å; C = O···H−C, and $CH_3$···N) between **5** and molecules of acetone trapped within the lattice.

**Photochemical Characterization.** All of the new fluorubine derivatives were characterized by UV−vis absorption and fluorescence-emission spectroscopy; the results are depicted in Figure 2 and summarized in Table 1. In solutions



DOI: 10.1021/acs.joc.7b00676
*J. Org. Chem.* 2017, 82, 6153−6162

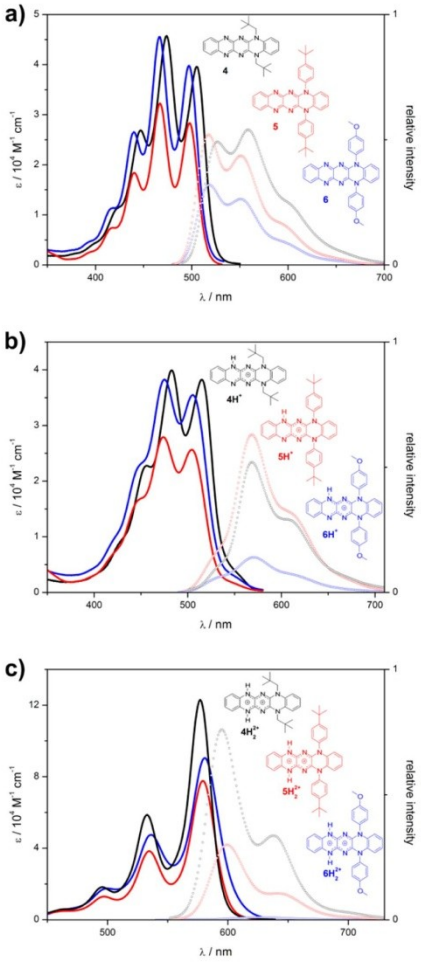


**Figure 2.** UV−vis (solid lines) and fluorescence (broken lines) spectra of the dyes **4**, **5**, and **6** in $CHCl_3$ solutions (a: neutral forms). The protonation states were realized by adding acetic acid (b) and trifluoroacetic acid (c), respectively. The fluorescence-emission spectra are normalized with regard to their relative intensities.

of $CHCl_3$, the derivatives show strong, vibronically structured-absorption bands with molar-absorption coefficients of $\varepsilon = 4.5 \times 10^4$ (**4**, **6**) and $3.2 \times 10^4$ $M^{-1}$ $cm^{-1}$ (**5**), in the green region of the visible spectrum. Typically for rigid chromophores,[54] the $S_{0-1}$ transitions are structured vibronically and show four maxima in the region of 400−520 nm at $\lambda$ = 420, 440, 470, and 500 nm. The absorption spectra of all of the derivatives are nearly identical, except for that the features in the UV−vis spectrum of the *neo*-pentyl derivative **4** are shifted slightly to higher wavelengths. As we described recently, an effective conjugation or extension of the chomophoric system via substitution of the amine nitrogen atom is inhibited, because of the torsion of these phenyl residues (in derivatives **5**, **6**).[32] In contrast, the weak electron-donating character of the alkyl substituents does not depend on bond angles, which is in line with the observed red-shifts in the spectrum. The optical band gaps were estimated from the onset (10%) of the absorption spectra to $\Delta E^{opt} \sim 2.4$ eV.

Fluorubines can be easily protonated,[55] which leads to new properties coming from the resulting cationic dyes. Of course, the zwitterionic derivatives of Wudl's[55] and Langer's groups[56] or **3c** can be turned to single cations, which entails drastic photochemical changes. In the case of the noncharged **4**, **5**, and **6**, conversion to the monoprotonated amidinium salts $\mathbf{4H^+}$, $\mathbf{5H^+}$, and $\mathbf{6H^+}$ is possible; we have ascertained this from our experience with similar systems[45] by adding acetic acid to $CHCl_3$ solutions (pH ≈ 3.5). The geometry is changed drastically from being highly symmetric to asymmetric; hence, the properties also change. The absorption bands not only exhibit a bathochromic shift, which leads to slightly decreased optical gaps of $\Delta E^{opt}$ = 2.3 eV, but the nature of the absorption bands is also affected. They are less structured, which is due to tautomerism associated with the change of bond lengths. Absorptions of the $S_{0-1}$ transitions of the derivatives extend over 400−550 nm, showing two maxima at $\lambda$ = 480 and 510 nm, with $\varepsilon = 4 \times 10^4$ ($\mathbf{4H^+}$, $\mathbf{6H^+}$) and $2.8 \times 10^4$ $M^{-1}$ $cm^{-1}$ ($\mathbf{5H^+}$), respectively. In contrast to derivative **3b**, which exhibits a bathochromic shift of 35 nm upon protonation, the absorption maxima of our novel derivatives are slightly shifted by 10 nm.

By further decreasing the pH using trifluoroacetic acid (pH ≈ 0.5), the fluorubines are turned into double amidinium salts. As *N*-heteroaromatics are known for this feature,[57] a strong bathochromic shift, recognizable by three separated absorption bands at $\lambda$ = 500, 530, and 580 nm, within the spectra of the dyes $\mathbf{4H_2^{2+}}$, $\mathbf{5H_2^{2+}}$, and $\mathbf{6H_2^{2+}}$ is the result of the double protonation. Outstanding molar absorption coefficients of $\varepsilon = 12 \times 10^4$ ($\mathbf{4H_2^{2+}}$), $8 \times 10^4$ ($\mathbf{5H_2^{2+}}$), and $9 \times 10^4$ $M^{-1}$ $cm^{-1}$ ($\mathbf{6H_2^{2+}}$), respectively, at 580 nm were observed and were verified thoroughly for the derivatives. The optical band gaps decrease in comparison to the neutral species by 0.4 eV to $\Delta E^{opt}$ = 2.0 eV.

To obtain deeper insights into all possible tautomeric forms, density functional theory (DFT) and time-dependent density functional theory (DFT) at B3LYP, PBE, and PBE1/6-31+G(d,p) levels of theory were applied as implemented in the Gaussian09 program package.[58−60] By utilizing the polarizable continuum model, the effects of solvation ($CHCl_3$) were accounted for.[61] After an initial geometry optimization at the B3LYP/6-31+G(d,p) level of theory, all of the compounds in Scheme 3 were analyzed in terms of their energy by means of the Boltzmann distribution at 298.15 K (for further details, see the Supporting Information).

The computations show that the protonation of all of the studied derivatives proceeds selectively on the nitrogen atoms N3 (single protonation) and N3/N8 (double protonation), respectively (for further details, see the Supporting Information). On the basis of the optimized ground-state geometries, the single-point energies of the first ten excited singlet states were determined within the Franck−Condon approximation by applying different functionals (B3LYP, PBE, PBE0) and the 6-31+G(d,p) basis set under linear-responsive consideration of the solvent interaction. Considering the transitions with an oscillator strength $f > 0.1$, the results from the B3LYP and PBE calculations show a nearly identical average absolute error with



DOI: 10.1021/acs.joc.7b00676
J. Org. Chem. 2017, 82, 6153−6162

The Journal of Organic Chemistry Article

**Table 1. Summary of the Important Photochemical Properties of the Fluorubine Dyes**

| substance | $\lambda_{abs,max}$/nm ($\varepsilon$ /$10^4$ $M^{-1}$ $cm^{-1}$)[a] | $\lambda_{abs\ calc,\ max}$/nm[b] ($\Delta$abs./eV)[c] | $\lambda_{em,max}$/nm[a] ($\nu$/eV)[d] | $\Phi$/E $mol^{-1}$[e] | $\Delta E^{opt}$/eV[f] |
|---|---|---|---|---|---|
| **4** | 505 (3.96); 474 (4.57); 447 (2.69) | 468 (0.19) | 527; 559 (0.10) | 0.54 | 2.36 |
| **4H$^+$** | 515 (3.82); 483 (3.99) | 536 (0.09) | 568 (0.22) | 0.52 | 2.25 |
| **4H$_2^{2+}$** | 577 (12.3); 533 (5.86); 496 (1.82) | 561 (0.06) | 595; 638 (0.06) | 0.76 | 2.07 |
| **5** | 498 (2.83); 467 (3.23); 440 (1.84) | 460 (0.20) | 517; 551 (0.09) | 0.52 | 2.40 |
| **5H$^+$** | 504 (2.57); 474 (2.79) | 530 (0.12) | 568 (0.28) | 0.63 | 2.30 |
| **5H$_2^{2+}$** | 579 (7.77); 535 (3.84); 497 (1.3) | 558 (0.07) | 599; 642 (0.07) | 0.30 | 2.06 |
| **6** | 497 (3.98); 467 (4.55); 440 (2.66) | 460 (0.19) | 518; 550 (0.10) | 0.32 | 2.39 |
| **6H$^+$** | 505 (3.55); 475 (3.83) | 531 (0.12) | 571 (0.25) | 0.14 | 2.28 |
| **6H$_2^{2+}$** | 581 (9.05); 536 (4.75); 500 (1.75) | 581 (0.08) | 625 (0.15) | <0.01 | 2.03 |

[a]Measured in $CHCl_3$, $CHCl_3$/HAc (3:1), and $CHCl_3$/TFA (3:1), respectively. [b]TD-DFT calculation B3LYP/6-31+G(d,p). [c]Difference between experimental and theoretical values. [d]Relative to the maximum of the absorption band. [e]Measured as described in footnote[a], relative to fluorescein ($\lambda_{exc}$ = 470 nm; $\Phi$ = 0.91), rhodamine 6G ($\lambda_{exc}$ = 530 nm; $\Phi$ = 0.95), and cresyl violet ($\lambda_{exc}$ = 560 nm; $\Phi$ = 0.56).[65] [f]Calculated via the onset (10%) of the absorption spectra.

**Scheme 3. Depiction of the Theoretical Analyzed Tautomers[a]**

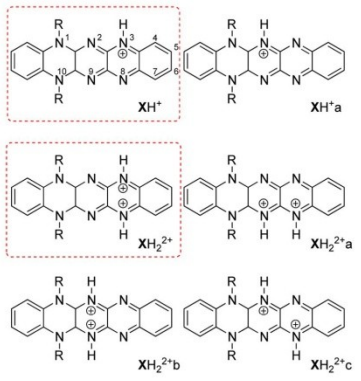


[a]The most-energetically stable structures are highlighted.

respect to the experimentally determined value for the $S_{0-1}$ transition of 0.13 eV. However, considering the much-lower standard deviation of the B3LYP absolute errors (B3LYP: 0.05 eV, PBE: 0.11 eV) it can be concluded that B3LYP is better suited to describe the electronic structure of these compounds. Moreover, it should be noted that none of the errors of the employed quantum-chemical calculations exceeds the limit of 0.3 eV, which is typical for TD-DFT calculations.[62,63]

All of the derivatives were investigated with fluorescence-emission spectroscopy (Figure 2). The fluorubines **4**, **5**, and **6** show broad, vibronically structured greenish-yellow fluorescence emission after photonic excitation at the appropriate absorption maximum ($\lambda_{em,max}$ ≈ 520 and 550 nm), with quantum yields of $\Phi$ = 0.5 (**4**, **5**) and 0.3 E $mol^{-1}$ (**6**) in $CHCl_3$.[64] As expected for such rigid systems, the loss of energy after excitation, the Stoke's shifts, are small (0.1 eV), and additional measurements in solvents of different polarity (toluene, $CH_3CN$, $CHCl_3$) revealed only weak solvatochromism of all derivatives with $\Delta E_{em,max}$ = 0.04–0.08 eV. Indeed, it is remarkable that the fluorescence-quantum yields increase in polar solvents such as $CH_3CN$ (up to 0.8 E $mol^{-1}$ for **5**, see table S1 in the Supporting Information). The amidinium ions **4H$^+$**, **5H$^+$**, and **6H$^+$** show an orange fluorescence emission, with larger Stoke's shifts of about 0.2 eV. Otherwise, as we have pointed out recently,[40,45] the quantum yields do not decrease when the molecule is protonated; the quantum yields of **4** and **4H$^+$**, and **5** and **5H$^+$** are nearly constant, and only that of the anisidyl derivative **6H$^+$** decreases to 0.1 E $mol^{-1}$.

Measurements of the double cationic dyes revealed strong fluorescence emissions (except for **6H$_2^{2+}$**, which shows no considerable emission) in the red region of the spectrum with two separated maxima at $\lambda_{em,max}$ ≈ 600 and 640 nm. In the case of **4H$_2^{2+}$** a remarkable fluorescence quantum yield of 0.76 E $mol^{-1}$ was obtained.

**Electro- and Quantum Chemical Characterization.** To investigate the electrochemical properties of the derivatives, cyclic voltammetry was carried out (see Figure 3 and Figures S7–S9 in the Supporting Information). The *neo*-pentyl derivative **4** reveals a reversible one-electron reduction at a half-wave potential of $E_{1/2}$ = −1.88 V, whereas the phenyl derivatives show irreversible reductions. In the case of derivative **5**, reductions occur at −1.66 and −1.85 V, and at −1.85 V for the anisidyl derivative **6**. Within the oxidation cycles, all three dyes reveal an irreversible-oxidation step at approximately 0.6 V. In addition, in the case of **4**, a one-electron oxidation step occurs at $E_{1/2}$ = 0.75 V, whereas the $^t$butyl-phenyl (**5**) and anisidyl fluorubine (**6**) are oxidized irreversibly at 0.93 V. Electrochemically estimated frontier orbital energies were calculated via: $E_{HOMO} = -[E_{onset}$ (ox vs $Fc^+/Fc)+5.1$ eV] and $E_{LUMO} = -[E_{onset}$ (red vs $Fc^+/Fc)+5.1$ eV], respectively.[66] The HOMO energies lie at −5.6 eV, and the LUMO energies range from −3.3 (**4** and **6**) to −3.4 eV (**5**). These energies lead to electrochemical-band gaps of approximately 2.3 eV, which are in good agreement with the optical gaps and in the typical range of fluorubines.[30,40] The experimentally and theoretically estimated frontier orbital energies of all of the different protonation states are summarized in Table 2.

By lowering the pH to approximately 3.5, the monoprotonated amidinium salts are generated, which are highly electron deficient because of the cationic charge. The reductions of **4H$^+$**, **5H$^+$**, and **6H$^+$** shift to much lower potentials, and two one-electron reductions are observed. In the case of **4H$^+$**, the reduction steps are overlapped and occur at $E_{1/2}$ = −0.68 and −0.81 V. Better separation of the two-step, one-electron reduction was observed in the case of the phenyl-substituted derivatives **5H$^+$** and **6H$^+$**, with half-wave potentials of $E_{1/2}$ = −0.54/−0.79 V (**5H$^+$**) and −0.59/−0.78 V (**6H$^+$**), respectively. As a result of this strong electron affinity, the LUMOs of all of the amidinium dyes are decreased drastically compared to their



DOI: 10.1021/acs.joc.7b00676
J. Org. Chem. 2017, 82, 6153–6162

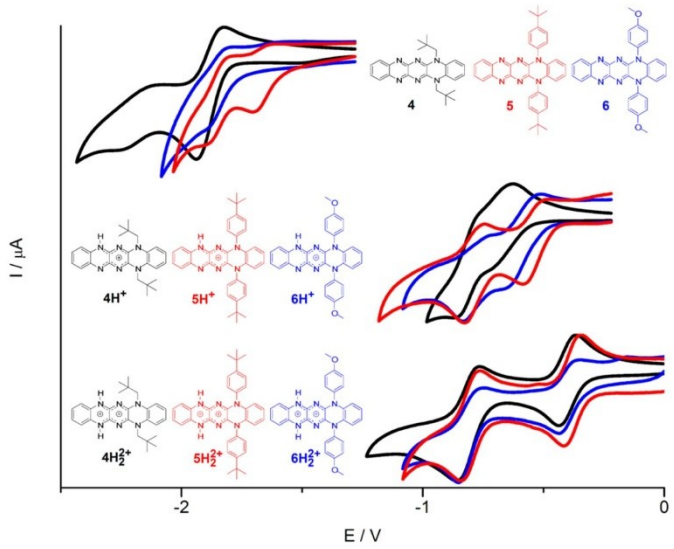


**Figure 3.** Depiction of the reduction waves recorded in 0.1 M solution of $TBAPF_6$ in THF solution at different pH. Protonation was accomplished by adding one droplet of TFA (singly protonated) and THF/TFA; 9:1 (doubly protonated), respectively. The voltammograms were calibrated externally against $Fc/Fc^+$.

**Table 2. Summary of the Frontier Orbital Energies Estimated Electrochemically and Theoretically**

| substance | LUMO/eV[a] ($LUMO^{DFT}$/eV)[b] | HOMO/eV[a] ($HOMO^{DFT}$/eV)[b] | $\Delta E^{CV}$/eV[c] | $\Delta E^{DFT}$ (error)/eV[c] |
|---|---|---|---|---|
| **4** | −3.28 (−2.50) | −5.64 (−5.18) | 2.36 | 2.67 (0.31) |
| $\mathbf{4H^+}$ | −4.55 (−4.06) | −6.80[d] (−6.30) | | 2.24 (−0.01) |
| $\mathbf{4H_2^{2+}}$ | −4.77 (−5.58) | −6.84[d] (−7.59) | | 2.01 (−0.06) |
| **5** | −3.37 (−2.52) | −5.65 (−5.24) | 2.28 | 2.72 (0.44) |
| $\mathbf{5H^+}$ | −4.64 (−4.08) | −6.94[d] (−6.35) | | 2.26 (−0.04) |
| $\mathbf{5H_2^{2+}}$ | −4.79 (−5.60) | −6.85[d] (−7.60) | | 2.01 (−0.05) |
| **6** | −3.33 (−2.52) | −5.62 (−5.24) | 2.29 | 2.72 (0.43) |
| $\mathbf{6H^+}$ | −4.60 (−4.08) | −6.88[d] (−6.34) | | 2.26 (−0.02) |
| $\mathbf{6H_2^{2+}}$ | −4.77 (−5.59) | −6.80[d] (−7.26) | | 1.67 (−0.36) |

[a]Recorded by cyclic voltammetry in 0.1 M solution of $TBAPF_6$ in THF at a scan rate of 50 mV/s (THF with one drop of TFA for the protonated species $\mathbf{4H^+}$, $\mathbf{5H^+}$, $\mathbf{6H^+}$; THF/TFA: 9:1 for the doubly protonated species $\mathbf{4H_2^{2+}}$, $\mathbf{5H_2^{2+}}$, $\mathbf{6H_2^{2+}}$) *vs* $E_{1/2}(Fc/Fc^+)$. $E_{LUMO} = -[E_{onset}(Red)+5.1]$, $E_{HOMO} = -[E_{onset}(Ox)+5.1]$. [b]HOMO: 50/50 PBE/6-31+G(d,p)/B3LYP/6-31+G(d,p); LUMO: PBE0/6-31+G(d,p)/B3LYP/6-31+G(d,p); Solvent: PCM THF. [c]Calculated via $\Delta E = -(E_{HOMO} - E_{LUMO})$. [d]$E_{HOMO} = E_{LUMO} - \Delta E^{opt}$.

neutral parent compounds by 1.3 eV to $E_{LUMO} = -4.6$ eV, which surpasses the LUMO levels of conventional acceptors such as fullerenes or perylenediimides and is in the range of Wangs 4Cl-4CN-perylenediimide, possessing an "ultralow LUMO" of −4.64 eV.[67−69] As expected, none of the amidinium ions showed an oxidation step within the range of the solvent (THF), but as the optical band gaps coincide with the ones estimated electrochemically (described above), the HOMO levels could be estimated via $E_{HOMO} = E_{LUMO} - \Delta E^{opt}$ to −6.8 ($\mathbf{4H^+}$) and −6.9 eV ($\mathbf{5H^+}$, $\mathbf{6H^+}$).

Stronger electron affinity is observed by turning the systems into their doubly protonated analogues ($\mathbf{4H_2^{2+}}$, $\mathbf{5H_2^{2+}}$, $\mathbf{6H_2^{2+}}$). These doubly cationic dyes show two well-separated one-electron reduction steps at half-wave potentials of $E_{1/2} = -0.4$ and −0.8 V, which lead to remarkably low LUMO levels of −4.8 eV. As already mentioned for the monoprotonated species ($\mathbf{4H^+}$, $\mathbf{5H^+}$, $\mathbf{6H^+}$), the doubly protonated forms do not show redox activity within the oxidation cycle and the HOMO levels were estimated via the optical gaps. As a result of the decreased band gap of the doubly protonated dyes ($\mathbf{4H_2^{2+}}$, $\mathbf{5H_2^{2+}}$, $\mathbf{6H_2^{2+}}$) and the lower LUMO levels, the HOMOs are nearly constant at −6.8 eV when compared to the monoprotonated species $\mathbf{4H^+}$, $\mathbf{5H^+}$, and $\mathbf{6H^+}$.

The energies of the HOMO and LUMO of the molecules were modeled using the optimized ground-state structures of the most-stable tautomer in each protonation state for further calculations. Again, several functionals (B3LYP, PBE, PBE0) were applied in order to compare the calculated energies of the HOMO and LUMO obtained from single-point calculations. A composite approach of HOMO (PBE) and LUMO (PBE0) was found to show a lower mean error of calculation than when both energy values from calculations with the same functional



DOI: 10.1021/acs.joc.7b00676
J. Org. Chem. 2017, 82, 6153−6162

were used. In earlier studies, we have already shown that this method is a viable approach and provides very accurate band gaps for fluorubines.[45]

## ■ CONCLUSIONS

We synthesized three novel derivatives of the fluorubine family via three (**5**, **6**) and four (**4**) simple consecutive reaction steps. All of the molecules and especially the $^t$butyl-bearing materials (**4**, **5**) displayed good solubility in organic solvents and crystallinity. Both **4** and **5** form one-dimensional $\pi$ stacks, with distances of 3.3 and 3.4 Å between the planes, which facilitate effective conductivity. The fluorubines **4**, **5**, and **6** show high molar-extinction coefficients (log $\varepsilon \approx 4.55$) in the blue-to-green region of the visible spectrum and high quantum yields of the greenish-yellow fluorescence. Because of their sensitivity to pH, the fluorubines can be converted into their amidinium counterparts ($\mathbf{4H}^+$, $\mathbf{5H}^+$, $\mathbf{6H}^+$), which results in drastically different properties. Not only are the absorptions shifted bathochromically, and hence the band gaps are decreased, the strong fluorescence emission is also shifted to the orange region of the spectrum. As a result of the protonation, significantly lowered LUMO energy levels of −4.6 eV are observed. A further decrease of the pH value affords the double-cationic amidinium ions ($\mathbf{4H_2}^{2+}$, $\mathbf{5H_2}^{2+}$, $\mathbf{6H_2}^{2+}$) which possess low-lying LUMOs (−4.8 eV), narrow band gaps (2 eV), and strong absorptions (up to log $\varepsilon$ = 5.1) in the orange region. Being endowed with easy synthetic access, good solubility, high molar extinction coefficients, as well as high fluorescence-quantum yields and tunable frontier-orbital energies, derivative **4** and its protonation states $\mathbf{4H}^+$, $\mathbf{4H_2}^{2+}$ is a viable candidate for application in organic electronics.

## ■ EXPERIMENTAL SECTION

Solvents for UV−vis and emission spectroscopy were of analytical grade and procured from Acros Organics ($CHCl_3$, stabilized with EtOH). Melting points were determined on a Galen III microscope from Cambridge Instruments equipped with a Lyca heating plate. The TGA experiment of **4** was measured on a Netzsch 449 F3 Jupiter (STA) under air. $^1$H and $^{13}$C NMR spectra and the corresponding correlation spectra were recorded on Bruker AC-250 (250 MHz), AC-300 (300 MHz), and AC-400 (400 MHz) spectrometers. The chemical shifts ($\delta$) are given relative to the deuterated solvents. UV−vis data for the compounds were collected with a PerkinElmer LAMBDA 45 UV−vis spectrometer and emission spectra were measured with a Jasco FP 6500 instrument. Elemental analysis was carried out with a Leco CHNS-932 instrument. The mass spectra were measured either with a Finnigan MAT SSQ 710 (EI) or a MAZ 95 XL (ESI) spectrometer. The X-ray diffraction data were collected on a Nonius Kappa CCD diffractometer, using graphite-monochromated Mo K$\alpha$ radiation. The data were corrected for Lorentz and polarization effects; absorption was taken into account on a semiempirical basis using multiple scans.[70−72] The structures were solved by direct methods (SHELXS)[73] and refined by full-matrix least-squares techniques against $F_0^2$ (SHELXL-97).[73] All of the hydrogen atoms of **10** were included at calculated positions with fixed thermal parameters. All of the non-hydrogen atoms were refined anisotropically.[73] The crystals of **5** were extremely thin and of low quality, resulting in a substandard data set; however, the refinement of the structure is accurate enough to show connectivity and geometry despite the high final R value. We are only publishing the conformation of the molecule and the crystallographic data. We will not deposit the data in the Cambridge Crystallographic Data Centre. MERCURY was used to generate the structure plots.[74] The TLC materials were from Merck (Polygram SIL G/UV254, aluminum oxide 60 F254). The material for column chromatography was also obtained from Merck (silica gel 60, 0.04−0.063 mm). The quantum yields were measured against fluorescein ($\Phi_F$ = 0.91 E mol$^{-1}$ in 1 M NaOH solution), rhodamine 6G ($\Phi_F$ = 0.95 E mol$^{-1}$ in EtOH), and cresyl violet ($\Phi_F$ = 0.56 E mol$^{-1}$ in EtOH) as the fluorescence standards.[64,65] The cyclovoltammetric measurements were performed at a Metrohm Autolab PGSTAT30 potentiostat in 0.1 M solution of $TBAPF_6$ in THF (**4**, **5**, **6**), THF with addition of one drop of TFA (pH ≈ 3.5) for $\mathbf{XH}^+$ and THF/TFA: 5:1 for $\mathbf{XH_2}^{2+}$ (concentrations: $1 \times 10^{-4}$ M) on a graphite working electrode with a scanning speed of 50 mV s$^{-1}$, platinum was used as counter and Ag/AgCl as the reference electrode. The data were calibrated externally versus ferrocene/ferrocenium.

***N,N′*-(1,2-Phenylene)bis(2,2-dimethylpropanamide) (17).**[75] To a mixture of *o*-phenylenediamine (**18**; 5.16 g, 47.6 mmol) and triethylamine (13.3 mL, 95.2 mmol) in 200 mL of THF, a mixture of pivaloyl chloride (11.75 mL, 95.2 mmol) in 30 mL of THF was added dropwise. The resulting reaction mixture was stirred overnight. After filtration, the precipitate was recrystallized from EtOH. The colorless crystals were washed with *n*-pentane and dried under reduced pressure to give **17** (11.6 g, 42 mmol; 88%): mp 174−175 °C; $^1$H NMR (400 MHz, $CDCl_3$): $\delta$ = 8.24 (s, 2H), 7.34−7.28 (m, 2H), 7.17−7.10 (m, 2H), 1.27 (s, 18H) ppm; $^{13}$C NMR (101 MHz, $CDCl_3$): $\delta$ = 178.2, 131.2, 126.0, 125.9, 77.2, 39.5, 27.8 ppm; Anal. calcd for $C_{16}H_{24}N_2O_2$: C, 69.53; H, 8.75; N, 10.14. Found: C, 69.51; H, 8.89; N, 10.01.

**1,2-Bis(neopentylamino)benzene (14).**[75] Compound **17** (11.6 g, 41.9 mmol) was added carefully to a suspension of $LiAlH_4$ (4.78 g, 125.9 mmol) in dry THF (160 mL) under nitrogen at 0 °C. After it was stirred under reflux and $N_2$ for 24 h, the reaction was quenched by a mixture of THF and water (5:1; 60 mL) while a precipitate was formed. After filtration, the filtrate was extracted with brine and evaporated to dryness to afford the crude product as a brown solid. Recrystallization from *n*-pentane yielded the desired compound **14** as colorless crystals (4.7 g, 18.9 mmol; 45%): mp 53−54 °C; $^1$H NMR (400 MHz, $C_6D_6$): $\delta$ = 7.03−6.97 (m, 2H), 6.78−6.70 (m, 2H), 3.28 (s, 2H), 2.69 (s, 4H), 0.90 (s, 18H) ppm; $^{13}$C NMR (101 MHz, $C_6D_6$): $\delta$ = 139.0, 128.1, 120.0, 113.2, 56.7, 31.4, 27.8 ppm; Anal. calcd for $C_{16}H_{28}N_2$: C, 77.36; H, 11.36; N 11.28. Found: C, 77.13; H, 11.49; N, 11.42.

***N,N′*-Bis(4-*tert*-butylphenyl)benzene-1,2-diamine (15).** A mixture of 1,2-dibromobenzene (**19**; 1 g, 4.3 mmol), 4-$^t$butylaniline (1.3 g, 8.6 mmol), and KO$^t$Bu (1 g, 9 mmol, 2.1 equiv) in 20 mL of toluene was purged with $N_2$ for 30 min, and $Pd(dba)_2$ (200 mg, 0.35 mmol, 8 mol %) and SPhos (280 mg, 0.68 mmol, 16 mol %) were added. The resulting dark reaction mixture was stirred under reflux and $N_2$ for 8 h and at 80 °C overnight. After the reaction was quenched with $NH_4Cl$ solution, the aqueous phase was extracted two times with toluene. The organic phases were combined, dried over $MgSO_4$, and evaporated under reduced pressure to afford the crude product as a dark oil. Column chromatography (silica; toluene; $R_f \sim 0.8$) yielded the diamine **15** as white oily solid (1.36 g, 3.7 mmol; 85%): mp 22−24 °C; $^1$H NMR (400 MHz, acetone-$d_6$): $\delta$ = 7.29−7.24 (m, 6H), 6.94 (d, $J$ = 8.6 Hz, 4H), 6.91 (dd, $J$ = 6.0, 3.5 Hz, 2H), 6.55 (s, 2H), 1.29 (s, 18H) ppm; $^{13}$C NMR (101 MHz, acetone-$d_6$): $\delta$ = 143.1, 143.0, 136.2, 126.6, 122.8, 120.4, 117.6, 34.5, 31.8, 29.8 ppm; MS (EI) $m/z$ = 372 [$M^{+\bullet}$], 357 [$(M-CH_3)^{+\bullet}$]; Anal. calcd for $C_{26}H_{32}N_2$: C, 83.82; H, 8.66; N, 7.52. Found: C, 84.08; H, 8.43; N, 7.67.

***N,N′*-Bis(4-methoxyphenyl)benzene-1,2-diamine (16).** To a mixture of 1,2-dibromobenzene (**19**; 1 g, 4.3 mmol), *p*-anisidine (1.1 g, 8.6 mmol), and KO$^t$Bu (1 g, 9 mmol, 2.1 equiv) in 20 mL of purged toluene, $Pd(dba)_2$ (200 mg, 0.35 mmol, 8 mol %) and SPhos (280 mg, 0.68 mmol, 16 mol %) were added. The reaction mixture was stirred under reflux and $N_2$ for 8 h and at 80 °C overnight. After extraction of the cooled mixture with water and $CH_2Cl_2$, the organic layer was dried over $MgSO_4$ and evaporated to dryness to give the crude product as a dark oil. To obtain the diamine **16** (1.3 g, 4.0 mmol; 95%) as a colorless oil, column chromatography (silica; toluene/ethyl acetate 19:1; $R_f \sim 0.7$) was carried out: mp 18−20 °C; $^1$H NMR (400 MHz, acetone-$d_6$): $\delta$ = 7.10 (dd, $J$ = 5.9, 3.5 Hz, 2H), 6.95 (d, $J$ = 8.9 Hz, 4H), 6.85−6.80 (m, 6H), 3.73 (s, 6H) ppm; $^{13}$C NMR (101 MHz, acetone-$d_6$): $\delta$ = 155.1, 138.6, 136.6, 122.3, 120.4, 119.1, 115.3, 55.7, 29.8 ppm; MS (EI) $m/z$ = 320 [$M^{+\bullet}$], 305 [$(M\text{-}CH_3)^{+\bullet}$]; Anal. calcd



DOI: 10.1021/acs.joc.7b00676
J. Org. Chem. 2017, 82, 6153−6162

for $C_{20}H_{20}N_2O_2$: C, 74.98; H, 6.29; N, 8.74. Found: C, 75.24; H, 6.11; N, 8.98.

**5,10-Dineopentyl-5,10-dihydropyrazino[2,3-*b*]quinoxaline-2,3-dicarbonitrile (10).** Diamine **14** (500 mg, 2 mmol) was dissolved in 20 mL of dioxane and the resulting solution was purged for 30 min with $N_2$. 5,6-Dichloropyrazine-2,3-dicarbonitrile (**13**; 400 mg, 2 mmol) was added, and the reaction was heated under reflux and $N_2$, until everything of **14** was consumed. After 8 h, the reaction was quenched with water, and the yellow precipitate was filtrated and washed with water. Recrystallization of the crude product from EtOH/$CHCl_3$ afforded the anthracene **10** as orange crystals (490 mg, 1.3 mmol; 65%): mp 226−227 °C; $^1$H NMR (250 MHz, $CDCl_3$): $\delta$ = 6.94−6.69 (m, 4H), 4.34 (s, 2H), 3.35 (s, 2H), 1.01 (s, 18H) ppm; $^{13}$C NMR (63 MHz, $CDCl_3$) $\delta$ = 148.2, 133.3, 124.3, 123.1, 115.9, 114.6, 77.2, 50.3, 34.6, 28.9 ppm; MS (EI) $m/z$ = 374 [$M^{+\bullet}$]; Anal. calcd for $C_{22}H_{26}N_6$: C, 70.56; H, 7.00; N, 22.44. Found: C, 70.21; H, 7.09; N, 22.32.

**5,10-Bis(4-*tert*-butylphenyl)-5,10-dihydropyrazino[2,3-*b*]-quinoxaline-2,3-dicarbonitrile (11).** A mixture of diamine **15** (750 mg, 2 mmol), pyrazine **13** (400 mg, 2 mmol), and Hünig's Base (700 $\mu$L, 4.1 mmol) in 10 mL of toluene was purged with $N_2$ for 30 min. After adding $Pd(dba)_2$ (92 mg, 0.16 mmol, 8 mol %) and RuPhos (150 mg, 0.32 mmol, 16 mol %), the reaction was stirred under reflux and $N_2$ for 10 h. The reaction was quenched by adding $NH_4Cl$ solution and the organic layer was separated and extracted with water. The aqueous phases were extracted with $CHCl_3$ and the organic layers were combined, dried over $MgSO_4$, and evaporated to dryness. After column chromatography (silica; $CHCl_3$; $R_f \sim 0.5$) the product was recrystallized from EtOH to give **11** as orange crystals (200 mg, 0.4 mmol; 20%): mp 356−357 °C; $^1$H NMR (400 MHz, DMSO-$d_6$): $\delta$ = 7.67 (d, $J$ = 7.6 Hz, 4H), 7.33 (d, $J$ = 7.6 Hz, 4H), 6.69−6.57 (m, 2H), 5.85−5.76 (m, 2H), 1.37 (s, $J$ = 0.8 Hz, 18H) ppm; $^{13}$C NMR (101 MHz, $CDCl_3$): $\delta$ = 152.7, 147.1, 133.3, 132.7, 128.3, 128.0, 124.5, 124.2, 116.0, 114.6, 77.2, 35.1, 31.5 ppm; MS (EI) $m/z$ = 498 [$M^{+\bullet}$]; Anal. calcd for $C_{32}H_{30}N_6$: C, 77.08; H, 6.06; N, 16.85. Found: C, 77.35; H, 6.17; N, 16.51.

**5,10-Bis(4-methoxyphenyl)-5,10-dihydropyrazino[2,3-*b*]-quinoxaline-2,3-dicarbonitrile (12).** Dissolved into 20 mL of purged dioxane was 750 mg (2.3 mmol) of **16**, and 470 mg (2.3 mmol) of **13** was added. The resulting dark reaction mixture was stirred under reflux and $N_2$ until everything of **16** was consumed (TLC: silica; toluene). After 20 h, the reaction was allowed to cool to room temperature and evaporated. The residue was dissolved in $CHCl_3$ and water. The organic layer was extracted two times with water, dried over $MgSO_4$, and evaporated to dryness. After column chromatography (silica; $CHCl_3$), the yellow product was recrystallized from EtOH to afford the anthracene **12** as orange powder (200 mg, 0.45 mmol; 20%): mp > 365 °C; $^1$H NMR (250 MHz, DMSO-$d_6$): $\delta$ = 7.31 (d, $J$ = 8.9 Hz, 4H), 7.18 (d, $J$ = 9.0 Hz, 4H), 6.67−6.57 (m, 2H), 5.87−5.78 (m, 2H), 3.84 (s, 6H) ppm; $^{13}$C NMR (101 MHz, DMSO-$d_6$): $\delta$ = 159.3, 147.8, 133.3, 129.8, 127.9, 124.0, 122.6, 115.9, 115.0, 114.7, 55.2, 39.5 ppm; MS (EI) $m/z$ = 446 [$M^{+\bullet}$]; Anal. calcd for $C_{26}H_{18}N_6O_2$: C 69.95, H 4.06, N 18.82; Found: C 70.30, H 4.19, N 18.64.

**General Procedure.** For the synthesis of fluorubines **4**, **5**, **6**: 200 mg of the corresponding anthracene derivative (**10**, **11**, or **12**) were dissolved in 20 mL of DMA and purged with $N_2$ for 30 min. After this, *o*-phenylenediamine (**13**; 3 equiv) and $Na_2CO_3$ (4 equiv) were added. The resulting reaction mixture was stirred under reflux and $N_2$ until everything of the anthracene derivative was consumed.

**5,14-Dineopentyl-fluorubine (4).** After 72 h, the reaction mixture was allowed to cool to room temperature and diluted with 60 mL of water. The aqueous slurry was extracted 5 times with $CHCl_3$. The organic layers were combined, dried over $MgSO_4$, and evaporated to dryness. The crude product was purified by column chromatography (silica; toluene/ethyl acetate 1:3) to give **4** (46 mg, 0.11 mmol; 20%): mp 317−318 °C; $^1$H NMR (250 MHz, $CDCl_3$): $\delta$ = 8.00 (dd, $J$ = 6.2, 3.5 Hz, 2H), 7.56 (dd, $J$ = 6.2, 2.9 Hz, 2H), 7.19 (dd, $J$ = 5.5, 3.7 Hz, 2H), 7.03 (dd, $J$ = 6.1, 3.5 Hz, 2H), 5.34 (d, $J$ = 15.5 Hz, 2H), 3.67 (d, $J$ = 14.2 Hz, 2H), 1.06 (s, 18H) ppm; $^{13}$C NMR (101 MHz, $CDCl_3$): $\delta$ = 145.3, 131.9, 130.2, 119.0, 118.9, 116.1, 113.3 110.5, 53.9, 35.3, 28.9 ppm; MS (EI) $m/z$ = 426 [$M^{+\bullet}$], 369 [$(M\text{-}^t\text{Bu})^{+\bullet}$]; MS (ESI-pos.) $m/z$ = 427.1 [$(M+H)^+$]; HRMS (ESI-pos.) calcd 427.2610, found: 427.2594; Anal. calcd for $C_{26}H_{30}N_6$: C, 73.21; H, 7.09; N, 19.70. Found: C, 73.47; H, 7.16; N, 19.49; UV−vis ($CHCl_3$): $\lambda$ ($\varepsilon$) = 505 nm ($3.96 \times 10^4$ $M^{-1}$ $cm^{-1}$), 474 nm ($4.57 \times 10^4$ $M^{-1}$ $cm^{-1}$), 447 nm ($2.69 \times 10^4$ $M^{-1}$ $cm^{-1}$).

**5,14-Bis(4-*tert*-butylphenyl)-fluorubine (5).** After 24 h, the mixture was allowed to cool to room temperature and diluted with 60 mL of water. The brown slurry was extracted 5 times with $CH_2Cl_2$. The combined organic layers were dried over $MgSO_4$ and evaporated to dryness. The crude product was purified by column chromatography (silica; toluene/ethyl acetate 5:1) and recrystallized from EtOH to give target compound **5** as red crystals (21 mg, 0.04 mmol; 10%): mp > 365 °C; $^1$H NMR (400 MHz, DMSO-$d_6$): $\delta$ = 7.76 (d, $J$ = 8.3 Hz, 4H), 7.68 (dd, $J$ = 6.1, 3.5 Hz, 2H), 7.51 (dd, $J$ = 6.3, 3.3 Hz, 2H), 7.47 (d, $J$ = 8.2 Hz, 4H), 6.87 (dd, $J$ = 6.0, 3.4 Hz, 2H), 6.20 (dd, $J$ = 5.5, 3.5 Hz, 2H), 1.45 (s, 18H) ppm; $^{13}$C NMR (63 MHz, acetone-$d_6$): $\delta$ = 154.3, 137.7, 134.5, 131.5, 128.7, 128.5, 127.6, 122.8, 118.7, 118.3, 113.7, 109.2, 35.7, 31.6 ppm; MS (EI) $m/z$ = 550 [$M^{+\bullet}$]; MS (ESI-pos.) $m/z$ = 573.3 [$(M+Na)^+$]; HRMS (ESI-pos.) calcd 573.2743, found 573.2751; Anal. calcd for $C_{36}H_{34}N_6$: C, 78.52; H, 6.22; N, 15.26. Found: C, 78.85; H, 6.30; N, 15.08. UV−vis ($CHCl_3$): $\lambda$ ($\varepsilon$) = 498 nm ($2.83 \times 10^4$ $M^{-1}$ $cm^{-1}$), 467 nm ($3.23 \times 10^4$ $M^{-1}$ $cm^{-1}$), 440 nm ($1.84 \times 10^4$ $M^{-1}$ $cm^{-1}$).

**5,14-Bis(4-methoxyphenyl)-fluorubine (6).** After 48 h, the mixture was allowed to cool to room temperature and diluted with 60 mL of water. The brown slurry was extracted 5 times with $CH_2Cl_2$. The combined organic layers were dried over $MgSO_4$ and evaporated to dryness. The crude product was purified by column chromatography (silica; $CHCl_3$/acetone 19:1) and recrystallized from EtOH to give target compound **6** as orange powder (18 mg, 0.04 mmol; 8%): mp > 365 °C; $^1$H NMR (300 MHz, DMSO-$d_6$): $\delta$ = 7.66 (dd, $J$ = 6.4, 3.4 Hz, 2H), 7.51 (dd, $J$ = 6.6, 3.3 Hz, 2H), 7.45 (d, $J$ = 8.6 Hz, 4H), 7.27 (d, $J$ = 8.8 Hz, 4H), 6.87 (dd, $J$ = 6.1, 3.5 Hz, 2H), 6.25 (dd, $J$ = 5.9, 3.5 Hz, 2H), 3.91 (s, 6H) ppm; $^{13}$C NMR (101 MHz, $CDCl_3$): $\delta$ = 161. 7, 149.2, 145.8, 132.4, 131.6, 130.0, 128.1, 126.4, 120.7, 119.7, 118.8, 116.3, 116.0, 113.1, 110.3, 77.2, 55.8 ppm; MS (EI) $m/z$ = 498 [$M^{+\bullet}$]; MS (ESI-pos.) $m/z$ = 499.3 [$(M+H)^+$]; HRMS (ESI-pos.) calcd: 499.1882, found 499.1872; Anal. calcd for $C_{30}H_{22}N_6O_2$: C, 72.28; H, 4.45; N, 16.86. found: C, 72.49; H, 4.58; N, 16.54; UV−vis ($CHCl_3$): $\lambda$ ($\varepsilon$) = 497 nm ($3.98 \times 10^4$ $M^{-1}$ $cm^{-1}$), 467 nm ($4.55 \times 10^4$ $M^{-1}$ $cm^{-1}$), 440 nm ($2.66 \times 10^4$ $M^{-1}$ $cm^{-1}$).

## ■ ASSOCIATED CONTENT

### Supporting Information

The Supporting Information is available free of charge on the ACS Publications website at DOI: 10.1021/acs.joc.7b00676.

X-ray data (CIF)

Solvatochromism measurements, oxidation waves of the cyclic voltammetry, photo and thermal stability tests, NMR spectra, details of the DFT calculations (PDF)

## ■ AUTHOR INFORMATION


### Corresponding Author

*E-mail: rainer.beckert@uni-jena.de

### ORCID

Panče Naumov: 0000-0003-2416-6569


### Notes

The authors declare no competing financial interest.

⊥Webpage: http://www.agbeckert.uni-jena.de/

## ■ REFERENCES


(1) Anthony, J. E. *Angew. Chem.* **2008**, *120*, 460.

(2) Braga, D.; Horowitz, G. *Adv. Mater.* **2009**, *21*, 1473.




DOI: 10.1021/acs.joc.7b00676
*J. Org. Chem.* 2017, 82, 6153−6162

(3) Mei, Y.; Loth, M. A.; Payne, M.; Zhang, W.; Smith, J.; Day, C. S.; Parkin, S. R.; Heeney, M.; McCulloch, I.; Anthopoulos, T. D.; Anthony, J. E.; Jurchescu, O. D. *Adv. Mater.* **2013**, *25*, 4352.
(4) Anthony, J. E. *Chem. Rev.* **2006**, *106*, 5028.
(5) Mas-Torrent, M.; Rovira, C. *Chem. Soc. Rev.* **2008**, *37*, 827.
(6) Mei, J.; Diao, Y.; Appleton, A. L.; Fang, L.; Bao, Z. *J. Am. Chem. Soc.* **2013**, *135*, 6724.
(7) Bunz, U. H.; Engelhart, J. U.; Lindner, B. D.; Schaffroth, M. *Angew. Chem., Int. Ed.* **2013**, *52*, 3810.
(8) Richards, G. J.; Hill, J. P.; Mori, T.; Ariga, K. *Org. Biomol. Chem.* **2011**, *9*, 5005.
(9) Bunz, U. H. *Chem. - Eur. J.* **2009**, *15*, 6780.
(10) Lindner, B. D.; Engelhart, J. U.; Tverskoy, O.; Appleton, A. L.; Rominger, F.; Peters, A.; Himmel, H. J.; Bunz, U. H. *Angew. Chem., Int. Ed.* **2011**, *50*, 8588.
(11) Jaung, J.; Fukunishi, K.; Matsuoka, M. *J. Heterocycl. Chem.* **1997**, *34*, 653.
(12) Kobayashi, T.; Kobayashi, S. *Eur. J. Org. Chem.* **2002**, 13, 2066.
(13) Koutentis, P. A. *ARKIVOC.* **2002**, *6*, 175.
(14) Schramm, F.; Walther, D.; Görls, H.; Käpplinger, C.; Beckert, R. *Z. Naturforsch.***2005**, *60*, 8, 843.
(15) Richards, G. J.; Hill, J. P.; Subbaiyan, N. K.; D'Souza, F.; Karr, P. A.; Elsegood, M. R.; Teat, S. J.; Mori, T.; Ariga, K. *J. Org. Chem.* **2009**, *74*, 8914.
(16) Tang, Q.; Liang, Z.; Liu, J.; Xu, J.; Miao, Q. *Chem. Commun.* **2010**, *46*, 2977.
(17) Miao, Q. *Synlett* **2012**, *23*, 326.
(18) Lindner, B. D.; Paulus, F.; Appleton, A. L.; Schaffroth, M.; Engelhart, J. U.; Schelkle, K. M.; Tverskoy, O.; Rominger, F.; Hamburger, M.; Bunz, U. H. F. *J. Mater. Chem. C* **2014**, *2*, 9609.
(19) Paulus, F.; Lindner, B. D.; Reiß, H.; Rominger, F.; Leineweber, A.; Vaynzof, Y.; Sirringhaus, H.; Bunz, U. H. *J. Mater. Chem. C* **2015**, *3*, 1604.
(20) Miao, S.; Brombosz, S. M.; Schleyer, P. V.; Wu, J. I.; Barlow, S.; Marder, S. R.; Hardcastle, K. I.; Bunz, U. H. *J. Am. Chem. Soc.* **2008**, *130*, 7339.
(21) Wu, J. I.; Wannere, C. S.; Mo, Y.; von Ragué Schleyer, P.; Bunz, U. H. F. *J. Org. Chem.* **2009**, *74*, 4343.
(22) Lindner, B. D.; Zhang, Y.; Höfle, S.; Berger, N.; Teusch, C.; Jesper, M.; Hardcastle, K. I.; Qian, X.; Lemmer, U.; Colsmann, A.; Bunz, U. H. F.; Hamburger, M. *J. Mater. Chem. C* **2013**, *1*, 5718.
(23) Biegger, P.; Stolz, S.; Intorp, S. N.; Zhang, Y.; Engelhart, J. U.; Rominger, F.; Hardcastle, K. I.; Lemmer, U.; Qian, X.; Hamburger, M.; Bunz, U. H. *J. Org. Chem.* **2015**, *80*, 582.
(24) Li, J.; Zhang, Q. *ACS Appl. Mater. Interfaces* **2015**, *7*, 28049.
(25) Wetzel, C.; Mishra, A.; Mena-Osteritz, E.; Walzer, K.; Pfeiffer, M.; Baeuerle, P. *J. Mater. Chem. C* **2016**, *4*, 3715.
(26) Bryant, J. J.; Zhang, Y.; Lindner, B. D.; Davey, E. A.; Appleton, A. L.; Qian, X.; Bunz, U. H. *J. Org. Chem.* **2012**, *77*, 7479.
(27) Zhao, J.; Li, G.; Wang, C.; Chen, W.; Loo, S. C. J.; Zhang, Q. *RSC Adv.* **2013**, *3*, 9653.
(28) Schramm, S.; Monteiro Leite Ciscato, L. F.; Oesau, P.; Krieg, R.; Richter, J. F.; Navizet, I.; Roca-Sanjuán, D.; Weiß, D.; Beckert, R. *ARKIVOC.* **2015**, *5*, 44.
(29) Schramm, S.; Navizet, I.; Naumov, P.; Nath, N. K.; Berraud-Pache, R.; Oesau, P.; Weiss, D.; Beckert, R. *Eur. J. Org. Chem.* **2016**, *2016*, 678.
(30) Fleischhauer, J.; Beckert, R.; Jüttke, Y.; Hornig, D.; Günther, W.; Birckner, E.; Grummt, U. W.; Görls, H. *Chem. - Eur. J.* **2009**, *15*, 12799.
(31) Strathausen, R.; Beckert, R.; Fleischhauer, J.; Müller, D.; Görls, H. *Z. Naturforsch., B: J. Chem. Sci.* **2014**, *69*, 641.
(32) Gampe, D. M.; Kaufmann, M.; Jakobi, D.; Sachse, T.; Presselt, M.; Beckert, R.; Görls, H. *Chem. - Eur. J.* **2015**, *21*, 7571.
(33) Hinsberg, O.; Schwantes, E. *Ber. Dtsch. Chem. Ges.* **1903**, *36*, 4039.
(34) Akimoto, Y. *Bull. Chem. Soc. Jpn.* **1956**, *29*, 460.
(35) CIBA-SOCIETE. BE614457, 1962.
(36) Deuschel, W.; Riedel, G. DE1142981B1, 1963.
(37) Riedel, G.; Deuschel, W. GB970.472, 1964.
(38) Riedel, G.; Deuschel, W. GB970.471, 1964.
(39) Foster, C. E.; GB2.430.936A, 2005.
(40) Fleischhauer, J.; Zahn, S.; Beckert, R.; Grummt, U.-W.; Birckner, E.; Görls, H. *Chem. - Eur. J.* **2012**, *18*, 4549.
(41) Stöckner, F.; Beckert, R.; Gleich, D.; Birckner, E.; Günther, W.; Görls, H.; Vaughan, G. *Eur. J. Org. Chem.* **2007**, *2007*, 1237.
(42) Mateo-Alonso, A.; Kulisic, N.; Valenti, G.; Marcaccio, M.; Paolucci, F.; Prato, M. *Chem. - Asian J.* **2010**, *5*, 482.
(43) Richards, G. J.; Ishihara, S.; Labuta, J.; Miklik, D.; Mori, T.; Yamada, S.; Ariga, K.; Hill, J. P. *J. Mater. Chem. C* **2016**, *4*, 11514.
(44) Li, G.; Wu, Y.; Gao, J.; Wang, C.; Li, J.; Zhang, H.; Zhao, Y.; Zhao, Y.; Zhang, Q. *J. Am. Chem. Soc.* **2012**, *134*, 20298.
(45) Gampe, D. M.; Schramm, S.; Kaufmann, M.; Görls, H.; Beckert, R. *New J. Chem.* **2016**, *40*, 10100.
(46) Bloking, J. T.; Han, X.; Higgs, A. T.; Kastrop, J. P.; Pandey, L.; Norton, J. E.; Risko, C.; Chen, C. E.; Brédas, J.-L.; McGehee, M. D.; Sellinger, A. *Chem. Mater.* **2011**, *23*, 5484.
(47) Chen, Y.; Wan, X.; Long, G. *Acc. Chem. Res.* **2013**, *46*, 2645.
(48) Yao, H.; Chen, Y.; Qin, Y.; Yu, R.; Cui, Y.; Yang, B.; Li, S.; Zhang, K.; Hou, J. *Adv. Mater.* **2016**, *28*, 8283.
(49) Kohl, B.; Rominger, F.; Mastalerz, M. *Org. Lett.* **2014**, *16*, 704.
(50) Kohl, B.; Rominger, F.; Mastalerz, M. *Angew. Chem., Int. Ed.* **2015**, *54*, 6051.
(51) Gampe, D. M.; Hänsch, V. G.; Schramm, S.; Menzel, R.; Weiß, D.; Beckert, R. *Eur. J. Org. Chem.* **2017**, *2017*, 1369.
(52) Lange, N. A. *Lange's Handbook of Chemistry*, 15 ed.; Dean, J., Ed.; McGraw-Hill, Inc.: New York, 1999.
(53) Miao, Q. *Adv. Mater.* **2014**, *26*, 5541.
(54) Bendikov, M.; Wudl, F.; Perepichka, D. F. *Chem. Rev.* **2004**, *104*, 4891.
(55) Wudl, F.; Koutentis, P. A.; Weitz, A.; Ma, B.; Strassner, T.; Houk, K. N.; Khan, S. I. *Pure Appl. Chem.* **1999**, Vol. *71*, 295.10.1351/pac199971020295
(56) Langer, P.; Bodtke, A.; Saleh, N. N.; Görls, H.; Schreiner, P. R. *Angew. Chem., Int. Ed.* **2005**, *44*, 5255.
(57) Zucchero, A. J.; McGrier, P. L.; Bunz, U. H. F. *Acc. Chem. Res.* **2010**, *43*, 397.
(58) Halgren, T. A. *J. Comput. Chem.* **1996**, *17*, 490.
(59) Yanai, T.; Tew, D. P.; Handy, N. C. *Chem. Phys. Lett.* **2004**, *393*, 51.
(60) Frisch, M. J.; Trucks, G. W.; Schlegel, H. B.; Scuseria, G. E.; Robb, M. A.; Cheeseman, J. R.; Scalmani, G.; Barone, V.; Mennucci, B.; Petersson, G. A.; Nakatsuji, H.; Caricato, M.; Li, X.; Hratchian, H. P.; Izmaylov, A. F.; Bloino, J.; Zheng, G.; Sonnenberg, J. L.; Hada, M.; Ehara, M.; Toyota, K.; Fukuda, R.; Hasegawa, J.; Ishida, M.; Nakajima, T.; Honda, Y.; Kitao, O.; Nakai, H.; Vreven, T.; Montgomery, Jr., J. A.; Peralta, J. E.; Ogliaro, F.; Bearpark, M. J.; Heyd, J.; Brothers, E. N.; Kudin, K. N.; Staroverov, V. N.; Kobayashi, R.; Normand, J.; Raghavachari, K.; Rendell, A. P.; Burant, J. C.; Iyengar, S. S.; Tomasi, J.; Cossi, M.; Rega, N.; Millam, N. J.; Klene, M.; Knox, J. E.; Cross, J. B.; Bakken, V.; Adamo, C.; Jaramillo, J.; Gomperts, R.; Stratmann, R. E.; Yazyev, O.; Austin, A. J.; Cammi, R.; Pomelli, C.; Ochterski, J. W.; Martin, R. L.; Morokuma, K.; Zakrzewski, V. G.; Voth, G. A.; Salvador, P.; Dannenberg, J. J.; Dapprich, S.; Daniels, A. D.; Farkas, Ö.; Foresman, J. B.; Ortiz, J. V.; Cioslowski, J.; Fox, D. J. *Gaussian 09, Revision A.02*; Gaussian, Inc.: Wallingford, CT, 2009.
(61) Tomasi, J.; Mennucci, B.; Cammi, R. *Chem. Rev.* **2005**, *105*, 2999.
(62) Jacquemin, D.; Wathelet, V.; Perpète, E. A.; Adamo, C. *J. Chem. Theory Comput.* **2009**, *5*, 2420.
(63) Jacquemin, D.; Perpète, E. A.; Ciofini, I.; Adamo, C. *Theor. Chem. Acc.* **2011**, *128*, 127.
(64) Fery-Forgues, S.; Lavabre, D. *J. Chem. Educ.* **1999**, *76*, 1260.
(65) Brouwer, A. M. *Pure Appl. Chem.* **2011**, *83*, 2213.
(66) Cardona, C. M.; Li, W.; Kaifer, A. E.; Stockdale, D.; Bazan, G. C. *Adv. Mater.* **2011**, *23*, 2367.
(67) Singh, J.; Naragyan, M. R. *Nanosci. Technol.***2013**, *1*, 8.



DOI: 10.1021/acs.joc.7b00676
*J. Org. Chem.* 2017, 82, 6153−6162

(68) More, S.; Bhosale, R.; Mateo-Alonso, A. *Chem. - Eur. J.* **2014**, *20*, 10626.
(69) Gao, J.; Xiao, C.; Jiang, W.; Wang, Z. *Org. Lett.* **2014**, *16*, 394.
(70) Otwinowski, Z.; Minor, W. *Methods Enzymol.* **1997**, *276*, 307.
(71) *Collect: Data collection software*; Nonius BV: Delft, The Netherlands, 1998.
(72) *SADABS 2.10*; Bruker AXS, Inc.: Madison, Wisconsin, 2002
(73) Sheldrick, G. *Acta Crystallogr., Sect. A: Found. Crystallogr.* **2008**, *64*, 112.
(74) Macrae, C. F.; Edgington, P. R.; McCabe, P.; Pidcock, E.; Shields, G. P.; Taylor, R.; Towler, M.; van de Streek, J. *J. Appl. Crystallogr.* **2006**, *39*, 453.
(75) Danièle, S.; Drost, C.; Gehrhus, B.; Hawkins, S. M.; Hitchcock, P. B.; Lappert, M. F.; Merle, P. G.; Bott, S. G. *Dalton Trans.* **2001**, 3179.



DOI: 10.1021/acs.joc.7b00676
*J. Org. Chem.* 2017, 82, 6153−6162